AN INVESTIGATION OF GENE DELIVERY BARRIERS FOR POLY(BETA-AMINO ESTER)S AND HYBRID GOLD-POLYMERIC NANOPARTICLES

by

Corey John Bishop

A dissertation submitted to Johns Hopkins University in conformity with the requirements for the degree of Doctor of Philosophy

Baltimore, Maryland

May 2015

Abstract

Gene therapy is promising because nearly all inheritable diseases and cancer has an underlying genetic component. However, the development of a gene vector capable of delivering nucleic acids efficiently while remaining safe has been a challenge. Generally speaking, viral vectors are highly adept at delivering nucleic acids intracellularly. Viral vectors, however, have been known to be associated with insertional mutagenesis and immunogenicity and in severe cases, death. Furthermore, viral vectors are difficult to chemically modify for optimization and to mass produce.

To date, despite that there have been more than 2000 gene therapy clinical trials worldwide, the U.S. FDA has yet to approve a gene therapy application. The lack of gene therapy approval by regulatory bodies delineates the need for safer and more effective vectors. A safer alternative to viral-based vectors are cationic, amine-containing polymeric vectors. Cationic polymers are capable of ionically complexing nucleic acid and forming nanoparticles on the order of 100-250 nm. This particle diameter is capable of extravasating through mal-formed tumor vasculature. The polymers can be engineered to have a buffering ability that allows the nucleic acid cargo to escape the lysosomal degradation pathway post-endocytosis. Ester-containing backbone polymers are capable of hydrolytic degradation, which helps mitigate toxicity. However, much is unknown regarding how polymer structure affects gene delivery. To date, the polymer vectors which work well have been discovered through empirical methods. Understanding how polymer structure affects gene delivery function would allow for a more rational approach to designing new vectors for gene delivery.

The objective of this work has been two-fold: the first objective has been to elucidate non-viral gene delivery barriers – in particular investigating polymer structure-function relationships for polymeric vectors; the second objective has been to develop a polymeric/inorganic hybrid, theranostic-enabling nanoparticle platform technology capable of co-delivering DNA and siRNA and modulating temporal release.

More specifically, this work details how polymer structure of poly(β-amino ester)s (PBAEs) affects polymer-DNA binding and how binding affects transfection levels, viability, and nanoparticle physical properties (zeta potential and diameter). We found transfection levels are biphasic with respect to binding in two human cancer cell lines and that binding constants in the range of $(1\text{-}6)\text{x}10^4$ M^{-1} were necessary but not sufficient for optimal transfection. We also investigated the comparative binding strengths of branched and linear polyethyleneimine, poly(L-lysine) and PBAEs with plasmid DNA and found PBAEs have the weakest binding.

This work also details new bioassays including a more high throughput method for assessing cellular and nuclear uptake rates using flow cytometry. This method may be used for elucidating structure-function relationships in various cell types. An auto-fitting, first order mass-action kinetic model was developed in MatLab to quantify the intracellular delivery rate constants for comparing delivery bottlenecks of various polymer structures in various cell lines. This model was used to assess rate differences between polymers which do not transfect well, tansfect mediocre, and transfect well in primary human glioblastoma *in vitro*. The model recapitulated the experimental data with good agreement without needing to extrapolate data from literature.

Principal component analysis is a method to look at large data sets with unknown

variable correlations and to quantify how each variable is correlated with another, as well as which and to what degree each variable may drive another. Principal component analysis was utilized to look at 27 physico-chemical properties and cell gene delivery outcomes (i.e., uptake, transfection levels, and viability). We found that certain key parameters, such as hydrophobicity, drove uptake and transfection.

The development of a theranostic-enabling platform technology involved gold nanoparticles and a layer-by-layer coating process to create polymer-inorganic hybrids. Gold nanoparticles are relatively biocompatible, are monodisperse, have interesting optical properties, have photothermal capabilities, and are easily chemically modified via thiol bonds. Gold nanoparticles can be synthesized to absorb a desired wavelength of electromagnetic radiation and can be imaged through various modalities such as photoacoustics or X-rays for diagnostic purposes.

The theranostic-enabling technology was capable of co-delivering DNA and siRNA as well as delivering two layers of DNA with two different expression time profiles. Co-delivering DNA and siRNA could allow for the knockdown of a dysfunctional aberrant protein while replacing it with a functional protein. The ability to express proteins with different time profiles could have multiple applications such as controlling stem cell differentiation.

Thesis Committee

Jordan J. Green, Ph.D. *(primary advisor, reader)*

Associate Professor, Departments of Biomedical Engineering, Ophthalmology, Neurosurgery, and Materials Science & Engineering,

Johns Hopkins University School of Medicine

Hai-Quan Mao, Ph.D. *(reader)*

Professor, Department of Materials Science and Engineering,

Johns Hopkins University

Kevin J. Yarema, Ph.D.

Associate Professor, Department of Biomedical Engineering,

Johns Hopkins University

Warren L. Grayson, Ph.D.

Assistant Professor, Department of Biomedical Engineering,

Johns Hopkins University School of Medicine

Acknowledgments

I would like to sincerely thank Dr. Jordan Green for his mentorship. We have had countless conversations over the years. I have always found his advice extremely helpful in terms of my experiments and also in terms of life in general. I look up to Dr. Green a great deal as a scientist, an engineer, and as a person. Dr. Green is incredibly intelligent and his kindness and patience is truly admirable. Our lab comments all the time how we all feel so incredibly lucky to have Dr. Green as our mentor. I feel a tremendous feeling of gratitude that I was able to be a member of his group. I have thoroughly enjoyed my time here at Hopkins under Dr. Green's tutelage. I will be forever grateful to Dr. Jordan Green and all that he has done for me and my family.

I would like to thank the other faculty members who served on my thesis committee: Dr. Hai-Quan Mao, Dr. Warren Grayson, and Dr. Kevin Yarema. Their insight and suggestions have been incredibly helpful as well. I could not have asked for a better committee.

I would like to thank my collaborators from the University of Helsinki and the Tampere University of Technology: Marjo Yliperttula, Elina Vuorimaa-Laukkanen, and Tiia Ketola. I would also like to thank my lab mates: Nupura Bhise, Joel Sunshine, Stephany Tzeng, Ron Shmueli, Kristen Kozielski, Jay Young, Randall Meyer, and David Wilson. I would like to thank them for all of the advice, suggestions, and also their friendship. We have shared a lot of laughs together. I look up to each and every one of them. I would also like to thank the undergraduates I have worked with: Rebecca Majewski, Richard Murdock, Toni Guiriba, Allen Liu, David Lee, Peter Nelson, Philip Harding, and Evan Smith. They have helped me a great deal throughout my time here.

I would also like to thank my parents and parents-in-law, John and Elaine Bishop, and Mark and Christine Gottfredson, for all of their support and encouragement. They have always believed in me fully and have inspired me to be my best. Where would we be without parents?

I would also like to thank my dear sweet wife, Becca. I would like to thank her for her never ending support and encouragement. I want to thank her for enabling me to come on this adventure. I want to thank her for being willing to have me be a student for such an extended period of time while we raise a family on a student's salary. She is an amazing mother of our beautiful 4 children. Connor is 6, Stella is 3.5, and McKay and Caleb are about 6 months old now. I would like to thank my kids for their love of life and for all of their laughs and smiles. My family fulfills me. I strive to be my best for them. They are what bring joy into my life. They are my everything. I will do everything in my power to give them the life they deserve.

Dedication

I would like to dedicate my thesis to Rebecca, my wife, and my children, Connor, Stella, McKay, and Caleb. I would also like to dedicate my thesis to my parents, John and Elaine Bishop and also my parents-in-law, Mark and Christine Gottfredson. I love you all dearly!

"The achievement of one goal should be the starting point of another."

-Alexander Graham Bell

Contents

List of figures

2.2.12 Figure 3. Gene expression of PBAE vs. adenovirus. A) Gene expression histogram comparing adenovirus (blue), PBAE (green), and negative control. B) Comparison of various PBAE formulations with adenovirus with respect to % positive cells and normalized expression. Images of GFP+ cells 24 hrs post transfection with C) PEI, D) C32-103, and E) 500 MOI (multiplicity of infection) adenovirus. Reproduced with permission.

2.2.12 Figure 4. Nuclear import through the nuclear pore complex. Reproduced with permission.

2.3.15 Figure 1. Structures of commonly used cationic polymers and polysaccharides used in gene delivery.

2.3.15 Figure 2. A: TEM of AuNP spheres; B: TEM of Au nanoparticle rods; C: AFM topography of AuNP shells coating platinum; D: Multi-walled CNT. E: Representative TEM of carbon samples produced by catalysis; F: Mesoporous silica nanoparticles; G: Quantum dots – top and bottom row are illuminated under visible and UV, respectively; H: Doxorubicin-loaded SPIONs with a diameter of 8 +/- 2 nm; I: TEM of pristine layered double hydroxide NPs of $Mg_2Al(OH)_6NO_3$ - inset NPs are associated with siRNA. Figures adapted with permission.

2.3.15 Figure 3. A: TEM images of HeLa cells. A: PBAE-siRNA-AuNPs; B: siRNA-AuNPs without PBAE; C: unmodified AuNPs; D: No nanoparticles (control). Adapted with permission.

3.5 Figure 1. GPC curves of fractionated polymers by group (relative RI shift (mV/max mV) versus elution time (min.); varying molecular weight (Low, Med, and High) (A), backbone (B), sidechain (C), and endcaps (D).

3.5 Figure 2. Fraction of bound DNA as a function of amine concentration of polymer 442.

3.5 Figure 3. Hill plots of polymer series varying M_w (A), backbone (B), sidechain (C), and endcaps (D).

3.5 Figure 4. Binding constants (M^{-1}) of each of the series comparing M_w (A), backbone (B), sidechain (C), and endcaps (D). (Statistical analysis was accomplished by a one-way ANOVA and a Tukey post-hoc analysis; *=P-value < 0.05; **=P-value < 0.01; ***=P-value < 0.001).

3.5 Figure 5. The effect of binding constant on transfection efficacy in MDA-MB-231 cells (A, C, E, G) and GBM319 cells (B, D, F, H) for each of the series comparing M_w (A and B), backbone (C and D), sidechain (E and F), and endcaps (G and H).

3.5 Figure 6. The effect of binding constant on relative metabolic activity in MDA-MB-231 cells (A, C, E, G) and GBM319 cells (B, D, F, H) for each of the series comparing M_w (A and B), backbone (C and D), sidechain (E and F), and endcaps (G and H).

3.5 Figure S1. ^{1}H NMR spectra of polymers 44 High (A, C), Med (E), Low M_w (G), 442 (B), 444 (D), 446 (F), and 447 (H). These spectra are consistent with NMR analyses published previously (Sunshine, Akanda, et al.) along with spectra of the other polymers used in this study. (See below for further peak analyses.)

3.5 Figure S2. Decay-associated spectra. The fluorescence lifetimes of ethidium bromide bound to DNA and free in the solution are 22.58 and 1.81 ns, respectively, in this particular case.

3.5 Figure S3. Hill plot of peptide $(KK)_2KGGC$.

3.5 Figure S4. The relationship between polyplex diameter and the binding constant (M^{-1}) of each of the series comparing M_w (A), backbone (B), sidechain (C), and endcaps (D).

3.5 Figure S5. All diameters versus binding constants (A); dependence of transfection efficacy on polyplex diameters in MDA-MB-231 (B) and GBM319 cells (C).

3.5 Figure S6. Diameter of four representative polymers at various pHs and ionic strengths. (White group was via NTA; remainder was via DLS.)

3.5 Figure S7. The relationship between zeta potential and the binding constant (M^{-1}) of each of the series comparing M_w (A), backbone (B), sidechain (C), and endcaps (E).

3.5 Figure S8. All ZP values irrespective of series versus binding constants (A); dependence of transfection efficacy on ZP in MDA-MB-231 (B) and GBM319 cells (C).

3.5 Figure S9. ZP of four representative polymers at various pHs and ionic strengths.

3.5 Figure S10. Normalized geometric (A) and arithmetic (B) means versus transfection efficacy in the MDA-MB-231 and GBM319 cell lines.

3.5 Figure S11. Positive (Lipofectamine 2000 at 100 and 200 ng/well) and negative controls (naked DNA and untreated) for transfection and relative metabolic activity in MDA-MB-231 and GBM319 cells.

3.5 Figure S12. All binding constants for each of the series of comparison against transfection efficacy in MDA-MB-231 cells (A) and GBM319 cells (B), as well as cytotoxicity in MDA-MB-231 cells (C) and GBM319 cells (D).

3.5 Figure S13. All binding constants against transfection efficacy using 70% serum in the GBM319 cell line.

3.5 Figure S14. Heparin (ranging from 0 to 512 μg/mL) competition release assay of four representative polymers using gel electrophoresis; binding constants range from 526 (weakest *K* measured) to 1.23×10^5 M^{-1} (strongest *K* measured).

4.6 Figure 1. TEM images of each of the layered stages showing nanoparticle size. The addition of the DNA layer results in initial clustering of multiple gold nanoparticle cores together to form a single particle.

4.6 Figure 2. Diameter (A) and zeta potential (B) at each of the layering stages.

4.6 Figure 3. SiRNA-mediated knockdown over time of GFP in human brain cancer cells resulting from delivery of MAu/DNA/siRNA LbL particles. Nanoparticle dosages and amount of 447 polymer in the outer layer were varied. Optimized particles had higher knockdown than the optimized formulation of the leading commercially available reagent Lipofectamine® 2000.

4.6 Figure 4. SiRNA-mediated knockdown of MAu/DNA/siRNA LbL particles on day 7 and relative metabolic activity at 24 hours post transfection of LbL NPs.

4.6 Figure 5. Fluorescence microscope images of the eGFP channel showing GFP knockdown following transfection with various MAu/DNA/siRNA LbL nanoparticles; the Lipofectamine® 2000 conditions shown are 240 ng 0.5:1 and 160 ng 2.5:1 (200 ms eGFP exposure time; magnification of 5x; "scr" refers to scrambled siRNA and "si" refers to active anti-eGFP siRNA).

4.6 Figure 6. Fluorescence microscope images showing exogenous dsRed expression following transfection of MAu/DNA/siRNA LbL nanoparticles. Lipofectamine® 2000 was added at a 100 ng dosage 2.5 μL:1 μg dsRed DNA; (200 ms eGFP and 600 ms dsRed exposure time; magnification of 10x).

4.6 Figure 7. DNA transfection efficacy and relative metabolic activity of MAu/DNA/siRNA LbL nanoparticles. Lipofectamine® 2000 was added at a 100 ng (2.5:1) dose and is not statistically different from nanoparticle formulation HD5. Lipofectamine® 2000's expression was statistically significantly greater than all other formulations (p-value < 0.0001).

4.6 Figure 8. TEM of MAu/DNA/siRNA LbL nanoparticles of formulation HD5 in GBM319 cells. **A** and **B**: show particles that are ~200 nanometers. **C**: Two left arrows indicate putative endosomes with multiple gold nanoparticle aggregates.

4.6 Figure S1. Absorbance spectra of citrate-stabilized CAu and 11-MUA-conjugated MAu at pH 7.1, similar to the storage conditions. MAu resists aggregation whereas CAu aggregates as indicated by the increase in the SPR wavelength.

4.6 Figure S2. UV-Vis spectra of CAu (left) and MAu (right) solutions in various concentrations of NaAc ranging from 0 to ~100 mM. The NaAc concentration after the first layer (PEI) is ionically complexed to AuNPs is approximately 60 mM.

4.6 Figure S3. Fluorescence recovery percentages using YO-PRO®-1, Picogreen, and Ribogreen to quantify nucleic acid.

4.6 Figure S4. Compartmentalization percentages of nucleic acid. DNA and siRNA content of what was ionically complexed during the layering process and in the two supernatants during the washing steps.

4.6 Figure S5. Nucleic acid lost to plasticware surface contact. **A**-**B**: Pipette tip and vial without contact with the co-delivery LbL formulation and without YO-PRO®-1, respectively. **C**: Vial with LbL formulation without YO-PRO®-1. **D**: Vial with LbL formulation and YO-PRO®-1. **E-F**: Vial and pipette tip with all of the LbL formulation removed with YO-PRO®-1, showing DNA and or siRNA not retained in the layering process.

4.6 Figure S6. Optimization of siRNA delivery to human brain cancer cells using Lipofectamine® 2000 over time with varying ratios. Efficacy measured by fluorescence on a plate reader for conditions where the relative metabolic activity was greater than 70%, normalized to the untreated group.

4.6 Figure S7. Optimization of siRNA delivery to human brain cancer cells using Lipofectamine® 2000 and polymer 447 on day 7. Knockdown on day 7 and relative metabolic activity at 24 hours post transfection using Lipofectamine® 2000 (Lipo X:Y; where X = Lipo μL; Y = μg DNA) and 447.

4.6 Figure S8. Fluorescence images of the various LbL formulations showing eGFP expression and their associated brightfield images overlaid to their right.

4.6 Figure S9. DNA transfection efficacy of dsRed expression and relative metabolic activity of various formulations. Lipofectamine® 2000 was delivered using 2.5 μL:1 μg DNA.

5.6 Figure 1. TEM of complete LbL formulation. Scale bars are 500 nm.

5.6 Figure 2. Hydrodynamic diameter (left) and zeta potential (right) of each of the 7 layers, respectively.

5.6 Figure 3. Transfection efficacies (top) and normalized transfection efficacies (bottom) in time for the outer (eGFP) and inner (dsRed) pDNA layers using 10% (left) and 50% (right) serum conditions.

5.6 Figure 4. Fluorescence microscopy images of the GB319 cells in 10% serum transfected with the full 7 layers on days 2, 5, 9, 14, and 21 post-transfection.

5.6 Figure S1. Polymer structure of B4-S4-E7 (447).

5.6 Figure S2. Layered nucleic acid content of the inner (dsRed) and outer (eGFP) pDNA layers; nucleic acid content in the supernatant of the first and second washings (SN1 and SN2) after the nucleic acid layer incubation.

5.6 Figure S3. The flow cytometry dot plots of the eGFP and dsRed channels in time of the 10% serum condition which qualitatively shows the expression maxima of the outer (eGFP) and inner (dsRed) pDNA layers to be on days 2 and 9, respectively.

5.6 Figure S4. The relative metabolic activities of GB319 cells incubated with the full 7 layers in either 10% or 50% serum.

5.6 Figure S5. dsRed and eGFP expression efficacies of Lipo2k dosages at 100, 200, or 328 ng (same dsRed:eGFP pDNA ratio) at varying Lipo2k µL:pDNA µg ratios.

6.6 Figure 1. Isolated nuclei stained with DAPI.

6.6 Figure 2. Cells and nuclei washing challenge (polyplex incubation for 1 hour at 4ºC) using 50 µg/mL heparin in PBS to eliminate associated DNA or DNA that was not uptaken. The washed cells and nuclei returned to their untreated fluorescence values, indicating successful washing.

6.6 Figure 3. Percentages (left) and NGM (right) of Cy3 for both cells (top) and nuclei (bottom). Pcyto, Pne, and Pni are plasmids which are in the cytoplasm, and plasmids which are extranuclear and intranuclear, respectively.

6.6 Figure 4. First order mass-action model (dotted lines; bi-exponential degradation) for the $P_{Corr\ cyto}$, $P_{Corr\ ne}$, and $P_{Corr\ ni}$ experimental data points.

6.6 Figure 5. The experimental and first order mass action kinetic models overlaid for polymers 44 (**A**), 446 (**B**), and 447 (**C**).

6.6 Figure S1. Normalized fluorescence of Cy3, showing no statistical difference at pH 7.4 (150 mM PBS) and 5.2 (150 mM NaAc).

6.6 Figure S2. Purity of nuclei. Flow cytometry was used to assess the eGFP presence of eGFP-stably expressing cells and their isolated nuclei to ascertain the purity of the nuclei; the eGFP protein in adhered cytoplasm would have caused nuclei to fluoresce.

6.6 Figure S3. Top: Ungated cells and nuclei (FSC-H vs SSC-H). The nuclei had a lower FSC-H value as expected due to their smaller size. Bottom: FSC-H Histogram for gated cells and nuclei.

6.6 Figure S4. Cell flow cytometry data for the untreated, and the 0 and 2 hour time points. There is a great deal of population overlap for the untreated and the 0 hour time point, as would be expected.

6.6 Figure S5. Calibration curve for converting bulk fluorescence on a plate reader to a plasmid number.

6.6 Figure S6. Gel electrophoresis of qPCR products (left, middle and rights lanes: DNA ladder, and qPCR products of eGFP and β-actin, respectively).

6.6 Figure S7. Plasmids in time calculated using the plate reader ($Plasmid_{PR}$) method compared to qPCR ($Plasmid_{qPCR}$).

6.6 Figure S8. $Plasmid_{PR}$ (top) and $Plasmid_{Corr}$ (bottom) in time for cells and nuclei.

6.6 Figure S9. $Plasmid_{qPCR}$ values from 2 to 24 hours for fitting the degradation constant, k_{deg}, showing mono- (dotted line) and bi-exponential degradation fittings.

6.6 Figure S10. Available number of plasmids in the media per cell in time. The dotted line shows what was used for modeling purposes.

6.6 Figure S11. Fluorescence microscopy images of the eGFP channel (left) and the eGFP and brightfield channels combined (right) for untreated (top) and for 447 30 w/w (bottom) at 48 hours post transfection.

6.6 Figure S12. Convergences of k_{cell}, k_{ne}, k_{ni}, and k_{bd} through optimization iteration.

6.6 Figure S13. Error minimizations for the 19^{th} or last iteration of optimization for k_{cell}, k_{ne}, k_{ni}, and k_{bd}.

6.6 Figure S14. First order mass-action model (dotted lines; mono-exponential degradation) for the $P_{Corr\ cyto}$, $P_{Corr\ ne}$, and $P_{Corr\ ni}$ experimental data points.

7.4 Figure 1. Top: the variances are explained for the first 5 PCs. The top 4 variables of the 27 are ranked by the degree to which they contribute to the PCs according to their associated coefficients and listed above the variances. The "(-)" indicates a negative contribution; Bottom: The loading plot of all of the variables showing relative correlations.

7.4 Figure 2: **A**: The scores plot versus transfection efficacy with red being the highest level of transfection; **B**: region B of 3A with a B+S (sum of carbons in backbone and sidechain) value of 7; **C**: region C of 3A with a B+S value of 8; **D**: region D of 3A with a B+S value of 9.

7.4 Figure S1. The loading plot of the variables in the boxed region of **Figure 1** showing other variables (Mw, PDI, Mn, MR, CV) which are positively correlated to transfection and uptake (quadrant IV) which are difficult to visibly differentiate.

List of Schemes

List of tables

experimental setups are likely different. Key: β-Gal = β-galactosidase; CAAT = chloramphenicol acetyltransferase; (e) GFP = (enhanced) green fluorescent protein; hESC = human embryonic stem cell; hpt = hours post transfection; Luc = Luciferase; PBAE = poly(β-amino esters); PEI = poly(ethylene imine); PLL = Poly(L-lysine); SPION = superparamagnetic iron oxide nanoparticles; RFP = red fluorescent protein; RLU = relative light unit.

3.7 Table S1. List of PBAE polymers and their number average molecular weights (M_n), weight average molecular weights (M_w), polydispersity indices (PDI), degree of polymerizations (DP), Hill coefficients (α), binding constants (*K*), diameters (nm), and zeta potentials (ZP; mV).

4.8 Table 1. Nucleic acid dosages and mass ratio of the 447 polymer to DNA (w/w) values of the various layered formulations. The w/w values are calculated from the most outer layer of polymer as described in section 2.6

4.8 Table S1. Nucleic acid dosages and weight/weight (w/w) values of the various layered formulations of polymers 447 for DNA and siRNA.

6.8 Table 1. GPC data (M_n, M_w, PDI) and rate constants for polymers 44, 446, and 447.

7.6 Table 1. Ranking of variables for transfection, uptake and viability. The value of Acos(Θ) indicates the strength of the correlation.

7.6 Table S1. The ranking of all variables according to the degree to which they contribute to each of the first 5 PCs. The notation '(-)' indicates the contribution is negative.

8.4 Table 1. Literature summary for "Biomolecule delivery to engineer the cellular microenvironment.

Derivation

6.8 Table S1. Derivation of degradation term in the differential equations.

1 Chapter 1: Introduction to the thesis

1.1 Objectives

As inheritable diseases and cancer can result from inactive genes[2,3], delivering DNA and shRNA to encode and generate a functional copy or to inhibit mRNA expression of a non-functioning protein can potentially treat and cure many genetic diseases. Despite being generally less effective than viruses, degradable cationic polymers are attractive as they are generally safer, are easier to manufacture and have more functional capabilities.[4] Varying a polymer's structure and functional groups allow optimization of delivery properties via high-throughput analyses of vast combinatorial libraries, but rational design of structure to control function would be more efficient.[5-7] I am interested in evaluating polymer structure-function relationships to further our mechanistic understanding of, and to improve polymeric materials for non-viral gene delivery. PBAEs are promising due to their ability to condense DNA into nanoparticles and thereby protect the DNA in the extracellular space, facilitate cellular uptake[8], mediate endosomal escape and subsequently release the DNA effectively within the cell.[9-12] Designing such systems require proper understanding of the binding between DNA and polycations.[13,14] One challenge in the field in evaluating and optimizing polymer structure is that synthetic polymers can be polydisperse, with variable extents of reaction and molecular weight heterogeneity.[15-17] Isolating precise polymer structures and uniform molecular weight are key to being able to evaluate polymer structure-function relationships and has been a confounding factor. I will quantify how poly(beta-amino ester) (PBAE) structural properties affect polmer/DNA binding thermodynamics and

gene delivery in **Aim 1**.

Aim 2. Improved nanobiotechnologies which enable multi-functional imaging and intracellular delivery of difficult to deliver biologics such as DNA and siRNA are needed. Gold nanoparticles (AuNPs) are easy to synthesize, monodisperse, relatively biocompatible, have optical properties useful for colorimetric sensor applications, and can be diversely functionalized with chemical moieties. AuNPs have been used as biosensors, imaging agents[18-20], and as therapeutic vectors (i.e., conjugation or ionic complexation to small molecules[21], or various nucleic acids, such as DNA[22], short hairpin RNA[23] or short interfering RNA (siRNA)[24] for promoting or inhibiting protein expression) for theranostic applications; the nanoscale size and the ability to functionalize with tumor/cancer-specific small molecules or antibodies allows passive and active targeting, respectively.[25-27] AuNPs may be tuned for photothermal therapy at wavelengths transparent to biological tissue on the order of centimeters.[28] Photothermal therapy takes advantage of tumors' decreased ability to self-thermoregulate.[29] Layer-by-layer (LbL) approaches coat a surface or a core with multiple layers of charge-alternating polyelectrolytes.[22,30-34] Nanoparticle LbL approaches are ideal for complexing ionically charged macromolecules into relevant particle sizes for systemic administration. LbL approaches can be accomplished using aqueous solvents, are versatile regarding molecular structure as natural and synthetic polyelectrolytes are able to be used, and are easily tuned by varying the number and order of the layers.[31,35] I will demonstrate a degradable hybrid gold/polymeric nanoparticle theranostic platform technology capable of delivering nucleic acid via a modifiable LbL approach in **Aim 2**.

In designing new biomaterials for gene delivery, a thorough understanding of the intracellular barriers is critical. Although there are a number of intracellular barriers for successful expression[4], cellular and nuclear entry are key. I will quantify the rates of cellular and nuclear uptake in **Aim 3** which will help further elucidate the bottlenecks of non-viral gene delivery.[36] In addition, there is currently a need to methodically understand how polymeric structure affects rates of cellular and nuclear uptake which I undertake using PBAEs to better understand structure-function relationships which will help in designing new non-viral biomaterial vectors. I develop a new method to quantify the number of plasmids within the cells and nuclei based on flow cytometry, which can be more efficient than using Polyermase Chain Reaction (PCR) which requires isolation and purification of the plasmid and genomic DNA for all samples. In the new method, after PCR is used to establish the degradation kinetics within each cell type, flow cytometry can then be used for multiple types of polymers within the cell type of interest.

The gene delivery field has observed certain general polymer properties that result in increased or decreased transfection levels. For example, generally speaking, it was previously known that as hydrophobicity of polymers increase, transfection levels increase; or that there is an optimal molecular weight which results in optimal transfection levels. However, there has not been a methodical mathematical approach applied to a large biomaterial library set used for non-viral gene delivery to date which quantifies correlative relationships between variables of interest. In **Aim 3**, I use Principal Component Analysis to methodically quantify which and to what degree physicochemical properties drive transfection, uptake, and viability.

Aim 1. To quantify how poly(beta-amino ester) (PBAE) structural properties affect polymer/DNA binding thermodynamics and gene delivery. I hypothesize that there is an optimal binding constant that will maximize exogenous gene expression.

a. Synthesize a library of PBAE polymers which vary only in the following: molecular weight; the number of carbons in the backbone which varies the amine density and hydrophobicity; the number of carbons in the sidechain which varies the distance of a hydroxyl group from the backbone and its hydrophobicity; and the endcap type (primary, secondary, tertiary amines and no endcap or diacrylate terminated).

b. Assess the binding affinity between the various polymers mentioned in Specific Aim 1a and DNA and how the binding affinity impacts DNA delivery functionality, namely transfection and cytotoxicity in human breast and brain cancer *in vitro*, as well as the physical properties of the polyplexes. In addition, the binding affinity between poly(L-lysine), and linear and branched PEI and DNA will be quantified.

Aim 2. Develop a hybrid gold/polymeric nanoparticle theranostic platform technology capable of delivering nucleic acid via a modifiable Layer-by-Layer (LbL) approach. I hypothesize that nanoparticles beginning with a gold nanoparticle (AuNP) core and

layered in multiple types of nucleic acids and polymers with differing degradable mechanisms are capable of resulting in effective transfection with tunable release.

a. Develop an siRNA and DNA-co-delivering formulation using a gold nanoparticle core via an LbL approach using cationic polymers which degrade mechanistically differently, via hydrolysis and reduction, and assess physicochemical properties.

b. Assess simultaneous knockdown and expression in human brain cancer

c. Tune multilayers to be able to control the timing of protein expression from two independent layers of plasmid DNA

Aim 3. Quantify transport as a major non-viral gene delivery barrier, namely the rates of cellular and nuclear uptake of DNA carried by polymeric nanoparticles; also to assess which and to what degree polymer physicochemical properties drive transfection and uptake. I hypothesize that nuclear uptake is the major barrier to polymeric gene delivery and rates will vary as a function of polymer structure.

a. Develop an assay to quantify kinetics of cellular uptake and nuclear uptake in a more high-throughput fashion

b. Via the assay from Specific Aim 3a, determine how polymer structure affects cellular uptake and nuclear uptake rate constants

c. Via principal component analysis, determine which and to what degree polymer physicochemical properties drive cellular transfection levels, uptake, and viability

1.2 Summary of contributions

The major contributions and accomplishments that have resulted from this work are as follows:

Chapter 2: State of the Art
CJ Bishop, J Kim, JJ Green. Biomolecule delivery to engineer the cellular microenvironment for regenerative medicine. *Ann. Biomed. Eng.* 2013, 42(7), 1557-72.

JC Sunshine, **CJ Bishop**, JJ Green. Advances in Polymeric and Inorganic Vectors for Non-viral Nucleic Acid Delivery. *Therapeutic Delivery.* 2011, 2(4), 493-521.

Chapter 3: The Effect and Role of Carbon Atoms in Poly(β-amino ester)s for DNA Binding and Gene Delivery

CJ Bishop, T Ketola, SY Tzeng, et al. The effect and role of carbon atoms in poly(β-amino ester)s for DNA binding and gene delivery. *J. Am. Chem. Soc.*, 2013, 135(18), 6951-7.

T Ketola, M Hanzlikova, L Leppanen, R Manuela, **CJ Bishop**, et al. Independent vs cooperative binding in polyethyleneimine-DNA and poly(L-lysine)-DNA polyplexes. *J. Phys. Chem. Part B*., 2013, 117(36), 10405-13.

CJ Bishop, SY Tzeng, JJ Green. Structure-Functional Relationships Between Poly(β-amino ester)s for DNA Binding and Gene Delivery. American Society for Gene and Cell Therapy. May 2014, 351, Poster presentation in Washington D.C.

TM Ketola, **CJ Bishop**, JJ Green, M Hanzlíková, H Lemmetyinen, A Urtti, M Yliperttula, E Vuorimaa. The influence of pH and polymer structure on the cationic polymer-DNA complexes revealed by time-resolved fluorescence studies. XXIV IUPAC Symposium on Photochemistry, 15-20 July 2012, Coimbra, Portugal. Poster presentation.

Chapter 4: Degradable Polymer-Coated Gold Nanoparticles for Co-delivery of DNA and siRNA

CJ Bishop, SY Tzeng, JJ Green. Nano-Gold/Degradable Polymer Hybrid Nanoparticles for Co-Delivery of DNA and siRNA. *Acta Biomaterialia,* 2014. 2014, 42(7), 1557-72.

CJ Bishop, SY Tzeng, JJ Green. A Layer-by-layer Gene Therapy Approach for Promoting Exogenous and Inhibiting Endogenous Protein Expression. *Society for Biomaterials.* April 2014 Denver Colorado; Oral Presentation; Honorable Mention STAR Award

CJ Bishop, SY Tzeng, JJ Green. A Layer-by-Layer Approach to Co-deliver DNA and siRNA Via AuNPs: A Potential Platform for Modifying Release Kinetics; BMES Oct. 2012; PS269A. Presented in Atlanta, Georgia.

CJ Bishop, SY Tzeng, JC Sunshine, JJ Green. Nano-gold/degradable polymer hybrid nanoparticles for co-delivery of DNA and siRNA. 23rd Annual Wilmer Research Meeting, April 2012, M5. Poster presentation.

CJ Bishop, JC Sunshine, JJ Green. Nano-gold/degradable polymer hybrid nanoparticles for co-delivery of DNA and siRNA. Nucleic Acid Delivery; BMES Oct. 2011, PS58A. Presented in Hartford, Connecticut.

Chapter 5: Inorganic/Polymeric Layer-by-layer Approach for Gene Delivery: Controlling Protein Expression

CJ Bishop, AL Liu, DS Lee, et al. Inorganic/polymeric layer-by-layer nanoparticles for gene delivery: controlling protein expression. In preparation for submission 2015.

Chapter 6: Cellular and Nuclear Uptake Rate Evaluation of Exogenous DNA via Flow Cytometry

CJ Bishop, RL Majewski, TR Guiriba, NS Bhise, JJ Green. Quantifying biomaterial-mediated cellular and nuclear uptake rates of exogenous DNA via flow cytometry. In preparation for submission 2015.

Chapter 7: Poly(β-amino ester) Monomer and Polymer Structure Function Relationships Elucidated Via Principal Component Analysis

CJ Bishop, B Abubaker-Sharif, TR Guiriba, JJ Green. Gene delivery polymer structure-function relationships elucidated via principal component analysis. Submitted 2015.

This work will also be presented at the Society for Biomaterials Annual Meeting in April 2015 (North Carolina).

2 Chapter 2: State of the Art

2.1 Biomolecule Delivery to Engineer the Cellular Microenvironment

Regenerative medicine has the potential to repair many cells and tissues to dramatically improve the quality of life of patients suffering from a myriad of diseases. In cases where a patient's own cells and tissues are used, rather than allogenic cells transplanted from another source, the complications of tissue rejection are prevented. The ability to regenerate tissue would also afford patients healthcare independent from a limited supply of allogenic cells or tissue. Although promising, regenerative medicine is still a nascent field requiring further refinement of bioengineered materials, cells, and biological microenvironmental cues, which are all necessary for integrative solutions to be found.

Tissue regeneration is not a new concept as it has been discussed for organisms such as the hydra, anurous batrachians and the midwife toad since at least 1744, 1769, and 1898, respectively.[1-3] Furthermore, in humans it is known that an embryo's wound healing process is faster than that of adult tissue and that it is better able to re-gain full functionality with reduced scar formation.[4] Understanding how such biological systems

Chapter 2.1 is published as "Bishop CJ, Kim J, Green, JJ. Biomolecule delivery to engineer the cellular microenvironment for regenerative medicine. *Ann. Biomed. Eng.* 2014;42(7):1557-72" and chapter 2.1.1 is published in "Sunshine JC, Bishop CJ, Green, JJ. Advances in polymeric and inorganic vectors for nonviral nucleic acid delivery. *Ther. Deliv.* 2011;2(4):493-521".

.

are capable of self-regeneration has been of great interest in the scientific community due to its translational potential.

To engineer a tissue to be a particular type and have a desired function, the microenvironment of the cells within the tissue must be controlled. Key controlling elements of cellular microenvironments or niches can be subdivided into four signaling categories which control the critical actions of cells including their cellular proliferation and death, migration, and differentiation. These signaling categories are: 1) Outside-in soluble biological factors that direct internal cell signaling; 2) Outside-in insoluble factors of the extracellular matrix (ECM) that direct cell-ECM signaling and 3) Cell-cell interactions and 4) Endogenous and exogenous genetic instructions within the cell functioning from the inside-out (Figure 1A).[5,6] In this review, we describe the current state of the art in engineering microenvironments (i.e., stem cell niches) through biomolecule delivery, highlighting biomolecule presentation to cells in soluble (i.e., autocrine/paracrine) or insoluble form, through cell-cell or cell-ECM interactions, as well as intracellular delivery of nucleic acids for regenerative medicine (Figure 1B).[7] Although mechanical cues, such as substrate elasticity and topography, are also important and an interesting avenue of research to control cellular responses, this is outside the scope of the current review; we refer interested readers to other reviews or articles on this topic such as Higuchi or Khetan, et al.[8,9]

Biomolecules delivered to cells can affect cells' interactions with each other and their microenvironment, and as a result promote the repair of defective tissues. Exogenous biomolecules can be presented to the cell microenvironment through various methods including: 1) loading in microparticles, nanoparticles, or controlled release

devices, 2) adsorbing or conjugating to a scaffold that may present the signal in a particular orientation, and 3) freely dissolving in a solution that is injectable and that may also contain other components such as injectable scaffolds. The box labeled "Exogenous Delivery: Outside-In" in Figure 1A provides a schematic diagram of three methods of exogenous delivery of biomolecules. When successfully delivered, these biomolecules can trigger intracellular signaling, promote cell-cell interactions, and control cell-ECM interactions. Such events can induce healing through mechanisms of ECM remodeling or specific differentiation of stem cells towards a tissue of interest.

2.1.1 Biomolecule Delivery and Release of Soluble Signals

Natural ECM regulates the biological activities in a tissue through soluble, bioactive effectors such as growth factors and morphogens.[10] The ECM locally binds, stores, and releases these biomolecules to meet the needs of cells for tissue repair or remodeling. Such interactions between soluble biomolecules and the ECM provide increased concentration of signaling molecules, localized morphogenetic activity, and protection against degradation.[11] There is a need to engineer the delivery of biomolecules so that the needed factor is provided to the right cells at the right time and place to properly control cell and tissue function. Approaches to engineer biomolecule delivery systems for regenerative medicine applications have focused on mimicking the biological release dynamics of the ECM by incorporating the biomolecules into scaffolds or controlled release devices.

Several strategies have been designed to incorporate growth factors within scaffolds: through diffusion into porous scaffold, direct incorporation into a hydrogel for

controlled release, or encapsulation in particulate delivery vehicles that are localized within a scaffold.[12,13] The simplest method of generating scaffolds that contain soluble biomolecules is by allowing the biomolecules to diffuse in and/or adsorb onto the scaffold. In order to create transplantable tissues, porous scaffolds seeded with cells *ex vivo* are incubated in bioreactors that contain flowing media with growth factors that spread through the scaffolds by convection and diffusion. For example, Davis, et al. showed that a mineralized, apatite-coated polymeric scaffold containing human mesenchymal stem cells (hMSCs) adsorbed bone morphogenetic protein-2 (BMP-2) from a BMP-2 solution and that the adsorbed BMP-2 induced osteogenic differentiation of hMSCs.[14] In another study, new mature cartilage tissue was formed *in vivo* from a chondrocyte-collagen composite, into which basic fibroblast growth factor (bFGF) had diffused prior to implantation.[15]

An alternative approach is to incorporate soluble signals into hydrogels. A hydrogel system is composed of hydrophilic polymer(s) in a solution that solidifies into a gel upon different cues, such as a change in temperature, pH, biomolecular interactions, or UV light.[13] Hydrogels in solutions with biomolecules can be gelled *ex vivo* and implanted or injected for subsequent cross-linking *in vivo*. For example, a UV-crosslinked chitosan hydrogel was able to release entrapped fibroblast growth factor-2 (FGF-2) upon *in vivo* biodegradation of the hydrogel and thereby accelerate the wound healing process.[16] In another example, Hea Kyung, et al. used a pH / temperature-sensitive hydrogel based on a synthetic polymer. The polymer was injected into mice as a solution mixed with recombinant human bone morphogenetic protein-2 (rhBMP-2) and

hMSCs, and then cross-linked *in situ* to form the hydrogel, which subsequently induced osteogenesis successfully.[17]

In an effort to better mimic physiologically relevant environments, growth factors have been incorporated into degradable matrices as well by means of cleavable covalent and separable non-covalent interactions.[18] Chemical conjugation or enzymatic cross-linking techniques are used to covalently bind growth factors to the backbone polymers of matrices. Lorentz *et al*. demonstrated that fibrin matrix cross-linked with α2-plasmin inhibitor-fused insulin-like growth factor-1 at bladder lesion sites *in vivo* induced significant increase in smooth muscle cell proliferation.[19] Non-covalent binding occurs via growth factors' specific interactions with ECM components. For example, bone morphogenetic protein-2 with high heparin-binding affinity added to collagen/heparin matrix significantly improved bone formation *in vivo*.[20] Also, in many situations, physiological "on-demand release" is mimicked via proteolytic degradation by proteases, a key step during tissue remodeling. Natural and synthetic hydrogels with specific protease cleavage domains can release their cross-linked growth factors upon physiological demand i*n situ*. Lutolf et al. showed that poly(ethylene-glycol) hydrogel with matrix metalloproteinase as linkers efficiently delivered human bone morphogenetic protein-2, recruited primary human fibroblasts, and remodeled bony tissue in rat crania *in situ*.[21]

An often-used delivery strategy is to utilize a particulate delivery system for controlled release. Micro- and nanoparticles are constructed from biomaterials, such as polymers, and incorporate therapeutic agents either throughout the particle or concentrated at the core. The particles can protect sensitive biological cargo from quick

degradation and clearance by the body, thereby significantly extending activity of the biomolecule.[22] The particles may be further surface-modified to render them hydrophilic and/or neutral in charge in order to evade non-specific protein adsorption, minimize immune response and clearance, and prolong circulation time. Some of the conventional methods include coating particles with polyethylene glycol, polyacrylamide, polysaccharides such as dextran, albumin, and transferrin.[23-27] Another primary advantage of using a particulate delivery system is the ability for controlled release of the encapsulated biomolecules. Particle-based release can enable constant release of a desired drug or biological factor to maintain a gradient or an effective concentration at a target site over time. Particulate delivery systems can be combined to enable programmed temporal release of multiple factors simultaneously or sequentially such as the release of BMP-2 and BMP-7 from particles to promote MSC differentiation and osteogenic activity.[28] Polymeric particle release kinetics can be controlled and modeled by the design of a material's physicochemical characteristics such as chemical bond degradation rate and diffusivity of water through the polymer as well as the length scale of the particle.[29,30]

Microparticles and nanoparticles can be either injected alone or incorporated into a scaffold. Seshadri, et al. demonstrated that the direct injection of superoxide dismutase encapsulated in polyketal microparticles in the myocardium following myocardial infarction significantly reduced myocyte apoptosis and improved cardiac function.[31] In an application related to bone tissue engineering, Park, at el. showed that rabbit bone marrow mesenchymal stem cells encapsulated in an oligo(poly(ethylene glycol) fumarate) hydrogel were able to differentiate into a chondrogenic lineage upon exposure

to transforming growth factor-β1 (TGF) released from co-encapsulated gelatin microparticles.[32] The authors of this study demonstrated that only the hydrogel containing TGF-β1 loaded microparticles induced stem cells to express chondrocyte-specific type II collagen and aggrecan in a dose-dependent manner. Particles can also be combined into hydrogels to facilitate sequential delivery of multiple growth factors, such as a system composed of alginate hydrogels and poly(lactic-co-glycolic acid) (PLGA) microparticles for sequential release of vascular endothelial growth factor (VEGF) and platelet-derived growth factor (PDGF) to promote angiogenesis.[33]

As multiple soluble factors can have synergistic function for regenerative medicine and this activity is often dependent on kinetics, the temporally controlled sequential delivery of multiple biomolecules can be critical.[34] A single delivery system may be used to achieve multiple stages of release by incorporating drugs at the core and the surface.[35] On the other hand, combining more than one system may also provide temporal control of the release of multiple biomolecules. In one study to engineer a vascularized bone tissue, Kempen, et al. formulated a composite with PLGA microparticles encapsulating BMP-2 embedded within a poly(propylene) scaffold which was in turn surrounded by a gelatin hydrogel loaded with VEGF.[36] Figure 2 shows enhanced vasculature and bone formation in the scaffold loaded with both BMP-2 and VEGF after 8 weeks of subcutaneous implantation.[36]

2.1.2 Insoluble Biomolecule Delivery Affecting Cell-Cell and Cell-Extracellular Microenvironment Interactions

Soluble factors in the previous section act by triggering cells' intracellular signaling to affect cell fate and promote tissue regeneration. However, cells in native

tissue are surrounded by neighboring cells as well as ECM that also influence the decisions that cells make through insoluble signals. Much research has focused on delivering exogenous biomolecules that support desired cell-cell and cell-ECM interactions.

Cells are in close proximity with homotypic or heterotypic cells in a living tissue. These cells need to communicate with each other through gap, adherens, and tight junctions as part of their cell-cell interactions in order to support tissue function and structure.[37] Due to the important roles that cell-cell interaction plays in tissue function, research in tissue engineering has aimed to mimic such architecture within an engineered construct.[38] A widely employed technique in this area of research is the patterned coculture of cells by utilizing a three-dimensional microfluidic system[39], a molded hydrogel[40], or thermally responsive cell sheets using poly(*N*-isopropylacrylamide) (PIPAAm).[41] Also, a layer-by-layer deposition method can be used to coculture cells together, such as fibroblasts and hepatocytes. This method involves sequential coating of different biomolecules to a substrate, utilizing ionic adsorption of charged polyelectrolytes such as hyaluronic acid (HA) and poly-L-lysine.[42] The function of hepatocytes can be modulated by the degree of heterotypic interaction with fibroblasts and by the extent of homotypic interaction between two fibroblasts. Such artificial tissue constructs have potential applications in not only the regeneration of the liver, but also other tissues with specific architecture for cell-cell interaction.

The ECM is a three-dimensional support for cells that provides biomolecular as well as mechanical cues and guides tissue formation and regeneration processes. Because of the similar viscoelastic and diffusive properties between natural ECM and hydrogels,

many types of artificial scaffolds used in tissue engineering are synthetic hydrogels.[11] Other types of hydrogels composed of more hydrophobic constituents are aimed at providing stronger mechanical architecture.[13] Scaffold designs often integrate biologically important molecules which mimic structural and functional aspects of natural, tissue-specific microenvironments. In this manner key insoluble biomolecules can be delivered and presented in a biomimetic manner. Examples include presentation of receptor-binding ligands for cell adhesion as well as proteolytic degradability for cell migration and ECM remodeling.[43,44]

Various ligands of small oligopeptide sequence promoting cell adhesion have been identified and are incorporated into tissue scaffolds.[44] One of the most commonly used motifs is the Arginine-Glycine-Aspartate (RGD) sequence that specifically recognizes and binds to integrin receptors. Many studies have tested the effectiveness of RGD peptide coated scaffolds for cell adhesion and their influence on cell behavior with respect to tissue engineering.[45] For example, Yang, et al. studied the growth and differentiation of human osteoprogenitor cells with RGD containing scaffolds.[46] Human bone marrow cells were able to adhere, grow, migrate and undergo osteogenesis on a three-dimensional PLGA scaffold modified with GRGDS peptides. In a more recent study, Wang, et al. showed that differential RGD nanospacing on a poly(ethylene glycol) (PEG) hydrogel directed preferential lineage commitment of mesenchymal stem cells (MSCs).[47] Adipogenic/osteogenic co-induction of MSCs on large RGD nanospacings resulted in a more robust differentiation into osteoblasts. These studies reinforce that defined and controlled presentation of insoluble cell-adhesion ligands on scaffolds is a critical parameter for engineering cells and tissues.

Other biomolecules are used to promote scaffold interaction with cell surface glycosaminoglycans (GAGs). Peptide sequences in this category are mostly derived from extracellular matrix proteins, such as laminin, fibronectin and vitronectin. For example, a vitronectin-derived GAG-binding peptide GKKQRFRHRNRKG was linked to a polyacrylamide hydrogel, into which human pluripotent stem cells were seeded. This hydrogel, which was unable to adhere nor self-renew stem cells prior to modification, was able to control self-renewal and maintain pluripotency in its peptide modified form.[48] Silva, et al. investigated cell-ECM interactions in inducing specific differentiation of neural progenitor cells (NPC) into neurons but not astrocytes.[49] They showed that NPCs increased expression of β–tubulin (neuronal marker) when cultured in a three-dimensional nanofiber matrix in the presence of bioactive epitope IKVAV of laminin, which is known to promote adhesion of neurons, further demonstrating how delivery and presentation of insoluble factors is key to control cell fate.

Cell migration through natural extracellular matrices is one of the key processes in tissue development, maintenance and regeneration.[11] Cells in synthetic three-dimensional scaffolds can migrate in two different ways. In the first case, cells can migrate in matrices with macroscopic pores of size larger than the cell diameter.[50] Secondly, cells can actively pave their migration path by utilizing proteases, such as matrix metalloproteinases (MMP), collagenase, serine proteases, and hyaluronidases that degrade extracellular proteins and proteoglycans.[51,52] In one example, smooth muscle cells (SMC) were able to migrate through PEG hydrogels functionalized with an RGD sequence and a polyalanine peptide sequence by secreting elastase which degraded the polyalanine peptide sequences.[53,54] The degradation, migration and formation of void

space in a scaffold can allow the natural process of tissue formation by allowing cellular synthesis and deposition of biomolecules such as collagen.

2.1.3 Intracellular Nucleic Acid Delivery for Engineering the Cellular Microenvironment

In contrast to engineering cells from the outside-in via soluble or insoluble factors, nucleic acid delivery approaches allow the engineering of the cell from the inside-out through promoting or inhibiting protein expression as a result of delivering nucleic acid. Intracellular nucleic acid delivery to the cytoplasm or nucleus is more challenging than delivery to the extracellular space, but can enable novel regeneration modalities by turning on and off exogenous and endogenous genes. **Figure 3**, taken from Sunshine, et al.,[55] depicts barriers of gene delivery which must be overcome for successful gene modulation that include: 1) Complexation or condensation of the nucleic acids, nanoparticle formation, and protection against nucleases; 2) Cellular uptake (i.e., via endocytosis); 3) Endosomal escape of the particle to the cytosol; 4) Release of the cargo from the gene carrier into the cytosol, which is the target location of short interfering RNA (siRNA); 5) Degradation of the gene carrier to minimize cytotoxicity; 6) Nuclear import for the case of DNA and short hairpin RNA (shRNA) plasmids.[55]

Nucleic acids are delivered using either viral or non-viral vectors. Viral methods can be effective, but the efficacy can diminish with repeated administration due to an adaptive immune response against the viral vector. Furthermore, viral vectors can have delivery limitations such as small cargo capacity and safety limitations such as insertional mutagenesis. Despite these complications, viral vectors are the most commonly used modality for gene transfer in clinical trials. Non-viral methods, albeit typically less

effective in comparison to viral vectors, have a higher cargo capacity, can be more easily functionalized for tissue targeting, more easily manufactured, are less immunogenic, and can be engineered to be relatively non-toxic.

However, both viral and non-viral gene delivery vectors have difficulty delivering their cargo intracellularly *in* vivo. To bypass *in vivo* nucleic acid delivery challenges, researchers often genetically manipulate autologous or allogenic cells *ex vivo* then deliver the modified cells for the specific regenerative medicine application. Caution is still warranted however as transplanting cells can be potentially associated with graft versus host disease, immunosuppression requirements, tumor formation, and unregulated protein synthesis.[56]

2.1.4 Viral Vectors for *Ex Vivo* Cell Engineering

Many researchers have utilized viruses to *ex vivo* engineer cells that are subsequently injected into animal models. In one example to aid cardiac regeneration after an ischemic heart attack, Haider, et al. supplied a source of myoblasts as well as growth factors to promote angiogenesis.[57] Haider, et al. created $VEGF_{165}$ expressing human skeletal myoblasts which were transduced by adenoviral vectors carrying human VEGF ($hVEGF_{165}$) and a *lac-z* reporter gene. $3x10^8$ transduced cells were injected at 20 different intramyocardial sites in Yorkshire swine, which were used as a model for chronic infarction. The authors found this angiomyogenesis regeneration method safe and able to result in improved perfusion, myocardial contractility and overall performance.

To promote vascularization in a rat myocardial infarct model, human embryonic stem cells (hESC) were transduced by an adenovirus to express $VEGF_{165}$ to enhance the

stem cells' differentiation down the endothelial cell line.[58] The obtained endothelial progenitor cells were then transplanted intramyocardially into the infarcted and peri-infarcted regions in the rat model; the progenitor cells were able to survive in the infarct model and aided infarcted myocardium regeneration (size and mature blood vessel density).

For osteogenic applications, Blum, et al. transfected and transduced rat marrow stromal cells to overexpress human bone morphogenetic protein 2 (hBMP-2) via Lipofectamine® Plus™ and an adenovirus or retrovirus and found that the adenovirus was the only vector capable of expressing detectable hBMP-2.[59] The authors were able to significantly increase endogenous alkaline phosphatase activity which indicates successful osteogenic differentiation. $4x10^5$ stromal cells were then seeded onto Ti-mesh scaffolds for *in vivo* osteogenic application assessment in an orthotopic, critically-sized, rat cranium. The authors found there was a small, statistically significant improvement in osteogenesis when using the adenoviral vector.[59]

To repair large nonunion bone defects, Wojtowicz, et al. retrovirally transduced bone marrow stromal cells (BMSC) to overexpress Runx2, a transcription factor regulating osteoblast differentiation.[60] These modified BMSCs were delivered in rats, which had a critical-sized femur defect, on polycaprolactone scaffolds with type I collagen mesh. The authors observed accelerated healing in the large bone defects compared to unmodified BMSCs.[60]

Cerebral vascular diseases of an occlusive nature lead to brain ischemia, causing neuropathological complications. Zhao, et al, endeavored to induce marrow stromal cells to express hepatocyte growth factor (HGF) using a herpes simplex virus type-1 vector.[61]

Marrow stromal cells themselves are capable of releasing cytokines and growth factors and are able to migrate towards damaged areas, improving functional recovery after cerebrovascular accidents. HGF has been associated with anti-apoptosis, angiogenesis, increased neurite growth, and neuroprotective properties post-ischemia and Zhao, et al. observed a significant neurological recovery when they intracerebrally transplanted transduced stromal cells into a rat occluded artery model.[61]

2.1.5 Viral Vectors for *In Vivo* Applications

While *in vivo* gene therapy is more challenging than *ex vivo* gene therapy, several studies suggest that may be a promising avenue for regenerative medicine. As there is limited osseointegration for allografts used in critical bone defects, Yazici, et al. endeavored to coat allografts in 10^{10} self-complementary adeno-associated virus (AAV) serotype 2.5 vector, delivering the BMP-2 gene.[62] The coated allograft was able to form cortical shells that were indistinguishable from those formed by live autografts; furthermore, there was reduced bone resorption, which led to increased bone volume than the autograft which rendered superior biomechanical properties.[62]

Gelse, et al. investigated complementary DNA (cDNA) delivery using adenoviral vectors encoding for bone morphogenetic protein or insulin-like growth factor 1 for an articular cartilage repair application.[63] Hyaline repair cartilage in the defect was produced in most partial thickness lesions in the rat model that was used. However, cells that failed to be transduced did not fill the defect or were associated with type I collagen.[63]

To assess spinal cord injury regeneration, Shea, et al used a rat spinal cord hemisection injury model using PLGA multichannel bridges.[64] Lentiviruses encoding for

brain derived neurotrophic factor and neurotrophin 3 transduced a number of cells including, astrocytes, macrophages, fibroblasts, and Schwann cells for at least 4 weeks, resulting in a significant induction of myelinated axons into the bridge in comparison to bridges with lentiviruses encoding for β-galactosidase.

In a final example, Bainbridge, et al. used recombinant adeno-associated viral vectors carrying a gene encoding for retinal pigment epithelium (RPE65) using the RPE65 promoter for three patients suffering from Leber's congenital amaurosis which is associated with infantile-onset rod-cone dystrophy.[65] There were no adverse events due to the subretinal vector delivery, nor changes in visual acuity, peripheral visual fields, and retinal responses to electroretinography, indicating the vision was stabilized.[65] Thus, *in vivo* viral gene therapy may be a promising approach for certain regenerative medicine applications.

2.1.6 Non-viral Vectors for *Ex Vivo* Cell Engineering

Numerous non-viral approaches for *ex vivo* gene transfer for regenerative medicine have been described. Autologous bone grafts from the iliac crest are commonly used for spinal arthrodeses for stabilizing adjacent disks and minimizing back pain. However, to avoid donor site morbidity complications Sheyn, et al. non-virally nucleofected primary porcine adipose tissue-derived stem cells to over express recombinant hBMP-6 which is capable of osteogenesis induction.[66] Post-transfection, $5x10^6$ cells were injected into the lumbar paravertebral muscle of mice. The authors found this gene transfer method to be safe and the mice exhibited temporary overexpression of BMP-6. Enough bone was formed in the lumbar region to fuse two to four vertebrae of the spine.[66]

Post-myocardial ischemia, overexpression of VEGF may result in the formation of angioma. Lei, et al. complexed a hypoxia-regulated VEGF plasmid with the cationic polymer, polyethyleneimine (PEI), to form particles and delivered them to rabbit skeletal myoblasts and then transplanted the transfected myoblasts to an acute myocardial infarcted rabbit model.[67] $1x10^7$ transfected cells were intramyocardially injected into the infarcted and peri-infarcted areas. The authors found that the ability to repair the infarcted tissue, as well as the global left ventricular function was improved.

With the purpose of increasing neovascularization for myocardial ischemia and peripheral vascular disease, human umbilical cord blood-derived progenitor cells were used in conjunction with polyethersulfone (PES) electrospun nanofibers by Das, et al.[68] The purpose of the nanofibers were to expand the stem/progenitor cells many fold without differentiation in an *ex vivo* environment; the progenitor cells were able to retain their phenotype prior to *in vivo* delivery. The progenitor cells were transfected using Nucleofector® technology to overexpress the VEGF-A_{164} and PDGF-BB growth factors. $5x10^5$ cells were delivered per immunodeficient NOD/SCID mouse, in a hind limb vascular injury animal model. The growth factor-overexpressing cells were able to promote angiogenesis more effectively compared to non-expressing progenitor cells.[68]

2.1.7 Non-viral Vectors for *In Vivo* Applications

Large bone implant osseointegration presents healing challenges even while using autologous bone grafts. Park, et al. investigated whether liposomal vectors delivering BMP-2 cDNA mixed with crushed bone and delivered onto the implant surface as well as the peri-implant defect could transfect trabecular-lined cells and induce bone—graft osseointegration in pig calvariae.[69] The authors found that the liposomal vector was able

to induce abundant BMP-2 protein production throughout the defect, enhance bone formation and caused the particulate bone to become trabecular, in contrast to the control groups.[69]

As there are still no optimal solutions for nonunion bone defects, Kimelman-Bleich, et al. endeavored to recruit host progenitor cells to nonunion radius bone defect sites in mice using a collagen sponge.[70] A plasmid encoding BMP-9 was injected into the radial defects and electroporation was accomplished 10 days after the defect was created. The authors found that the gene expression was localized to the site of the defect and that bone formation bridged the nonunion gap; whereas the gaps remained in the control groups.[70]

Trentin, et al. demonstrated that they were able to achieve upregulation of VEGF-A_{165} in full-thickness dermal wounds in a mouse model with vessel maturity by delivering a mutated hypoxia-inducible factor (HIF)-1α gene lacking the oxygen sensor so that the gene was constitutively on.[71] The gene was delivered using an intracellularly reducible disulfide-containing, cysteine-flanked lysine peptide in a fibrin matrix.[71]

Shea, et al. investigated the efficacy of delivering of FGF-2-encoding plasmids using a porous PLGA scaffold formed via a gas foaming method in the intraperitoneal fat of C57BL/6 male mice.[72] They found the expression peaked after the first couple of days and subsided over the following week or two and that the vascular volume fraction increased 40% in comparison to the controls at week two.

Park, et al. demonstrated the ability to significantly increase vascular endothelial growth factor and stromal cell-derived factor-1α chemokine in mice with full-thickness dermal wounds by intradermally delivering the sonic hedgehog gene using poly(β-amino

ester) polymers.[73] By varying the type of small molecule endcap, they were able to optimize toxicity and achieve higher transfection of the morphogen than commercially available reagents such as Lipofectamine® 2000 *in vitro*.[73] Thus, emerging non-viral approaches are able to achieve efficacy *in vivo* for regenerative medicine challenges, while also reducing potential safety concerns as compared to viruses.

2.1.8 Combination Biomolecule and Cell Therapy Application

There have been several biomolecule and cell-based combination therapies used for regenerative medicine. One of particular interest involves the treatment of Duchenne muscular dystrophy (DMD). Filareto, et al. investigated an autologous cell-based combination therapy in a DMD mouse model which involved the following procedures: the extraction of fibroblasts and their induction of pluripotency; gene delivery to correct for the missing micro-utrophin gene in the fibroblasts; the promotion of myogenic progenitor cells using Pax3; and the eventual re-implantation of the corrected myogenic progenitor cells into a DMD mouse model.[74]

More specifically, Filareto, et al. retrovirally transduced dystrophin/utrophin-double knockout (dKO) tail-tip fibroblast cells with Oct4, Sox2, and Klf4 to obtain the dystrophic induced pluripotent stem cells (iPSC), which were then expanded **(Figure 4)**.[74] The dystrophic iPSCs were corrected by delivering the micro-utrophin gene via the Sleeping Beauty transposon system to allow for precise excision and relocation of a DNA segment. Pax3 was then used to promote skeletal muscle stem/progenitors cells. Flk-1 and PDGFα receptor expression were shown to establish pluripotency using differentiated embryoid bodies. The micro-utrophin-corrected myogenic precursors were

then autologously re-implanted back into the same dKO mice. The muscles of such mice had improved contractility and muscle regeneration *in vivo*.[74]

2.1.9 Current Limitations

The development of thick complex tissues requires multiple cell types and involves microenvironments that may overlap, greatly increasing complexity. Although many of the techniques discussed in this article can be used for temporal and spatial control of delivery in a broad sense, they generally do not control *in vivo* delivery with the cellular and subcellular spatial resolution and second-scale temporal resolution that may be in many ways ideal. Coupled with this engineering limitation is the basic science limitation of not having precise knowledge about these precise spatial and temporal requirements. Despite the use of various computer-controlled 3D cell printing techniques, spatiotemporally controlling multiple microenvironments within close regions remains a challenge. Newer techniques involving computational topology design and solid free-form fabrication help alleviate some disadvantages, yet the remaining challenges include but are not limited to vascularization, host integration, resolution and porosity, and the seeding and co-culturing of multiple cell types.[75,76] Furthermore, the mechanisms by which complex tissues are orchestrated to develop and heal are largely unknown.[77] Therefore, there are opportunities in the field for the invention of higher resolution *in vivo* biosensing technologies, extracellular and intracellular drug delivery technologies with increased spatial and temporal control, and cell delivery and scaffold technologies with increased spatial control and organization of diverse cell types.

2.1.10 Clinical Trials

As of June 2010, according to the Journal of Gene Medicine website[1], there have been a total of 1,644 gene therapy clinical trials approved worldwide. The leading diseases being treated in the gene therapy clinical trials are cancer (64.5%), cardiovascular diseases (8.7%), and monogenic diseases (8.2%). The majority (60.5%) of the clinical trials are in phase I. The most common gene types used have been antigens (19.8%), cytokines (18.4%), tumor suppressors (10.5%), and growth factors (7.7%). **Table 1** is a summary of non-viral gene therapy clinical trials detailing the type, the current or last clinical phase, the nucleic acid being delivered, and the disease target. This data highlights that the majority of clinical trial thus far have been with viral vectors (~75%), and the leading non-viral approaches in clinical trials are "naked" free DNA (18%) followed by Lipofection (7%). Polymeric and inorganic vectors for gene delivery, although promising for the future, are for the most part still in preclinical stages of development. However, one recent approach in polymeric gene delivery to reach clinical trials is Mark Davis and Calando Pharmaceuticals work with cyclodextrin-based polymers [78,79]. In this work it has been demonstrated that biocompatible polymeric nanoparticles can reach solid tumors following systemic administration in humans and within these tumors the particles can cause siRNA-specific knockdown of a target gene.

2.1.11 Conclusions

A key element important to consider for bioengineered delivery is that the needed factor be provided to the right cells at the right time and place to properly control cell and tissue function. Engineering a cell from the outside-in via delivery of soluble and insoluble factors to the outside of the cell was compared to engineering a cell from the

inside-out via gene transfer using both viral and non-viral methods. Combinations of delivery of biomolecules, scaffolds, and cells were demonstrated as approaches that are promising for *in vivo* regenerative medicine therapeutics.

2.1.12 Figures

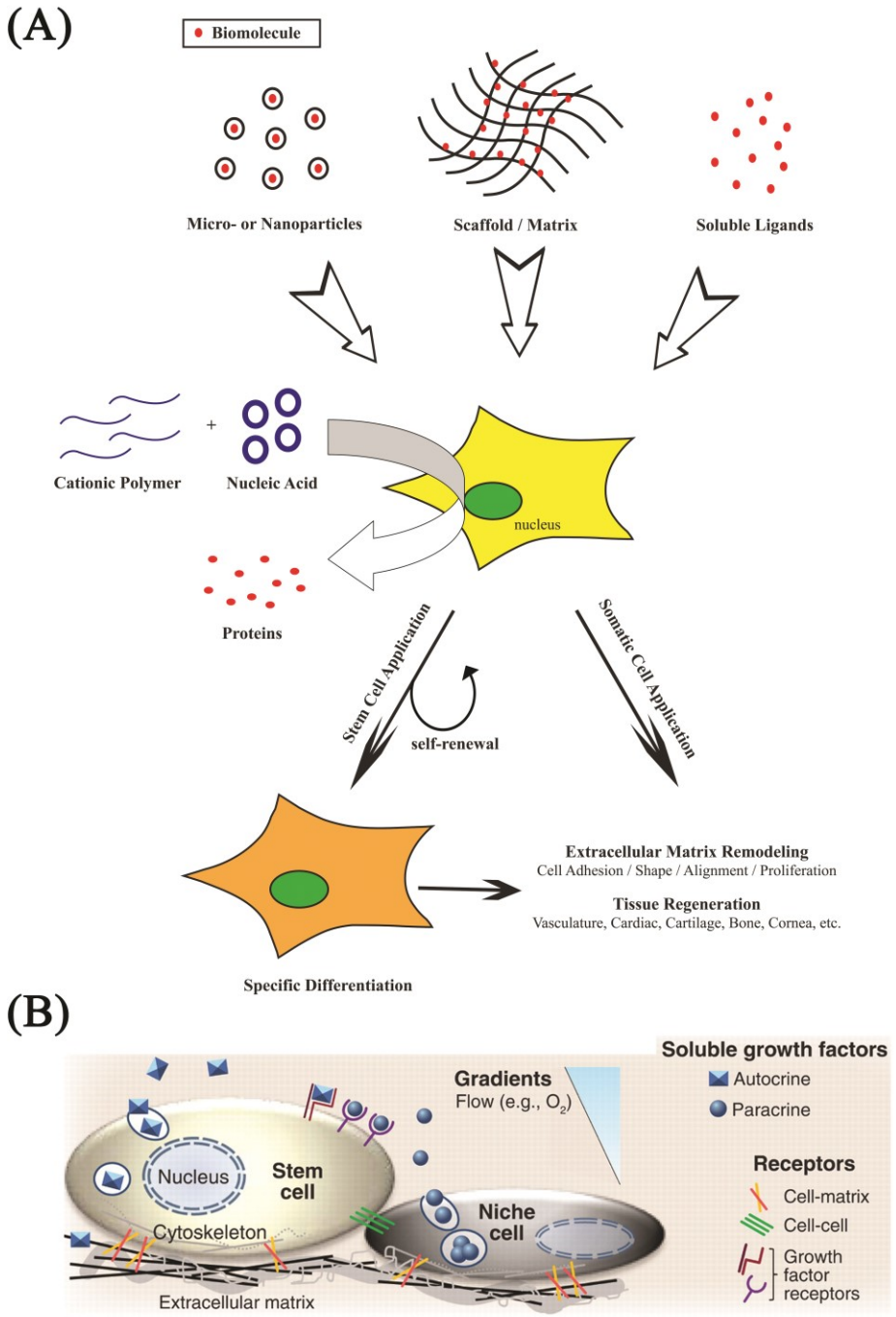

Figure 1 (A) Key controlling signals regulating cellular responses (B) A depiction of niche factors which control microenvironments: soluble growth factors which could be either autocrine or paracrine acting, cellular receptors involved in binding other cells or the ECM, as well as growth factor receptors; from Discher, et al. Growth factors, matrices, and forces combine and control stem cells. *Science* 324:1673-1677, 2009.[7] Reprinted with permission from AAAS.

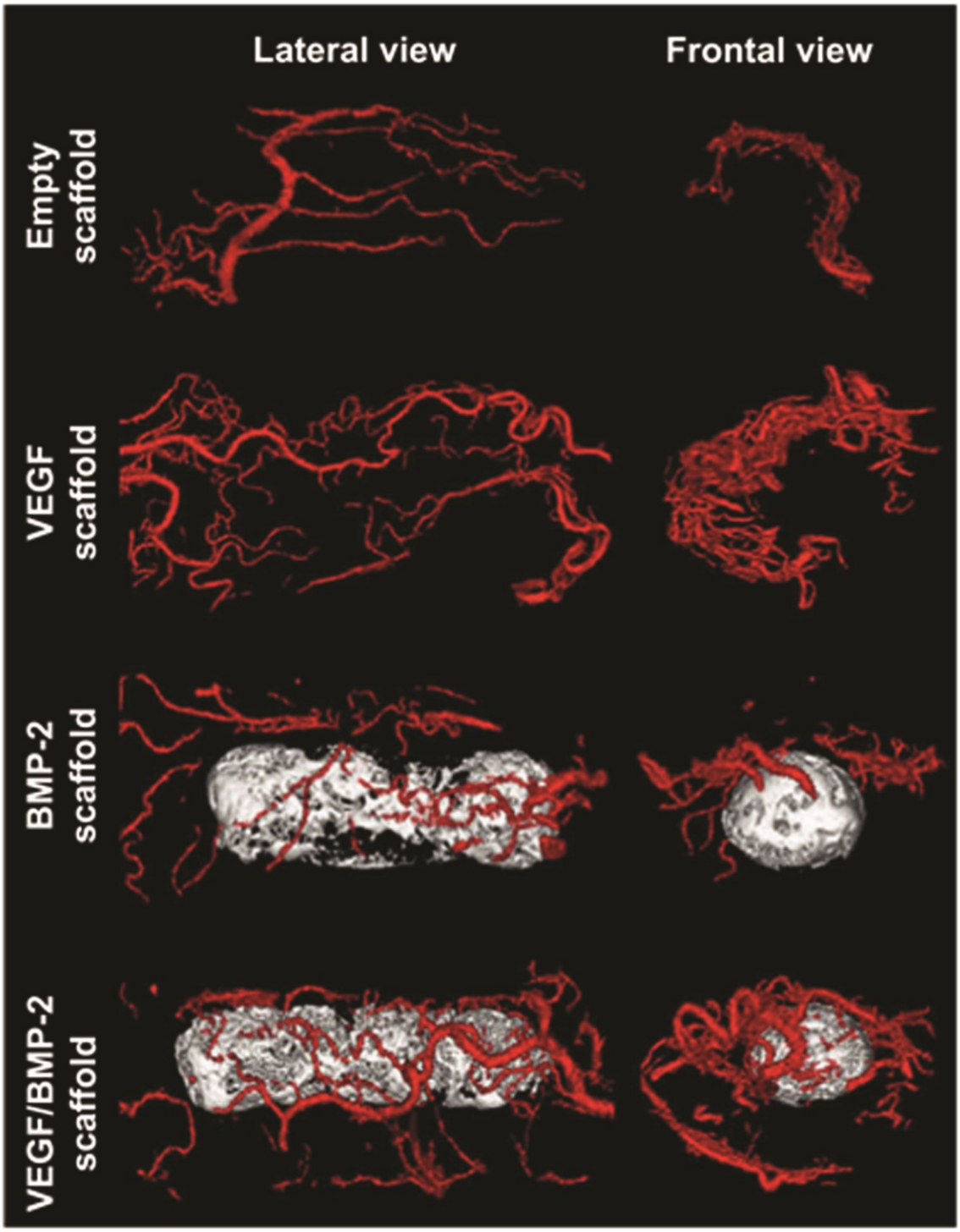

Figure 2. A depiction of enhanced vasculature and bone formation in the scaffold loaded with both BMP-2 and VEGF after 8 weeks of subcutaneous implantation. Reprinted from Biomaterials, Vol. 30, Kempen, et al., Effect of local sequential VEGF and BMP-2 delivery on ectopic and orthotopic bone regeneration, pages 2816-2825, Copyright (2009), with permission from Elsevier.[36]

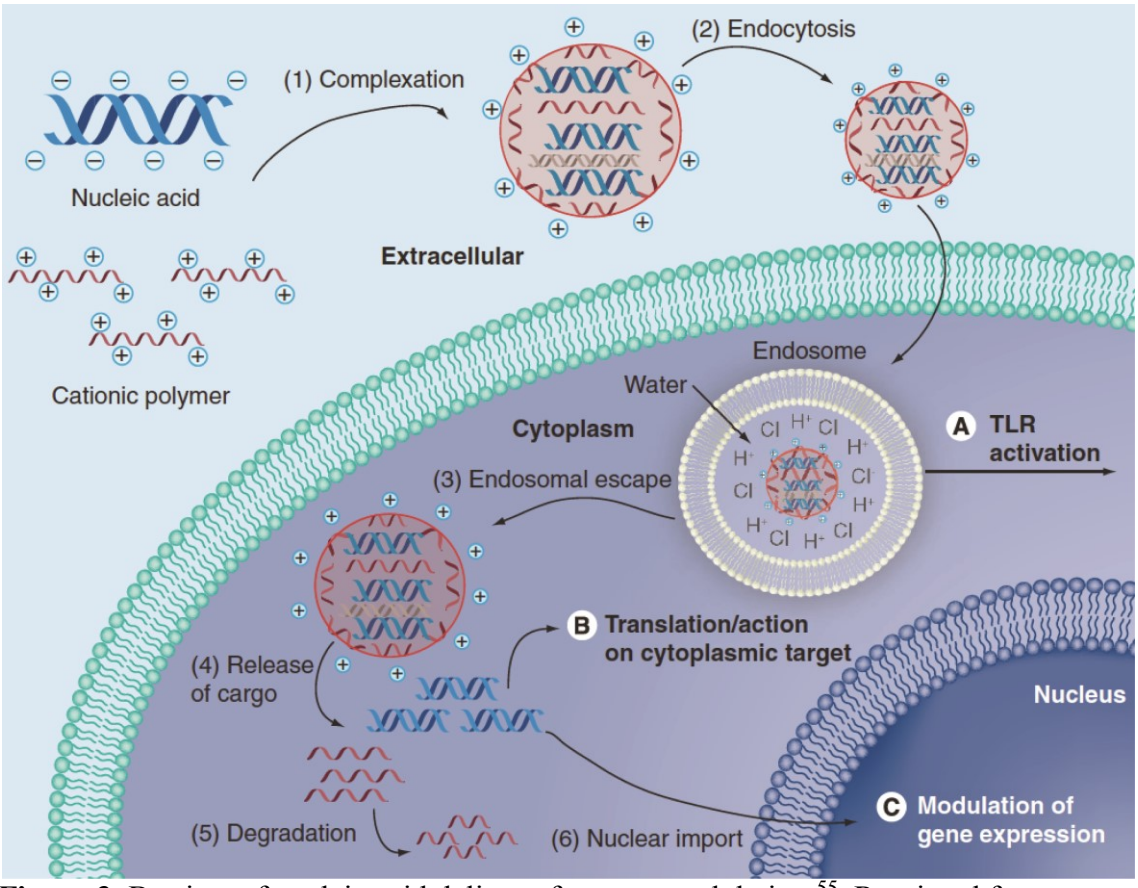

Figure 3. Barriers of nucleic acid delivery for gene modulation.[55] Reprinted from Therapeutic Delivery, Vol. 2, Sunshine, et al., Advances in polymeric and inorganic vectors for nonviral nucleic acid delivery, pages 493-521, Copyright (2011), with permission from Future Science Ltd.

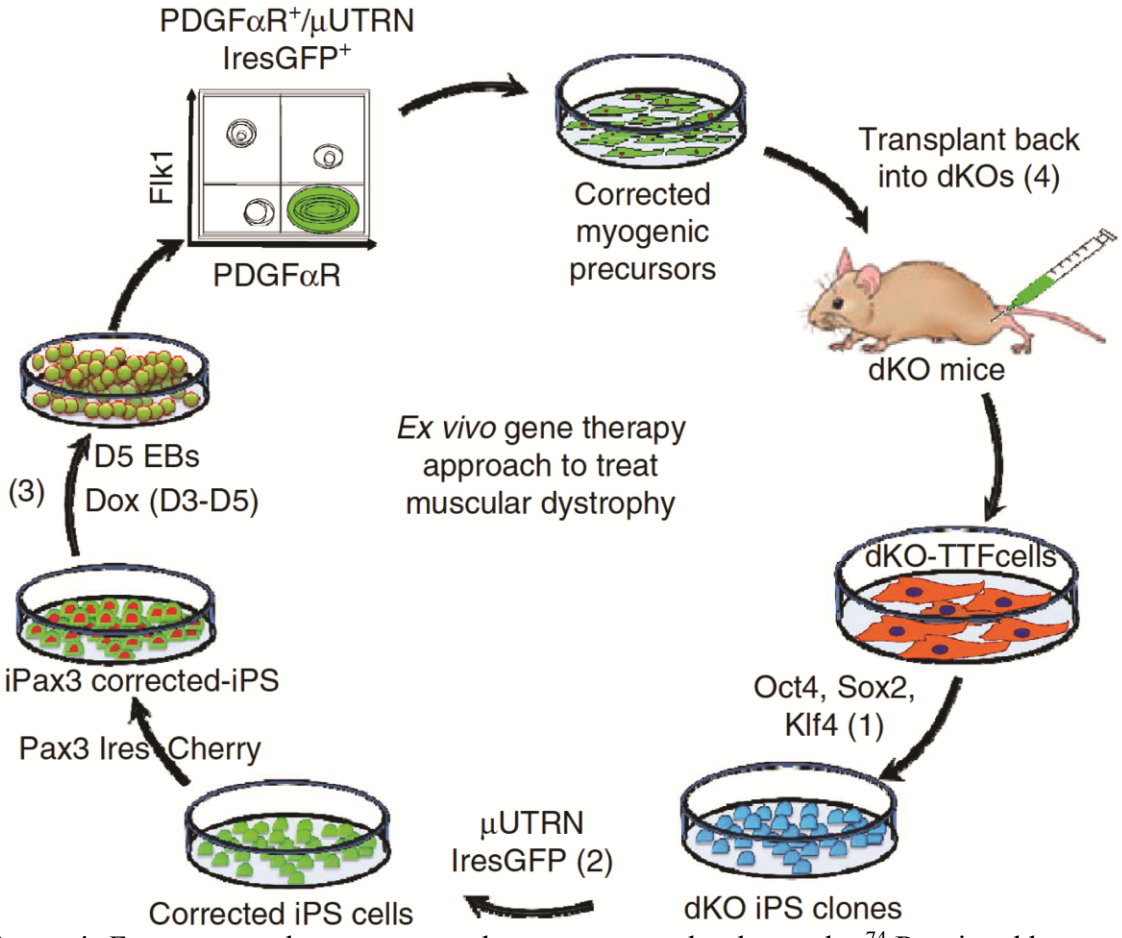

Figure 4. *Ex vivo* gene therapy approach to treat muscular dystrophy.[74] Reprinted by permission from Macmillan Publishers Ltd: Nature Communications, Copyright (2013).[74]

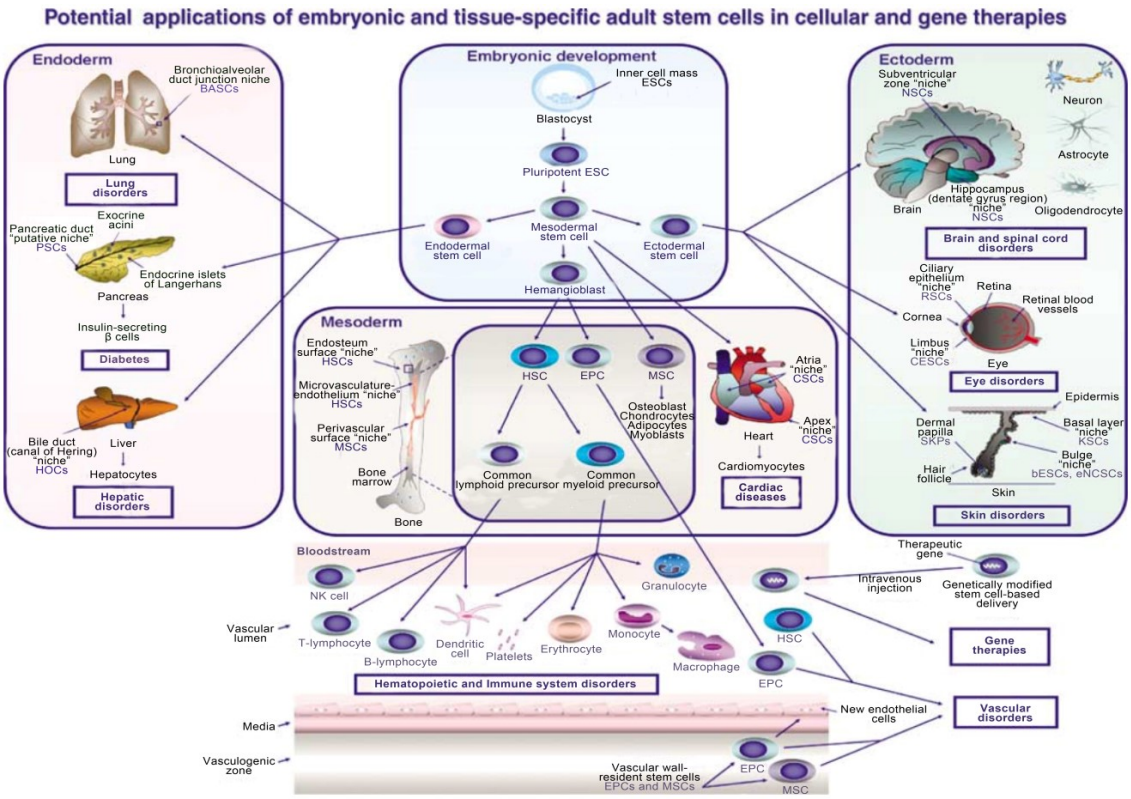

Figure 5. A depiction of applicable avenues of gene and cell therapies using stem cells.[80] Reproduced by permission from Macmillan Publishers Ltd: Clinical Pharmacology and Therapeutics, Copyright (2007).[80]

2.1.13 Tables

Table 1. Summary of clinical trials (some of which are ongoing)
*Acronyms: AMD = Age-related macular degeneration; CNV = choroidal neovascularization; DC-Chol = 3B[N-(iV',W-dimethylaminoet hane)-carbamoyllcholesterol; FGF = fibroblast growth factor; GMC-SF = Granulocyte-macrophage colony stimulating factor; heNOS = human endothelial nitric oxide synthase; HGF = hepatocyte growth factor; IL = interleukin; PAOD = peripheral artery occlusive disease; RSV = Respiratory syncytial virus;

Type	Clinical Phase	Nucleic Acid	Disease Target
Naked Plasmid/DNA (intramyocardial)[81]	II/III	VEGF	Angina
Naked Plasmid/DNA (lung injection)[82]	II	heNOS*	Hypertension
Naked Plasmid/DNA (intramuscular)[83]	II	FGF*	PAOD*
Gene Gun (intravenous)[84]	I/II	IL*-7,12; GM-CSF*	Malignant Melanoma
Gene Gun (intradermal)[85]	I	GM-CSF*	Malignant Melanoma, Sarcoma
Lipofection (intratumoral)[86]	II	HLA-B7/β 2-μglobulin	Malignant melanoma
Lipofection (intratumoral)[87]	II	IL*-2	Renal cell cancer
Lipofection (intraperitoneal)[88]	II	E1A	Ovarian Cancer
Lipofection (intravenous)[89]	I	P53	Solid tumors
Lipofection (intradermal)[90]	II	B7.1 (CD80), HLA-A1/2	Non-small cell lung cancer
siRNA (intravenous)[91,92]	I	I5NP	Acute Renal Failure
Naked DNA (corpus cavernosum injection) [93]	I	hSlo DNA	Erectile Dysfunction
siRNA (intravitreal) [94]	III	Bevasiranib (anti-VEGF)	AMD*
siRNA (inhalation)[95]	IIa/b	Anti-RSV nucleocapsid gene	RSV*

siRNA (systemic, Lipid-ionic complexation)[96]	I	Plasmid DNA => 4 RNAi, inhibiting all viral genotypes	Hepatitis B-virus
siRNA (topical)[97]	II	Bevasiranib/Cand5 Anti-VEGF	Diabetic molecular oedema
siRNA (injected into callus on foot)[98]	I	TD101	Pachyonychia Congenita
siRNA (intravitreal)[99]	II	AGN211745	AMD*/CNV*
cDNA encoding two growth factor isoforms (intramuscular)[100]	II	VM202 (HGF*-723/728)	Critical limb ischemia
Anti-sense DNA (intratumoral), DC-Chol* liposomes[101]	I	EGFR	Head/neck cancer
Anti-sense DNA (intratumoral injection)[102]	I/II	EGFR	Head/Neck Squamous Cell carcinoma

2.1.14 References

(1) Ridewood, W. G. *P. Zool. Soc. Lond.* **1898**, *66*, 101-106.
(2) Spallanzani *Leipzig* **1769**.
(3) Trembley, A. *Leiden: Verbeek* **1744**.
(4) Martin, P.; Lewis, J. *Nature* **1992**, *360*, 179-183.
(5) Fisher, O. Z.; Khademhosseini, A.; Langer, R.; Peppas, N. A. *Accounts Chem. Res.* **2010**, *43*, 419-428.
(6) Cha, C.; Liechty, W. B.; Khademhosseini, A.; Peppas, N. A. *ACS Nano* **2012**, *6*, 9353-9358.
(7) Discher, D. E.; Mooney, D. J.; Zandstra, P. W. *Science* **2009**, *324*, 1673-7.
(8) Higuchi, A.; Ling, Q. D.; Chang, Y.; Hsu, S. T.; Umezawa, A. *Chem. Rev.* **2013**.
(9) Khetan, S.; Guvendiren, M.; Legant, W. R.; Cohen, D. M.; Chen, C. S.; Burdick, J. A. *Nat. Mater.* **2013**, *12*, 458-465.
(10) Ramirez, F.; Rifkin, D. B. *Matrix Biol.* **2003**, *22*, 101-107.
(11) Lutolf, M. P.; Hubbell, J. A. *Nat. Biotechnol.* **2005**, *23*, 47-55.
(12) Babensee, J. E.; McIntire, L. V.; Mikos, A. G. *Pharm. Res.* **2000**, *17*, 497-504.
(13) Drury, J. L.; Mooney, D. J. *Biomaterials* **2003**, *24*, 4337-4351.
(14) Davis, H. E.; Case, E. M.; Miller, S. L.; Genetos, D. C.; Leach, J. K. *Biotechnol. Bioeng.* **2011**, *108*, 2727-2735.
(15) Fujisato, T.; Sajiki, T.; Liu, Q.; Ikada, Y. *Biomaterials* **1996**, *17*, 155-162.
(16) Obara, K.; Ishihara, M.; Ishizuka, T.; Fujita, M.; Ozeki, Y.; Maehara, T.; Saito, Y.; Yura, H.; Matsui, T.; Hattori, H.; Kikuchi, M.; Kurita, A. *Biomaterials* **2003**, *24*, 3437-3444.
(17) Kim, H. K.; Shim, W. S.; Kim, S. E.; Lee, K. H.; Kang, E.; Kim, J. H.; Kim, K.; Kwon, I. C.; Lee, D. S. *Tissue Eng. Part A* **2009**, *15*, 923-933.
(18) Rice, J. J.; Martino, M. M.; De Laporte, L.; Tortelli, F.; Briquez, P. S.; Hubbell, J. A. *Adv. Healthcare Mater.* **2013**, *2*, 57-71.
(19) Lorentz, K. M.; Yang, L. R.; Frey, P.; Hubbell, J. A. *Biomaterials* **2012**, *33*, 494-503.
(20) Johnson, M. R.; Boerckel, J. D.; Dupont, K. M.; Guldberg, R. E. *Clin. Orthop.* **2011**, *469*, 3111-3117.
(21) Lutolf, M. R.; Weber, F. E.; Schmoekel, H. G.; Schense, J. C.; Kohler, T.; Muller, R.; Hubbell, J. A. *Nat. Biotechnol.* **2003**, *21*, 513-518.
(22) Mundargi, R. C.; Babu, V. R.; Rangaswamy, V.; Patel, P.; Aminabhavi, T. M. *J. Control. Release* **2008**, *125*, 193-209.
(23) Owens, D. E.; Peppas, N. A. *Int. J. Pharm.* **2006**, *307*, 93-102.
(24) Torchilin, V. P.; Trubetskoy, V. S. *Advanced Drug Delivery Reviews* **1995**, *16*, 141-155.
(25) Lemarchand, C.; Gref, R.; Couvreur, P. *Eur. J. Pharm. Biopharm.* **2004**, *58*, 327-341.
(26) Simoes, S.; Slepushkin, V.; Pires, P.; Gaspar, R.; de Lima, M. C. P.; Duzgunes, N. *Biochimica Et Biophysica Acta-Biomembranes* **2000**, *1463*, 459-469.

(27) Kircheis, R.; Wightman, L.; Schreiber, A.; Robitza, B.; Rossler, V.; Kursa, M.; Wagner, E. *Gene Ther.* **2001**, *8*, 28-40.
(28) Yilgor, P.; Sousa, R. A.; Reis, R. L.; Hasirci, N.; Hasirci, V. *J. Mater. Sci. Mater. Med.* **2010**, *21*, 2999-3008.
(29) von Burkersroda, F.; Schedl, L.; Gopferich, A. *Biomaterials* **2002**, *23*, 4221-31.
(30) Rothstein, S. N.; Federspiel, W. J.; Little, S. R. *Biomaterials* **2009**, *30*, 1657-64.
(31) Seshadri, G.; Sy, J. C.; Brown, M.; Dikalov, S.; Yang, S. C.; Murthy, N.; Davis, M. E. *Biomaterials* **2010**, *31*, 1372-9.
(32) Park, H.; Temenoff, J. S.; Tabata, Y.; Caplan, A. I.; Mikos, A. G. *Biomaterials* **2007**, *28*, 3217-3227.
(33) Sun, Q. H.; Silva, E. A.; Wang, A. X.; Fritton, J. C.; Mooney, D. J.; Schaffler, M. B.; Grossman, P. M.; Rajagopalan, S. *Pharm. Res.* **2010**, *27*, 264-271.
(34) Richardson, T. P.; Peters, M. C.; Ennett, A. B.; Mooney, D. J. *Nat. Biotechnol.* **2001**, *19*, 1029-1034.
(35) Serda, R. E.; Godin, B.; Blanco, E.; Chiappini, C.; Ferrari, M. *BBA-Gen. Subjects* **2011**, *1810*, 317-329.
(36) Kempen, D. H.; Lu, L.; Heijink, A.; Hefferan, T. E.; Creemers, L. B.; Maran, A.; Yaszemski, M. J.; Dhert, W. J. *Biomaterials* **2009**, *30*, 2816-25.
(37) Cowan, D. B.; Lye, S. J.; Langille, B. L. *Circ. Res.* **1998**, *82*, 786-793.
(38) Khademhosseini, A.; Langer, R.; Borenstein, J.; Vacanti, J. P. *Proc. Natl. Acad. Sci. U. S. A.* **2006**, *103*, 2480-2487.
(39) Chiu, D. T.; Jeon, N. L.; Huang, S.; Kane, R. S.; Wargo, C. J.; Choi, I. S.; Ingber, D. E.; Whitesides, G. M. *Proc. Natl. Acad. Sci. U. S. A.* **2000**, *97*, 2408-2413.
(40) Tang, M. D.; Golden, A. P.; Tien, J. *J. Am. Chem. Soc.* **2003**, *125*, 12988-12989.
(41) Yamato, M.; Konno, C.; Utsumi, M.; Kikuchi, A.; Okano, T. *Biomaterials* **2002**, *23*, 561-7.
(42) Bhatia, S. N.; Balis, U. J.; Yarmush, M. L.; Toner, M. *Biotechnol. Prog.* **1998**, *14*, 378-387.
(43) Hoffman, A. S. *Adv. Drug Deliv. Rev.* **2002**, *54*, 3-12.
(44) Shin, H.; Jo, S.; Mikos, A. G. *Biomaterials* **2003**, *24*, 4353-4364.
(45) Hersel, U.; Dahmen, C.; Kessler, H. *Biomaterials* **2003**, *24*, 4385-415.
(46) Yang, X. B.; Roach, H. I.; Clarke, N. M. P.; Howdle, S. M.; Quirk, R.; Shakesheff, K. M.; Oreffo, R. O. C. *Bone* **2001**, *29*, 523-531.
(47) Wang, X.; Yan, C.; Ye, K.; He, Y.; Li, Z. H.; Ding, J. D. *Biomaterials* **2013**, *34*, 2865-2874.
(48) Musah, S.; Morin, S. A.; Wrighton, P. J.; Zwick, D. B.; Jin, S.; Kiessling, L. L. *ACS Nano* **2012**, *6*, 10168-10177.
(49) Silva, G. A.; Czeisler, C.; Niece, K. L.; Beniash, E.; Harrington, D. A.; Kessler, J. A.; Stupp, S. I. *Science* **2004**, *303*, 1352-5.
(50) Behravesh, E.; Mikos, A. G. *J. Biomed. Mater. Res. Part A* **2003**, *66A*, 698-706.
(51) Liu, D. C.; Pearlman, E.; Diaconu, E.; Guo, K.; Mori, H.; Haqqi, T.; Markowitz, S.; Willson, J.; Sy, M. S. *Proc. Natl. Acad. Sci. U. S. A.* **1996**, *93*, 7832-7837.
(52) Friedl, P. *Curr. Opin. Cell Biol.* **2004**, *16*, 14-23.
(53) Gertler, A.; Hofmann, T. *Can. J. Biochem.* **1970**, *48*, 384-&.
(54) Mann, B. K.; Gobin, A. S.; Tsai, A. T.; Schmedlen, R. H.; West, J. L. *Biomaterials* **2001**, *22*, 3045-3051.

(55) Sunshine, J. C.; Bishop, C. J.; Green, J. J. *Ther. Deliv.* **2011**, *2*, 493-521.
(56) Naldini, L. *Nat. Rev. Genet.* **2011**, *12*, 301-315.
(57) Haider, H. K.; Ye, L.; Jiang, S. J.; Ge, R. W.; Law, P. K.; Chua, T.; Wong, P.; Sim, E. K. W. *J. Mol. Med.-JMM* **2004**, *82*, 539-549.
(58) Rufaihah, A. J.; Haider, H. K.; Heng, B. C.; Ye, L.; Tan, R. S.; Toh, W. S.; Tian, X. F.; Sim, E. K. W.; Cao, T. *Regen. Med.* **2010**, *5*, 231-244.
(59) Blum, J. S.; Barry, M. A.; Mikos, A. G.; Jansen, J. A. *Human Gene Therapy* **2003**, *14*, 1689-1701.
(60) Wojtowicz, A. M.; Templeman, K. L.; Hutmacher, D. W.; Guldberg, R. E.; Garcia, A. J. *Tissue Eng. Part A* **2010**, *16*, 2795-2808.
(61) Zhao, M. Z.; Nonoguchi, N.; Ikeda, N.; Watanabe, T.; Furutama, D.; Miyazawa, D.; Funakoshi, H.; Kajimoto, Y.; Nakamura, T.; Dezawa, M.; Shibata, M. A.; Otsuki, Y.; Coffin, R. S.; Liu, W. D.; Kuroiwa, T.; Miyatake, S. I. *J. Cereb. Blood Flow Metab.* **2006**, *26*, 1176-1188.
(62) Yazici, C.; Takahata, M.; Reynolds, D. G.; Xie, C.; Samulski, R. J.; Samulski, J.; Beecham, E. J.; Gertzman, A. A.; Spilker, M.; Zhang, X. P.; O'Keefe, R. J.; Awad, H. A.; Schwarz, E. M. *Mol. Ther.* **2011**, *19*, 1416-1425.
(63) Gelse, K.; von der Mark, K.; Aigner, T.; Park, J.; Schneider, H. *Arthritis Rheum.* **2003**, *48*, 430-441.
(64) Tuinstra, H. M.; Aviles, M. O.; Shin, S.; Holland, S. J.; Zelivyanskaya, M. L.; Fast, A. G.; Ko, S. Y.; Margul, D. J.; Bartels, A. K.; Boehler, R. M.; Cummings, B. J.; Anderson, A. J.; Shea, L. D. *Biomaterials* **2012**, *33*, 1618-1626.
(65) Bainbridge, J. W.; Smith, A. J.; Barker, S. S.; Robbie, S.; Henderson, R.; Balaggan, K.; Viswanathan, A.; Holder, G. E.; Stockman, A.; Tyler, N.; Petersen-Jones, S.; Bhattacharya, S. S.; Thrasher, A. J.; Fitzke, F. W.; Carter, B. J.; Rubin, G. S.; Moore, A. T.; Ali, R. R. *N Engl J Med* **2008**, *358*, 2231-9.
(66) Sheyn, D.; Pelled, G.; Zilberman, Y.; Talasazan, F.; Frank, J. M.; Gazit, D.; Gazit, Z. *Stem Cells* **2008**, *26*, 1056-1064.
(67) Ye, L.; Zhang, W.; Su, L. P.; Haider, H. K.; Poh, K. K.; Galupo, M. J.; Songco, G.; Ge, R. W.; Tan, H. C.; Sim, E. K. W. *Biomaterials* **2011**, *32*, 2424-2431.
(68) Das, H.; Abdulhameed, N.; Joseph, M.; Sakthivel, R.; Mao, H. Q.; Pompili, V. J. *Cell Transplant.* **2009**, *18*, 305-318.
(69) Park, J.; Lutz, R.; Felszeghy, E.; Wiltfang, J.; Nkenke, E.; Neukam, F. W.; Schlegel, K. A. *Biomaterials* **2007**, *28*, 2772-2782.
(70) Kimelman-Bleich, N.; Pelled, G.; Zilberman, Y.; Kallai, I.; Mizrahi, O.; Tawackoli, W.; Gazit, Z.; Gazit, D. *Mol. Ther.* **2011**, *19*, 53-59.
(71) Trentin, D.; Hall, H.; Wechsler, S.; Hubbell, J. A. *Proc. Natl. Acad. Sci. U. S. A.* **2006**, *103*, 2506-11.
(72) Rives, C. B.; des Rieux, A.; Zelivyanskaya, M.; Stock, S. R.; Lowe, W. L.; Shea, L. D. *Biomaterials* **2009**, *30*, 394-401.
(73) Park, H. J.; Lee, J.; Kim, M. J.; Kang, T. J.; Jeong, Y.; Um, S. H.; Cho, S. W. *Biomaterials* **2012**, *33*, 9148-9156.
(74) Filareto, A.; Parker, S.; Darabi, R.; Borges, L.; Iacovino, M.; Schaaf, T.; Mayerhofer, T.; Chamberlain, J. S.; Ervasti, J. M.; McIvor, R. S.; Kyba, M.; Perlingeiro, R. C. *Nat. Commun.* **2013**, *4*, 1549.
(75) Hollister, S. J. *Nat. Mater.* **2005**, *4*, 518-524.

(76) Seol, Y. J.; Kang, T. Y.; Cho, D. W. *Soft Matter* **2012**, *8*, 1730-1735.
(77) Place, E. S.; Evans, N. D.; Stevens, M. M. *Nat. Mater.* **2009**, *8*, 457-470.
(78) Davis, M. E. *Mol. Pharm.* **2009**, *6*, 659-68.
(79) Davis, M. E.; Zuckerman, J. E.; Choi, C. H.; Seligson, D.; Tolcher, A.; Alabi, C. A.; Yen, Y.; Heidel, J. D.; Ribas, A. *Nature*, *464*, 1067-70.
(80) Mimeault, M.; Hauke, R.; Batra, S. K. *Clin. Pharmacol. Ther.* **2007**, *82*, 252-264.
(81) Steward DJ. Multicentre, Randomized,Double Blind,Placebo Controlled Trial of Myocardial Angiogenesis Using VEGF165, Intramyocardial Gene Delivery in Patients With Severe Angina. Gene Therapy Clinical Trials Worldwide (2002). www.abedia.com/wiley/record_detail. php?ID=68
(82) Ward M. The PHACeT Trial: pulmonary hypertension: assessment of cell therapy (Phase II). Gene Therapy Clinical Trials Worldwide (2006). www.abedia.com/wiley/record_detail. php?ID=70
(83) Baumgartner. Gene therapy in patients with severe peripheral artery occlusive disease (PAOD). Gene Therapy Clinical Trials Worldwide (2001), www.abedia.com/wiley/record_detail. php?ID=104
(84) Schadendorf D. Gene therapy in patients with melanoma. Gene Therapy Clinical Trials Worldwide. www.abedia.com/wiley/record_detail. php?ID=149
(85) Figlin R. Phase II study of direct gene transfer of IL-2 plasmid DNA/DMRIE/DOPE lipid complex (Leuvectin) as an immunotherapeutic regimen in patients with metastatic renal cell carcinoma. Gene Therapy Clinical Trials Worldwide (1998). www.abedia.com/wiley/record_detail. php?ID=856
(86) Mahvi D: Phase I/IB study of immunization with autologous tumor cells transfected with the GM–CSF gene by particle-mediated transfer in patients with melanoma or sarcoma. Gene Therapy Clinical Trials Worldwide (1996). www.abedia.com/wiley/record_detail. php?ID=755
(87) Dreicer R. Phase II study of direct gene transfer of HLA-B7 plasmid DNA/DMRIE/ DOPE lipid complex (Allovectin-7) as an immunotherapeutic agent in patients with stage III or IV melanoma with no treatment alternatives. Gene Therapy Clinical Trials Worldwide (1998). www.abedia.com/wiley/record_detail. php?ID=830
(88) Ueno N. A Phase II Study of intraperitoneal E1A-lipid complex for patients without advanced epithelial ovarian cancer without HER-2/neu overexpression. Sponsor: Targeted Genetics Corporation. Gene Therapy Clinical Trials Worldwide (2000). www.abedia.com/wiley/record_detail. php?ID=1012
(89) Marshall J. An open-label safety study of escalating doses of sgt-53 for systemic injection in patients with advanced solid tumor malignancies. Gene Therapy Clinical Trials Worldwide (2003). www.abedia.com/wiley/record_detail. php?ID=1188
(90) Raez L. A Phase II clinical trial of adjuvant immunotherapy with an allogeneic B7.1/HLAA transfected tumor cell vaccine in patients with stage I-II non-small cell lung cancer. Gene Therapy Clinical Trials Worldwide (2004). www.abedia.com/
(91) Whitehead, K. A.; Langer, R.; Anderson, D. G. *Nature Reviews Drug Discovery* **2010**, *9*, 412-412.
(92) Weinreb G. Quark Pharmaceuticals raises $27m. IVC Weekly Newsletter (2008). www.ivc-online.com/ivcWeeklyItem. asp?articleID=6841
(93) Melman, A.; Rojas, L.; Christ, G. *Curr. Opin. Urol.* **2009**, *19*, 595-600.

(94) Singerman, L. *Retina-the Journal of Retinal and Vitreous Diseases* **2009**, *29*, S49-S50.
(95) Vaishnaw A. A status report on RNAi therapeutics. *J. Silence* 1(1), 14 (2010).
(96) Nucleonics initiates hepatitis B clinical trial with expressed interfering RNA therapeutic. EurekAlert (2011). http://www.eurekalert.org/pub_releases/2008-2001/ka-nih011008.php (2008).
(97) O'Shaughnessy D. Safety and Efficacy Study of Small Interfering RNA Molecule (Cand5) to Treat Diabetic Macular Edema. Clinical Trials (2008). http://clinicaltrials.gov/show/NCT00306904
(98) Leachman SA. Study of TD101, a Small Interfering RNA (siRNA) Designed for Treatment of Pachyonychia Congenita. Clinical Trials (2008). http://clinicaltrials.gov/ct2/show/NCT00716014?term=Pachyonychia+Congenita+AND+TransDerm&rank=00716011
(99) Allergan I. A Study Using Intravitreal Injections of a Small Interfering RNA in Patients With Age-Related Macular Degeneration. Clinical Trials (2006). http://clinicaltrials.gov/ct2/show/NCT00395057?term=Allergan+AND+siRNA+AND+AMD&rank=00395052
(100) Mendelsohn F. Safety and Efficacy Study Using Gene Therapy for Critical Limb Ischemia. Clinical Trials (2010). http://clinicaltrials.gov/ct2/show/NCT01064440?term=dna+gene+therapy&rank=01064443
(101) Grandis J. Gene Therapy in Treating Patients With Advanced Head and Neck Cancer. Clinical Trials (2001). http://clinicaltrials.gov/ct2/show/NCT00009841?term=dna+gene+therapy&rank=00009841
(102) Argiris A. Safety and Efficacy of Radiation/Cetuximab Plus EGFR Antisense DNA for Head and Neck Squamous Cell Carcinoma. Clinical Trials (2009). http://clinicaltrials.gov/ct2/show/NCT00903461?term=dna+gene+therapy+head+and+neck+squamous&rank=00903461

2.2 Non-viral Gene Delivery Barriers

Nucleic acid therapies have enormous potential in the clinic, from treatment of specific genetic diseases such as cystic fibrosis [1], Leber hereditary optic neuropathy [2], hemoglobinopathies [3,4] and hemophilia [5], to the treatment of cancer [6,7] and cardiovascular

Chapter 2.2 is published as "Sunshine JC, Bishop CJ, Green, JJ. Advances in polymeric and inorganic vectors for nonviral nucleic acid delivery. *Ther. Deliv.* 2011;2(4):493-521".

disease [8] and the use of genetic vaccines [9]. Additionally, nucleic acid delivery plays a crucial role in cellular engineering and basic biomedical research through the ability to knock in and knock down genes and proteins in the lab, as well as in the creation of induced-pluripotent stem-cells (iPSCs) via viral methods [10,11] and investigations into the induction of iPSCs via non-viral [12] methods.

The central challenge for effective therapy using nucleic acids is finding a safe and effective delivery system [13]. With regards to gene therapy, since viral gene therapy can have serious safety concerns [14], recent efforts have focused on non-viral methods.

These non-viral methods can be used to deliver various nucleic acids (Table 1), including DNA [15], small interfering RNA (siRNA) [16,17], immunostimulatory RNA [18], short hairpin RNA (shRNA) [19], anti-gene RNA (agRNA), and small-activating RNA (saRNA) [20]. The choice of nucleic acid to deliver may influence where the nanocarrier needs to deliver its cargo (Fig 1). For example, to target Toll-like receptors (TLRs) such as TLR3, TLR7, and TLR8, isRNA should be targeted to the endosome itself [18]. siRNA needs to get into the cytoplasm, so vectors that carry these cargoes, if they are trafficked through the endosome, need some method to escape it. Finally, DNA, shRNA-encoding plasmids, agRNA, and saRNA all need to be further transported from the cytoplasm into the nucleus to be expressed, to interfere with, or to promote gene expression.

There are several barriers to cellular entry and delivery of the nucleic acid cargo that challenge the development of an effective delivery vehicle (Fig. 1). The vehicle needs to form a stable complex with its nucleic acid cargo, protect it from degradation extracellularly, arrive at the cell of interest, get internalized (typically via either receptor-

mediated endocytosis and or non-specific endocytic pathways), escape endo-lysosomal degradation, release its cargo, and harmlessly degrade or otherwise be eliminated.

After escaping the endosomal compartment and making it into the cytoplasm, nucleic acids such as DNA and agRNA, need to make it to the nucleus. This is among the largest challenges remaining for non-viral gene delivery. Simply getting the plasmid into the cytoplasm of the cell is not sufficient; in order to achieve the same level of transfection, delivery of 30 to 100-fold more DNA to the cytoplasm is required compared to direct delivery of DNA to the nucleus [21]. Dividing cells are more easily transfected due to the breakdown of the nuclear membrane that occurs during mitosis [22]. While this breakdown can enhance localization of plasmids to the nucleus and transfection efficiency, cell division is not a requirement for successful transfection [22]. Plasmids can also enter the nucleus through nuclear pore complexes (NPCs) when they are coupled to nuclear localization signals, but this process is not as efficient [22].

Here we will review the current progress in non-viral nucleic acid delivery, especially highlighting the progress in the use of cationic polymers and inorganic nanoparticles (as well as their hybrids). Lipid-based materials for nucleic acid delivery are outside the scope of this review and are well-described elsewhere for siRNA delivery [23] and gene delivery [24]. In this review general properties and biomedical applications of polymeric and inorganic materials are described first. This is followed by further discussion of new approaches to solving the barriers to non-viral delivery. Subsequently, an overview of past and present gene therapy clinical trials will be discussed in terms of the type of delivery system, its current clinical phase, the gene of interest being delivered, and the targeted disease.

When designing gene therapy vectors it is important to note that physical properties such as size, aspect ratio, molecular weight, surface area, shape, polydispersity, zeta potential, and others, can have an impact on cytotoxicity and delivery [25]. To meet certain barrier requirements for gene delivery, surface modifications can be used to modify the physical properties of the delivery system to improve circulation time and solubility (i.e., PEGylation) [26], localization (i.e., folic acid, RGD) [27], biostability (i.e., zeta potential: amine or carboxylic groups) [26], cytotoxicity (addition of carboxyl or hydroxyl groups) [28,29], internalization, and inhibition of reticuloendothelial system clearance [30,31]

2.2.1 Shape/Surface Morphology

Recently, manipulation of particle shape has come into focus as a new method for modulating drug delivery [32]. Local shape of the particle where it makes contact with the cell and not necessarily the overall shape dictate whether or not the particle is internalized by macrophages [33]. Elongated particles have been shown to circulate longer and avoid phagocytosis more effectively than spherical particles [34], however, spherical particles are much more efficiently internalized into target tissues as compared to elongated particles [35]. Seeking to take advantage of this property, Yoo et al. has recently constructed PLGA-based shape shifting particles (one way, from ellipsoid to spherical) in response to temperature, pH, or a chemical signal and demonstrated efficient uptake of the spheres as compared to the ellipsoids [36] (Fig 2). It is also possible to complex anisotropic faces of AuNPs with DNA oligonucleotides to form sticky patches which allows for complicated self assembly [37].

Other nanoparticle morphologies may prove worthwhile to investigate to tune cytotoxicity and nucleic acid delivery of potential vectors. Spherical silver nanoparticles can be induced via light to transform into triangular prisms with efficiency nearing 100%. This is accomplished by irradiating a solution of silver nanoparticles with a halogen lamp at 150 watts for 5 hours (bandpass filter at 550 nm) [38]. DeSimone and coworkers have elegantly used soft lithography using polydimethylsiloxane and perfluoropolyether to make molds enabling nanoparticle replication in a non-wetting template. Using this, nanoparticles with diverse shapes are able to be fabricated (i.e., 200 nm trapezoidal particles, 200 x 800 nm bar particles, 3 μm arrow particles, and 2.5 x 1 μm^2 hexnut particles with 1 μm holes) [39].

Tuning surface morphology has recently been shown to be another important aspect of controlling nanoparticle delivery [40]. Verma et al. showed that gold nanoparticles with surface "ribbon-like" domains of alternating hydrophobic/hydrophilic composition were able to enter the cell without the membrane disruption associated with cationic nanoparticle systems; control particles with random surface organization were unable to penentrate cells at all [41]. Cell penetrating peptides appear to have similar functionality [41,42]. This property should reduce the toxicity usually associated with membrane disruption [41].

2.2.2 Size

Polymer nanoparticles have been developed with a wide variety of sizes for different purposes. Nanoparticles of approximately 100 nm show prolonged blood circulation and a relatively low rate of mononuclear-phagocyte system uptake. [43] Particles

with a 1-5 μm diameter are likely to be trapped in the liver and phagocytosed by Kupffer cells [36]. Larger than 5 μm particles are likely to be trapped in the capillary beds [36]. When NPs are greater than 200 nm they are likely to be filtered in the spleen, whereas the NPs less than 100 nm are likely to leave the blood vessels through fenestrations in the endothelial lining [36]. NPs that are ~50-200 nm have been known to accumulate in tumors by the enhanced permeability and retention (EPR) effect (as a result of leaky vasculature and the absence of a draining lymphatic system) [44,45]. It has been suggested that particles must not exceed 300 nm to take advantage of the EPR effect [46]. Nanoparticles smaller than 50 nm are more likely to enter most cells, and those with sizes smaller than 20 nm can get out of the blood stream and into tissues [45,47]. The glomerular apparatus' capillary wall has fenestrations ~4-5 nm and it has been reported that nanoparticles >8 nm cannot be filtered through the glomerular filtration system [25] as a result would increase circulation half-life [48].

2.2.3 Charge

To best avoid nonspecific interaction and escape the reticuloendothelial system, nanoparticles should be designed to have neutral or slightly negative zeta potentials [49]. On the other hand, a positive zeta potential enhances nanoparticle-cell contact and promotes uptake and internalization through stronger affinity for anionic proteoglycans on the cell surface [50]. For example, the zeta potentials of lysine-, arginine-, and histidine modified nanoemulsions were reported to be 50 mV, 43 mV, and 7 mV, with transfection efficiency decreasing with neutralization of the zeta potential [51]. Some nanoparticles may be more or less cytotoxic depending on their charge (i.e., AuNPs are less cytotoxic when

anionic) [52]. It is important to consider zeta potentials when complexing nucleic acids via ionic interactions. The interaction must be strong enough to condense the nucleic acid to protect against restriction enzymes. It is important to note that zeta potentials of nanoparticles can switch signs when in the presence of serum and this should be considered in the design and testing process [53,54].

2.2.4 Biocompatibility

Biocompatibility is crucial for maintaining an appropriate host response during gene therapy. In depth assessments and characterizations are required to elucidate the physicochemical differences responsible for low cytotoxicity and acceptable viability.

PEI lacks degradable linkages and is too toxic for therapeutic applications, inducing both apopotosis and necrosis in an endothelial cell model [55]. As a result, a number of investigators have synthesized an array of degradable PEIs consisting of LMW PEIs and degradable cross-linkers, in the hopes of achieving higher efficacy with the reduced cytotoxicity of low molecular weight PEIs [56,57].

Other groups have focused on developing new, biodegradable polymers for non-viral gene delivery, which we will review here by method of degradation. Biodegradable polymers should be able to both reduce the cytotoxicity associated with the transfection reagent as well and potentially improve dissociation of the vector from its cargo to allow the cargo to be utilized intracellularly.

Multiple strategies have been formulated using ester bonds to allow hydrolytic cleavage of the polymer. Amine containing hydrolyzable polymers have been utilized which are effective gene delivery agents with significantly decreased cytotoxicity as

compared to non-degradable polymers such as poly(ethylenimine) (PEI) [58] and poly(lysine) (PLL) [59]. These structures include poly(lactide-*co*-glycolide) (PLGA) [60], hyperbranched poly(amino ester)s [61], poly(lactic acid) (PLA) [62], and linear poly(β-amino ester)s (PBAE) [63], among others.

Libraries of PBAEs have been developed for gene vector screening [64,65]. Studies have shown that amine-terminated PBAEs are more effective at pDNA transfection than acrylate-terminated versions. Modification of the polymer ends with different amines can lead to virus-like efficacy in human primary cells in vitro [66] (Fig. 3). Tuning of polymer end group leads to significant differences in transfection efficacy, and the optimal end-group for each cell type appears to be different [67,68]. PBAEs also have been shown to be non-toxic to human primary cells in vitro [69] and in mice in vivo [70,71].

2.2.5 Stealth Properties

The binding of serum proteins to nanoparticle surfaces after intravenous injection allows the nanoparticles to be recognized and internalized by macrophages, resulting in removal of nanoparticles from circulation [72]. Addition of hydrophilic moieties, like poly(ethylene glycol) (PEG), poly(N-(2-hydroxypropyl-methacrylamide) (pHPMA), and various oligosaccharides, have been shown to increase solubility, prolong circulation time, neutralize zeta potential, and reduce interactions with the environment within the bloodstream due to a higher tolerance against incubation with serum proteins [73,74]. One disadvantage of this approach is that while it may stabilize the polyplex in serum and reduce cytotoxicity, it may also interfere with complexation and reduce transfection efficiencies depending on the extent of addition [75]. Modification of the surface of

preformed particles with PEG/pHPMA that can bind to exposed surface amino groups has been shown to alleviate this problem [73,76]. Recently, Yuan et al. showed that adding PEG to PAMAM dendrimers via bis-aryl hydrazone bond linkages into the vector significantly enhanced the buffering capacity of the vector even with a high degree of PEGylation [77]. PEG can be added to a variety of nanoparticles and can be further modified to provide targeting [78-81], or can be attached by degradable bonds (such as matrix metaloproteinases (MMP)) that can be cleaved to expose underlying functionalities [82-86]. Electrostatic coatings can also be used to improve the delivery properties of a charged particle without significantly altering the core particle [87,88].

2.2.6 Nucleic Acid Complexation

Many polymers for nucleic acid delivery rely on electrostatic interaction between a cationic polymer and the anionic phosphate backbone of nucleic acid substrate. For polymer-DNA complexes, requirements include condensation of the plasmid to an appropriate scale for internalization, neutralization of the negatively charged phosphate backbone of the DNA, and protection of DNA from degradation both intra- and extracellularly [89,90]. Sufficient cationic charge is crucial to condense DNA, but it is also correlated with increased cytotoxicity, and higher DNA binding affinity may lead to decreased DNA release and reduced transport through the cytoplasm [91]. Gold nanoparticles can use electrostatic methods for complexation with nucleic acids as well. AuNP rods conjugated with cationic cetyltrimethylammonium bromide were electrostatically complexed with siRNA (anti-DARPP-32 gene in dopaminergic neuronal cells) with 98% cell viability and 67% expression knockdown at 120 hr post-transfection

[49]. Alternatively, hydrolytically degradable nanoparticles can be formed through encapsulation of DNA by non-cationic polymers such as PLGA. These particles degrade to release their nucleic acid cargo and the size of the particle can be controlled in the nanometer to micrometer range, depending on the method of particle formation used. Methods have been developed to protect the cargo from destruction during these processes [60] but are still limited by low encapsulation efficiency and potential DNA degradation in the hydrolyzing polymer core [92].

Chitosan can form nanoparticles through a process called ionotropic gelation with polyanions such as sodium tripolyphosphate [93]. Chitosan has been optimized to allow for the encapsulation of both hydrophilic and hydrophobic drugs and has been utilized in nucleic acid delivery [94,95], most successfully as hybrid co-polymers with various polycations [96-99].

Inorganic nanoparticles can be complexed with nucleic acids via ionic complexation or covalent bond. For example, AuNPs (4.1 nm) can be covalently attached to cationic N-dodecyl polyethylenimine (2 kDa) and complexed with β-gal pDNA. When this conjugated complex was delivered to COS-7 cells, there was 67% cell viability and 50% transfection efficacy which compared favorably to regular PEI and PEI25 which had 4 and 8% transfection, respectively (~93% cell viability) [100].

Another nucleic acid complexation technique involved 11-mercaptoundecanoic acid which was deposited on Au to bind oppositely charged polyelectrolyte solutions. The deposited Au combined with PEI (23kDa MW) and double-stranded 21-mer anti-EGFP siRNA and was then coated again in a PEI layer. This complex was delivered to

CHO-K1 cells resulting in ~95% cell viability and ~72% knockdown of EGFP expression[101].

2.2.7 Cellular Targeting

By utilizing a targeting moiety, smaller dosages can elicit comparable therapeutic responses while minimizing side effects and reducing the cost of therapy [102]. There are two types of targeting; passive and active. Passive targeting utilizes natural processes such as the enhanced permeability and retention effect (EPR), in which the leaky tumor vasculature and lack of efficient lymphatic drainage in a solid tumor leads to passive accumulation of drugs or particles at the tumor site, given sufficient circulation time [103]. Active targeting consists of an additional ligand to assist in localization or internalization such as antibodies or their fragments (i.e., J591 against prostate-specific membrane antigens [104], anti-HER2 (Trastuzumab) [105], etc) [106], folic acid([107]), sugars (i.e., galactose, mannose, and lactose) [108], peptides (RGD) [109,110], transferrin [111], and nucleic acid aptamers [112]. Large targeting moieties, however, may hamper internalization and gene unpacking and having triggered removal of the target moiety at the cell surface may be worthwhile [102]. Targeting moieties are typically attached chemically but can be physically adsorbed to the delivery system as well [88]. Interestingly, it has been shown that biodistribution of cargo at the accumulation site can be independent of the presence of targeting ligands [45]**.** The reason for improved functionality when targeting ligands are used appears to be due to an increase in cell internalization and specificity of the nanoparticles rather than tissue localization. Passively targeted nanoparticles have a

propensity to end up in the extracellular space of tumors and in tumor-associated macrophages [45].

Cationic polymers have been modified with targeting ligands for various applications. For example, the addition of lung surfactant to ternary nanoparticles for aerosol-based gene therapy enhances gene delivery to the lung, resulting in 12-fold higher transfection compared to pure nanoparticles and 30-fold higher compared to polyethylenimine [113]. Insulin adsorption significantly increased gene expression of PEI-pDNA nanoparticles up to 16-fold on alveolar epithelial cells but not on bronchial epithelial cells [114].

AuNPs can be complexed with PEG-NH_2 and folic acid via non-covalent interactions and can be taken up by cancer cells (OV167, OV202, OVCAR-5) proportional to the degree of folic acid receptors expressed on them. However, unintended delivery to the liver and kidneys can also occur due to over-expression of folic acid receptors there as well [115,116].

AuNPs and the monoclonal antibody CD11b have been targeted to RAW264.7 macrophages and resulted in 81% cell death post 30 J/cm^2 exposure as opposed to 0.9% cell death with non-labeled cells [31].

2.2.8 Enhancing Internalization

AuNP can be internalized to a greater degree via electroporation which causes membranes to become permeabilized by pulsed electric fields (several kV/cm amplitude and submicrosecond duration). Membrane pores occur momentarily as a result, allowing for easier passage of gene therapy systems. However, electroporation can also cause

osmotic lysis of the cells. Kawano et al has delivered AuNP-SS-mPEG-pDNA *in vivo* in combination with electrical pulses to the mouse liver and observed greater stability in circulation and a gene expression increase by ten-fold in comparison to naked DNA [117]. Multi-walled CNTs combined with irradiation of microwaves for 8 seconds can aid gene delivery by creating transient nanochannels in the cell while maintaining cell viability at 100% [118]. Hexagonal layered double hydroxide nanoparticles (LDHs) are most likely taken up by clathrin-mediated endocytosis and localize to the perinuclear area of the cytoplasm (where siRNA/mRNA complexes can degrade). In contrast, rod-like LDHs concentrate in the nucleus [119].

Gene-associated magnetic nanoparticles (i.e., SPIONs) can be guided toward a particular region of the body via external magnetic fields. Application of external magnetic fields to aid traversing membrane barriers and enhancing cell contact is known as magnetofection [120]. CNTs with ferromagnetic-nickel tips have been known to be able to align in an external magnetic field to spear cell membranes. This increases the shuttling efficiency of cargo by 107 fold and was shown to increase transfection rates to approximately 100% to mammalian cells in vitro [121] Ultrasound is non-invasive and safe at a broad range of frequencies and intensities and can be used to enhance gene delivery. The main mechanism responsible for increased gene delivery is cavitation, where reversible nanopores are formed (up to 100 nm with a half life of a few seconds) by microbubble expansion and collapse. [122]. Stride et al. endeavored to combine ultrasound-mediated gene delivery and magnetofection and showed significantly improved transfection over magnetofection and ultrasound alone [123].

Gene guns are biological ballistic hand held delivery systems which physically propel nucleic acid-complexed nanoparticles (i.e., AuNP) into cell cytoplasm and nuclei with a low pressured propellant (i.e., helium). Chitosan and poly-g-glutamic acid (150-250 nm) nanoparticles have been used to encapsulate reporter genes and transfect liver cells via the gene gun method which increases delivery by 2 log orders of magnitude in terms of luciferase RLU/mg protein compared to naked DNA [124].

2.2.9 Endosomal Escape

In early experiments with non-viral gene delivery, non-degradable polycations, including poly(l-lysine) (PLL) and polyethylenimine (PEI) were used. Compared to PLL, a major advantage of PEI is the "proton sponge" effect due to PEI's extensive buffering capacity. When PEI:DNA complexes gain entry to the endosome, the secondary and tertiary amines in PEI function to buffer acidification of the endosome. This causes an influx of negatively charged chloride ions into the endosome to maintain electroneutrality as protons are continually pumped into the endosome. Eventually, this leads to osmotic swelling and rupture of the endosomes and release of the vector and cargo into the cytoplasm [125]. This mechanism has been widely explored for gene and siRNA delivery [58,126]. This concept has also been extended and heavily used in the design of next-generation biodegradable vectors which also contain this buffering capacity.

A widely used buffering moiety is the imidazole ring of histidine. It is a weak base with a (pKa ~ 6) capable of buffering the endosome. For example, a poly(phosphazene) based polymer has been histidylated, and the resulting polymer

showed improved transfection and reduced cytotoxicity when compared to the histidine-free polymer and branched PEI [127].

Newer methods for endosomal escape involve functionalizing a polymer with peptides that enhance endosomal release. Melittin enhances endosomal escape and nuclear transport via cationic C-terminal lysine-arginine-lysine-arginine cluster [128]. Modifying melittin either by reversible acetylation of a lysine residue in melittin [129] or replacement of two glutamines with glutamic acids which get neutralized at acidic pH [130] takes advantage of the acidification of the endosome to induce membrane lysis only in the endosomal compartment and reduces the cytotoxicity associated with use. Functionalizing polylysine with polyethylene glycol and a pH-responsive melittin peptide was shown to be an efficient siRNA delivery agent [131].

Protonation of glutamate residues (pKa 5-5.5) within "anionic fusogenic peptides" within the endosome triggers disruption of the endosomal membrane via the formation of an alpha-helical structure in the peptide [132-134]. Adding these peptides to polymeric vehicles was shown to enhance the endosomal escape rate constant by two orders of magnitude [135].

2.2.10 Release of Cargo/Degradation

Nucleic acids must be released from the vector to have an effect. This can be done by taking advantage of the redox potential gradient [136], acidic environment of the endosome [137], MMPs [138,139], photocatalysis [140], and hydrolytic degradation of the carrier [63,141,142]. It has been shown that plasmid unpacking can be a limiting step with regards to gene expression for sufficiently large polymer constructs [143].

Bioreducible polymers

Using bioreducible polymers via incorporation of disulfide linkages takes advantage of the relative reducing environment of the intracellular space. Intracellular reduction of the disulfide bond occurs via the glutathione (GSH) pathway. GSH is regenerated from its oxidized form by glutathione reductase, and is an important component in many cellular pathways and plays a major role in cellular defense against oxidative stress. Disulfide bonds are stable extracellularly, preventing particle breakdown before the nano-complex reaches the cell surface, whereas the reducing environment of the intracellular space allows for enhanced polymer breakdown and nucleic acid release [144-148].

Disulfide bonds have been shown to degrade intracellularly within 3 hours [149]. When cell lines with different intrinsic glutathione levels were compared, increased cellular GSH levels were associated with improved transfection of mRNA polyplexes. In other experiments, no clear trend was observed for plasmid DNA or siRNA containing complexes and GSH levels; rather, the cell line which demonstrated the best DNA transfection was the fastest dividing cell line [150].

Enhancing release of the pDNA cargo can lead to dramatic gains in transfection efficiency. Chen et al synthesized a series of reducible hyperbranched poly(amido amine)s and found that reducible polymers were able to achieve nearly 200-fold higher transfection as compared to control polymers [151]. Combining hydrolyzable and bioreducible functional groups as a single polymer might also help further tune the release profile [152,153].

Reducible polymers have also been used to deliver siRNA. Histidine containing reducible polycations based on CH(6)K(3)H(6)C monomers (His6 RPCs) were examined for their utility in delivering siRNA. Co-delivery of EGFP siRNA with EGFP DNA reduced reporter gene expression by 85%. Interestingly, while as with most polymer systems, larger polymer size correlated with increased DNA transfection efficiency, effective delivery of siRNA was only possible with smaller polymers (36-80kDa) [154].

Low molecular weight PEI has also been crosslinked via disulfide linkages to show reduced cytotoxicity and equivalent DNA transfection efficacy to higher MW PEI [155]. In one study, reducible poly(amido ethylenimine) (SS-PAEI) was synthesized by addition copolymerization of triethylenetetramine and cystamine bis-acrylamide (poly(TETA/CBA)) and used as a carrier for siRNA. Under normal conditions there was significantly higher suppression of VEGF with poly(TETA/CBA) than with linear-polyethylenimine. The addition of dl-buthionine sulfoxamine, which reduces intracellular level of reduced glutathione reduced the RNAi activity level of poly(TETA/CBA) formulation to that of L-PEI, showing that reduction of the polymer was crucial to gene knockdown [156].

Jere et al used a reducible polyspermine (RPS) carrier composed of multiple spermine units with disulfide linkages and showed improved efficacy in gene delivery and in gene knockdown compared to 25K PEI. RPS delivered anti-Akt1 sh/si/ssiRNA and altered the cancer cell survival, proliferation and metastasis to different extents depending on the nature of siRNA treatment [157].

Acid labile linkages

Acid labile linkages would also be useful for endosomal escape and for enhanced cargo release into the cytoplasm, as they take advantage of the acidification of the endosome to allow for release of the cargo. Acid labile acetal and ketal bond bearing polycations were recently developed for this purpose. Oligoethylenimines linked by either acid-degradable ketal or acetal linkers in a copolymer with 5 kDa PEG formed complexes with half-lives of 3 min at pH 5.0, and 5 h (OEI-MK) or 3.5 h (OEI-BAA) at physiological pH 7.4 [84]. Using acylhydrazides or pyridylhydrazines to link a PEG shield to the polymer backbone enhanced transfection by two (*in vitro*) or one (*in vivo*) order(s) of magnitude compared to complexes whose PEG shield was not acid-hydrolyzable [82].

Irradiation-released

An Nd:YAG laser was used to release DNA from a 44 nm spherical AuNP complex conjugated to PEG-orthopyridyl-disulfide. The Nd:YAG laser irradiation was applied at 80 mJ/pulse (~10 ns, 6 mm diameter). DNA was released without any degradation seen [140].

When EGFP DNA-SS-AuNR was delivered to HeLa cells and was controlled remotely using femtosecond near-infra red (NIR), a shape change from rod to sphere was observed. It was proposed that this transformation induces DNA release from its conjugate [158]. Also using NIR, AuNR-EGFP-DNA conjugates were delivered to HeLA cells and there was expression detected at the irradiated spots of NIR exposure (79 uJ/pulse for 1 min). There was 80% cell viability observed and the NIR irradiation induced plasmid release without structural degradation [159].

AuNRs of different aspect ratios can be melted selectively at their unique longitudinal plasmon resonance by morphing to a sphere to release DNA oligonucleotides. Aspect ratios at 4.0 and 5.4 will have a longitudinal plasmon resonance at 800 and 1100 nm, respectively. By irradiating a combined sample of the aspect ratios at one wavelength 50-60% of the intended oligonucleotides can be released and are still functional whereas the unintended oligonucleotides from the other aspect ratio released <10% of its cargo [160].

2.2.11 Nuclear Translocation

Diffusion of DNA longer than 250 base pairs in length is significantly reduced in the cytoplasm compared with water due to the involvement of the cytoskeleton [161]. The nuclear pore complex (NPC) forms a selective permeability barrier, allowing free diffusion of molecules (e.g. ions, small proteins, and metabolites) with a mass/size less than about 40 kDa/10 nm proteins [162]. Macromolecules greater than ~40 kDa are transported actively across the nuclear envelope through the nuclear pore complexes (NPCs) using soluble transport factors or carrier molecules (β-karyopherins) that cycle between the cytoplasm and nucleus [163]. In the classical case, nuclear localization signals (NLS) are recognized by importin-α, which then binds to importin-β, and this complex is allowed through the NPC. Once inside the nucleus, the importin-β binding domain is released by binding to RanGTP and the cargo is released [163] (Fig. 4). By utilizing electron microscopy and gold nanoparticles complexed to NLSs, Panté and Kann were able to show that the largest rigid particle to achieve nuclear entry through NPCs was ~39 nm in diameter including NLSs [164].

Strategies for obtaining access to the nucleus have relied primarily on diffusion through the cytoplasm and presentation of NLS to allow pDNA access to the nucleus [22]. Numerous groups have tried to complex synthetic or naturally occurring NLS peptides with the delivered DNA, with variable efficacy [22], and transfection enhancement may be due to NLS peptides inducing improved nanoparticle complexation and not increased nuclear import [22]. A single NLS has been shown to be sufficient to carry the DNA through the NLS [22], but the addition of hundreds of NLS sequences to a plasmid lead to no nuclear localization of the plasmids [22], Multiple NLS sites might lead to cellular machinery attempting to pull a single plasmid in multiple directions at the same time, as well as potentially inhibit translation.

2.2.12 Figures

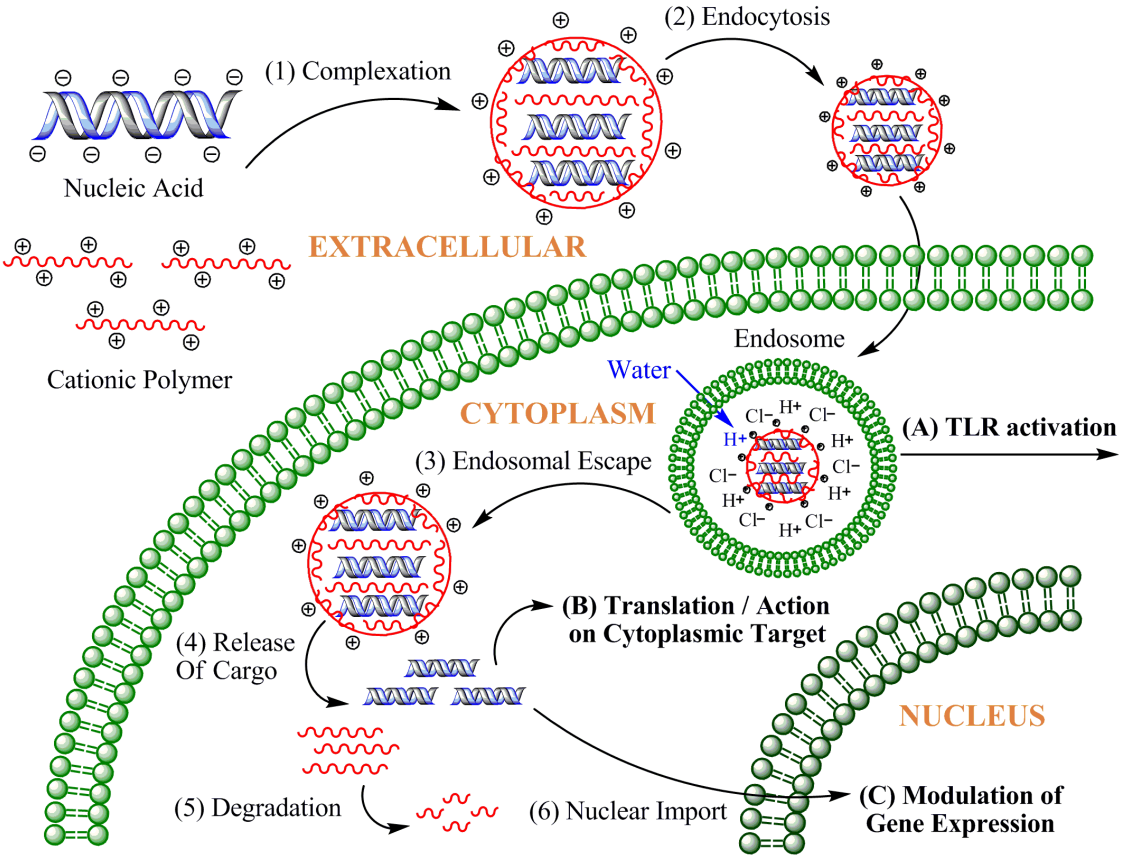

Figure 1: Barriers to intracellular nucleic acid delivery. (1) Nucleic acid must be complexed to the nanocarrier and protected from degradation as it makes its way to the target cell. (2) The nanocarrier and cargo must be internalized successfully. **(A)** TLR7 is localized to the endosome; for isRNA activity, endosomal escape is not required. For other nucleic acid, (3) endosomal escape is required. (4) For cytoplasmic activity **(B)**, nucleic acid must be released intracellularly. (5) Nanocarrier degradation is not required, but is useful for reduced toxicity. (6) For DNA, shRNA-encoding plasmids, and agRNA, nuclear import is required for successful effect **(C).**

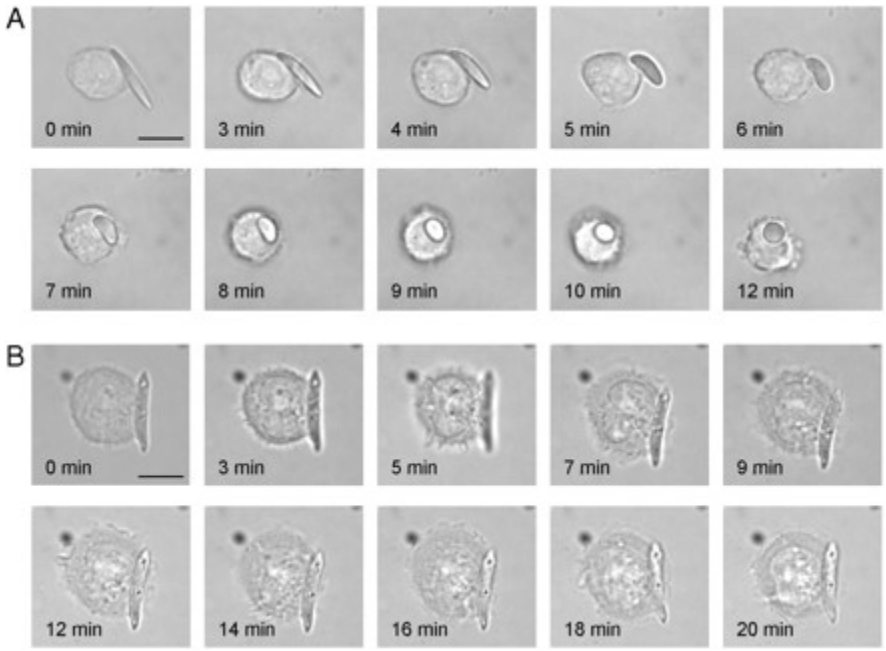

Figure 2: Time-lapse video microscopy clips of shape-dependent phagocytosis by macrophage. (A) Shape-switching PLGA-ester elliptical disk (ED) allows macrophage internalization. (*B*) PLGA-ester elliptical disk (ED) which does not switch shape prevents internalization (Scale bar: 10 μm.) Used with permission from [36].

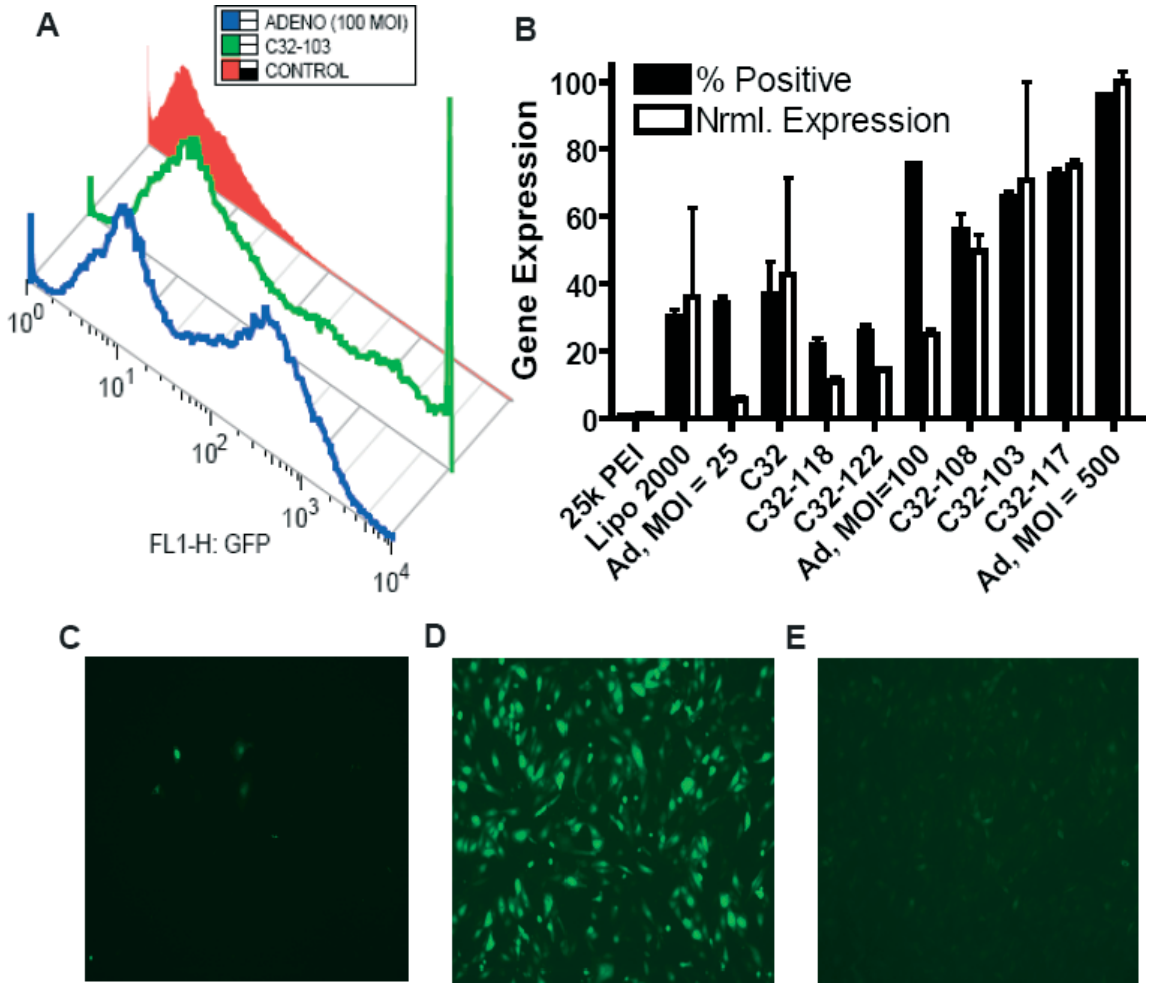

Figure 3. Gene expression of PBAE vs. adenovirus. A) Gene expression histogram comparing adenovirus (blue), PBAE (green), and negative control. B) Comparison of various PBAE formulations with adenovirus with respect to % positive cells and normalized expression.
Images of GFP+ cells 24 hrs post transfection with C) PEI, D) C32-103, and E) 500 MOI (multiplicity of infection) adenovirus. Used with permission from [66].

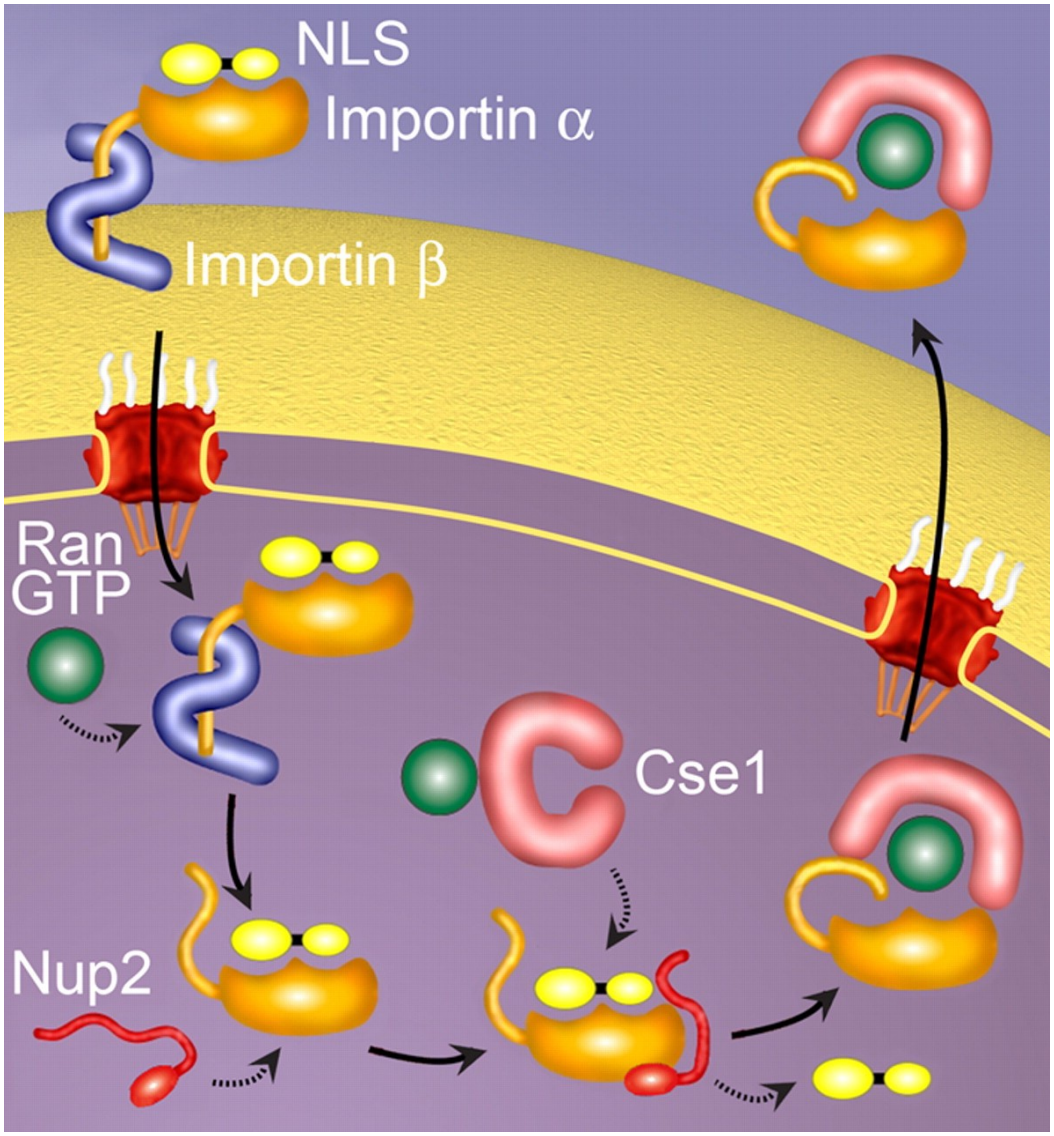

Figure 4: Nuclear import through the nuclear pore complex. Used with permission from [163].

2.2.13 Table

Table 1: Summary of results of various polymeric and inorganic vectors for delivering genes. It is important to note that direct comparisons are difficult as the experimental setups are likely different.

Ref. #	Materials used & size	Cargo (DNA)	Target	Cell viability	Transfection efficacy
[165]	Folate PLL, chloroquine	Luc	KB cells	Not reported in detail	6x higher than w/o folate @ 24 hpt
[166]	Partially histidylated PLL	Luc	HepG2	No cytotox. 4-24 incubation hours	~ 5 log orders of higher RLU than PLL @ 48 hpt
[167]	Galactosylated PLL (Gal_{13}-PLL_{13000}; ~179 nm	CAAT	Human epitome cell line HepG2	Not reported in detail	~850 mU/mg @ 48 hpt
[58]	800 kDa PEI (nitrogen to DNA base = 9)	Luc	3T3 cells	Only toxicity above concent. for optimal efficiency	4 log orders more efficient than PLL (light units/mg protein)
[168]	Low molecular weight PEI at 11.9 kDa; High molecular weight PEI at 1620 kDa	Luc	ECV304	MTT assay: LMW, none up to 1 mg/mL; HMW, IC_{50} = 35 μg/mL	LMW PEI (N/P = 66.66) RLU was 100-fold higher than HMW PEI (N/P = 13.33)
[169]	Fully deacetylated (deAc) linear PEI: 25-kDA (PEI25) and 87-kDa (PEI87)	β-gal *in vitro*; Luc *in vivo* (mouse)	A549 cells *in vitro;* Lungs *in vivo*	>80% viability with N/P ratio <20; increasing toxicity with increasing N/P; deAc-PEI was more toxic than PEI	deAc-PEI25 21x higher than Ac-PEI25 *in vitro*; 115x-higher expression vs. PEI25 seen by deAc-PEI87 *in vitro*; 10 N/P deAc-PEI25 showed 5 log orders of higher RLU and 1500-fold enhancement in lung specificity vs. PEI25 *in vivo*
[170]	PBAE (C32); 71 nm; 1.2:1 amine/acrylate ratio	Luc	COS-7	No cytotoxicity observable	Better than Lipofectamine 2000

[53]	PBAE (C32-117); <200 nm	Luc	HUVEC	2 orders of magnitude lower than 25 kDa PEI	~adenovirus and lentivirus; 2 log orders greater than 25 kDa PEI
[12]	PBAE (C32-117); ~200 nm	GFP & RFP	hESC	70% @ 24 hpt	50% @ 24 hpt
[171]	(Mannose/galactose)-PEG-PAMAM linear-dendritic hybrid polymers (~150 nm)	Luc	P388D1 murine macrophages bearing Man-receptor	60-80% for G5.0 and 50-70% for G6.0 when transfecting P388D1 cells	Man-PEG-G6.0 transfected P388D1 1.6-1.8-fold more efficiently than PEI with no serum and 4-fold more efficiently in the presence of serum
[172]	Chitosan (~150 nm)	Arah2 (peanut allergy gene)	Oral administration	Not reported in detail.	Decreased IgE levels in response to anaphylaxis induction
[173]	Biomineral solution ($CaCl_2$, KH_2PO_4, NaCl, KCl, $MgSO_4$, $MgCl_2$, $NaHCO_3$) (Fig. 3)	β-galactosidase	MG-63	>90% at 24 hours using concentrations ranging from 1-20 μg/mL	Transfection is greater than Transfast (1μg/mL) using inorganic mineral solutions at 1, 10, and 20 μg/mL
[174]	tetra(piperazino) fullerene epoxide	eGFP	C57/BL6 mice	No acute toxicity for liver or kidney	Increased plasma insulin levels and reduced blood glucose concentrations
[175]	ZnO quantum dots with poly(2-(dimethylamino)ethyl methacrylate)	Luc	COS-7	90% at 50 μg/ml. However, at 100 μg/ml (experimental levels) viability was 18% which is most likely due to quantum dot vectors	~1 log order lower than PEI(25k) @ 48 hpt
Ref. #	**Materials used & size**	**Cargo (siRNA)**	**Target**	**Cell viability**	**Expression Knockdown**

[176]	PLGA nanoparticles (slightly <200 nm) with spermidine or protamine used as a counter ion to the siRNA in the loading process	anti-MAPK1 (ERK2) siRNA *in vitro*, anti-eGFP siRNA *in vivo*	Vaginal epithelium	*In vitro* no observed decreased cell viability up to 10 mg/ml; *in vivo* no histological changes (mice significant inflammation when treated with siRNA lipopolyplexes)	spermidine improved loading by >40-fold; *in vitro* ≥ gene silencing compared to Lipofectamine™ RNAiMax; *in vivo* 50-60% knockdown in vaginal epithelium and submucosa
[119]	$Mg_2Al(OH)_6NO_3$; layered double hydroxide nanoparticles; ~100 nm	anti-MAPK1 (ERK2) siRNA	HEK293T	>80% over 3 day period; IC_{50}: 0.125 mg mL^{-1}	RLU for NP alone and w/ siRNA: ~1.1 a.u. @ 24 hpt, and ~0.1 a.u., respectively @8 hpt
[30]	PBAE (C32-221)-siRNA-SS-PEG-AuNP; ~100 nm	Anti-Luc siRNA	HeLa	~90% @ 24 hpt	~95% @ 24 hpt
[177]	Mesoporous silica nanoparticles-PEI; ~100 nm	Anti-eGFP siRNA	PANC-1	Not reported in detail	61.7% 72 hpt
[101]	AuNP, siRNA, MUA, 25 kDa PEI (LbL); 26.8 nm	Anti-eGFP siRNA	CHO-K1	~95% @ 0.37 nM AuNP	~72%@ 0.37 nM AuNP
[178]	Lipospheres, cationic lipid Metafectene, dioleoylphosphatidyl-ethanolamine functionalized with SPION	Anti-eGFP and Anti- Luc siRNA	eGFP-HeLa, firefly luciferase-HeLa	Anti-eGFP siRNA: Not significantly affected; Anti-Luciferase: 50% viability; likely due to transfection	90% @ 48 hpt

2.2.14 References

(1) Pringle, I. A.; Hyde, S. C.; Gill, D. R. *Expert Opin Biol Ther* **2009**, *9*, 991-1003.
(2) Lam, B. L.; Feuer, W. J.; Abukhalil, F.; Porciatti, V.; Hauswirth, W. W.; Guy, J. *Arch Ophthalmol*, *128*, 1129-35.
(3) Sadelain, M.; Riviere, I.; Wang, X.; Boulad, F.; Prockop, S.; Giardina, P.; Maggio, A.; Galanello, R.; Locatelli, F.; Yannaki, E. *Ann N Y Acad Sci*, *1202*, 52-8.
(4) Perumbeti, A.; Malik, P. *Ann N Y Acad Sci*, *1202*, 36-44.
(5) Viiala, N. O.; Larsen, S. R.; Rasko, J. E. *Semin Thromb Hemost* **2009**, *35*, 81-92.
(6) Phalon, C.; Rao, D. D.; Nemunaitis, J. *Expert Rev Mol Med*, *12*, e26.
(7) Sangro, B.; Mazzolini, G.; Ruiz, M.; Ruiz, J.; Quiroga, J.; Herrero, I.; Qian, C.; Benito, A.; Larrache, J.; Olague, C.; Boan, J.; Penuelas, I.; Sadaba, B.; Prieto, J. *Cancer Gene Ther*.
(8) Karvinen, H.; Yla-Herttuala, S. *Curr Opin Pharmacol*, *10*, 208-11.
(9) Nguyen, D. N.; Green, J. J.; Chan, J. M.; Langer, R.; Anderson, D. G. *Adv Mater* **2009**, *21*, 847-867.
(10) Yu, J.; Vodyanik, M. A.; Smuga-Otto, K.; Antosiewicz-Bourget, J.; Frane, J. L.; Tian, S.; Nie, J.; Jonsdottir, G. A.; Ruotti, V.; Stewart, R.; Slukvin, II; Thomson, J. A. *Science* **2007**, *318*, 1917-20.
(11) Takahashi, K.; Tanabe, K.; Ohnuki, M.; Narita, M.; Ichisaka, T.; Tomoda, K.; Yamanaka, S. *Cell* **2007**, *131*, 861-72.
(12) Green, J. J.; Zhou, B. Y.; Mitalipova, M. M.; Beard, C.; Langer, R.; Jaenisch, R.; Anderson, D. G. *Nano Lett.* **2008**, *8*, 3126-30.
(13) Putnam, D. *Nat. Mater.* **2006**, *5*, 439-51.
(14) Check, E. *Nature* **2005**, *433*, 561.
(15) Viola, J. R.; El-Andaloussi, S.; Oprea, II; Smith, C. I. *Expert Opin Drug Deliv*, *7*, 721-35.
(16) Hamilton, A. J.; Baulcombe, D. C. *Science* **1999**, *286*, 950-2.
(17) Guo, J. F.; Fisher, K. A.; Darcy, R.; Cryan, J. F.; O'Driscoll, C. *Molecular Biosystems* **2010**, *6*, 1143-1161.
(18) Schlee, M.; Hornung, V.; Hartmann, G. *Mol Ther* **2006**, *14*, 463-70.
(19) Paddison, P. J.; Caudy, A. A.; Bernstein, E.; Hannon, G. J.; Conklin, D. S. *Genes Dev.* **2002**, *16*, 948-958.
(20) Janowski, B. A.; Younger, S. T.; Hardy, D. B.; Ram, R.; Huffman, K. E.; Corey, D. R. *Nat Chem Biol* **2007**, *3*, 166-73.
(21) Miller, A. M.; Dean, D. A. *Adv Drug Deliv Rev* **2009**, *61*, 603-13.
(22) Lam, A. P.; Dean, D. A. *Gene Therapy* **2010**, *17*, 439-447.
(23) Schroeder, A.; Levins, C. G.; Cortez, C.; Langer, R.; Anderson, D. G. *Journal of Internal Medicine* **2010**, *267*, 9-21.
(24) Tros de Ilarduya, C.; Sun, Y.; Duzgunes, N. *Eur J Pharm Sci*, *40*, 159-70.
(25) Gormley, A. J.; Ghandehari, H. *Evaluation of Toxicity of Nanostructures in Biological Systems*; John Wiley & Sons, Ltd, 2009.
(26) van Vlerken, L. E.; Vyas, T. K.; Amiji, M. M. *Pharm. Res.* **2007**, *24*, 1405-14.
(27) Wang, J. Q.; Tao, X. Y.; Zhang, Y. F.; Wei, D. Z.; Ren, Y. H. *Biomaterials* **2010**, *31*, 4426-4433.

(28) Sayes, C. M.; Liang, F.; Hudson, J. L.; Mendez, J.; Guo, W.; Beach, J. M.; Moore, V. C.; Doyle, C. D.; West, J. L.; Billups, W. E.; Ausman, K. D.; Colvin, V. L. *Toxicol Lett* **2006**, *161*, 135-42.
(29) Zhang, B. L.; Chen, Q. O.; Tang, H.; Xie, Q. J.; Ma, M.; Tan, L. A.; Zhang, Y. Y.; Yao, S. Z. *Colloid Surface B* **2010**, *80*, 18-25.
(30) Lee, J. S.; Green, J. J.; Love, K. T.; Sunshine, J.; Langer, R.; Anderson, D. G. *Nano Lett.* **2009**, *9*, 2402-6.
(31) Pissuwan, D.; Niidome, T.; Cortie, M. B. *J Control Release* **2009**.
(32) Champion, J. A.; Katare, Y. K.; Mitragotri, S. *Journal of Controlled Release* **2007**, *121*, 3-9.
(33) Champion, J. A.; Mitragotri, S. *Proceedings of the National Academy of Sciences of the United States of America* **2006**, *103*, 4930-4934.
(34) Geng, Y.; Dalhaimer, P.; Cai, S. S.; Tsai, R.; Tewari, M.; Minko, T.; Discher, D. E. *Nature Nanotechnology* **2007**, *2*, 249-255.
(35) Muro, S.; Garnacho, C.; Champion, J. A.; Leferovich, J.; Gajewski, C.; Schuchman, E. H.; Mitragotri, S.; Muzykantov, V. R. *Molecular Therapy* **2008**, *16*, 1450-1458.
(36) Yoo, J. W.; Mitragotri, S. *Proceedings of the National Academy of Sciences of the United States of America* **2010**, *107*, 11205-11210.
(37) Glotzer, S. C.; Anderson, J. A. *Nat. Mater.* **2010**, *9*, 885-887.
(38) Xue, C.; Metraux, G. S.; Millstone, J. E.; Mirkin, C. A. *J. Am. Chem. Soc.* **2008**, *130*, 8337-8344.
(39) Jeong, W.; Napier, M. E.; DeSimone, J. M. *Nanomed.* **2010**, *5*, 633-639.
(40) Verma, A.; Stellacci, F. *Small*, *6*, 12-21.
(41) Verma, A.; Uzun, O.; Hu, Y.; Han, H. S.; Watson, N.; Chen, S.; Irvine, D. J.; Stellacci, F. *Nat. Mater.* **2008**, *7*, 588-95.
(42) Herbig, M. E.; Assi, F.; Textor, M.; Merkle, H. P. *Biochemistry* **2006**, *45*, 3598-609.
(43) Li, S. D.; Huang, L. *Molecular Pharmaceutics* **2008**, *5*, 496-504.
(44) Tang, C.; Russell, P. J.; Martiniello-Wilks, R.; Rasko, J. E.; Khatri, A. *Stem Cells*.
(45) Phillips, M. A.; Gran, M. L.; Peppas, N. A. *Nano Today*, *5*, 143-159.
(46) Reilly, R. M. *J. Nucl. Med.* **2007**, *48*, 1039-1042.
(47) Sekhon, B. S.; Kamboj, S. R. *Nanomedicine*, *6*, 516-522.
(48) Tong, R.; Cheng, J. J. *Polymer Reviews* **2007**, *47*, 345-381.
(49) Bonoiu, A. C.; Mahajan, S. D.; Ding, H.; Roy, I.; Yong, K. T.; Kumar, R.; Hu, R.; Bergey, E. J.; Schwartz, S. A.; Prasad, P. N. *Proc. Natl. Acad. Sci. U. S. A.* **2009**, *106*, 5546-5550.
(50) Ortiz Mellet, C.; Benito, J. M.; Garcia Fernandez, J. M. *Chemistry*, *16*, 6728-42.
(51) Liu, C. H.; Yu, S. Y. *Colloids Surf B Biointerfaces*, *79*, 509-15.
(52) Goodman, C. M.; McCusker, C. D.; Yilmaz, T.; Rotello, V. M. *Bioconjug Chem* **2004**, *15*, 897-900.
(53) Green, J. J.; Langer, R.; Anderson, D. G. *Accounts of Chemical Research* **2008**, *41*, 749-759.
(54) Arsianti, M.; Lim, M.; Marquis, C. P.; Amal, R. *Langmuir*, *26*, 7314-26.
(55) Godbey, W. T.; Wu, K. K.; Mikos, A. G. *Biomaterials* **2001**, *22*, 471-480.
(56) Kloeckner, J.; Wagner, E.; Ogris, M. *Eur J Pharm Sci* **2006**, *29*, 414-25.
(57) Jere, D.; Jiang, H. L.; Arote, R.; Kim, Y. K.; Choi, Y. J.; Cho, M. H.; Akaike, T.; Chot, C. S. *Expert Opinion on Drug Delivery* **2009**, *6*, 827-834.

(58) Boussif, O.; Lezoualc'h, F.; Zanta, M. A.; Mergny, M. D.; Scherman, D.; Demeneix, B.; Behr, J. P. *Proc Natl Acad Sci U S A* **1995**, *92*, 7297-301.
(59) Laemmli, U. K. *Proc Natl Acad Sci U S A* **1975**, *72*, 4288-92.
(60) Ando, S.; Putnam, D.; Pack, D. W.; Langer, R. *Journal of Pharmaceutical Sciences* **1999**, *88*, 126-130.
(61) Lim, Y.; Kim, S. M.; Lee, Y.; Lee, W.; Yang, T.; Lee, M.; Suh, H.; Park, J. *J Am Chem Soc* **2001**, *123*, 2460-1.
(62) Shive, M. S.; Anderson, J. M. *Adv Drug Deliv Rev* **1997**, *28*, 5-24.
(63) Lynn, D. M.; Langer, R. *Journal of the American Chemical Society* **2000**, *122*, 10761-10768.
(64) Akinc, A.; Lynn, D. M.; Anderson, D. G.; Langer, R. *J. Am. Chem. Soc.* **2003**, *125*, 5316-23.
(65) Lynn, D. M.; Anderson, D. G.; Putnam, D.; Langer, R. *J Am Chem Soc* **2001**, *123*, 8155-6.
(66) Green, J. J.; Zugates, G. T.; Tedford, N. C.; Huang, Y.; Griffith, L. G.; Lauffenburger, D. A.; Sawicki, J. A.; Langer, R.; Anderson, D. G. *Adv Mater* **2007**, *19*, 2836-2842.
(67) Sunshine, J.; Green, J. J.; Mahon, K.; Yang, F.; Eltoukhy, A.; Nguyen, D. N.; Langer, R.; Anderson, D. G. *Adv Mater* **2009**, *21(48)*, 4947-4951.
(68) Zugates, G. T.; Tedford, N. C.; Zumbuehl, A.; Jhunjhunwala, S.; Kang, C. S.; Griffith, L. G.; Lauffenburger, D. A.; Langer, R.; Anderson, D. G. *Bioconjug Chem* **2007**, *18*, 1887-96.
(69) Green, J. J.; Shi, J.; Chiu, E.; Leshchiner, E. S.; Langer, R.; Anderson, D. G. *Bioconjug Chem* **2006**, *17*, 1162-1169.
(70) Anderson, D. G.; Peng, W.; Akinc, A.; Hossain, N.; Kohn, A.; Padera, R.; Langer, R.; Sawicki, J. A. *Proc Natl Acad Sci U S A* **2004**, *101*, 16028-33.
(71) Huang, Y. H.; Zugates, G. T.; Peng, W.; Holtz, D.; Dunton, C.; Green, J. J.; Hossain, N.; Chernick, M. R.; Padera, R. F., Jr.; Langer, R.; Anderson, D. G.; Sawicki, J. A. *Cancer Res* **2009**, *69*, 6184-91.
(72) Opanasopit, P.; Nishikawa, M.; Hashida, M. *Critical Reviews in Therapeutic Drug Carrier Systems* **2002**, *19*, 191-233.
(73) Ogris, M.; Brunner, S.; Schuller, S.; Kircheis, R.; Wagner, E. *Gene Therapy* **1999**, *6*, 595-605.
(74) Harada, A.; Kimura, Y.; Kojima, C.; Kono, K. *Biomacromolecules*, *11*, 1036-42.
(75) Petersen, H.; Fechner, P. M.; Martin, A. L.; Kunath, K.; Stolnik, S.; Roberts, C. J.; Fischer, D.; Davies, M. C.; Kissel, T. *Bioconjugate Chemistry* **2002**, *13*, 845-854.
(76) Subr, V.; Konak, C.; Laga, R.; Ulbrich, K. *Biomacromolecules* **2006**, *7*, 122-130.
(77) Yuan, Q.; Yeudall, W. A.; Yang, H. *Biomacromolecules*, *11*, 1940-7.
(78) Liu, Y.; Li, J.; Shao, K.; Huang, R.; Ye, L.; Lou, J.; Jiang, C. *Biomaterials*, *31*, 5246-57.
(79) Chen, Y.; Wu, J. J.; Huang, L. *Mol Ther*, *18*, 828-34.
(80) Liu, Z.; Tabakman, S. M.; Chen, Z.; Dai, H. *Nat Protoc* **2009**, *4*, 1372-82.
(81) Davis, M. E. *Molecular Pharmaceutics* **2009**, *6*, 659-668.
(82) Walker, G. F.; Fella, C.; Pelisek, J.; Fahrmeir, J.; Boeckle, S.; Ogris, M.; Wagner, E. *Mol Ther* **2005**, *11*, 418-25.
(83) Knorr, V.; Ogris, M.; Wagner, E. *Pharm Res* **2008**, *25*, 2937-45.

(84) Knorr, V.; Russ, V.; Allmendinger, L.; Ogris, M.; Wagner, E. *Bioconjug. Chem* **2008**, *19*, 1625-34.
(85) Carlisle, R. C.; Etrych, T.; Briggs, S. S.; Preece, J. A.; Ulbrich, K.; Seymour, L. W. *J Gene Med* **2004**, *6*, 337-44.
(86) Murthy, N.; Campbell, J.; Fausto, N.; Hoffman, A. S.; Stayton, P. S. *J Control Release* **2003**, *89*, 365-74.
(87) Harris, T. J.; Green, J. J.; Fung, P. W.; Langer, R.; Anderson, D. G.; Bhatia, S. N. *Biomaterials* **2010**, *31*, 998-1006.
(88) Shmueli, R. B.; Anderson, D. G.; Green, J. J. *Expert Opin. Drug Deliv.* **2010**, *7*, 535-550.
(89) Abdelhady, H. G.; Allen, S.; Davies, M. C.; Roberts, C. J.; Tendler, S. J. B.; Williams, P. M. *Nucleic Acids Research* **2003**, *31*, 4001-4005.
(90) Lechardeur, D.; Sohn, K. J.; Haardt, M.; Joshi, P. B.; Monck, M.; Graham, R. W.; Beatty, B.; Squire, J.; O'Brodovich, H.; Lukacs, G. L. *Gene Therapy* **1999**, *6*, 482-497.
(91) Schaffer, D. V.; Fidelman, N. A.; Dan, N.; Lauffenburger, D. A. *Biotechnology and Bioengineering* **2000**, *67*, 598-606.
(92) Walter, E.; Moelling, K.; Pavlovic, J.; Merkle, H. P. *Journal of Controlled Release* **1999**, *61*, 361-374.
(93) Shu, X. Z.; Zhu, K. J. *J Microencapsul* **2001**, *18*, 237-45.
(94) Weecharangsan, W.; Opanasopit, P.; Ngawhirunpat, T.; Rojanarata, T.; Apirakaramwong, A. *Aaps Pharmscitech* **2006**, *7*, -.
(95) Zhao, X.; Yin, L. C.; Ding, J. Y.; Tang, C.; Gu, S. H.; Yin, C. H.; Mao, Y. M. *Journal of Controlled Release* **2010**, *144*, 46-54.
(96) Lou, Y. L.; Peng, Y. S.; Chen, B. H.; Wang, L. F.; Leong, K. W. *Journal of Biomedical Materials Research Part A* **2009**, *88A*, 1058-1068.
(97) Rethore, G.; Mathew, A.; Naik, H.; Pandit, A. *Tissue Engineering Part C-Methods* **2009**, *15*, 605-613.
(98) Yuan, X. D.; Shah, B. A.; Kotadia, N. K.; Li, J. A.; Gu, H.; Wu, Z. Q. *Pharmaceutical Research* **2010**, *27*, 1285-1295.
(99) Mao, H. Q.; Roy, K.; Troung-Le, V. L.; Janes, K. A.; Lin, K. Y.; Wang, Y.; August, J. T.; Leong, K. W. *J Control Release* **2001**, *70*, 399-421.
(100) Thomas, M.; Klibanov, A. M. *Proc Natl Acad Sci U S A* **2003**, *100*, 9138-43.
(101) Elbakry, A.; Zaky, A.; Liebl, R.; Rachel, R.; Goepferich, A.; Breunig, M. *Nano Lett.* **2009**, *9*, 2059-64.
(102) Bauhuber, S.; Hozsa, C.; Breunig, M.; Göpferich, A. *Advanced Materials* **2009**, *21*, 3286-3306.
(103) Greish, K. *J Drug Target* **2007**, *15*, 457-64.
(104) Moffatt, S.; Cristiano, R. J. *Int J Pharm* **2006**, *317*, 10-3.
(105) Liu, Y.; Li, K.; Liu, B.; Feng, S. S. *Biomaterials*.
(106) Pissuwan, D.; Valenzuela, S. M.; Killingsworth, M. C.; Xu, X. D.; Cortie, M. B. *Journal of Nanoparticle Research* **2007**, *9*, 1109-1124.
(107) Dauty, E.; Remy, J. S.; Zuber, G.; Behr, J. P. *Bioconjug Chem* **2002**, *13*, 831-839.
(108) Hashida, M.; Nishikawa, M.; Yamashita, F.; Takakura, Y. *Adv Drug Deliv Rev* **2001**, *52*, 187-96.
(109) Kunath, K.; Merdan, T.; Hegener, O.; Haberlein, H.; Kissel, T. *J Gene Med* **2003**, *5*, 588-599.

(110) Green, J. J.; Chiu, E.; Leshchiner, E. S.; Shi, J.; Langer, R.; Anderson, D. G. *Nano Lett* **2007**, *7*, 874-9.
(111) Ogris, M.; Walker, G.; Blessing, T.; Kircheis, R.; Wolschek, M.; Wagner, E. *J. Controlled Release* **2003**, *91*, 173-181.
(112) Levy-Nissenbaum, E.; Radovic-Moreno, A. F.; Wang, A. Z.; Langer, R.; Farokhzad, O. C. *Trends Biotechnol* **2008**, *26*, 442-9.
(113) Nguyen, J.; Reul, R.; Betz, T.; Dayyoub, E.; Schmehl, T.; Gessler, T.; Bakowsky, U.; Seeger, W.; Kissel, T. *Journal of Controlled Release* **2009**, *140*, 47-54.
(114) Elfinger, M.; Pfeifer, C.; Uezguen, S.; Golas, M. M.; Sander, B.; Maucksch, C.; Stark, H.; Aneja, M. K.; Rudolph, C. *Biomacromolecules* **2009**, *10*, 2912-2920.
(115) Alexis, F.; Rhee, J. W.; Richie, J. P.; Radovic-Moreno, A. F.; Langer, R.; Farokhzad, O. C. *Urol Oncol* **2008**, *26*, 74-85.
(116) Liao, H.; Hafner, J. H. *Chemistry of Materials* **2005**, *17*, 4636-4641.
(117) Kawano, T.; Yamagata, M.; Takahashi, H.; Niidome, Y.; Yamada, S.; Katayama, Y.; Niidome, T. *J Control Release* **2006**, *111*, 382-9.
(118) Rojas-Chapana, J.; Troszczynska, J.; Firkowska, I.; Morsczeck, C.; Giersig, M. *Lab Chip* **2005**, *5*, 536-9.
(119) Ladewig, K.; Niebert, M.; Xu, Z. P.; Gray, P. P.; Lu, G. Q. M. *Biomaterials* **2010**, *31*, 1821-1829.
(120) Tang, M.; Russell, P. J.; Khatri, A. *Discov Med* **2007**, *7*, 68-74.
(121) Cai, D.; Mataraza, J. M.; Qin, Z. H.; Huang, Z. P.; Huang, J. Y.; Chiles, T. C.; Carnahan, D.; Kempa, K.; Ren, Z. F. *Nat. Methods* **2005**, *2*, 449-454.
(122) Rahim, A.; Taylor, S. L.; Bush, N. L.; ter Haar, G. R.; Bamber, J. C.; Porter, C. D. *Ultrasound Med Biol* **2006**, *32*, 1269-79.
(123) Stride, E.; Porter, C.; Prieto, A. G.; Pankhurst, Q. *Ultrasound Med Biol* **2009**, *35*, 861-8.
(124) Lee, P. W.; Peng, S. F.; Su, C. J.; Mi, F. L.; Chen, H. L.; Wei, M. C.; Lin, H. J.; Sung, H. W. *Biomaterials* **2008**, *29*, 742-51.
(125) Sonawane, N. D.; Szoka, F. C., Jr.; Verkman, A. S. *J Biol Chem* **2003**, *278*, 44826-31.
(126) Akinc, A.; Thomas, M.; Klibanov, A. M.; Langer, R. *Journal of Gene Medicine* **2005**, *7*, 657-663.
(127) Yang, Y. X.; Xul, Z. H.; Chen, S. W.; Gao, Y.; Gu, W. W.; Chen, L. L.; Pei, L. Y.; Li, Y. P. *International Journal of Pharmaceutics* **2008**, *353*, 277-282.
(128) Ogris, M.; Carlisle, R. C.; Bettinger, T.; Seymour, L. W. *J Biol Chem* **2001**, *276*, 47550-5.
(129) Rozema, D. B.; Ekena, K.; Lewis, D. L.; Loomis, A. G.; Wolff, J. A. *Bioconjugate Chemistry* **2003**, *14*, 51-57.
(130) Boeckle, S.; Fahrmeir, J.; Roedl, W.; Ogris, M.; Wagner, E. *Journal of Controlled Release* **2006**, *112*, 240-248.
(131) Meyer, M.; Philipp, A.; Oskuee, R.; Schmidt, C.; Wagner, E. *Journal of the American Chemical Society* **2008**, *130*, 3272-3273.
(132) Murata, M.; Kagiwada, S.; Hishida, R.; Ishiguro, R.; Ohnishi, S.; Takahashi, S. *Biochem Biophys Res Commun* **1991**, *179*, 1050-5.
(133) Midoux, P.; Mayer, R.; Monsigny, M. *Biochim Biophys Acta* **1995**, *1239*, 249-56.

(134) Wagner, E.; Plank, C.; Zatloukal, K.; Cotten, M.; Birnstiel, M. L. *Proc. Natl Acad. Sci.* **1992**, *89*, 7934-8.
(135) Moore, N. M.; Sheppard, C. L.; Barbour, T. R.; Sakiyama-Elbert, S. E. *J Gene Med* **2008**, *10*, 1134-49.
(136) Hwang, C.; Sinskey, A. J.; Lodish, H. F. *Science* **1992**, *257*, 1496-502.
(137) Mellman, I. *Annu Rev Cell Dev Biol* **1996**, *12*, 575-625.
(138) Coussens, L. M.; Fingleton, B.; Matrisian, L. M. *Science* **2002**, *295*, 2387-2392.
(139) Gross, J.; Lapiere, C. M. *Proc. Natl. Acad. Sci. U. S. A.* **1962**, *48*, 1014-&.
(140) Niidome, Y.; Niidome, T.; Yamada, S.; Horiguchi, Y.; Takahashi, H.; Nakashima, K. *Molecular Crystals and Liquid Crystals* **2006**, *445*, 201 - 206.
(141) Jon, S.; Anderson, D. G.; Langer, R. *Biomacromolecules* **2003**, *4*, 1759-1762.
(142) Jewell, C. M.; Zhang, J. T.; Fredin, N. J.; Wolff, M. R.; Hacker, T. A.; Lynn, D. M. *Biomacromolecules* **2006**, *7*, 2483-2491.
(143) Schaffer, D. V.; Lauffenburger, D. A. *J Biol Chem* **1998**, *273*, 28004-9.
(144) Lin, C.; Engbersen, J. F. *Expert Opin Drug Deliv* **2009**, *6*, 421-39.
(145) Lin, C.; Lammens, T. M.; Zhong, Z. Y.; Gu, H.; Lok, M. C.; Jiang, X.; Hennink, W. E.; Feijen, J.; Engbersen, J. F. *J Control Release* **2006**, *116*, e79-81.
(146) Lin, C.; Zhong, Z.; Lok, M. C.; Jiang, X.; Hennink, W. E.; Feijen, J.; Engbersen, J. F. *J Control Release* **2006**, *116*, 130-7.
(147) Piest, M.; Lin, C.; Mateos-Timoneda, M. A.; Lok, M. C.; Hennink, W. E.; Feijen, J.; Engbersen, J. F. *J Control Release* **2008**, *130*, 38-45.
(148) Saito, G.; Swanson, J. A.; Lee, K. D. *Advanced Drug Delivery Reviews* **2003**, *55*, 199-215.
(149) Lee, Y.; Mo, H.; Koo, H.; Park, J. Y.; Cho, M. Y.; Jin, G. W.; Park, J. S. *Bioconjug. Chem* **2007**, *18*, 13-8.
(150) Manickam, D. S.; Li, J.; Putt, D. A.; Zhou, Q. H.; Wu, C.; Lash, L. H.; Oupicky, D. *J Control Release*, *141*, 77-84.
(151) Chen, J.; Wu, C.; Oupicky, D. *Biomacromolecules* **2009**, *10*, 2921-7.
(152) Sunshine, J.; Bhise, N.; Green, J. J. *Conf Proc IEEE Eng Med Biol Soc* **2009**, *2009*, 2412-5.
(153) Bhise, N. S.; Gray, R. S.; Sunshine, J. C.; Htet, S.; Ewald, A. J.; Green, J. J. *Biomaterials*, *31*, 8088-96.
(154) Stevenson, M.; Ramos-Perez, V.; Singh, S.; Soliman, M.; Preece, J. A.; Briggs, S. S.; Read, M. L.; Seymour, L. W. *J Control Release* **2008**, *130*, 46-56.
(155) Gosselin, M. A.; Guo, W. J.; Lee, R. J. *Bioconjug Chem* **2001**, *12*, 989-994.
(156) Hoon Jeong, J.; Christensen, L. V.; Yockman, J. W.; Zhong, Z.; Engbersen, J. F.; Jong Kim, W.; Feijen, J.; Wan Kim, S. *Biomaterials* **2007**, *28*, 1912-7.
(157) Jere, D.; Kim, J. E.; Arote, R.; Jiang, H. L.; Kim, Y. K.; Choi, Y. J.; Yun, C. H.; Cho, M. H.; Cho, C. S. *Biomaterials* **2009**, *30*, 1635-47.
(158) Chen, C. C.; Lin, Y. P.; Wang, C. W.; Tzeng, H. C.; Wu, C. H.; Chen, Y. C.; Chen, C. P.; Chen, L. C.; Wu, Y. C. *J Am Chem Soc* **2006**, *128*, 3709-15.
(159) Takahashi, H.; Niidome, Y.; Yamada, S. *Chem Commun (Camb)* **2005**, 2247-9.
(160) Wijaya, A.; Schaffer, S. B.; Pallares, I. G.; Hamad-Schifferli, K. *ACS Nano* **2009**, *3*, 80-6.
(161) Dauty, E.; Verkman, A. S. *Journal of Biological Chemistry* **2005**, *280*, 7823-7828.

(162) Pouton, C. W.; Wagstaff, K. M.; Roth, D. M.; Moseley, G. W.; Jans, D. A. *Advanced Drug Delivery Reviews* **2007**, *59*, 698-717.
(163) Stewart, M. *Nature Reviews Molecular Cell Biology* **2007**, *8*, 195-208.
(164) Pante, N.; Kann, M. *Molecular Biology of the Cell* **2002**, *13*, 425-434.
(165) Mislick, K. A.; Baldeschwieler, J. D.; Kayyem, J. F.; Meade, T. J. *Bioconjug. Chem.* **1995**, *6*, 512-515.
(166) Midoux, P.; Monsigny, M. *Bioconjug. Chem.* **1999**, *10*, 406-411.
(167) Nishikawa, M.; Takemura, S.; Takakura, Y.; Hashida, M. *J. Pharmacol. Exp. Ther.* **1998**, *287*, 408-415.
(168) Fischer, D.; Bieber, T.; Li, Y. X.; Elsasser, H. P.; Kissel, T. *Pharm. Res.* **1999**, *16*, 1273-1279.
(169) Thomas, M.; Lu, J. J.; Ge, Q.; Zhang, C.; Chen, J.; Klibanov, A. M. *Proc. Natl Acad. Sci.* **2005**, *102*, 5679-84.
(170) Anderson, D. G.; Akinc, A.; Hossain, N.; Langer, R. *Mol. Ther.* **2005**, *11*, 426-434.
(171) Wood, K. C.; Little, S. R.; Langer, R.; Hammond, P. T. *Angew Chem Int Ed Engl* **2005**, *44*, 6704-8.
(172) Roy, K.; Mao, H. Q.; Huang, S. K.; Leong, K. W. *Nat. Med.* **1999**, *5*, 387-91.
(173) Shen, H.; Tan, J.; Saltzman, W. M. *Nat. Mater.* **2004**, *3*, 569-574.
(174) Maeda-Mamiya, R.; Noiri, E.; Isobe, H.; Nakanishi, W.; Okamoto, K.; Doi, K.; Sugaya, T.; Izumi, T.; Homma, T.; Nakamura, E. *Proc. Natl. Acad. Sci. U. S. A.* **2010**, *107*, 5339-5344.
(175) Zhang, P.; Liu, W. G. *Biomaterials* **2010**, *31*, 3087-3094.
(176) Woodrow, K. A.; Cu, Y.; Booth, C. J.; Saucier-Sawyer, J. K.; Wood, M. J.; Saltzman, W. M. *Nat. Mat.* **2009**, *8*, 526-533.
(177) Hom, C.; Lu, J.; Liong, M.; Luo, H. Z.; Li, Z. X.; Zink, J. I.; Tamanoi, F. *Small* **2010**, *6*, 1185-1190.
(178) del Pino, P.; Munoz-Javier, A.; Vlaskou, D.; Gil, P. R.; Plank, C.; Parak, W. J. *Nano Lett.* **2010**, *10*, 3914-3921.

2.3 Polymer and Inorganic Vectors for Nucleic Acid Delivery

2.3.1 Cationic Polymers

Various cationic polymer systems have been utilized for nucleic acid delivery. A wide range of structures have been explored, including linear and branched non-

Chapter 2.3 is published as "Sunshine JC, Bishop CJ, Green, JJ. Advances in polymeric and inorganic vectors for nonviral nucleic acid delivery. *Ther. Deliv.* 2011;2(4):493-521".

degradable polycations as well as biodegradable and bioreducible polycations and oligosacharides. Some of the most commonly used polymer structures are shown in Fig. 1. All of the cationic polymers have primary amine groups which are protonated at neutral pH, which enables electrostatic interaction with the anionic nucleic acid.

Poly-L-lysine (PLL) was one of the first polymeric gene transfection agents developed, and was shown to condense DNA into small complexes with rod (25-50 nm) or toroidal (40 to 80 nm) structure [1]. PLL can be synthesized by several-step polymerization of ε,N-benzyloxycarbonyl-α,N-carboxy-L-lysine anhydride[2]. PLL is especially limited for intracellular delivery by its lack of an endosomal escape mechanism and endosomolytic groups like histidine [3] have been used to improve delivery. To reduce serum interaction and increase cell uptake, a variety of other molecules such as poly(ethylene glycol) (PEG)[4], and targeting ligands such as asialoorosomucoid [5], transferrin [6], galactose [7,8], lactose [9], and folate [10] have been conjugated to PLL. Poly(ethylenimine) (PEI) was the second polymeric transfection agent developed [11]. Branched PEI (b-PEI) can be synthesized from aziridine monomers under acidic conditions, and linear PEI (l-PEI) can be synthesized by the hydrolysis of poly(2-proplyl-2-oxazoline)[12], or by polymerization of aziridine monomers at lower temperatures [13]. Compared to later generation nucleic acid delivery agents, PEI is cytotoxic, leading to necrosis and apoptosis [14]. The high proportion of nitrogen atoms provides for a strong buffering effect ("the proton sponge effect") which is advantageous for endosomal escape, as described below. 25 kDa b-PEI has been shown to be an efficient transfection reagent with reduced toxicity as compared to higher molecular weight b-PEI [15]. For delivery of shorter nucleic acids (e.g. mRNA) low molecular weight

PEI (2 kDa or less) leads to enhanced biological effect, as complexes with higher molecular weight PEI are more stable and do not release the nucleic acid as efficiently into the cytoplasm [16]. Standard PEI has also been modified by deacylation to boost delivery of DNA and siRNA by orders of magnitude *in vitro* and *in vivo* [17].

Poly(lactide-co-glycolide) (PLGA) microspheres have been used in nucleic acid delivery in part for their relative biocompatibility and biodegradability. PLGA is synthesized by co-polymerization of cyclic dimers of glycolic acid and lactic acid with various catalysts. Microparticles can be formed from pre-made polymer by emulsion evaporation, emulsion diffusion, solvent displacement and salting out techniques, and particle size depends on the formulation conditions and molecular weight of the starting material [18]. Both the polymer and its degradation products are well tolerated in animal studies [19,20]. PLGA has recently been used to delivery siRNA *in vivo* and achieved sustained gene silencing when delivered to the vaginal mucosa [21].

Poly(β-amino ester)s (PBAE) are synthesized by Michael addition of either primary or bis(secondary) aliphatic amines to diacrylate compounds [22], and their simple chemistry leads them naturally to a combinatorial approach to synthesis and screening of polymer libraries [23-27]. They are hydrolytically degradable at the backbone ester linkages which allow for release of nucleic acid cargoes and reduced cytotoxicity.

As opposed to mostly linear, cross-linked, or other branched systems, dendrimers such as poly(amido amine) (PAMAM) dendrimers are synthesized iteratively to produce nanoscale structures characterized by dendritic connectivity and radial symmetry. Advantages of dendrimeric systems include precise, nanoscale, structural control, dense and tunable surface chemistry (for addition of targeting ligands, modification of surface

charge, etc.), and high charge density for complexation and buffering. PAMAM dendrimers were first synthesized in the mid 1980s [28]. Typically, ethyenediamine or ammonia are used as cores and allowed to undergo repeating two-step reactions whereby methyl acrylate is added by Michael addition to all the primary amines, and then the ester groups are amidated by a large excess of ethylenediamine to produce primary amine termini. They have been extensively studied for gene delivery [29,30] as well as oligonucleotide delivery [31-34]. Interestingly, thermal degradation of the dendrimers was shown to increase transfection efficacy [35]. Dendrons, rather than full dendrimers, have also been used for successful gene delivery [36]. Mannose-PEG-PAMAM linear-dendritic hybrid polymers successfully delivered the luciferase gene to P388D1 murine macrophages bearing the mannose-receptor, and showed 1.6 to 1.8-fold more efficient transfection of these cells than PEI with no serum and 4-fold more efficient transfection in the presence of serum; this boosted transfection was shown to be targeting ligand dependant [36].

2.3.2 Oligosaccharides

Sugars are crucial in a wide variety of biological applications. They are hydrophilic molecules composed predominantly of carbon, hydrogen and oxygen, and exist both in ring form as well as in extended conformations. Every extracellular protein in the human body is glycosylated (addition of oligosaccharides to proteins). The ABO blood group antigens are oligosaccharides, and oligosaccharides play a crucial role in tethering and rolling via the interaction of selectins to sialyl-lewis X [37]. Glycosylation is a

crucial consideration in the production of monoclonal antibodies (mAb) for therapeutics in terms of optimization of biological activity [38] and improved pharmacological profile [39].

Due to the hydrophilic nature of oligosaccharides and the fact that sugars are relatively well tolerated by the body, cationic polysaccharides have been explored for gene and nucleic acid delivery. Cyclodextrins (CD) are produced by the degradation of starch by the enzyme glucosyltransferase. This generates natural cyclic oligosaccharides composed of 6, 7, or 8 D(+)-glucose units known as alpha, beta and gamma cyclodextrins. Cyclodextrins are of particular interest because in addition to showing low toxicity, good biocompatibility, they can form inclusion complexes with small, hydrophobic compounds. This ability allows for modification of the surface of the cyclodextrin-based particles without interfering with polycation/nucleic acid interactions and particle morphology [40]. Polycationic cyclodextrins have been shown to transfect cells in serum in a comparable level to 1,2-dioleoyl-3-trimethylammonium propane (DOTAP) [41]. Grafting of cyclodextrins onto a PEI polymer lead to reduced transfection efficacy depending on the extent of modification (increased modification lead to further decreases in transfection efficacy) but significantly reduced toxicity [40]. Interestingly, however, grafting of cyclodextrins onto PAMAM dendrimers increased their transfection efficacy (100x that of the dendrimer alone and comparable to Lipofectin and TransFast); the optimal formulation used α-cyclodextrin [42].

One excellent recent example of utilizing cyclodextrins for nucleic acid delivery currently in clinical trials is CALAA-01. CALAA-01 is a cyclodextrin-containing polymer (CDP) for siRNA delivery which is sterically stabilized by PEGylation and modified to contain human transferrin (Tf) for targeting [43,44]. The CDPs are synthesized

by condensing two difunctionalized comonomers. In addition, imidazole end group modifications were added to enhance endosomal escape [45]. Interestingly, separate *in vivo* studies using earlier constructs for for DNA and DNAzyme delivery showed that nanoparticle localization to the tumors was independent of the targeting ligand but addition of the targeting ligand increased tumor cell uptake [46,47]. CALAA was later formulated for siRNA delivery, and after animal studies was used to treat the first patient in a phase I clinical trial in May 2008 [45]; this trial was able to provide evidence of inducing an RNAi mechanism of action in a human from the delivered siRNA for the first time [44].

Another sugar used significantly in drug and nucleic acid delivery is chitosan. Chitosan is formed by the deacetylation of chitin. It is mucoadhesive and biodegradable, with a reasonable toxicity profile, and has been specifically useful in transmucosal drug delivery [48]. Oral administration of chitosan and Arah2 (a peanut allergy gene) was shown to significantly decrease IgE levels in response to anaphylaxis induction [49]. N-alkylated chitosan was investigated for gene delivery, and lengthening the side chains to 8-carbons was found to improve gene delivery [50]. The optimal trimethyl chitosan-cysteine conjugate showed 1.5-fold higher in-vitro and 4.1-fold higher in-vivo transgene expression when compared to Lipofectamine 2000 [51]. Imidazole-modified chitosan siRNA delivery showed good gene knockdown in the lungs and the liver [52]. Chitosan hydroxybenzotriazole showed ~60% knockdown of the control enhanced green fluorescent protein gene expression [53].

2.3.3 Inorganic Materials

Many types of inorganic nanoparticles are in use today for gene therapy and have properties that can be exploited for multifunctional use (i.e., theranostics – therapy and diagnostics). A large portion of these are gold nanoparticles (AuNP) [54-70] (Fig. 2A-C), carbon nanotubes (CNTs) [71-76]] (Fig. 2D,E), silica [71,77-81] (Fig. 2F), quantum dots (QD) [82-89] (Fig. 2G), superparamagnetic iron oxide nanoparticles (SPION) (Fig. 2H) [88,90-93], layered double hydroxide nanoparticles (LDH) [94] (Fig. 2I).

2.3.4 Gold Nanoparticles

AuNPs' structures can be solid spheres (Fig. 2A), rods (Fig. 2B), or shells (Fig. 2D). Many investigators synthesize AuNP spheres by dissolving tetrachloroauric acid ($HAuCl_4$) in purified water and then adding a reducing agent (i.e., sodium borohydride, sodium citrate) converting Au(III) to its neutral form [54,57-59,95]. To make gold nanorods (AuNR), a seed solution and a growth solution can be prepared separately and mixed. A possible seed solution uses CTAB, $HAuCl_4$, and $NaBH_4$ and a possible growth solution uses CTAB, $AgNO_3$, $HAuCl_4$, and ascorbic acid [60]. When AuNP shells are synthesized, a shell forms around a core. Investigators have used the reverse micelle method [61] or the Stöber method [62] to synthesize AuNP shells. AuNP shells have encapsulated SiO_2 [63], Fe [61,64], Pt [56] and other materials. Other ways to synthesize AuNPs are citrate reduction or the Brust-Schiffrin method as reported by Daniel et al. [65] . The timing and the relative amounts of reagents used can be varied to tune the size of the AuNPs [65].AuNPs are known to have low cytotoxicity, can be synthesized with decent monodispersity, and can be conjugated at high densities with a wide range of organic molecules [66,67]. AuNPs can

be functionalized with antibodies for the detection of molecules. The detection is made possible because AuNPs have surface plasmon resonance effects which scatter light at various intensities and absorb light at different wavelengths dependent on their size and degree of aggregation [68]. For example, the high expression of a surface receptor (i.e., folic acid receptor [107], EGFR [68], HER2 [62]) due to the presence of a cancer can cause an increase in AuNP-antibody local concentration which causes a shift in optical properties and detection. In addition, AuNPs do not undergo photobleaching [68].

Furthermore, AuNPs can be used to localize photothermal cancer therapy. Spatially localizing the thermal therapy minimizes collateral damage. The AuNPs can be excited at near-infrared wavelengths to produce heat in an aspect-ratio dependent manner [55,62,69]. The near-infrared light can be applied externally as biological tissue does not attenuate the energy significantly which allows for control over timing of the thermotherapy.

2.3.5 Fullerenes

Fullerenes are carbon-only nanostructures (i.e., spherical, cylindrical, ellipsoidal). The two most common nanostructures applied to nanomedicine are carbon nanotubes (CNT) and spherical fullerenes (C-60 buckyballs) as discussed below.

2.3.6 Carbon Nanotubes

CNTs are highly ordered and hollow [70]. They are single atom thick cylinders of sp^2- bonded carbon atoms [70]. CNTs can be synthesized by a variety of methods including laser ablation, arc discharge, thermal chemical deposition, and plasma-enhanced chemical

vapor deposition [72] (Refer to cited literature for an in depth discussion of methods (i.e., [73]). Post synthesis, CNTs can be sonicated to a desired length with some size restraints [74].

Single-walled and multi-walled CNT diameters can be 1-2 nm and 2 to 25 nm, respectively [74] (Fig. 2D,E). Spherical, hydrophobic carbon-nanostructures can be cationically functionalized via amine groups to become soluble and to enable ionic complexation with nucleic acids [75] for gene delivery applications. Carbon nanostructures can be conjugated to antibodies to increase specificity [96]. The single-walled CNTs have Raman signal to improve cancer detection and near-infrared absorption for photothermal applications [96] similar to AuNPs. CNTs have unprecedented high tensile strength [72] and CNTs' electrical and thermal conductivities make them useful for biosensor applications [72]. CNTs also have high surface area for dense loading of cargo [23,97]. Its needle-like shape can also enable the penetration of cell membranes with greater ease [97], however, its structural similarity to asbestos warrants further research [98]. Nanotoxicology of these materials and other nanomedicines is important to consider prior to any clinical experimentation[89].

CNTs are cytotoxic as there is lipid membrane peroxidation due to residual metal catalysts. Due to this toxicity CNTs are known to down-regulate adhesive proteins and increase cell death (aspect ratio dependent), but can be non-toxic to primary immune cells when functionalized appropriately [99]. Poly(amido amine) dendrimers can be used to coat multi-walled CNTs to improve biocompatibility and cellular uptake [99]. Glycodendrimers can be used to coat single-walled CNTs to lower cytoxicity as well [100]. DNA-CNT complexes have been demonstrated to be non-toxic and non-mitogenic to activated or non-activated lymphocytes [101]. Larger carbon nanomaterials (i.e., fibers, flakes) are less

toxic than single-walled or multi-walled CNTs, possibly due to their different interaction with the cellular membrane [102]. Aggregation of CNTs can influence their toxicity due to the alteration of their physical properties [103]. Fullerenes can be stabilized via functional groups to decrease cell death. For example, functionalization using SWNT in 1% Pluronic F108 at 2 μg/ml, di-carboxylation with a carbon to functional group ratio of 23 at 2 mg/mL, SO_3H with a carbon to functional group ratio of 80, 41, and 18 at 2 mg/mL resulted in ~65, 50, 40, 15, and nearly 0% cell death, respectively [104,105].

2.3.7 Spherical Fullerenes

Carbon-60 Spherical fullerenes (buckyballs) are around 1 nm in diameter. They have a propensity to aggregate, and are hydrophobic but can be made to be hydrophilic by the addition of functional groups (i.e., amine, carboxyl), particularly by the Hirsch-Bingel reaction [106]. Hydrophilic buckyballs mainly localize in the liver and have slow metabolism [106]. Buckyballs can function as an anti-oxidant for neuroprotective applications[76], an anti-viral agent such as HIV, a gene delivery carrier (particularly amine-derivatized fullerenes), and as a photosensitizer for photodynamic therapy applications [106]. Buckyballs can carry an unstable atom (i.e., Gd^{3+}, ^{99m}Tc -- which mainly localizes in macrophages of the bone marrow, liver, and spleen) which is not released into the biological system and can then be used as an MRI contrast agent, X-ray imaging agent, or radiopharmaceutical [106].

2.3.8 Silica Nanoparticles

Mesoporous silica nanoparticles (Fig. 2F) used for gene therapy are commonly synthesized using tetraethyl orthosilicate and cetyltrimethyl ammonium bromide (CTAB) under basic conditions using sodium hydroxide [78,79] or aqueous ammonia [107] at ~80°C. By varying the amount of CTAB added the nanoparticles' size can be modified [107]. Mesoporous silica nanoparticles are used in gene delivery because they have relatively large surface areas for dense conjugation, tunable pore sizes for cargo encapsulation, and are surface modifiable [78].

A few non-exhaustive applications of silica nanoparticles include the delivery of nucleic acids (siRNA) by functionalization of PEI for ionic complexation [78], the delivery of GFP to osteoblasts by ionic complexation of conjugated Ca-silica [81], and the delivery of genes (luciferase) to the Achilles tendon [70].

Silica nanoparticles can activate macrophages and produce pro-inflammatory cytokines and reactive oxygen species [108]. Positively charged silica nanotubes are significantly more toxic than their bare counterparts. Toxicity was also significantly greater for positively charged silica nanotubes that were 200 nm versus 500 nm for a given mass in both HUVEC and MDA-MB-231 cell lines [109]. It was reported that the smaller particles have a greater extent of interaction with cells and therefore increased cytotoxicity [109].

2.3.9 Quantum Dots

Quantum dots (QD) are composed in pairs of semiconductor elements (i.e., ZnS, CdS, CdSe, InP, CdTe, PbS, PbTe). For example, CdSe QDs can be synthesized by

adding cadmium oxide to tetradecylphosphonic acid and trioctylphosphine oxide at 300ºC under Ar flow to dissolve the Cd. At 270ºC, a Se solution of tri-n-octylphosphine is injected. The QDs can be grown at 250ºC for different lengths of time to control size. This solution can then be injected into chloroform and the CdSe will then precipitate out of solution [82].

For biological applications QDs are sometimes synthesized in a core-shell fashion. The shell is chosen such that the band gap is winder than the core. This improves fluorescence properties, passivates the core, and prevents leaching (i.e., of toxic Cd ions) [83]. Heavy metal ions (i.e., Cd2+) are toxic at low concentrations (0.65 μM); however, when using silica shells and silane-PEGylation (methoxy(polyethyleneoxy)propyltrimethoxysilane (Gelest P/N SIM6492.7) (MW=450-600)), there was no toxicity observed at quantum dot concentrations up to 30 μM [110].

QDs' photoluminescence spectra are resistant to photobleaching [84] and emission is narrow, symmetrical, and tunable as a function of core size [83]. Figure 2G shows the color dependence of different radii of CdSe core QDs with emission [77]. The intensity of the fluorescence typically has a half-life of 27 hours which is many fold greater than other fluorescence agents (i.e., Alexaflour, R-phycoerythrin, and FITC) [83].

QDs can be carboxylated to conjugate peptidyl amine residues or aminated by 2-aminoethane thiol hydrochloride for maleimide derivatization. Thiolated and polyhistidine-conjugated biologicals can also directly interact and self-assemble on the surface of QDs, respectively [83].

QDs have been encapsulated in chitosan nanoparticles to track and monitor siRNA delivery and transfection of SKBR3 breast cancer cells [87]. QDs have been used to

quantify and monitor changes in transgene expression of two similar prostate cancer cell lines (PC3 and PC3-PSMA) due to changes in microtubule dynamics [86]. QDs have been used for multiplex fluorescence imaging, tumor cell extravasation tracking, and real-time *in vivo* imaging [84].

2.3.10 Superparamagnetic Iron Oxide Nanoparticles

Superparamagnetism relates to the stochastic magnetization changes of nanoparticles. In the absence of a magnetic field, the nanoparticles have an average magnetic state of zero. However, under an external magnetic field, magnetism is induced and their magnetic susceptibility is stronger to that of paramagnets [111]. Superparamagnetic Iron Oxide Nanoparticles (SPION) are typically comprised of a crystalline iron-oxide core coated with a biomaterial (i.e., dextran, starch) [90] and synthesized by co-precipitation in water [91]. In one example, SPIONs can be synthesized by precipitation in a reverse water-in-oil microemulsion system of water/SDS and 1-butanol/cyclohexane [92]. SPIONs can also be synthesized in an aqueous solution by co-precipitation of ferric and ferrous chlorides in alkaline medium [88].

SPIONs constitute a hydrophobic crystalline iron-oxide core which can be coated with relatively hydrophilic and or biocompatible materials (i.e., dextran, starch, polyol derivatives, phospholipids, silica, or amphiliphilic polymers) [89]. SPIONs can be conjugated with targeting moieties and gene delivery carriers. Figure 2H shows doxorubicin-loaded SPIONs.

SPIONS are rapidly cleared by the reticuloendothelial system (also known as the mononuclear phagocyte system). SPIONs (namely Ferumoxides and Ferumoxtran-10,

magnetic resonance contrast agents) are mainly cleared in the liver by Kupffer cells in a nanoparticle size-dependent manner [112]. Another SPION formulation (AMI-25) resulted in 80% uptake of the initial dose by Kupffer cells and its half life was 10 minutes [113].

SPIONs can be used for delivery systems via magnetofection, contrast enhancers for magnetic resonance imaging for T2 and T2* weighted imaging [89,114], tissue repair, immunoassays, detoxification, and anticancer magnetic hyperthermia [92,93]. Iron oxide nanoparticles that are associated with Metafectene and dioleoylphosphatidyl-ethanolamine delivering anti-eGFP and firefly luciferase have been known to accomplish at least 90% knockdown at 48 hours post transfection with reasonable cell viability using the HeLa cell line [115].

SPIONs are metabolized in the hepato-renal system and are capable of entering the endogenous iron reserves by means of hematopoiesis [116].

2.3.11 Layered Double Hydroxide Nanoparticles

Layered double hydroxide nanoparticles (LDHNP) are anionic clay materials which can be generally written as $[M^{II}_{n}M^{III}(OH)_{2+2n}]^{+}(A^{m-})_{1/m}$ x H_20 (n=2-4) ($M^{II/III}$ = di/trivalent metal cation, A^{m-} = anion) [94]. LDHNPs can be synthesized by dissolving 3 mmol of $Mg(NO_3)_2$ and 1 mmol of $Al(NO_3)_3$ in 10 mL of deionized water and quickly added to 40 mL of 6 mmol NaOH [94]. The mixture is then stirred for 10 min. The slurry can be purified and heated at 100^{o}C for 16 hours [94] to obtain the inorganic crystals. LDHNPs can be synthesized in controlled sizes.

LDHNPs can be used in cellular drug and gene delivery, are relatively biocompatible, have large cargo capacities, and can be tailored to have pH-controlled

release of their cargo. LDHNPs can complex with siRNA which helps protect the nucleic acids and can efficiently deliver the siRNA *in vitro* [94].

LDH was found to have negligible effects on cell viability and proliferation at 0.050 mg/mL. Furthermore, there was a significant decrease in HEK293T protein which was targeted using siRNA. LDHNP's IC50 is 0.125 mg/mL. Greater than 94% viability was maintained at concentrations less than 0.050 mg/mL of LDH [94].

2.3.12 Co-precipitating Mineral Solutions

Macromolecules such as DNA is thought to be capable of co-depositing with inorganic minerals (biomineralization) and form bioactive nanocomposites in close proximity to cells to promote DNA uptake with controllable surface-mediated release [117]. An inorganic mineral solution constituting (i.e., $CaCl_2$, KH_2PO_4, NaCl, KCl, $MgSO_4$, $MgCl_2$, $NaHCO_3$) was used to co-precipitate β-galactosidase DNA (Fig. 2) [117].

2.3.13 Multifunctional Nucleic Acid Carriers

Multifunctionalized constructs are typically a hybrid of materials which are intended to accomplish different objectives simultaneously such as gene therapy and diagnostics (i.e., imaging), commonly referred to as theranostics. Multifunctional hybrid vectors could also incorporate components to overcome multiple entry barriers discussed above: nucleic acid complexation, physical requirements (i.e., charge, biocompatibility), targeting, internalization, endosomal escape, cargo release, biodegradation, and nuclear translocation.

Hybrid Gold Nanoparticle/siRNA/PBAE System

Thiol-modified siRNA can be combined with PBAEs and complexed with thiol-modified gold nanoparticles by disulfide linkages for multiple functionality (AuNP for sensing, siRNA for silencing, and reduction-triggered release of cargo) (Fig. 3). PEG was used as a spacer between the disulfide bond and the AuNP surface as the Au can induce release of the cargo. This system has high stability and low aggregation of the ~100 nm particles. There was no significant cytotoxicity reported and the system resulted in ~95% gene knockdown of luciferase expression in HeLa cells [66].

Multifunctional QDs

ZnO QDs have been reported to have dual functionality (pDNA delivery and cell labeling) when capped with poly(2-(dimethylamino)ethyl methacrylate). This system was capable of condensing pDNA into nanoplexes and delivering DNA to COS-7 cells with real-time imaging of gene transfection under UV [118].

Mesoporous Silicon

Mesoporous silica nanoparticles have been tri-functionalized (imaging, targeting, therapy). To enable traceable imaging an optical agent ATTO 647N was used. cRGDyK peptides were used as the targeting moiety which binds specifically to $\alpha_v\beta_3$ integrin. $\alpha_v\beta_3$ integrins are overexpressed in tumor metastatic and endothelial cells. An oxygen sensing porphyrin-based photosensitizer was used to enhance the photo-induced cytotoxicity for photodynamic therapy. *In vitro* experiments using MCF-7 human breast cancer cells and U87-MG human glioblastoma cells demonstrated that there was excellent specificity,

minimal collateral damage, and potent photodynamic effects [119]. Mesoporous silica can also be used in other ways for combination/theranostic use [120].

2.3.14 Conclusion

Polymeric and inorganic based-vectors for nucleic acid delivery need to overcome many crucial barriers in the delivery process, and a variety of novel approaches have been investigated to overcome these challenges. A wide array of materials have been investigated for their potential in this area, including degradable and non-degradable cationic polymers, oligo- and polysaccharides, fullerenes, carbon nanotubes, quantum dots, and gold, silver, silica, layered-double hydroxide, and iron-oxide nanoparticles. Each has unique properties and potential advantages.

For effective delivery, the vector first must be stably complexed to the nucleic acid cargo and needs to stay compacted until cellular entry. The size, shape, surface charge, and surface functionality of the gene delivery particles are critical to efficient delivery, increased circulation time, and specific cellular entry. Size is a crucial parameter in determining the passive biodistribution of a nanoparticle delivery system and charge shielding / PEGylation has been shown to improve circulation time and increase accumulation at tumor sites as a result of the EPR effect. Particles can be fabricated in a variety of different shapes and shape-shifting particles whose shape-change can be triggered by pH, heat, and light are also possible.

A majority of delivery systems achieve cellular entry via endocytosis. The desired delivery compartment within the cell is dependent on the type of nucleic acid being delivered. For delivery of isRNA, interaction with TLR7 in the endosome is the end-goal,

so particles should be designed to target and then remain in the endosome. For siRNA and all DNA based systems, there needs to be a mechanism for endosomal escape. Mechanisms employed by non-viral vectors for endosomal escape include the proton-sponge effect, endosomolytic peptide-based lysis, and acid-triggered hydrophobic residue exposure. Hydrolysis, bioreduction, and photolysis have been utilized to reduce toxicity and promote unpacking of nucleic acid cargo intracellularly. Finally, for cargo such as DNA that needs to localize to the nucleus, particles and nucleic acids can make use of endogenous cell machinery and NLS sequences to allow nuclear import via the NPC.

2.3.15 Figures

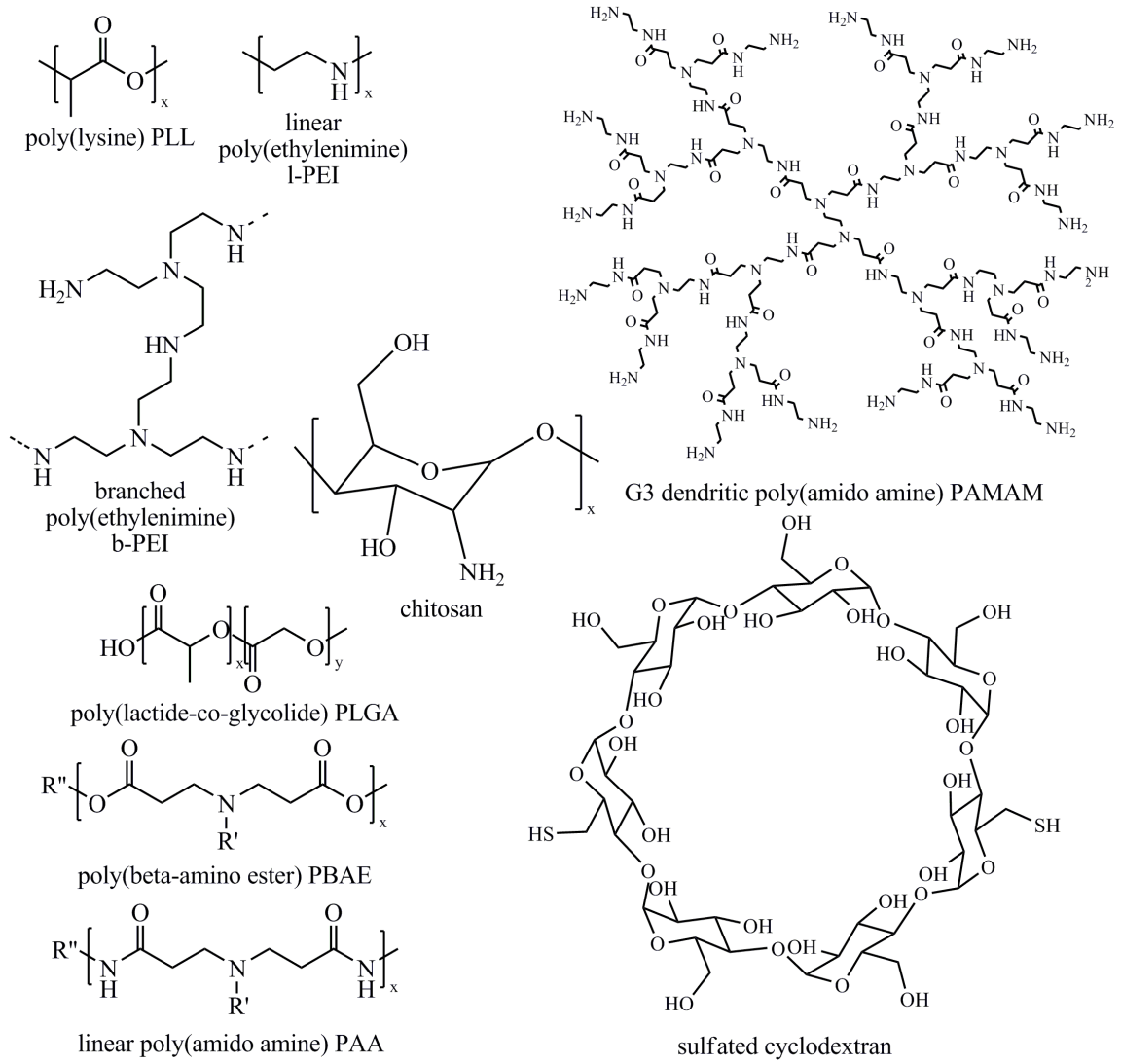

Figure 1: Structures of commonly used cationic polymers and polysaccharides used in gene delivery.

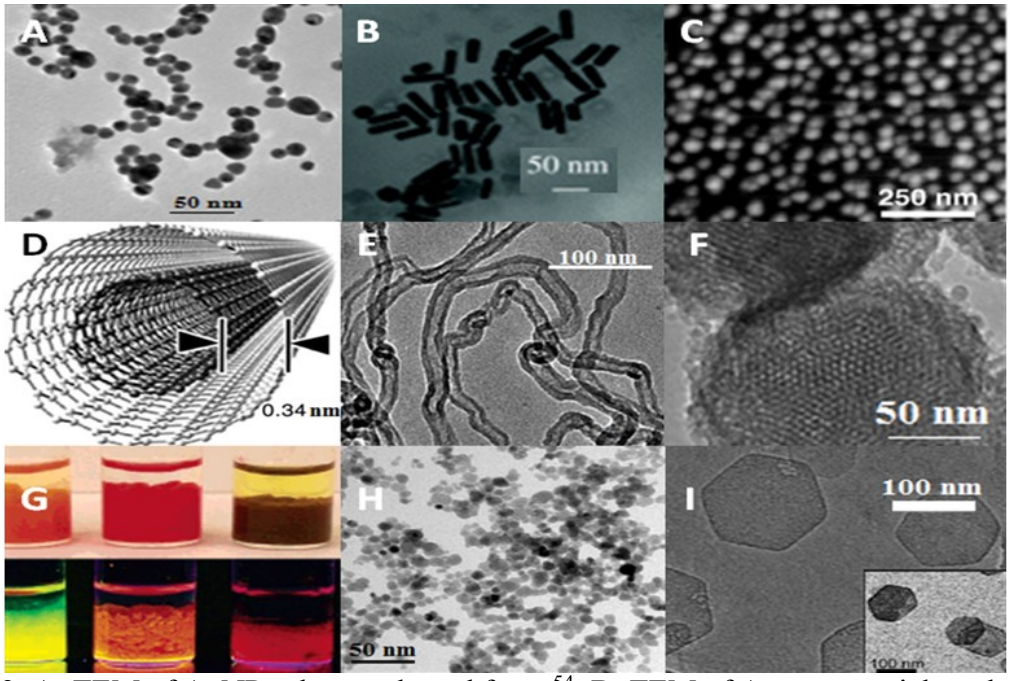

Figure 2. A: TEM of AuNP spheres adapted from [54]; B: TEM of Au nanoparticle rods adapted from [55]; C: AFM topography of AuNP shells coating platinum adapted from [56]; D: Multi-walled CNT adapted from [121]. E: Representative TEM of carbon samples produced by catalysis - adapted from [71]; F: Mesoporous silica nanoparticles adapted from [107]; G: Quantum dots – top and bottom row are illuminated under visible and UV, respectively - adapted from [77]; H: Doxorubicin-loaded SPIONs with a diameter of 8 +/- 2 nm - adapted from [88]; I: TEM of pristine layered double hydroxide NPs of $Mg_2Al(OH)_6NO_3$ - inset NPs are associated with siRNA - adapted from [94]. Figures adapted with permission.

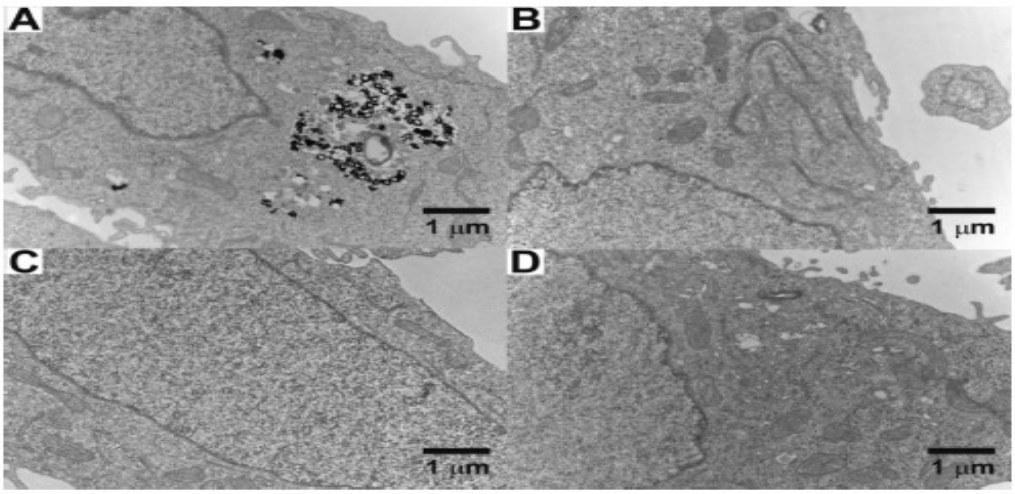

Figure 3: TEM images of HeLa cells. A: PBAE-siRNA-AuNPs; B: siRNA-AuNPs without PBAE; C: unmodified AuNPs; D: No nanoparticles (control). Adapted with permission from [66].

2.3.16 References

(1) Laemmli, U. K. *Proc Natl Acad Sci U S A* **1975**, *72*, 4288-92.
(2) Sela, M.; Arnon, R.; Jacobson, I. *Biopolymers* **1963**, *1*, 517-525.
(3) Midoux, P.; Monsigny, M. *Bioconjugate Chemistry* **1999**, *10*, 406-411.
(4) Choi, Y. H.; Liu, F.; Kim, J. S.; Choi, Y. K.; Park, J. S.; Kim, S. W. *J Control Release* **1998**, *54*, 39-48.
(5) Wu, G. Y.; Wu, C. H. *J Biol Chem* **1987**, *262*, 4429-32.
(6) Wagner, E.; Zenke, M.; Cotten, M.; Beug, H.; Birnstiel, M. L. *Proceedings of the National Academy of Sciences of the United States of America* **1990**, *87*, 3410-3414.
(7) Nishikawa, M.; Takemura, S.; Takakura, Y.; Hashida, M. *Journal of Pharmacology and Experimental Therapeutics* **1998**, *287*, 408-415.
(8) Hashida, M.; Takemura, S.; Nishikawa, M.; Takakura, Y. *Journal of Controlled Release* **1998**, *53*, 301-310.
(9) Midoux, P.; Mendes, C.; Legrand, A.; Raimond, J.; Mayer, R.; Monsigny, M.; Roche, A. C. *Nucleic Acids Research* **1993**, *21*, 871-878.
(10) Mislick, K. A.; Baldeschwieler, J. D.; Kayyem, J. F.; Meade, T. J. *Bioconjugate Chemistry* **1995**, *6*, 512-515.
(11) Boussif, O.; Lezoualc'h, F.; Zanta, M. A.; Mergny, M. D.; Scherman, D.; Demeneix, B.; Behr, J. P. *Proc Natl Acad Sci U S A* **1995**, *92*, 7297-301.
(12) Brissault, B.; Kichler, A.; Guis, C.; Leborgne, C.; Danos, O.; Cheradame, H. *Bioconjugate Chemistry* **2003**, *14*, 581-587.
(13) Fischer, D.; Bieber, T.; Li, Y. X.; Elsasser, H. P.; Kissel, T. *Pharmaceutical Research* **1999**, *16*, 1273-1279.
(14) Moghimi, S. M.; Symonds, P.; Murray, J. C.; Hunter, A. C.; Debska, G.; Szewczyk, A. *Mol Ther* **2005**, *11*, 990-5.
(15) Wightman, L.; Kircheis, R.; Rossler, V.; Carotta, S.; Ruzicka, R.; Kursa, M.; Wagner, E. *Journal of Gene Medicine* **2001**, *3*, 362-372.
(16) Bettinger, T.; Carlisle, R. C.; Read, M. L.; Ogris, M.; Seymour, L. W. *Nucleic Acids Research* **2001**, *29*, 3882-3891.
(17) Thomas, M.; Lu, J. J.; Ge, Q.; Zhang, C.; Chen, J.; Klibanov, A. M. *Proc. Natl Acad. Sci.* **2005**, *102*, 5679-84.
(18) Astete, C. E.; Sabliov, C. M. *Journal of Biomaterials Science-Polymer Edition* **2006**, *17*, 247-289.
(19) Visscher, G. E.; Robison, R. L.; Maulding, H. V.; Fong, J. W.; Pearson, J. E.; Argentieri, G. J. *Journal of Biomedical Materials Research* **1985**, *19*, 349-365.
(20) Shive, M. S.; Anderson, J. M. *Adv Drug Deliv Rev* **1997**, *28*, 5-24.
(21) Woodrow, K. A.; Cu, Y.; Booth, C. J.; Saucier-Sawyer, J. K.; Wood, M. J.; Saltzman, W. M. *Nat. Mat.* **2009**, *8*, 526-533.
(22) Lynn, D. M.; Langer, R. *Journal of the American Chemical Society* **2000**, *122*, 10761-10768.
(23) Anderson, D. G.; Akinc, A.; Hossain, N.; Langer, R. *Mol. Ther.* **2005**, *11*, 426-434.
(24) Green, J. J.; Langer, R.; Anderson, D. G. *Accounts of Chemical Research* **2008**, *41*, 749-759.
(25) Akinc, A.; Lynn, D. M.; Anderson, D. G.; Langer, R. *J. Am. Chem. Soc.* **2003**, *125*, 5316-23.

(26) Anderson, D. G.; Lynn, D. M.; Langer, R. *Angewandte Chemie-International Edition* **2003**, *42*, 3153-3158.
(27) Lynn, D. M.; Anderson, D. G.; Putnam, D.; Langer, R. *J Am Chem Soc* **2001**, *123*, 8155-6.
(28) Tomalia, D. A.; Baker, H.; Dewald, J.; Hall, M.; Kallos, G.; Martin, S.; Roeck, J.; Ryder, J.; Smith, P. *Polymer Journal* **1985**, *17*, 117-132.
(29) Haensler, J.; Szoka, F. C. *Bioconjugate Chemistry* **1993**, *4*, 372-379.
(30) Navarro, G.; de ILarduya, C. T. *Nanomedicine-Nanotechnology Biology and Medicine* **2009**, *5*, 287-297.
(31) Bielinska, A.; KukowskaLatallo, J. F.; Johnson, J.; Tomalia, D. A.; Baker, J. R. *Nucleic Acids Research* **1996**, *24*, 2176-2182.
(32) DeLong, R.; Stephenson, K.; Loftus, T.; Fisher, M.; Alahari, S.; Nolting, A.; Juliano, R. L. *Journal of Pharmaceutical Sciences* **1997**, *86*, 762-764.
(33) Axel, D. I.; Spyridopoulos, I.; Riessen, R.; Runge, H.; Viebahn, R.; Karsch, K. R. *Journal of Vascular Research* **2000**, *37*, 221-234.
(34) Ravina, M.; Paolicelli, P.; Seijo, B.; Sanchez, A. *Mini-Reviews in Medicinal Chemistry* **2010**, *10*, 73-86.
(35) Tang, M. X.; Redemann, C. T.; Szoka, F. C. *Bioconjugate Chemistry* **1996**, *7*, 703-714.
(36) Wood, K. C.; Little, S. R.; Langer, R.; Hammond, P. T. *Angew Chem Int Ed Engl* **2005**, *44*, 6704-8.
(37) Morgan, W. T.; Watkins, W. M. *Glycoconj J* **2000**, *17*, 501-30.
(38) Li, H.; Sethuraman, N.; Stadheim, T. A.; Zha, D.; Prinz, B.; Ballew, N.; Bobrowicz, P.; Choi, B. K.; Cook, W. J.; Cukan, M.; Houston-Cummings, N. R.; Davidson, R.; Gong, B.; Hamilton, S. R.; Hoopes, J. P.; Jiang, Y.; Kim, N.; Mansfield, R.; Nett, J. H.; Rios, S.; Strawbridge, R.; Wildt, S.; Gerngross, T. U. *Nat Biotechnol* **2006**, *24*, 210-5.
(39) Sinclair, A. M.; Elliott, S. *J Pharm Sci* **2005**, *94*, 1626-35.
(40) Pun, S. H.; Bellocq, N. C.; Liu, A. J.; Jensen, G.; Machemer, T.; Quijano, E.; Schluep, T.; Wen, S. F.; Engler, H.; Heidel, J.; Davis, M. E. *Bioconjugate Chemistry* **2004**, *15*, 831-840.
(41) Cryan, S. A.; Holohan, A.; Donohue, R.; Darcy, R.; O'Driscoll, C. M. *European Journal of Pharmaceutical Sciences* **2004**, *21*, 625-633.
(42) Arima, H.; Kihara, F.; Hirayama, F.; Uekama, K. *Bioconjug Chem* **2001**, *12*, 476-84.
(43) Davis, M. E. *Mol. Pharm.* **2009**, *6*, 659-68.
(44) Davis, M. E.; Zuckerman, J. E.; Choi, C. H.; Seligson, D.; Tolcher, A.; Alabi, C. A.; Yen, Y.; Heidel, J. D.; Ribas, A. *Nature*, *464*, 1067-70.
(45) Davis, M. E. *Molecular Pharmaceutics* **2009**, *6*, 659-668.
(46) Bellocq, N. C.; Davis, M. E.; Engler, H.; Jensen, G. S.; Liu, A. J.; Machemer, T.; Maneval, D. C.; Quijano, E.; Pun, S. Z. H.; Schluep, T.; Wen, S. F. *Molecular Therapy* **2003**, *7*, S290-S290.
(47) Pun, S. H.; Tack, F.; Bellocq, N. C.; Cheng, J. J.; Grubbs, B. H.; Jensen, G. S.; Davis, M. E.; Brewster, M.; Janicot, M.; Janssens, B.; Floren, W.; Bakker, A. *Cancer Biology & Therapy* **2004**, *3*, 641-650.
(48) Prego, C.; Garcia, M.; Torres, D.; Alonso, M. J. *Journal of Controlled Release* **2005**, *101*, 151-162.
(49) Roy, K.; Mao, H. Q.; Huang, S. K.; Leong, K. W. *Nat. Med.* **1999**, *5*, 387-91.

(50) Liu, W. G.; Zhang, X.; Sun, S. J.; Sun, G. J.; De Yao, K.; Liang, D. C.; Guo, G.; Zhang, J. Y. *Bioconjugate Chemistry* **2003**, *14*, 782-789.
(51) Zhao, X.; Yin, L. C.; Ding, J. Y.; Tang, C.; Gu, S. H.; Yin, C. H.; Mao, Y. M. *Journal of Controlled Release* **2010**, *144*, 46-54.
(52) Ghosn, B.; Singh, A.; Li, M.; Vlassov, A. V.; Burnett, C.; Puri, N.; Roy, K. *Oligonucleotides*, *20*, 163-72.
(53) Opanasopit, P.; Techaarpornkul, S.; Rojanarata, T.; Ngawhirunpat, T.; Ruktanonchai, U. *Oligonucleotides* **2010**, *20*, 127-136.
(54) Zhang, F. X.; Srinivasan, M. P. *Langmuir* **2007**, *23*, 10102-10108.
(55) Huang, X. H.; El-Sayed, I. H.; Qian, W.; El-Sayed, M. A. *J. Am. Chem. Soc.* **2006**, *128*, 2115-2120.
(56) Hartling, T.; Uhlig, T.; Seidenstucker, A.; Bigall, N. C.; Olk, P.; Wiedwald, U.; Han, L. Y.; Eychmuller, A.; Plettl, A.; Ziemann, P.; Eng, L. M. *Applied Physics Letters* **2010**, *96*, -.
(57) Mukherjee, P.; Bhattacharya, R.; Wang, P.; Wang, L.; Basu, S.; Nagy, J. A.; Atala, A.; Mukhopadhyay, D.; Soker, S. *Clin. Cancer Res.* **2005**, *11*, 3530-3534.
(58) Qiu, H. J.; Sun, Y. L.; Huang, X. R.; Qu, Y. B. *Colloid Surface B* **2010**, *79*, 304-308.
(59) Bonoiu, A. C.; Mahajan, S. D.; Ding, H.; Roy, I.; Yong, K. T.; Kumar, R.; Hu, R.; Bergey, E. J.; Schwartz, S. A.; Prasad, P. N. *Proc. Natl. Acad. Sci. U. S. A.* **2009**, *106*, 5546-5550.
(60) Nikoobakht, B.; El-Sayed, M. A. *Chemistry of Materials* **2003**, *15*, 1957-1962.
(61) Kayal, S.; Ramanujan, R. V. *J. Nanosci. Nanotechnol.* **2010**, *10*, 5527-5539.
(62) Loo, C.; Lowery, A.; Halas, N. J.; West, J.; Drezek, R. *Nano Lett.* **2005**, *5*, 709-711.
(63) Chang, Y. H.; Bau, D. T.; Lee, Y. S.; Chen, C. Y.; Huang, H. J.; Tsai, F. J.; Tsai, C. H.; Chen, C. Y. C. *Multi-Functional Materials and Structures Ii, Pts 1 and 2* **2009**, *79-82*, 565-568
2317.
(64) Chao, S. M.; Meen, T. H.; Chen, W. R.; Wu, K. H.; Liu, Y. S.; Tzou, W. C.; Huang, C. J. *High-Performance Ceramics Vi* **2010**, *434-435*, 799-802
885.
(65) Daniel, M. C.; Astruc, D. *Chem. Rev.* **2004**, *104*, 293-346.
(66) Lee, J. S.; Green, J. J.; Love, K. T.; Sunshine, J.; Langer, R.; Anderson, D. G. *Nano Lett.* **2009**, *9*, 2402-6.
(67) Pissuwan, D.; Niidome, T.; Cortie, M. B. *J Control Release* **2009**.
(68) El-Sayed, I. H.; Huang, X. H.; El-Sayed, M. A. *Nano Lett.* **2005**, *5*, 829-834.
(69) Huang, H. C.; Rege, K.; Heys, J. J. *ACS Nano* **2010**, *4*, 2892-2900.
(70) Suwalski, A.; Dabboue, H.; Delalande, A.; Bensamoun, S. F.; Canon, F.; Midoux, P.; Saillant, G.; Klatzmann, D.; Salvetat, J. P.; Pichon, C. *Biomaterials* **2010**, *31*, 5237-5245.
(71) Branca, C.; Frusteri, F.; Magazu, V.; Mangione, A. *Journal of Physical Chemistry B* **2004**, *108*, 3469-3473.
(72) Lim, S. H.; Luo, Z.; Shen, Z.; Lin, J. *Nanoscale Res Lett*, *5*, 1377-1386.
(73) Weber, J.; Singhal, R.; Zekri, S.; Kumar, A. *International Materials Reviews* **2008**, *53*, 235-255.
(74) Reilly, R. M. *J. Nucl. Med.* **2007**, *48*, 1039-1042.

(75) Maeda-Mamiya, R.; Noiri, E.; Isobe, H.; Nakanishi, W.; Okamoto, K.; Doi, K.; Sugaya, T.; Izumi, T.; Homma, T.; Nakamura, E. *Proc. Natl. Acad. Sci. U. S. A.* **2010**, *107*, 5339-5344.
(76) Sitharaman, B.; Zakharian, T. Y.; Saraf, A.; Misra, P.; Ashcroft, J.; Pan, S.; Pham, Q. P.; Mikos, A. G.; Wilson, L. J.; Engler, D. A. *Mol. Pharm.* **2008**, *5*, 567-578.
(77) Arachchige, I. U.; Brock, S. L. *J. Am. Chem. Soc.* **2007**, *129*, 1840-+.
(78) Hom, C.; Lu, J.; Liong, M.; Luo, H. Z.; Li, Z. X.; Zink, J. I.; Tamanoi, F. *Small* **2010**, *6*, 1185-1190.
(79) Liu, Y. Y.; Miyoshi, H. *J. Biomed. Nanotechnol.* **2008**, *4*, 25-32.
(80) Qian, J.; Li, X.; Wei, M.; Gao, X. W.; Xu, Z. P.; He, S. L. *Opt. Express* **2008**, *16*, 19568-19578.
(81) Moudgil, S.; Ying, J. Y. *Adv. Mater.* **2007**, *19*, 3130-+.
(82) Yang, X. T.; Zhang, Y. *Langmuir* **2004**, *20*, 6071-6073.
(83) Delehanty, J. B.; Boeneman, K.; Bradburne, C. E.; Robertson, K.; Medintz, I. L. *Expert Opin. Drug Deliv.* **2009**, *6*, 1091-1112.
(84) Barat, B.; Sirk, S. J.; McCabe, K. E.; Li, J. Q.; Lepin, E. J.; Remenyi, R.; Koh, A. L.; Olafsen, T.; Gambhir, S. S.; Weiss, S.; Wu, A. M. *Bioconjug. Chem.* **2009**, *20*, 1474-1481.
(85) Portney, N. G.; Ozkan, M. *Anal. Bioanal. Chem.* **2006**, *384*, 620-630.
(86) Barua, S.; Rege, K. *Biomaterials* **2010**, *31*, 5894-5902.
(87) Tan, W. B.; Jiang, S.; Zhang, Y. *Biomaterials* **2007**, *28*, 1565-1571.
(88) Munnier, E.; Cohen-Jonathan, S.; Linassier, C.; Douziech-Eyrolles, L.; Marchais, H.; Souce, M.; Herve, K.; Dubois, P.; Chourpa, I. *Int. J. Pharm.* **2008**, *363*, 170-176.
(89) Liu, Z.; Kiessling, F.; Gatjens, J. *Journal of Nanomaterials* **2010**, -.
(90) Tang, C.; Russell, P. J.; Martiniello-Wilks, R.; Rasko, J. E.; Khatri, A. *Stem Cells*.
(91) Schopf, B.; Neuberger, T.; Schulze, K.; Petri, A.; Chastellain, M.; Hofmann, M.; Hofmann, H.; von Rechenberg, B. *Journal of Magnetism and Magnetic Materials* **2005**, *293*, 411-418.
(92) Prijic, S.; Scancar, J.; Romih, R.; Cemazar, M.; Bregar, V. B.; Znidarsic, A.; Sersa, G. *J. Membr. Biol.* **2010**, *236*, 167-179.
(93) Gupta, A. K.; Gupta, M. *Biomaterials* **2005**, *26*, 3995-4021.
(94) Ladewig, K.; Niebert, M.; Xu, Z. P.; Gray, P. P.; Lu, G. Q. M. *Biomaterials* **2010**, *31*, 1821-1829.
(95) Bhattacharya, R.; Patra, C. R.; Earl, A.; Wang, S. F.; Katarya, A.; Lu, L.; Kizhakkedathu, J. N.; Yaszemski, M. J.; Greipp, P. R.; Mukhopadhyay, D.; Mukherjee, P. *Nanomedicine-Nanotechnology Biology and Medicine* **2007**, *3*, 224-238.
(96) Xiao, Y.; Gao, X. G.; Taratula, O.; Treado, S.; Urbas, A.; Holbrook, R. D.; Cavicchi, R. E.; Avedisian, C. T.; Mitra, S.; Savla, R.; Wagner, P. D.; Srivastava, S.; He, H. X. *BMC Cancer* **2009**, *9*, -.
(97) Gormley, A. J.; Ghandehari, H. *Evaluation of Toxicity of Nanostructures in Biological Systems*; John Wiley & Sons, Ltd, 2009.
(98) Kane, A. B.; Hurt, R. H. *Nature Nanotechnology* **2008**, *3*, 378-379.
(99) Zhang, B. L.; Chen, Q. O.; Tang, H.; Xie, Q. J.; Ma, M.; Tan, L. A.; Zhang, Y. Y.; Yao, S. Z. *Colloid Surface B* **2010**, *80*, 18-25.
(100) Wu, P.; Chen, X.; Hu, N.; Tam, U. C.; Blixt, O.; Zettl, A.; Bertozzi, C. R. *Angew Chem Int Ed Engl* **2008**, *47*, 5022-5.

(101) Cheung, W.; Pontoriero, F.; Taratula, O.; Chen, A. M.; He, H. *Adv Drug Deliv Rev*, *62*, 633-49.
(102) Smart, S. K.; Cassady, A. I.; Lu, G. Q.; Martin, D. J. *Carbon* **2006**, *44*, 1034-1047.
(103) Wick, P.; Manser, P.; Limbach, L. K.; Dettlaff-Weglikowska, U.; Krumeich, F.; Roth, S.; Stark, W. J.; Bruinink, A. *Toxicology Letters* **2007**, *168*, 121-131.
(104) Sayes, C. M.; Liang, F.; Hudson, J. L.; Mendez, J.; Guo, W.; Beach, J. M.; Moore, V. C.; Doyle, C. D.; West, J. L.; Billups, W. E.; Ausman, K. D.; Colvin, V. L. *Toxicol Lett* **2006**, *161*, 135-42.
(105) Lifeng, D.; et al. *Nanotechnology* **2008**, *19*, 255702.
(106) Bakry, R.; Vallant, R. M.; Najam-Ul-Haq, M.; Rainer, M.; Szabo, Z.; Huck, C. W.; Bonn, G. K. *Int. J. Nanomedicine* **2007**, *2*, 639-649.
(107) Lelong, G.; Bhattacharyya, S.; Kline, S.; Cacciaguerra, T.; Gonzalez, M. A.; Saboungi, M. L. *Journal of Physical Chemistry C* **2008**, *112*, 10674-10680.
(108) Park, E. J.; Park, K. *Toxicol Lett* **2009**, *184*, 18-25.
(109) Nan, A. J.; Bai, X.; Son, S. J.; Lee, S. B.; Ghandehari, H. *Nano Lett.* **2008**, *8*, 2150-2154.
(110) Kirchner, C.; Liedl, T.; Kudera, S.; Pellegrino, T.; Munoz Javier, A.; Gaub, H. E.; Stolzle, S.; Fertig, N.; Parak, W. J. *Nano Lett* **2005**, *5*, 331-8.
(111) Coussens, L. M.; Fingleton, B.; Matrisian, L. M. *Science* **2002**, *295*, 2387-2392.
(112) Raynal, I.; Prigent, P.; Peyramaure, S.; Najid, A.; Rebuzzi, C.; Corot, C. *Invest. Radiol.* **2004**, *39*, 56-63.
(113) Ferrucci, J. T.; Stark, D. D. *Am. J. Roentgenol.* **1990**, *155*, 943-950.
(114) Sekhon, B. S.; Kamboj, S. R. *Nanomedicine*, *6*, 516-522.
(115) del Pino, P.; Munoz-Javier, A.; Vlaskou, D.; Gil, P. R.; Plank, C.; Parak, W. J. *Nano Lett.* **2010**, *10*, 3914-3921.
(116) Tang, M.; Russell, P. J.; Khatri, A. *Discov Med* **2007**, *7*, 68-74.
(117) Shen, H.; Tan, J.; Saltzman, W. M. *Nat. Mater.* **2004**, *3*, 569-574.
(118) Zhang, P.; Liu, W. G. *Biomaterials* **2010**, *31*, 3087-3094.
(119) Cheng, S.-H.; Lee, C.-H.; Chen, M.-C.; Souris, J. S.; Tseng, F.-G.; Yang, C.-S.; Mou, C.-Y.; Chen, C.-T.; Lo, L.-W. *Journal of Materials Chemistry*, *20*, 6149-6157.
(120) Tasciotti, E.; Liu, X.; Bhavane, R.; Plant, K.; Leonard, A. D.; Price, B. K.; Cheng, M. M.-C.; Decuzzi, P.; Tour, J. M.; Robertson, F.; Ferrari, M. *Nat Nano* **2008**, *3*, 151-157.
(121) Iijima, S. *Physica B-Condensed Matter* **2002**, *323*, 1-5.

3 Chapter 3: The Effect and Role of Carbon Atoms in Poly(β-amino ester)s for DNA Binding and Gene Delivery

3.1 Introduction

Inheritable diseases and cancer can result from inactive genes (i.e., CFTR in cystic fibrosis or P53 as a tumor suppressor).[1,2] Delivering DNA and shRNA to encode and generate a functional copy or to inhibit mRNA expression of a non-functioning protein can potentially treat and cure many genetic diseases. Viruses have been used as delivery vectors as they are highly efficient in nucleic acid delivery, but they can cause insertional mutagenesis, immunogenic responses, and toxicity.[3] The safety and efficacy of the viral vectors depend on the viral vector type, route of administration and therapeutic target. To date there have been only two gene therapy formulations approved; one by the SFDA in China (2003) and one in Europe (2012) by the European Medicines Agency; there are still no FDA-approved gene therapies.[4] Degradable cationic polymers are an attractive alternative to viruses, as they are generally safer, are easier to manufacture and mass produce, and have more functional capabilities than viruses.[5] Varying a polymer's structure and functional groups allows one to optimize nucleic acid delivery properties while minimizing toxicity levels.[6] High-throughput analyses of

Chapter 3 is published as "Bishop CJ, Ketola T, Tzeng SY, et al. The effect and role of carbon atoms in poly(β-amino ester)s for DNA binding and gene delivery. *J. Am. Chem. Soc.* 2013;135(18):6951-7" and sections of chapter 3.3.13 are from "Ketola TM, Hanzlikova M, Leppanen L, Ravina M, CJ Bishop, et al. *J. Phys. Chem. B.* 2013;117(36):10405-13".

combinatorial biomaterial libraries can allow a vast number of polymers to be screened, but rational design of structure to control function would be more efficient.[7,8]

We are interested in evaluating polymer structure-function relationships to further our mechanistic understanding of, and to improve polymeric materials for non-viral gene delivery (Scheme 1). We have previously investigated poly(beta-amino esters) (PBAEs) as biodegradable cationic polymers capable of promoting gene delivery to various types of cells.[9-11] These polymers are promising due to their ability to condense DNA into nanoparticles containing many plasmids per particle,[12] facilitate cellular uptake,[13] and mediate endosomal escape.[14,15] Certain PBAE nanoparticles have been shown effective for *in vivo* gene delivery in the eye[16] and to tumors.[17] Despite this progress, gene delivery efficiency using polymers remains lower than with viral delivery. One challenge in evaluating and optimizing polymer structure is that synthetic polymers can be polydisperse, with variable extents of reaction and molecular weight heterogeneity.[18-20] Isolating precise polymer structures and uniform molecular weight are key to being able to evaluate polymer structure.

The interactions between a cationic polymer and DNA are critical to facilitate DNA protection, nanoparticle formation, cellular uptake, and subsequent DNA release.[21,22] Anionic phosphate groups on the DNA associate with and bind to positively charged amine groups on cationic polymers to cause nucleic acid condensation and protection. This is important because the degradation half-life of naked DNA in the presence of serum is on the order of minutes.[23] Upon binding with a cationic carrier (i.e., polymer), the nucleic acid half-life can increase substantially.[24,25] An optimal DNA carrier system should bind, condense, and protect DNA in the extracellular space, but

release DNA effectively within the cells. Designing such systems require proper understanding of the binding between DNA and polycations.[26,27]

In this manuscript, we use time-resolved fluorescence spectroscopy,[28,29] a new approach to quantitatively probe polymer-DNA interactions and binding. We report our findings of systematically investigating binding properties of DNA and monodisperse, size-fractionated poly(beta-amino ester)s with differential structures. In particular, we investigated series of polymers which varied the following: molecular weight; the number of carbons in the backbone which varied the amine density and hydrophobicity; the number of carbons in the sidechain which varied the distance of a hydroxyl group from the backbone and its hydrophobicity; and the endcap type (primary, secondary, tertiary amines and no endcap or diacrylate terminated). The effects of these small changes in the polymeric structures were characterized by fluorescence spectroscopy and gene delivery efficacy in human brain cancer and human breast cancer cells *in vitro*.[30] The experimental procedures, including materials and methods, can be found in the Supporting Information.

3.2 Materials and Methods

3.2.1 Materials (Reagents, Assays, Cells and Instruments)

The polymers were synthesized from commercially available monomers: 1,3-propanediol diacrylate (B3) (Monomer-Polymer and Dajac Laboratories Inc.), 1,4-butanediol diacrylate (B4) (Alfa Aesar), 1,5-pentanediol diacrylate (B5) (Monomer-Polymer and Dajac Laboratories Inc.), 1,6-hexanediol diacrylate (B6) (Alfa Aesar), 3-amino-1-propanol (S3), 4-amino-1-butanol (S4) (Alfa Aesar), 5-amino-1-pentanol (S5)

(Alfa Aesar), 6-amino-1-hexanol (S6) (Sigma Aldrich), 2,2-dimethyl-1,3-propanediamine (E2) (Sigma Aldrich), 2-methyl-1,5-diaminopentane (E4) (TCI America), 2-(3-aminopropylamino)ethanol (E6) (Sigma Aldrich), 1-(3-aminopropyl)-4-methylpiperazine (E7) (Alfa Aesar). Other reagents include the following and were used as received: peptide $(KK)_2KGGC$ (Biomatik), tetrahydrofuran (THF) (Sigma Aldrich), dimethyl sulfoxide (DMSO), (Sigma Aldrich), ethidium bromide (ETB; Sigma Aldrich), Lipofectamine™ 2000 (Invitrogen, Carlsbad, CA), OptiMEM I (Invitrogen), plasmid enhanced green fluorescent protein (pEGFP-N1) DNA (Clontech), amplified and purified by Aldevron (Fargo, ND). The breast cancer cell line (MDA-MB-231; ATCC) is of human origin and was cultured using DMEM high glucose 1x media and supplemented with 10% heat inactivated fetal bovine serum (FBS) and 100 U/mL of penicillin and 100 μg/mL of streptomycin (Invitrogen). The glioblastoma multiforme (GBM) cell line (GBM319) was derived from brain tumor stem cells from a 79-year old patient, was cultured as previously described in DMEM:Ham's F12 (1:1) (Invitrogen) supplemented with 10% heat inactivated FBS and 1x Antibiotic-Antimycotic (Invitrogen).[11] All cells were cultured in a humid 37ºC and 5% CO_2 atmosphere. Propidium iodide (PI) (Invitrogen), 25 mM sodium acetate buffer (NaAc, pH=5.2) (Sigma Aldrich), CellTiter® Aqueous One Solution Cell Proliferation Assay (Promega), Gel Permeation Chromatography (GPC) (Waters®, Breeze 2 software), a Bruker nuclear magnetic resonance (NMR) spectrometer, UV-Vis Spectrometer (Synergy2, BioTek®, Gen5 software), and a BD Accuri™ C6 flow cytometer equipped with HyperCyt® (Intellicyt Corp.) for high-throughput were used following manufacturer instructions. A Visi-Blue™ Transilluminator was used for imaging agarose gels. The single photon counting

instrumentation consisted of a PicoQuant GmBH, PicoHarp 300 controller and a PDL 800-B driver.

3.2.2 Polymer Synthesis and Fractionation

Diacrylate monomers that form the polymer backbones (B3, B4, B5, B6) and amine monomers that form the polymer side chains (S3, S4, S5, S6) were mixed neat using 1.05:1, 1.2:1, or 1.4:1 mole ratios and endcapped as previously described with slight modification (E2, E4, E6, E7) (Scheme 2).[6] Briefly, the base polymer (diacrylate and side chain) reactions were carried out for 24 hours at 90ºC, solvated in THF and endcapped for 1 hr using a 0.5 M amine monomer solution. Subsequently, the polymers were purified in anhydrous diethyl ether and vacuum dried for at least 24 hours and then fractionated by gel permeation chromatography (Waters Corp., Milford MA) using THF Styragel columns (3 7.8 x 300 mm in series). Two minute time fractions were collected at a 1 mL/min flow rate and again ether purified and vacuum dried for 48 hours. The polymers were then solvated in anhydrous DMSO to 100 mg/mL and stored at -20ºC in small aliquots to minimize freeze-thaw cycles. GPC was used to assess molecular weight of the fractionated polymers. Synthetic PBAE polymers are referred to by the order of their constituent monomers: backbone acrylate monomer, side chain amine monomer, and end group amine monomer. For example, B4-S4-E7 is 447 as an abbreviation (Scheme 2).

3.2.3 Nuclear Magnetic Resonance

Representative acrylate-terminated base polymers and amine-terminated end-capped polymers were analyzed via ^{1}H NMR. Polymers designated as "ether-purified" were synthesized in THF (or, in the case of 44 base polymer, dissolved in THF without reaction) and then precipitated into diethyl ether as described. After 48 hr drying under vacuum, polymers were dissolved in deuterated chloroform ($CDCl_3$) with 0.03% v/v tetramethylsilane (TMS) at 10-20 mg/mL Other 44 base polymers were not purified after neat synthesis and were similarly dissolved in $CDCl_3$ with TMS. All spectra were obtained with Bruker instruments (400 MHz, Topspin 2.0 or 2.1 software) and analyzed with NMR Processor v.12 (ACD Labs, Toronto, Canada).[6]

3.2.4 Fluorescence Measurements/Time-Correlated Single Photon Counting

Plasmid DNA encoding enhanced green fluorescent protein (pEGFP) at 0.0975 mg/mL (300 μM of phosphate concentration) was added to ETB (20 μM) in a 15:1 mole ratio in 250 μL of 25 mM sodium acetate (NaAc, pH 5.2). The resulting intercalated DNA-ETB complex was a homogeneous pink color. Subsequently, 250 μL of each polymer was added to the resulting solution in polymer weight to DNA weight ratio (w/w) ranging from 1.2 to 47 w/w (N/P ratios ranging from 1 to 40) and was immediately mixed thoroughly. The polyplexes were allowed to stabilize for 10 minutes before beginning fluorescence measurements. The time-resolved fluorescence was measured by a time-correlated single photon counting (TCSPC) system (PicoQuant GmBH) consisting of a PicoHarp 300 controller and a PDL 800-B driver. The samples were excited with the pulsed diode laser head LDH-P-C-485 at 483 nm with 130 ps time resolution. The signals

were detected with a microchannel plate photomultiplier tube (Hamamatsu R2809U). To diminish the influence of the scattered excitation, a cut-off filter was used in front of the monitoring monochromator. To study the decay associated spectra (DAS), the decays were collected with a constant accumulation time in the 560–670 nm wavelength range with 10 nm increments. The decays were simultaneously fitted to the sum of two exponents in the equation (1):

$$I(t,\lambda) = a_1(\lambda)e^{-t/\tau_1} + a_2(\lambda)e^{-t/\tau_2} \quad (1)$$

where τ_i is the global lifetime and $a_i(\lambda)$ is the local amplitude at a particular wavelength. The factors $a_i(\lambda)$ represent the DAS (Figure S2), which in the case of a mixture of different non-interacting fluorescing species corresponds to the individual spectra of the species (ETB bound to DNA and ETB free in solution). The photomultiplier tube becomes increasingly less sensitive at higher wavelengths which was taken into account. The spectral areas (A_i) of the components can be calculated by integrating the pre-exponential factors over the measured wavelength range as indicated in the following equation:

$$A_i = \int a_i(\lambda)d\lambda \quad (2)$$

The short-living component, corresponding to free ETB in the bulk solution, has a lower fluorescence quantum yield than the long-living component corresponding to ETB bound to DNA. The relative fluorescence quantum yield of the short-living component, ϕ_{rel} = 0.112 (equation 3), was calculated from the steady state absorption (UV-VIS spectrophotometer Shimadzu UV-3600) and fluorescence (Fluorolog Yobin Yvon-SPEX, l_{ex} = 483 nm) spectra according to the following equation:

$$\phi_{rel} = \frac{\phi_{ETB}}{\phi_{DNA-ETB}} = \frac{I_{ETB}A_{DNA-ETB}}{I_{DNA-ETB}A_{ETB}} \quad (3)$$

where ϕ_{ETB} is the quantum yield of ETB free in solution, $\phi_{DNA\text{-}ETB}$ is the quantum yield of the DNA-ETB complex, I_i is the area of the fluorescence spectra with an excitation wavelength of 483 nm and A_i is the absorbance at wavelength of 483 nm. The corrected spectral area (A_1^c) for the short living component is obtained by dividing A_1 by ϕ_{rel}. As polymer (P) is added to the DNA-ETB complex, the polymer binds DNA and the ETB is freed into solution as follows:

DNA-ETB + P ⇌ DNA-P + ETB (4)

The proportion of the short-living decay component of the total area of the DAS spectra, *B*, is the proportion or ratio of free ETB and is directly proportional to the amount of formed polyplexes (or the fraction of DNA bound to polymer). Thus, the bound fraction of DNA, B, can be assessed by monitoring the ratio of free ETB and can be calculated from the spectral areas of the components as follows:

$$B = \frac{A_1^c}{A_1^c + A_2} \quad (5)$$

The bound fraction of DNA as a function of amine concentration was assessed and the maximum was determined. All data points up to the maximum bound fraction were used to determine the binding constants. Of note, the initial concentration of ETB in the system is chosen such that without polymer there is no free ETB.

3.2.5 Cooperative Binding Constant Calculations

The Hill plot equation for multivalent ligands binding to multi-subunit substrates was used to estimate the cooperativity and binding constants for the polyplex formation[31-34].

$$\ln \frac{A_1^c}{A_2} = \alpha \ln [P] + \alpha \ln K \quad (6)$$

K^{α} is the overall binding constant for the reaction DNA + nP ⇌ DNA-P_n, K is the binding constant for the binding of one functional amine group according to the reaction DNA-P_{x-1} + P ⇌ DNA-P_x (X = 1, 2, …, n) and the slope of the Hill plot, □□ is the experimental Hill´s coefficient (α = 1 for non-cooperative systems, α < 1 for negative cooperativity and α > 1 for positive cooperativity). The error in K is calculated from the standard error of the y-value in the linearly fitted Hill plots.

3.2.6 Particle Diameter and Zeta Potential

Particle diameter was determined by nanoparticle tracking analysis (NTA) using a NanoSight NS500 (Amesbury, UK, 532 nm laser), and zeta potential was determined using a Malvern Zetasizer Nano ZS (Malvern Instruments, UK, detection angle 173°, 633 nm laser) in triplicate. Polymer/DNA nanoparticles were made at a 60 w/w ratio in 25 mM sodium acetate buffer (pH = 5.2) at a DNA concentration of 0.005 mg/ml and diluted into 1x PBS, pH 7.4. Particles were diluted 100-fold into PBS before NTA measurement. Particles were diluted 5-fold into PBS when using the Zetasizer; average electrophoretic mobilities were measured at 25°C, and zeta potentials (ZP) were analyzed using the Smoluchowski model. Additional experiments of representative polyplexes were conducted at concentrations comparable to delivery conditions at various pHs (5 and 7.4) and various ionic strengths (150, 75, 38, 19 mM) using dynamic light scattering (Malvern Instruments, UK).

3.2.7 Transfection and Cytotoxicity (Relative Metabolic Activity)

MDA-MB-231 and GBM319 cells were seeded in 96-well plates at 15,000 cells per well and allowed to adhere overnight at 37ºC and 5% CO_2. Polymers and DNA were diluted in 25 mM NaAc and mixed in a 1:1 v/v ratio at 30, 60, and 90 w/w. Particles were allowed to self-assemble for 10 minutes prior to *in vitro* delivery. Subsequently, 20 μL of particle solution was delivered to each well already containing 100 μL of media (10% or 70% serum) for a DNA dosage of 600 ng/well (5 μg/mL) in quadruplicate. Naked DNA at the same final concentration in 25 mM sodium acetate and an untreated group were used as negative controls. Lipofectamine 2000 was used as a positive control to deliver 100 and 200 ng of DNA per well using a 2.5:1 v/w ratio (Lipofectamine reagent:DNA) in quadruplicates (following manufacturer recommendations). After 4 hours of incubation, the wells were aspirated and replenished with fresh media. To assess relative metabolic activity as an indication of toxicity at 24 hours post-delivery, each of the wells were aspirated and incubated with 110 μL of a 10:1 mixture of culture media to CellTiter 96® Aqueous One Solution in quadruplicate according to the manufacturer's instructions. The absorbance at 490 nm was measured using the Synergy2 UV-Vis spectrometer.

3.2.8 Flow Cytometry

The transfection efficacy was assessed using flow cytometry at 48 hours post-delivery. The 96-well plates were aspirated, washed with PBS, and trypsinized. After quenching with 2% FBS (in PBS) with propidium iodide (PI) at 1:200 v/v, the contents were transferred to a round-bottom 96-well plate and centrifuged at 800 RPM for 5 minutes. After centrifuging, all but 30 μL of buffer was removed, and each cell pellet was

triturated before loading on the Hypercyt high-throughput reader. FlowJo (v. 7.6) was used for gating and further analysis. Singlets were identified using FSC-H vs SSC-H; dying cells were identified with PI (a DNA intercalator which fluoresces with a compromised cell membrane) using FSC-H vs FL3-H; FL1-H vs FL3-H was used to identify the GFP-positive population.

Geometric and arithmetic fluorescence means of the flow cytometer's FL1-A channel can be an indicator of the relative amount of EGFP present on a per cell basis. Normalized fluorescence means of the FL1-A channel were calculated by dividing the viable singlet population's FL1-A mean fluorescence by the untreated conditions' mean fluorescence.

3.2.9 Heparin Competition Release Assay

Gel electrophoresis was accomplished using 1% agarose gels containing 1 μg/mL of ETB in a 1x TAE buffer. The gels were loaded with 15 μL of polyplexes at 60 w/w (pEGFP-N1 of 0.01 mg/mL). The polyplexes were allowed to stabilize for 10 minutes. Just prior to the loading the polyplexes were added to glycerol (30% v/v). The gels were run for 1 hour using 100 volts and imaged using a Visi-Blue™ Transilluminator. Four representative polymers ranging from the weakest to the strongest binding constants were used for the release assay (44, 447 Low M_w, 446, 447 High M_w).

3.2.10 Statistics

All binding constants are reported as previously described; transfection and toxicity plots show the mean and standard error of the mean. All other physical characterizations and data plotted show the mean and standard deviation. One-way ANOVA tests were

used with Tukey post-hoc analyses to assess significance between multiple groups. Differences were considered significant with p-values < 0.05 (* < 0.05, ** < 0.01, *** < 0.001).

3.3 Results and Discussion

3.3.1 Polymer Synthesis and Fractionation

The 447 polymer series varying molecular weight ranged from 10.3 to 91.6 kDa (weight average molecular weight (M_w)). The polydispersity indices (PDI) increased as the M_w increased (PDIs: 1.3, 1.4, 2.9). The average M_w of the groups varying the backbone, sidechain and endcaps were 10 ± 1 kDa, 13 ± 2 kDa, and 10.9 ± 0.7 kDa, respectively. The PDIs of the groups varying backbone, sidechain and endcaps were 1.3 ± 0.1, 1.3 ± 0.1, and 1.34 ± 0.09, respectively (**Table S1**). The differences in the 447 molecular weight series and the similarities of the molecular weights in the groups which differ with respect to their backbone, sidechain and endcap groups are depicted in the normalized GPC curves per the refractive index detector (**Figure 1**). The similarity of the M_w and narrow PDIs of the comparable polymers with small differences in the backbone, sidechain and endcap allow comparisons between the groups and ensure differences are due to the monomer type as opposed to M_w or size heterogeneity.

Representative ^{1}H NMR spectra of polymers 44, 442, 444, 446 and 447 can be found in **Figure S1**.[6]

Some of the spectra above include the following sharp peaks corresponding to the solvent in which the polymer was synthesized (tetrahydrofuran, THF) or diethyl ether, used to precipitate the polymer:

THF: 1.85 ppm

Diethyl ether: 3.45-3.55 ppm (q, $CH_3C\boldsymbol{H_2}OC\boldsymbol{H_2}CH_3$)

Diethyl ether: 3.15-3.25 ppm (t, $C\boldsymbol{H_3}CH_2OCH_2C\boldsymbol{H_3}$)

Solvent peaks were not considered during analysis. Shown in the spectra below:

<u>44 (B4-S4) (all molecular weights)</u>

1.45-1.6 (m, $NCH_2C\boldsymbol{H_2}CH_2CH_2OH$ and $NCH_2CH_2C\boldsymbol{H_2}CH_2OH$)

1.6-1.75 (t, $COOCH_2C\boldsymbol{H_2}C\boldsymbol{H_2}CH_2OOC$)

2.35-2.6 (t, $COOC\boldsymbol{H_2}CH_2NCH_2C\boldsymbol{H_2}OOC$ and t, $NC\boldsymbol{H_2}CH_2CH_2CH_2OH$)

2.7-2.85 (t, $COOCH_2C\boldsymbol{H_2}NC\boldsymbol{H_2}CH_2OOC$)

3.55-3.7 (t, $NCH_2CH_2CH_2C\boldsymbol{H_2}OH$)

4.0-4.2 (t, $COOC\boldsymbol{H_2}CH_2CH_2C\boldsymbol{H_2}OOC$)

5.8-5.9 (d, $CH_2OOCCH=C\boldsymbol{H}H$)

6.1-6.2 (dd, $CH_2OOCC\boldsymbol{H}=CHH$)

6.35-6.5 (d, $CH_2OOCCH=CH\boldsymbol{H}$)

<u>442 (B4-S4-E2)</u>

0.9-0.95 (s, $NHCH_2C(CH_3)_2CH_2NH_2$)

1.45-1.6 (m, $NCH_2C\boldsymbol{H_2}CH_2CH_2OH$ and $NCH_2CH_2C\boldsymbol{H_2}CH_2OH$)

1.6-1.75 (t, $COOCH_2C\boldsymbol{H_2}C\boldsymbol{H_2}CH_2OOC$)

2.35-2.6 (t, $COOC\boldsymbol{H_2}CH_2NCH_2C\boldsymbol{H_2}OOC$ and t, $NC\boldsymbol{H_2}CH_2CH_2CH_2OH$ and t, $NHC\boldsymbol{H_2}C(CH_3)_2C\boldsymbol{H_2}NH_2$)

2.7-2.85 (t, $COOCH_2C\boldsymbol{H_2}NC\boldsymbol{H_2}CH_2OOC$)

3.55-3.7 (t, $NCH_2CH_2CH_2C\boldsymbol{H_2}OH$)

4.0-4.2 (t, $COOC\boldsymbol{H_2}CH_2CH_2C\boldsymbol{H_2}OOC$)

<u>444 (B4-S4-E4)</u>

0.9-1.0 (m, $NCH_2CH_2C\boldsymbol{H_2}CH(C\boldsymbol{H_3})CH_2N$)

1.45-1.6 (m, $NCH_2C\boldsymbol{H_2}CH_2CH_2OH$ and $NCH_2CH_2C\boldsymbol{H_2}CH_2OH$ and $NCH_2C\boldsymbol{H_2}CH_2C\boldsymbol{H}(CH_3)CH_2N$)

1.6-1.75 (t, $COOCH_2C\boldsymbol{H_2}C\boldsymbol{H_2}CH_2OOC$)

2.35-2.5 (t, $COOC\boldsymbol{H_2}CH_2NCH_2C\boldsymbol{H_2}OOC$ and t, $NC\boldsymbol{H_2}CH_2CH_2CH_2OH$ and m, $NC\boldsymbol{H_2}CH_2CH_2CH(CH_3)C\boldsymbol{H_2}N$)

2.7-2.85 (t, $COOCH_2C\boldsymbol{H_2}NC\boldsymbol{H_2}CH_2OOC$)

3.55-3.7 (t, $NCH_2CH_2CH_2C\boldsymbol{H_2}OH$)

4.0-4.2 (t, $COOC\boldsymbol{H_2}CH_2CH_2C\boldsymbol{H_2}OOC$)

<u>446 (B4-S4-E6)</u>

1.45-1.6 (m, $NCH_2C\boldsymbol{H_2}CH_2CH_2OH$ and $NCH_2CH_2C\boldsymbol{H_2}CH_2OH$)

1.6-1.75 (t, $COOCH_2C\boldsymbol{H_2}C\boldsymbol{H_2}CH_2OOC$ and quin, $NCH_2C\boldsymbol{H_2}CH_2NHCH_2CH_2OH$)

2.35-2.6 (t, $COOC\boldsymbol{H_2}CH_2NCH_2C\boldsymbol{H_2}OOC$ and t, $NC\boldsymbol{H_2}CH_2CH_2CH_2OH$ and m, $NC\boldsymbol{H_2}CH_2CH_2NHC\boldsymbol{H_2}CH_2OH$)

2.7-2.85 (t, $COOCH_2C\boldsymbol{H_2}NC\boldsymbol{H_2}CH_2OOC$)

3.55-3.7 (t, $NCH_2CH_2CH_2C\boldsymbol{H_2}OH$ and t, $NCH_2CH_2CH_2NHCH_2C\boldsymbol{H_2}OH$)

4.0-4.2 (t, $COOC\boldsymbol{H_2}CH_2CH_2C\boldsymbol{H_2}OOC$)

<u>447 (B4-S4-E7)</u>

1.45-1.6 (m, $NCH_2C\boldsymbol{H_2}CH_2CH_2OH$ and $NCH_2CH_2C\boldsymbol{H_2}CH_2OH$ and

t, $NCH_2C\boldsymbol{H_2}CH_2N<(CH_2CH_2)_2>NCH_3$)

1.6-1.75 (t, $COOCH_2C\boldsymbol{H_2}C\boldsymbol{H_2}CH_2OOC$)

2.3 (s, $NCH_2CH_2CH_2N<(CH_2CH_2)_2>NC\boldsymbol{H_3}$)

2.35-2.6 (t, $COOC\boldsymbol{H_2}CH_2NCH_2C\boldsymbol{H_2}OOC$ and t, $NC\boldsymbol{H_2}CH_2CH_2CH_2OH$ and m,

$NC\boldsymbol{H_2}CH_2C\boldsymbol{H_2}N<(C\boldsymbol{H_2}C\boldsymbol{H_2})_2>NCH_3$)

2.7-2.85 (t, $COOCH_2C\boldsymbol{H_2}NC\boldsymbol{H_2}CH_2OOC$)

3.55-3.7 (t, $NCH_2CH_2CH_2C\boldsymbol{H_2}OH$)

4.0-4.2 (t, $COOC\boldsymbol{H_2}CH_2CH_2C\boldsymbol{H_2}OOC$)

3.3.2 Cooperative Binding Constants for Polyplex Formation

The polyplex formation can be monitored by plotting the proportion of bound DNA, *B* in equation 5, against the concentration of amine. As an example the plot for polymer 442 is shown in **Figure 2**. The proportion of bound DNA increases with increasing polymer concentration until it reaches a saturation limit of approximately 76 % at w/w ratios of 24 in this case. Most PBAEs polymers saturated close to 80%. The saturation limit of polymer 44 and 346 is 60 and 96%, respectively. Polymers with negative cooperativity typically have saturation less than 100%, whereas polymers with high positive cooperativity saturate near 100%.

The Hill plots for the 447 molecular weight series are shown in **Figure 3A**. Similar linear curves with negative cooperativity (**Table S1**) were obtained for most of the polymers except polymer 646 (**Figure 3B-D)**. The fact that most polymers' Hill plots entail negative cooperativity and most polymers' bound fraction saturate close to 80% are in agreement.

While most polymers show a single linear Hill plot, varying the polymer backbone structure (646) may enable a biphasic response (**Figure 3B**). Polymer 646's Hill plot is associated with a negative and a positive cooperativity phase, which may account for why polymer 646 saturates at 96%.

This biphasic nature of binding suggests a change in the binding mechanism with increasing the molar amine to phosphate ratio. The analysis and discussion of polymer 646 will focus on the positive cooperativity slope associated with the higher amine to phosphate ratios, as all other experiments (i.e., transfection, toxicity, diameters, etc.) were carried out at weight/weights of 30, 60 or 90 (N/P ratios greater than 35). Polymers 346 and 546 (**Figure 3B)** have a data point which may either be an outlier or may also be associated with a binding mechanism which is biphasic, similar to polymer 646. Too few data points in these regions where there may be positive cooperativity for polymers 346 and 546 restrict further analysis. The multi-phase cooperativity is an interesting aspect for future investigation.

As the molecular weight of 447 increased, the binding constant per amine (K) increased (**Figure 4A**). Thus, larger polymer molecular weight led to increased polymer-DNA interaction and stronger binding. By utilizing this trend, one could potentially

fractionate a polymer with a particular molecular weight corresponding to a desired binding constant.

When evaluating the number of carbons that make up the polymer backbone repeat (3, 4, 5, or 6), the binding constants decreased as the number of carbons in the backbone monomer increased (**Figure 4B)**. The binding affinity reduced 400-fold when the number of carbons in the backbone increased from 3 to 6. The decrease in the binding constant is likely due to the decrease in amine density as the number of carbons in the backbone increases.

The binding constants in the sidechain series (437, 447 Med M_w, 457, 467) decreased with increasing side chain length (**Figure 4C**). As the sidechain was altered from 3 to 6 carbons, the binding affinity reduced 24-fold. Again, the decrease in the binding constant is likely due to the decrease in amine density as the number of carbons in the sidechain increases.

The base polymer (polymer 44) had a lower binding constant than any of the endcapped polymers (442, 444, 446, and 447 Low M_w). The binding constant increased 6.6 ± 0.1, 15.2, and 8.0-fold when the base polymer was endcapped using primary (442 and 444), secondary (446), and tertiary amines (447 Low M_w), respectively (**Figure 4D**). Considering the pK_a values of primary, secondary, and tertiary amines, one would suspect that there would be greater binding between primary versus tertiary; however, these differences would be diminished as the buffer was at a pH of 5.2. We observed a larger than expected value for the 446 K. This higher K value is understandable when the molecular weight of the 446 polymer is considered; the molecular weight of the 446 polymer was 14% higher than the other molecular weights of the endcap polymer series

(**Table S1)** which had 3-5 more amines per polymer strand than the other polymers in the group (un-endcapped, primary, secondary, and tertiary amine-type polymers had 40, 39, 44 and 41 amines per polymer strand, respectively.

3.3.3 Comparison of Binding Constant Calculation Methodology

The binding constant of a cationic peptide $(KK)_2KGGC$ was also evaluated to compare our time-resolved fluorescence spectroscopy binding assay to other binding assays found in the literature. The proportion of bound DNA, *B* in equation 5, as a function of $(KK)_2KGGC$ concentration displayed a saturation level close to 90 %. The Hill plot of the peptide presented in **Figure S3** shows the presence of two phases, similar to polymer 646. The kink point corresponds to the w/w ratio 3.6. The peptide, perhaps due to the presence of positive cooperativity (at low w/w) was associated with a higher saturation than most of the PBAEs, similar to what was observed with polymer 646. The Hill coefficient of the positive and negative cooperativity phases were 2.2 and 0.50, respectively, suggesting that further binding is hindered by the already bound amines. The overall binding constant, K^{α}, obtained from the positive cooperativity phase is $1.2 \pm 0.2\times10^7$ M^{-1}. Plank et al. obtained a value of $2.09x10^6$ M^{-1} with this peptide which is ~6 times smaller than by our method.[21]

3.3.4 Relationship Between Polyplex Diameter and Binding

The diameter of the polyplexes (nanoparticles) formed due to the binding and self assembly of cationic polymer with anionic DNA ranged from a mean diameter of 122 to

227 nm (**Figure S4 and S5**). While a polymer with one of the lowest binding constants (646, 1.19 x 10^3 M^{-1}) formed polyplexes of the largest size (227 nm) and the polymer with the largest binding constant (346, 4.8 x 10^5 M^{-1}) formed polyplexes of the smallest size (122 nm), there was not an overall trend between PBAE-DNA binding affinity and polyplex size (**Figure S4**). For the case of polymer backbone length, there was an apparent decrease in the diameter as the binding constant increased (or as the backbone length decreased (**Figure S4B**). As the backbone length increases the amine density decreases and hydrophobicity increases as well.

While an increased binding constant appears to correlate with smaller polyplex diameter, the trend is not very strong as a range of polymer binding constants and polymer structures can produce polyplexes of similar size (**Figure S5A**). Our data suggests that tighter binding constants may, but do not necessarily result in smaller polymer/DNA polyplexes. Complex size is affected by the number of plasmids and polymer chains per complex as well as the association of individual complexes in ion containing buffer solutions.

Polyplex/particle diameter does not appear to show any clear trends in transfection efficacies in either cell line (**Figure S5B and S5C**)**.** This finding suggests that the diameter of the polymer/DNA polyplexes is not a key determining factor for this class of PBAE particles in these cell lines. As all nanoparticles studied were relatively small in diameter they should be able to mediate successful endocytic cellular uptake.

Polyplexes were successfully formed at both pHs (5.2 and 7.4) and various ionic strengths (**Figure S6)**. At these conditions, the diameters of the polyplexes ranged from approximately 100 to 300 nm and no significant aggregation was observed (**Figure S6).**

3.3.5 Relationship Between Polyplex Zeta Potential and Binding

The polyplexes' zeta potentials (ZP) (**Figure S7 and S8**) ranged from +5 to +18 mV. There were no apparent trends between the binding constants and ZP (**Figure S7 and S8A**). In contrast to our cationic ZPs, Eltoukhy et al. found their PBAEs were neutral in sodium acetate, likely explained by the use of different polymer structures as well as 20-40 w/w formulations, which use less polymer than what was tested in our experiments (60 w/w).[18] Our nanoparticles are weakly positively charged, allowing interaction with a cell's anionic surface. Their charge is not excessive and they do not cause high toxicity when added to cells. When comparing all ZP measurements against transfection efficacies, there are no clear trends in either cell line (**Figure S8B and S8C).**

These findings suggests that ZP of the polymer/DNA particles is not a key determining factor for transfection for this class of PBAE particles in these cell lines. As all nanoparticles studied were relatively weakly positive in ZP, they should be able to mediate successful cellular uptake.

The ZP of the polyplexes at both pHs (5.2 and 7.4) and in various ionic strengths ranged from approximately +6 to +25 mV (**Figure S9**). The ZP appeared to be inversely proportional to pH. At a pH of 5.2, the ZP decreased as the salt content increased. At a pH of 7.4, the ZP did not appear to increase in all cases as the salt content decreased (**Figure S9)**. The ZPs of the 1:100 diluted condition was comparable to the undiluted.

3.3.6 Effect of Binding Constant on Transfection Efficacy

Two human cancer cell lines (MDA-MB-231 and GBM319) were utilized in these experiments to evaluate transfection efficacy. The former is derived from invasive triple negative human breast cancer and the latter is from human glioblastoma multiforme. Generally speaking, we have found both cell lines to be difficult to transfect, with MDA-MB-231 (**Figure 5A, 5C, 5E, 5G)** being more difficult to transfect than GBM319 (**Figure 5B, 5D, 5F, 5H**). The relative amount of EGFP per cell according to the normalized mean fluorescence linearly correlated with the transfection efficacy as measured by percent of cells with EGFP (**Figure S10)**.

The optimal molecular weight of the 447 polymer that resulted in the highest transfection efficacy was polymer 447 Med M_w at 90 w/w in both cell lines (**Figure 5A and 5B)**. By flow cytometry the 447 Med M_w polymer achieved 30 ± 4% and 69 ± 1% transfection in the MDA-MB-231 cell line and the GBM319 cell line, respectively. In MDA-MB-231 cells, the PBAE nanoparticle formulation with the highest transfection efficacy achieved 74% of the transfection percentage achieved with Lipofectamine 2000, a highly effective positive control widely used in the non-viral gene delivery community; positive and negative controls can be found in **Figure S11**. In GBM319 cells, the leading PBAE nanoparticles transfected 240% of the amount achieved with Lipofectamine 2000. Naked DNA, which is the same dose of plasmid DNA without added polymer, resulted in no transfection in both cell lines.

When all binding constants are analyzed with transfection efficacy, it is apparent that a biphasic trend is observed where the peak transfection occurs at an intermediate binding affinity (**Figure S12A and S12B)**. However, the correlation is not

straightforward, as similar binding affinities can also lead to dramatically lower transfection. This is to be expected as binding constants alone are likely insufficient to predict whether a particular polymer will deliver DNA successfully as there are many factors affecting gene delivery such as cellular uptake, endosomal escape, DNA release and nuclear import (Scheme 1).[5]

3.3.7 Effect of M_w on Binding Constants/Transfection Efficacy

In the MDA-MB-231 cells, a comparison of 447 polymers with incremental molecular weight (**Figure 5A**) revealed a biphasic response, with the highest transfection efficacy at intermediate polymer molecular weight (447 Med M_w) and intermediate binding affinity (58,000 M^{-1}). For the 30 w/w group, there was an increase in transfection efficacy as the molecular weight increased in the MDA-MB-231 cell line (**Figure 5A**) whereas there was a decrease in the GMB319 cell line (**Figure 5B)**. 447 Med M_w with a binding constant of 58,000 M^{-1} was the most effective binding constant evaluated in terms of transfection efficacy in the GBM319 cells (**Figure 5B**). This suggests that there is an optimal range: too low of a binding constant is unfavorable and too high of a binding constant is also unfavorable. Low binding constant polymers may not be able to sufficiently condense and protect the DNA and excessively high binding constants are likely to not release the DNA as efficiently.[22] As the molecular weight increased from 10.3 to 91.6 kDa, the transfection efficacy decreased from approximately 60% to 30% positive cells in the GBM319 cells.

3.3.8 Effect of Single Carbon Differences on Binding Constants/Transfection Efficacy

When holding molecular weight approximately constant and varying the backbone and sidechain, the optimal binding constant was near 58,000 M^{-1} (polymer 447 Med M_w) for MDA-MB-231 cells (**Figure 5C and 5E)** and transfection was similarly high (~70%) for GBM319 cells in the range of 1-6x10^4 M^{-1} (**Figures 5D and 5F**). In the case where the binding constant is smaller than 10^4 M^{-1}, increasing the binding constant correlates with increased transfection efficacy for MDA-MB-231 cells. GBM319 cells are better transfected by polymers with weaker binding constants (10^3-10^4 M^{-1}) than the MDA-MB-231 cells are and this is likely due to intrinsic differences in the gene delivery transport steps (**Scheme 1**) between these two cell types. For both cell types, when binding constant increased further (>10^5 M^{-1}), even with molecular weight constant, transfection decreased.

Although it is common practice to use 10% FBS for *in vitro* transfection experiments, higher media serum content may be more physiologically relevant. 70% serum was used to assess transfection efficacy and its correlation with the observed binding constants in the GBM319 cell line. The highest transfection achieved in the presence of high serum was similar to the highest transfection observed with low serum, approximately 70% of human cells positively transfected. A similar biphasic trend was also observed as in the 10% serum conditions (**Figure S13)** and a similar optimal range of binding constants, ~10^4 M^{-1}, was able to result in the highest transfection efficacy.

3.3.9 Effect of End Caps on Binding Constants/Transfection Efficacy

The MDA-MB-231 and GBM319 cell lines had very low transfection for un-endcapped, acrylate terminated (polymer 44) polymers. Furthermore, primary amine polymers (polymer 442 and 444) were not able to effectively transfect MDA-MB-231 cells; whereas primary, secondary and tertiary amines were able to transfect the GB319 cells.

Secondary or tertiary amine endcapped groups, depending on the w/w ratio, were required in the MDA-MB-231 cell line for effective transfection with these polymers. The GBM319 cell line was able to be transfected via primary amine-endcapped PBAE polymers 442 and 444 in addition to the polymers endcapped with secondary or tertiary amines. There did not appear to be a strong trend however with the binding constant and transfection efficacy in the endcapped series (**Figures 5G and 5H**).

3.3.10 Effect of Binding Constant, M_w, Single Carbon Differences, and End Caps on Cytotoxicity

In general, cytotoxicity increased with increasing polymer to DNA w/w ratio (**Figure 6**). In both cell lines tested it appeared there was low cytotoxicity with polymers that had binding constants in the 10^4-10^5 M^{-1} range (**Figures S11C and S11D**).

I. Effect of M_w

Particle-induced cytotoxicity increased as the binding constant (and the M_w) increased in both cell lines **(Figures 6A and 6B)**. There was relatively less toxicity in the

MDA-MB-231 cell line compared to the GB319 cell line, especially for the 447 High M_w polymer.

II. Effect of Single Carbon Differences

The cytotoxicity increased as the number of carbons in the backbone or sidechain increased in both cell lines. Thus, cytotoxicity decreased (and the relative metabolic activity increased) as the binding constant increased (**Figures 6C-6F).**

III. Effect of Endcaps

There was not significant cytotoxicity in the MDA-MB-231 cell line in the 44, 442, 444, 446 and 447 Low endcap series, whereas there appeared to be some cytotoxicity in the GBM319 cell line with the primary and tertiary amine endcaps. Secondary amine endcaps may be particularly less cytotoxic in the GBM319 cell line (**Figures 6G and 6H)**. There was not a clear trend in the relative metabolic activity when varying the type of endcap.

3.3.11 Heparin Competition Release

The 44 polymer associated with the weakest binding constant (526 M^{-1}) released its DNA with the lowest amount of heparin (<2 μg/mL) (**Figure S14)**. 447 Low M_w was associated with a binding constant of $4.2x10^3$ M^{-1} and released its DNA at a heparin concentration between 16 to 64 μg/mL (**Figure S14)**. The 446 and 447 High M_w polymers were associated with $7.97x10^3$ and $1.23x10^5$ M^{-1}, respectively and both released their DNA between 128 and 256 μg/mL. The 446 polymer has a faint

supercoiled DNA band at 128 μg/mL, suggesting 446 polymer likely releases its DNA at a lower heparin concentration than does 447 High M_w (**Figure S14)**. The DNA release from the polyplexes appears inversely proportional to the binding affinity between DNA and the polymers.

3.3.12 Comparison of Poly(β-amino ester) Binding to Poly(L-lysine), and Linear and Branched Polyethyleneimine

Branched polyethyleneimine (PEI), linear PEI and poly(L-lysine) (PLL) had binding constants per amine (*K;* M^{-1}) of (5.1±0.1)x10^3 M^{-1}, (4.3±0.2)x10^3 M^{-1}, and (5.5±0.2)x10^3 M^{-1}, respectively; the Hill coefficients, α, were 3.78, 3.16, and 2.63.[35] All of the PBAE αs were less than one, with the exception of polymer 646. In light of this, the overall binding constants, K^{α}, of the branched and linear PEI, as well as PLL were significantly higher than PBAE's. When considering the structure of PBAEs versus the other polymers of interest, there are also significantly less primary amines which are mainly responsible for binding; in contrast to tertiary amines which are more responsible for buffering the endosomes to allow the cargo to escape unscathed from the lysosomal degradation pathway. Primary amines, secondary amines, and tertiary amine pKa values are approximately 11, 8, and 5, respectively. It appears that the primary amines binding to anionic nucleic acid may results in a positive cooperativity effect due to avidity. Generally speaking, the binding ranking for each of the polymers would be: branched and linear PEI, PLL, followed by PBAE.

3.4 Conclusions

Evaluation of polymer-DNA binding constants using TCSPC compared to transfection efficacy allowed us to observe that binding constants between 1-6x10^4 M^{-1} were optimal for both human cancer cell lines tested. Our data reveals that polymer-DNA binding affinity for PBAEs is biphasic with transfection efficacy, with an intermediate binding affinity being optimal. A binding constant in the optimal range is necessary but not sufficient for effective transfection. This intermediate binding affinity can be independently tuned by adding single carbons to the backbone or side-chain structure, varying monomer ratios during synthesis and/or using GPC fractionation to tune the polymer molecular weight, and by modifying a small molecule endgroup used to endcap a linear polymer. By probing a specific gene delivery bottleneck with a class of polymers that were synthesized to have subtle structural differences, new quantitative and mechanistic insights were obtained concerning how they function for gene delivery.

3.5 Figures

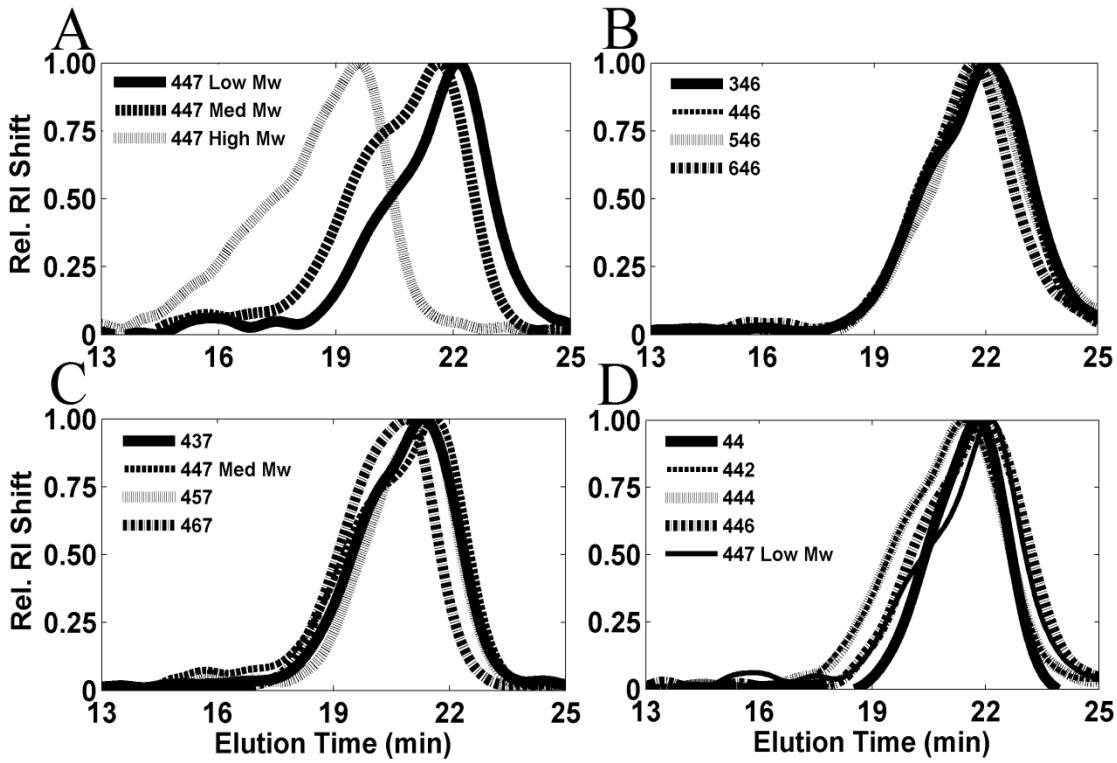

Figure 1. GPC curves of fractionated polymers by group (relative RI shift (mV/max mV) versus elution time (min.); varying molecular weight (Low, Med, and High) (A), backbone (B), sidechain (C), and endcaps (D).

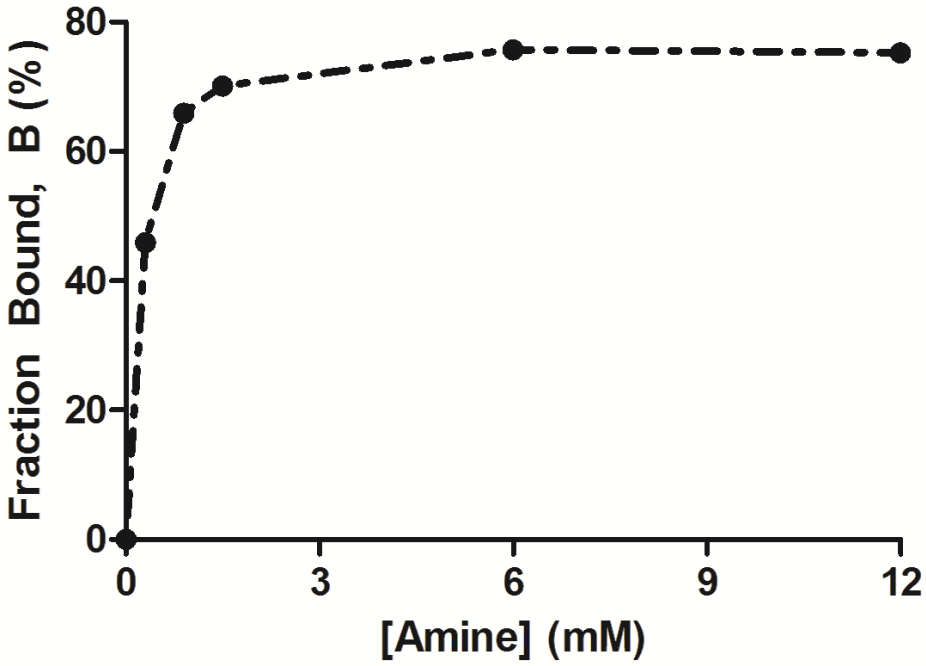

Figure 2. Fraction of bound DNA as a function of amine concentration of polymer 442.

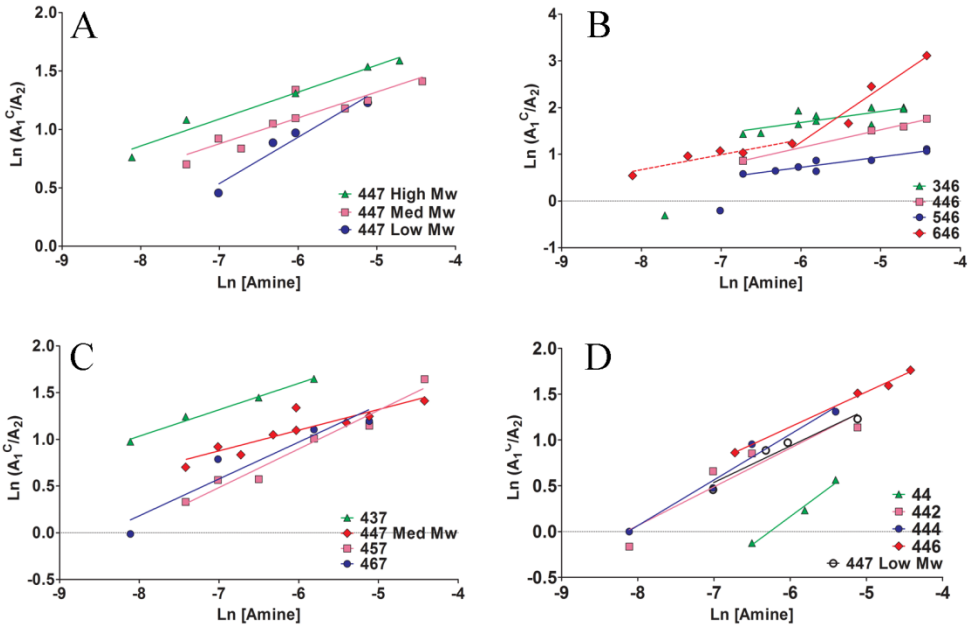

Figure 3. Hill plots of polymer series varying M_w (A), backbone (B), sidechain (C), and endcaps (D).

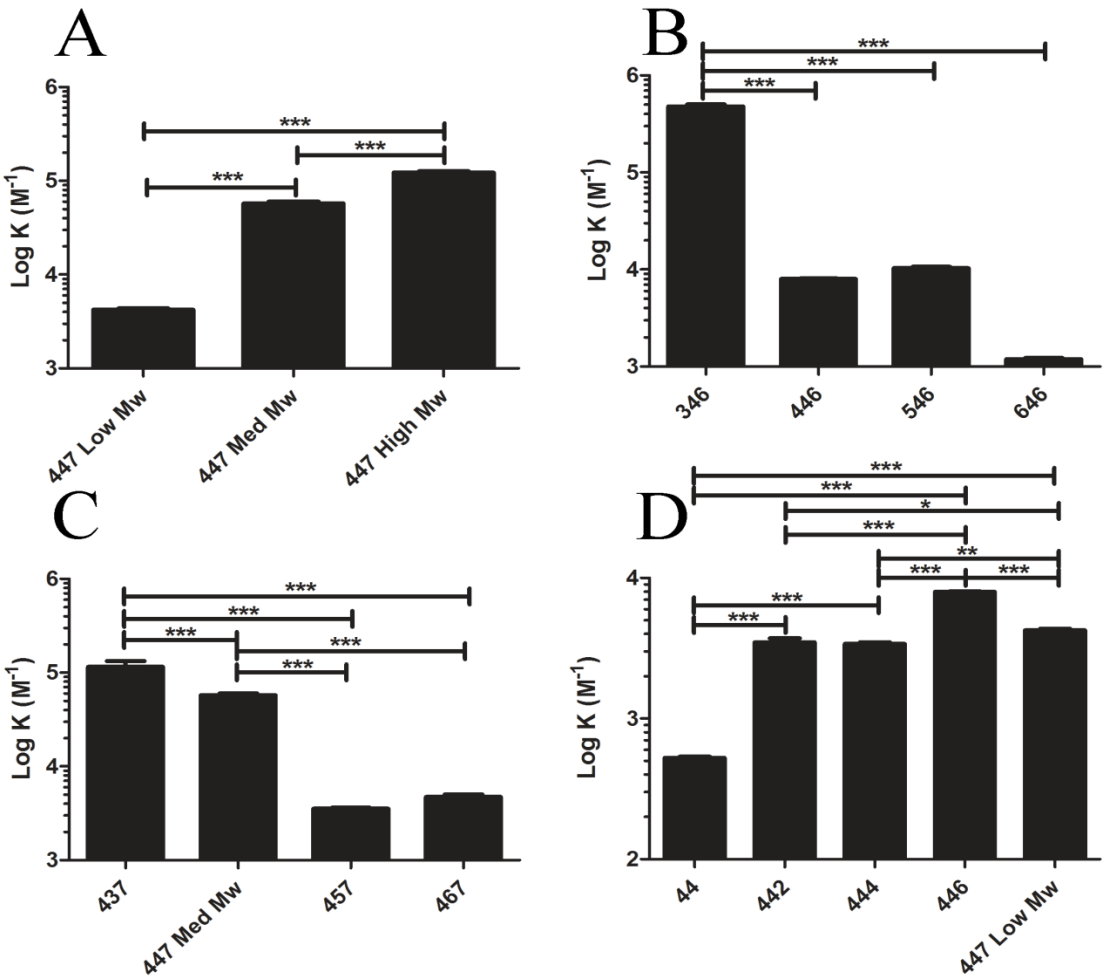

Figure 4. Binding constants (M^{-1}) of each of the series comparing M_w (A), backbone (B), sidechain (C), and endcaps (D). (Statistical analysis was accomplished by a one-way ANOVA and a Tukey post-hoc analysis; *=P-value < 0.05; **=P-value < 0.01; ***=P-value < 0.001).

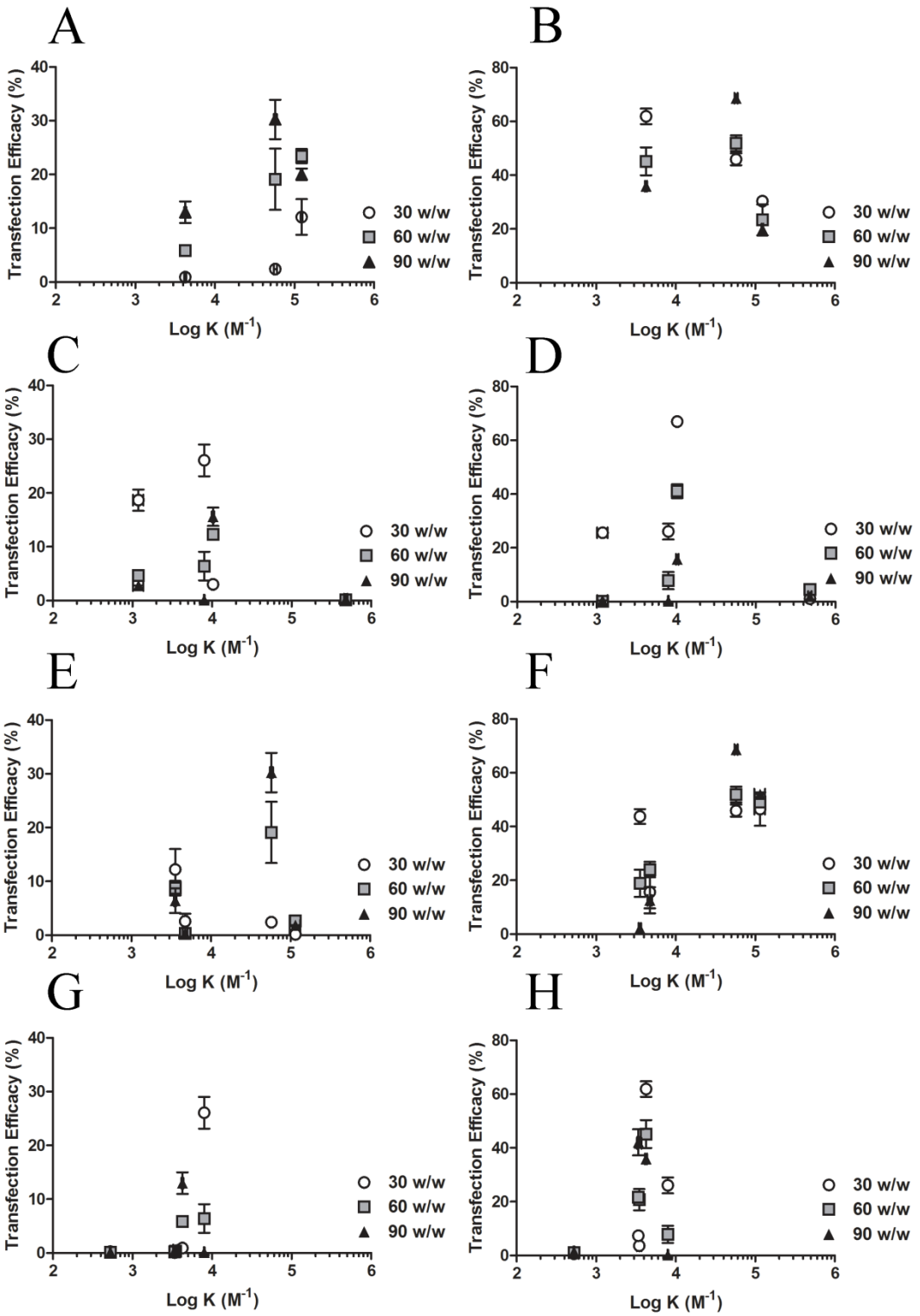

Figure 5. The effect of binding constant on transfection efficacy in MDA-MB-231 cells (A, C, E, G) and GBM319 cells (B, D, F, H) for each of the series comparing M_w (A and B), backbone (C and D), sidechain (E and F), and endcaps (G and H).

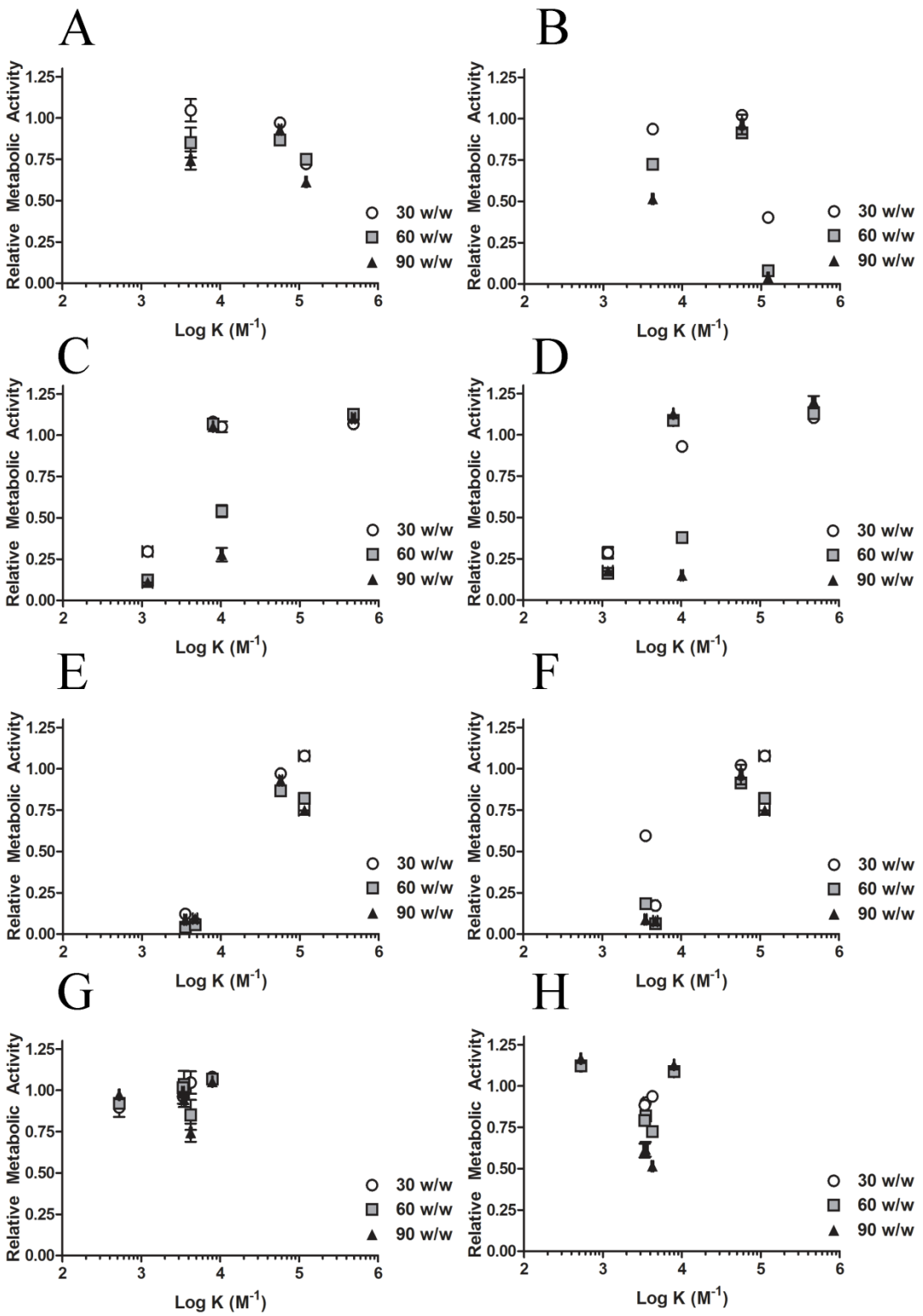

Figure 6. The effect of binding constant on relative metabolic activity in MDA-MB-231 cells (A, C, E, G) and GBM319 cells (B, D, F, H) for each of the series comparing M_w (A and B), backbone (C and D), sidechain (E and F), and endcaps (G and H).

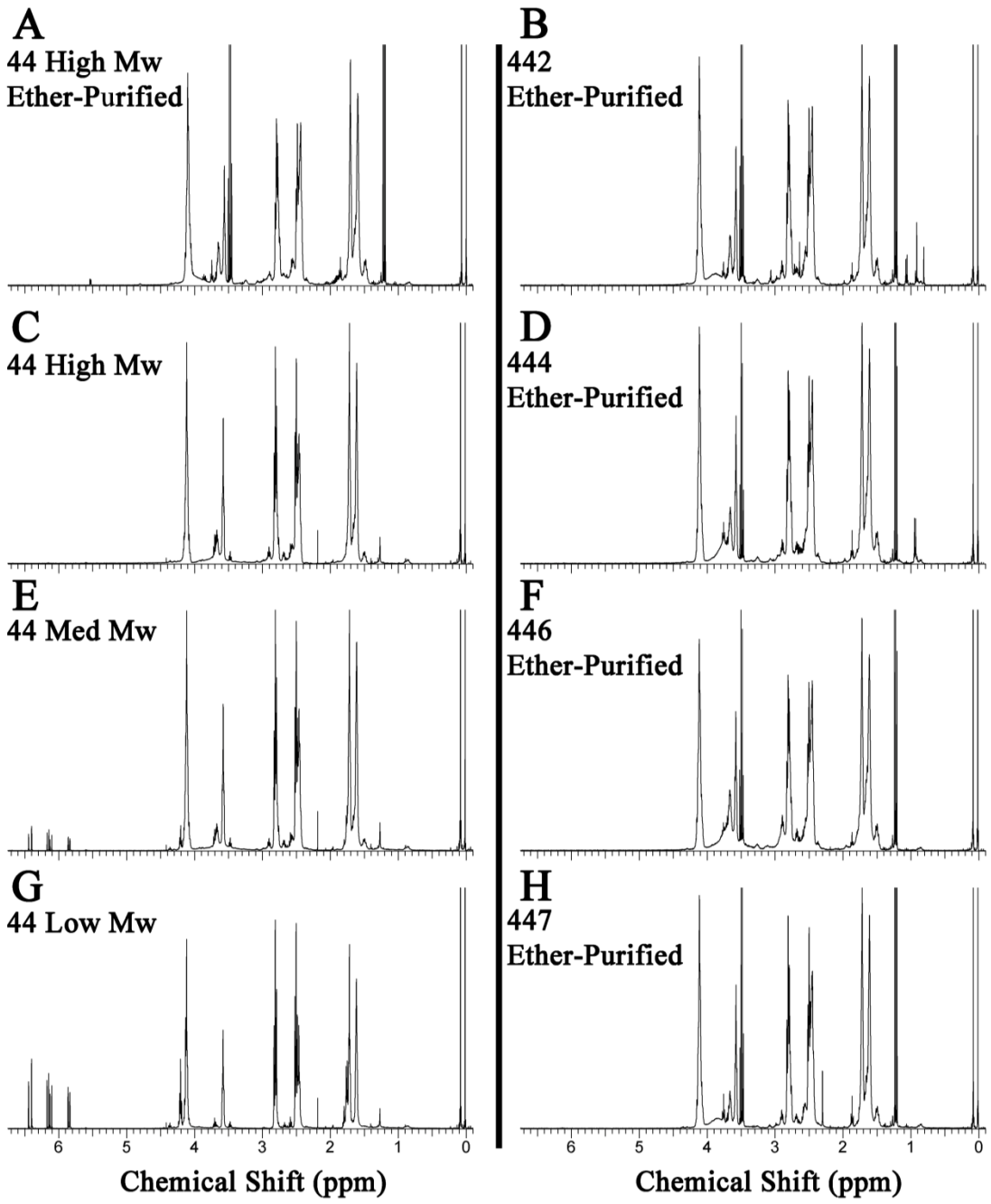

Figure S1. ^{1}H NMR spectra of polymers 44 High (A, C), Med (E), Low M_w (G), 442 (B), 444 (D), 446 (F), and 447 (H). These spectra are consistent with NMR analyses published previously (Sunshine, Akanda, et al.) along with spectra of the other polymers used in this study.[6] (See below for further peak analyses.)

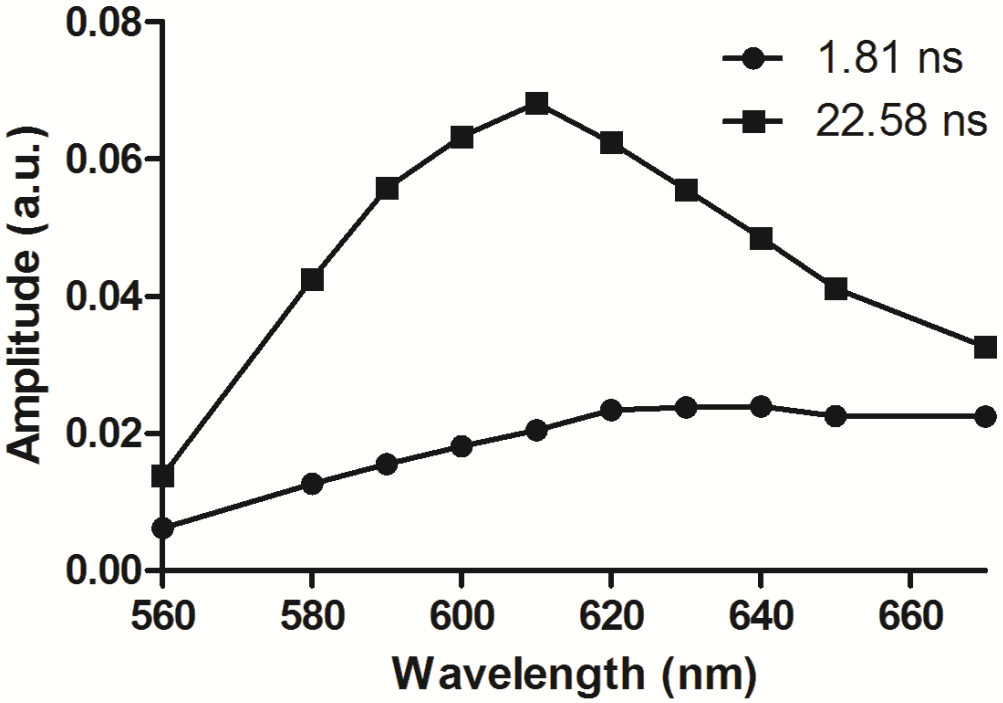

Figure S2. Decay-associated spectra. The fluorescence lifetimes of ethidium bromide bound to DNA and free in the solution are 22.58 and 1.81 ns, respectively, in this particular case.

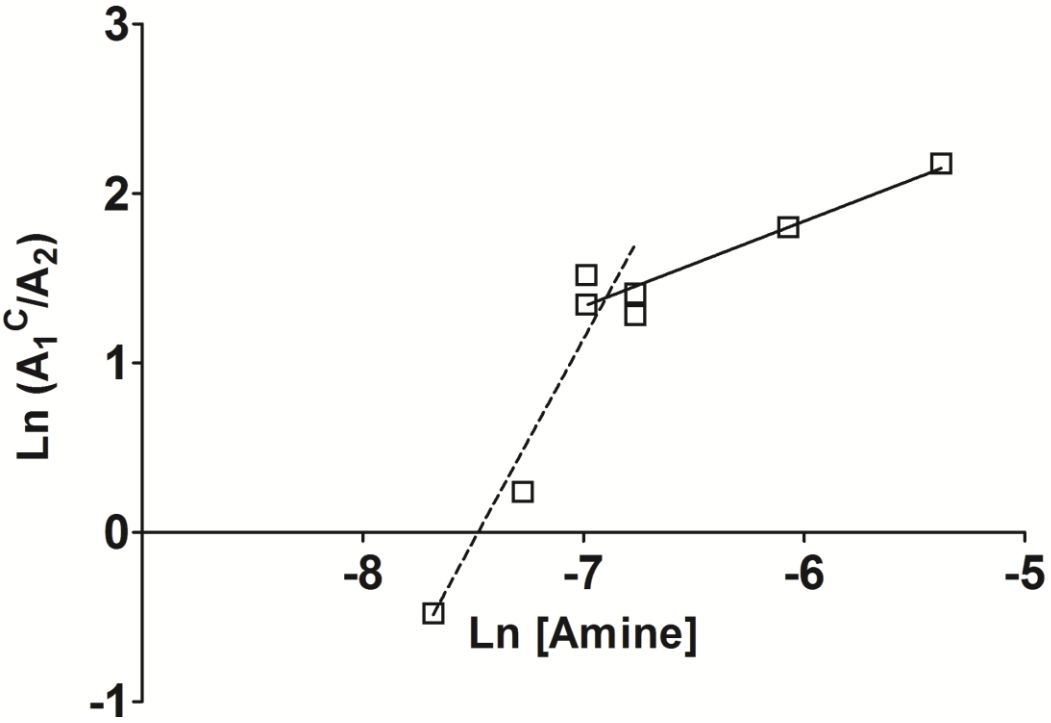

Figure S3. Hill plot of peptide $(KK)_2KGGC$.

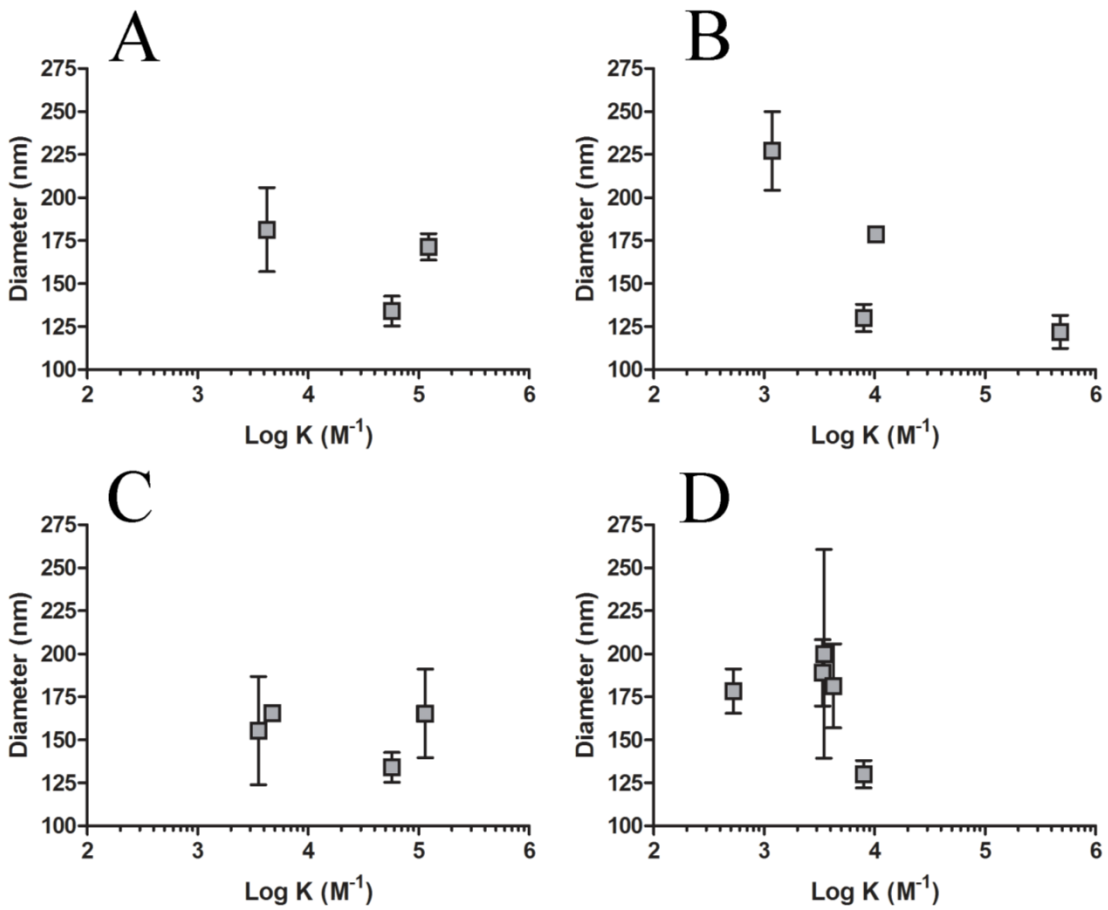

Figure S4. The relationship between polyplex diameter and the binding constant (M^{-1}) of each of the series comparing M_w (A), backbone (B), sidechain (C), and endcaps (D).

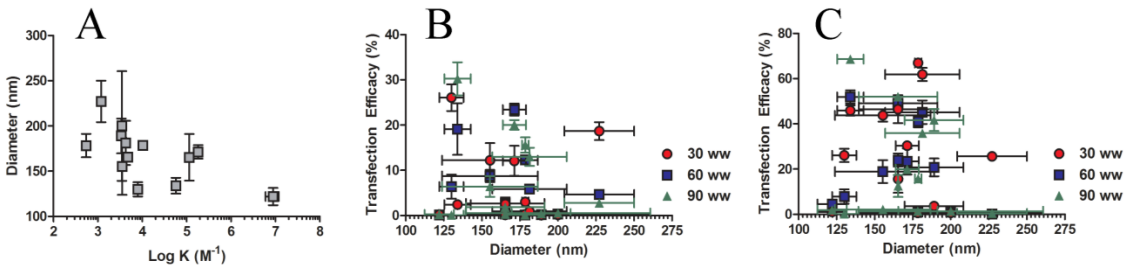

Figure S5. All diameters versus binding constants (A); dependence of transfection efficacy on polyplex diameters in MDA-MB-231 (B) and GBM319 cells (C).

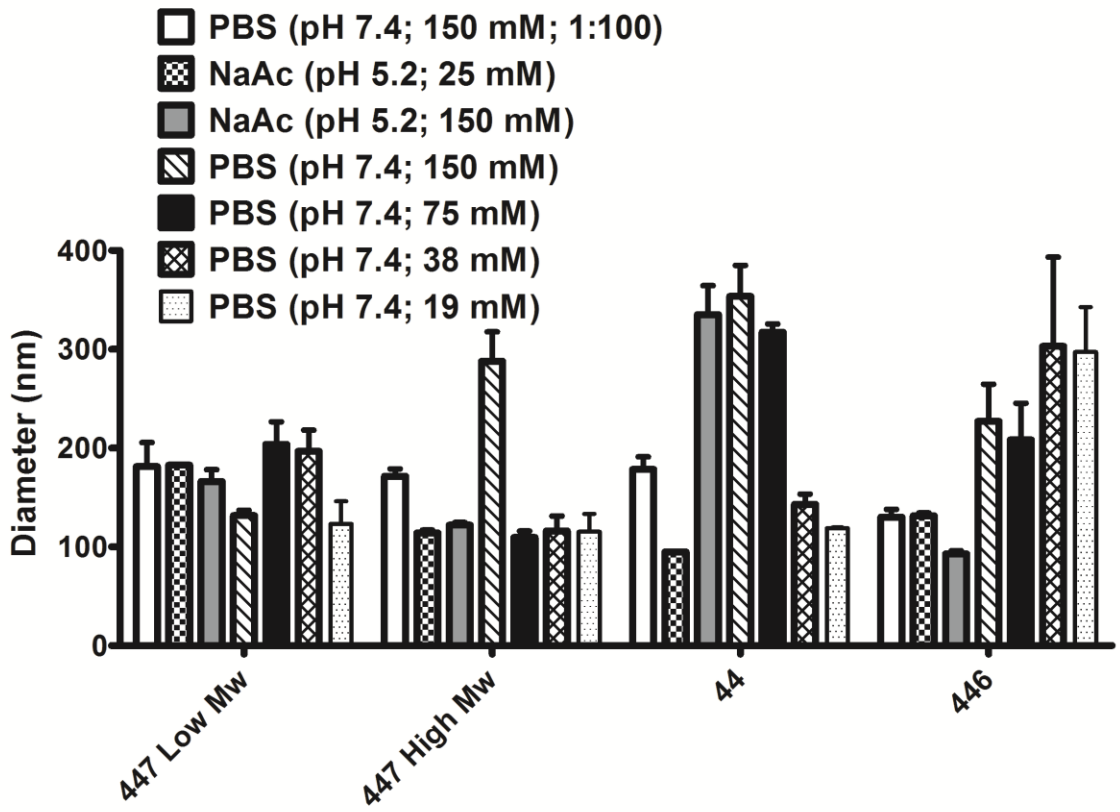

Figure S6. Diameter of four representative polymers at various pHs and ionic strengths. (White group was via NTA; remainder was via DLS.)

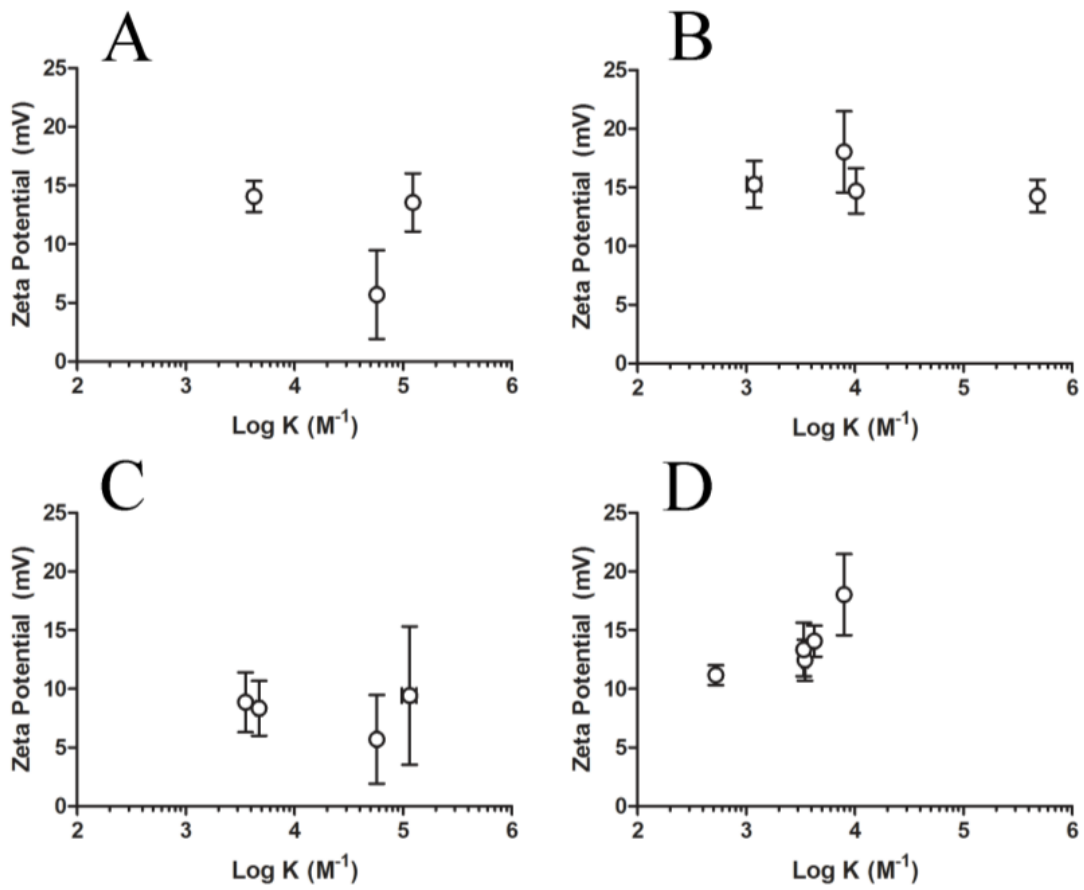

Figure S7. The relationship between zeta potential and the binding constant (M^{-1}) of each of the series comparing M_w (A), backbone (B), sidechain (C), and endcaps (E).

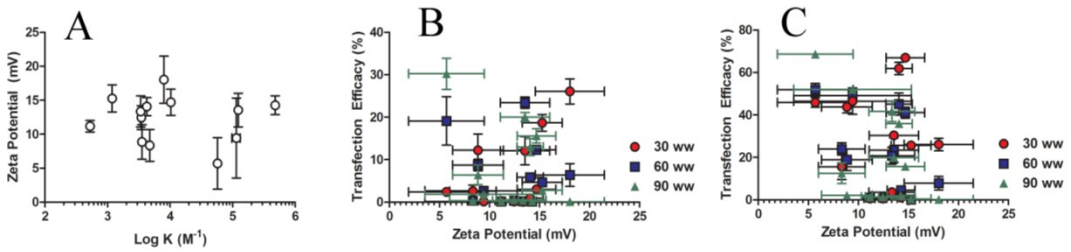

Figure S8. All ZP values irrespective of series versus binding constants (A); dependence of transfection efficacy on ZP in MDA-MB-231 (B) and GBM319 cells (C).

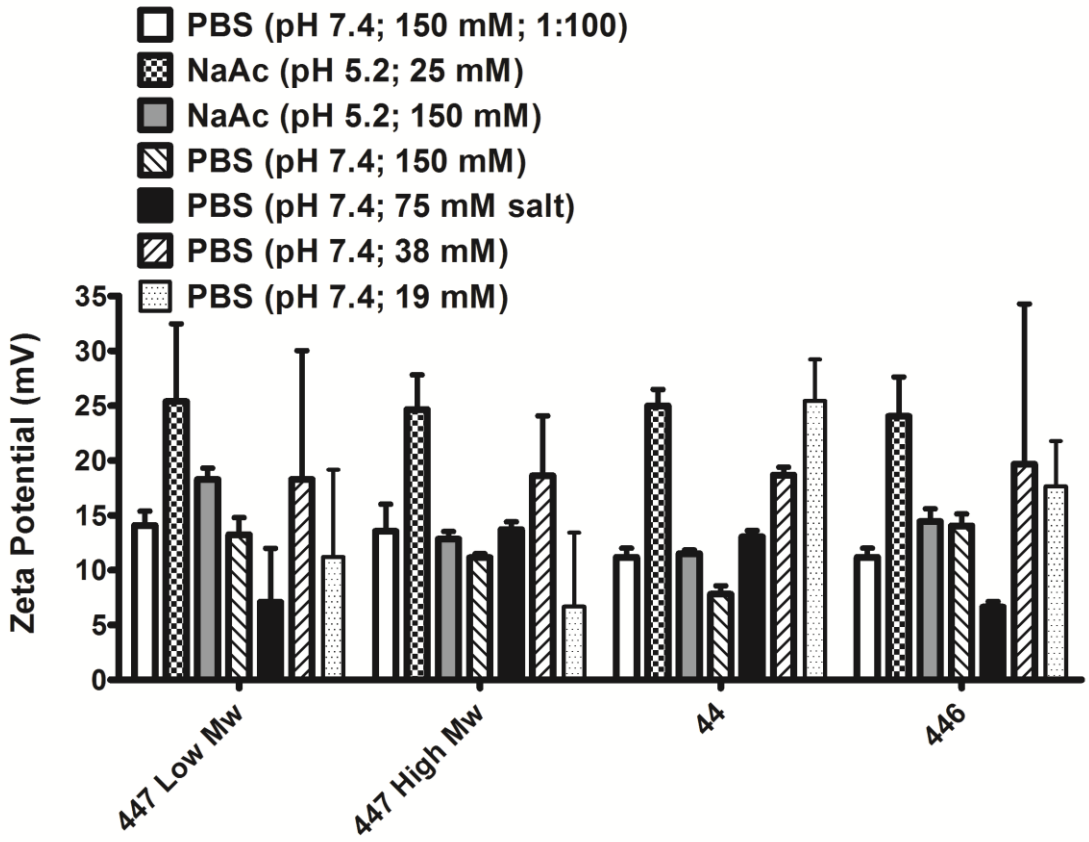

Figure S9. ZP of four representative polymers at various pHs and ionic strengths.

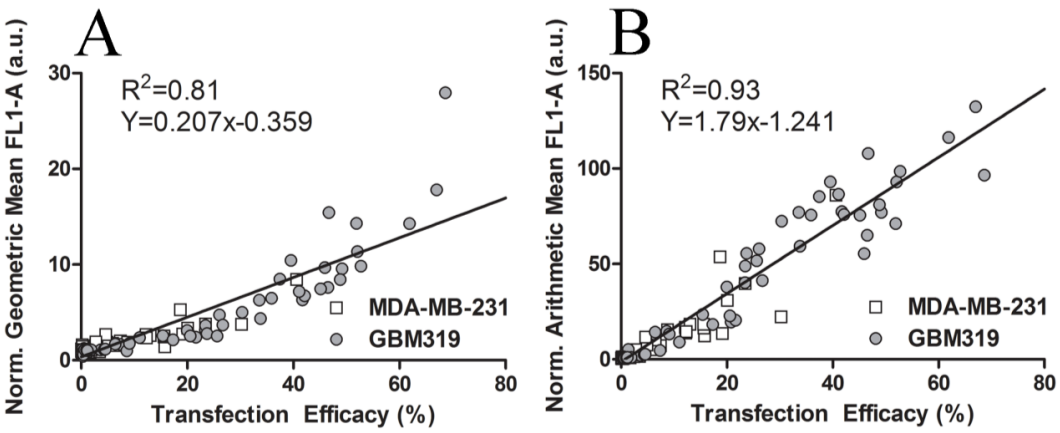

Figure S10. Normalized geometric (A) and arithmetic (B) means versus transfection efficacy in the MDA-MB-231 and GBM319 cell lines.

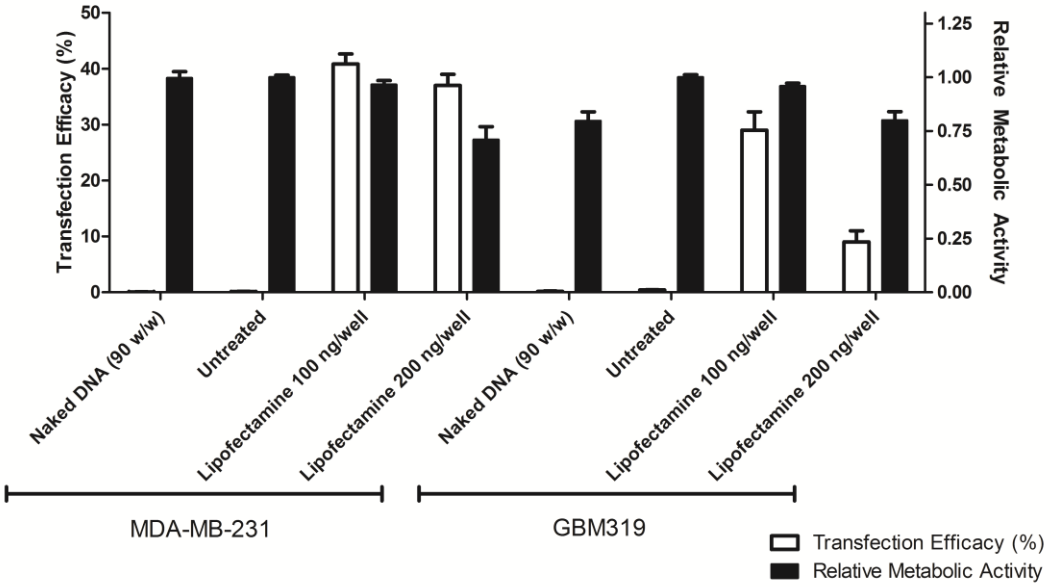

Figure S11. Positive (Lipofectamine 2000 at 100 and 200 ng/well) and negative controls (naked DNA and untreated) for transfection and relative metabolic activity in MDA-MB-231 and GBM319 cells.

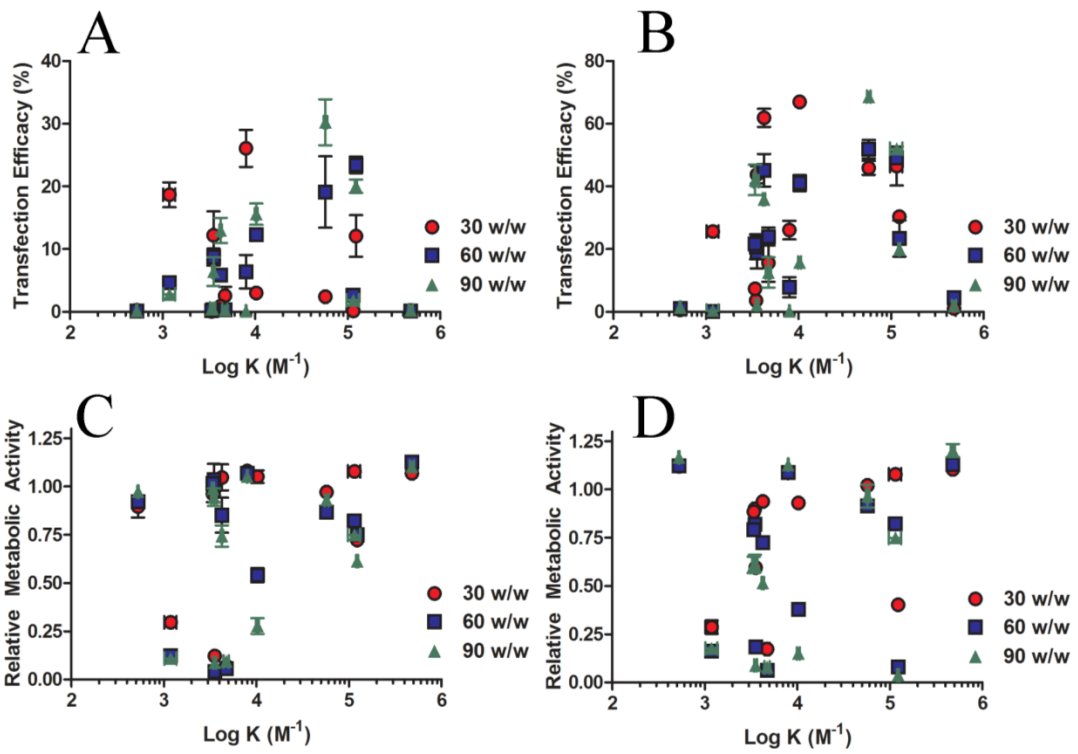

Figure S12. All binding constants for each of the series of comparison against transfection efficacy in MDA-MB-231 cells (A) and GBM319 cells (B), as well as cytotoxicity in MDA-MB-231 cells (C) and GBM319 cells (D).

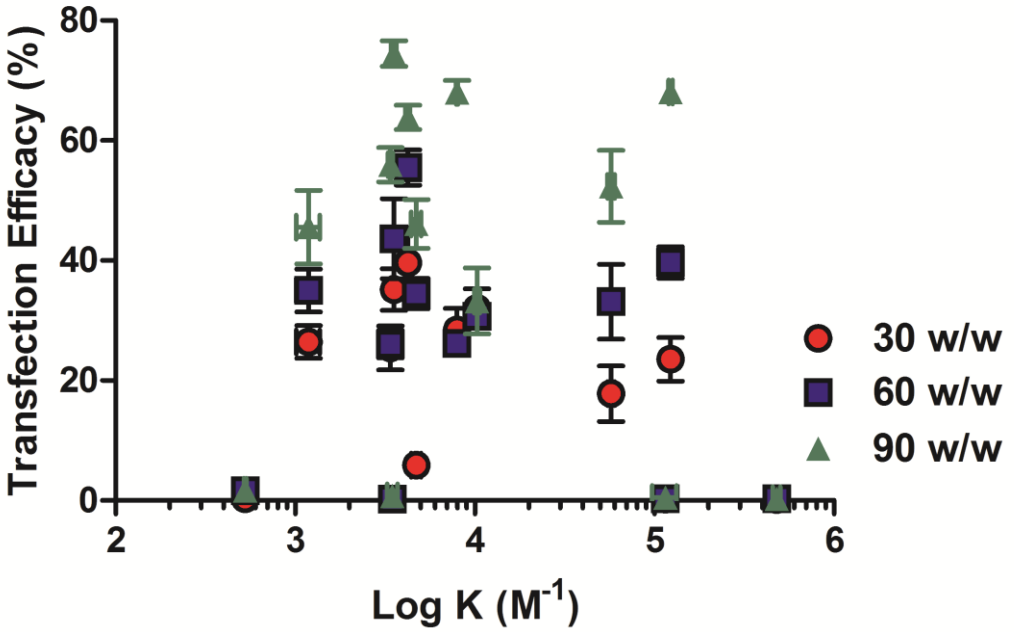

Figure S13. All binding constants against transfection efficacy using 70% serum in the GBM319 cell line.

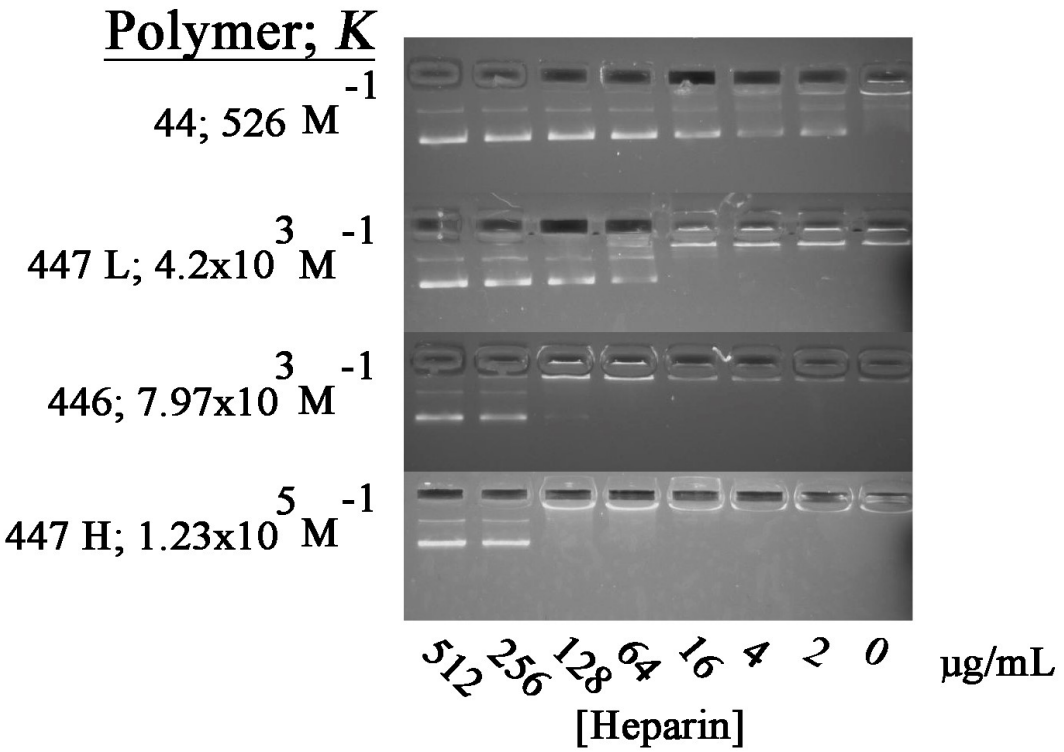

Figure S14. Heparin (ranging from 0 to 512 µg/mL) competition release assay of four representative polymers using gel electrophoresis; binding constants range from 526 (weakest *K* measured) to 1.23×10^5 M^{-1} (strongest *K* measured).

3.6 Schemes

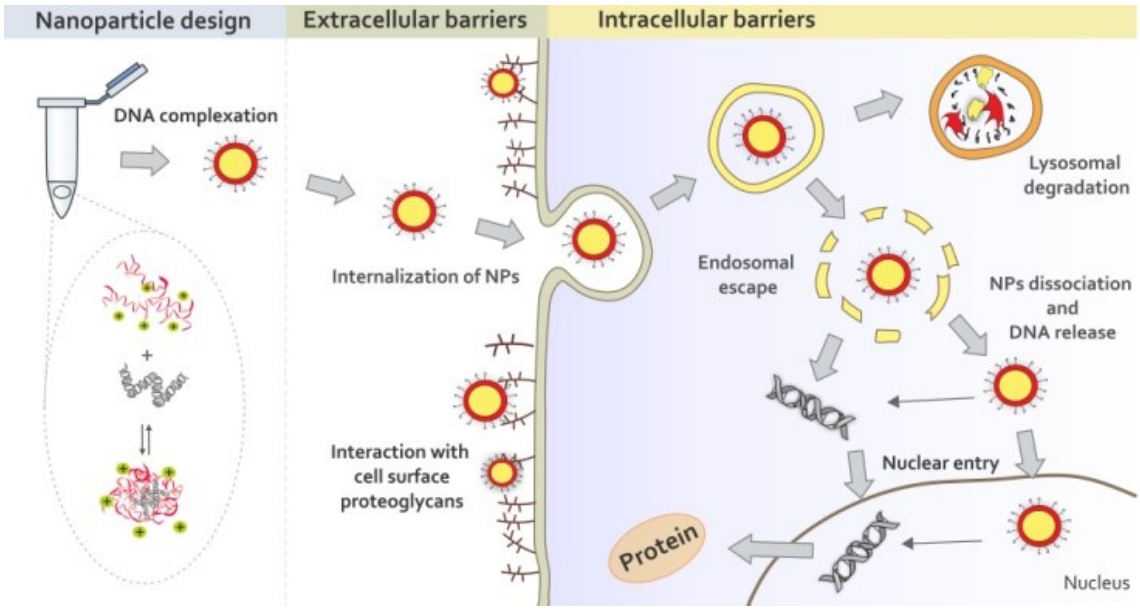

Scheme 1. Nanoparticle formulation, extracellular and intracellular barriers for successful gene delivery.

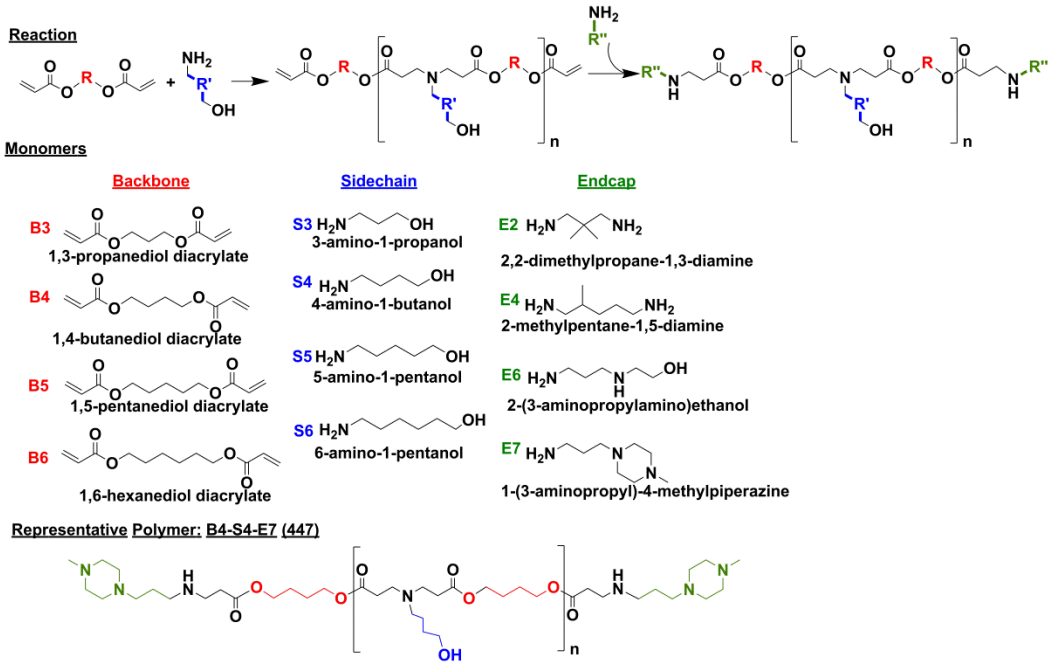

Scheme 2. Reaction of PBAE synthesis; backbone (B3-6), sidechain (s3-6) and various endcap (E2, E4, E6, E7) monomers used in the PBAE library. A representative polymer (447) is shown.

3.7 Tables

Table S1. List of PBAE polymers and their number average molecular weights (M_n), weight average molecular weights (M_w), polydispersity indices (PDI), degree of polymerizations (DP), Hill coefficients (α), binding constants (*K*), diameters (nm), and zeta potentials (ZP; mV).

Varying	Polymer	M_n (kDa)	M_w (kDa)	PDI	DP	α	*K* (M^{-1})	Diameter (nm)	ZP (mV)
Molecular Weight	447 Low M_w	7.9	10.3	1.3	27	0.40	$4.2 \pm 0.1 \times 10^3$	180	14
	447 Med M_w	10.4	14.7	1.4	35	0.22	$5.8 \pm 0.3 \times 10^4$	135	6
	447 High M_w	32.0	91.6	2.9	110	0.23	$1.23 \pm 0.03 \times 10^5$	171	14
Backbone	346	7.5	11.2	1.5	27	0.24	$4.8 \pm 0.2 \times 10^5$	122	14
	446	8.3	11.8	1.4	28	0.38	$7.97 \pm 0.09 \times 10^3$	130	18
	546	7.0	9.1	1.3	23	0.22	$1.03 \pm 0.04 \times 10^4$	178	15
	646	8.1	10.0	1.2	24	1.16	$1.19 \pm 0.04 \times 10^3$	230	15
Sidechain	437	8.1	10.3	1.3	29	0.28	$1.15 \pm 0.01 \times 10^5$	170	9
	447 Med M_w	10.4	14.7	1.4	35	0.22	$5.8 \pm 0.3 \times 10^4$	134	6
	457	10.3	13.1	1.3	33	0.41	$3.5 \pm 0.1 \mathrm{Ex} 10^3$	160	9
	467	10.3	12.5	1.2	31	0.39	$4.7 \pm 0.3 \times 10^3$	165	8
Endcap	44	9.3	11.6	1.2	32	0.62	526 ± 9	180	11
	442	7.5	10.4	1.4	25	0.42	$3.5 \pm 0.2 \times 10^3$	200	12
	444	7.4	10.3	1.4	25	0.50	$3.4 \pm 0.1 \times 10^3$	190	13
	446	8.3	11.8	1.4	28	0.38	$7.97 \pm 0.09 \times 10^3$	130	18
	447 Low M_w	7.9	10.3	1.3	27	0.40	$4.2 \pm 0.1 \times 10^3$	180	14

3.8 References

(1) Nielsen, L. L.; Maneval, D. C. *Cancer Gene Ther.* **1998**, *5*, 52-63.
(2) Ziady, A. G.; Kelley, T. J.; Milliken, E.; Ferkol, T.; Davis, P. B. *Mol. Ther.* **2002**, *5*, 413-9.
(3) Thomas, M.; Klibanov, A. M. *Appl. Microbiol. Biotechnol.* **2003**, *62*, 27-34.
(4) Pearson, S.; Jia, H. P.; Kandachi, K. *Nat. Biotechnol.* **2004**, *22*, 3-4.
(5) Sunshine, J. C.; Bishop, C. J.; Green, J. J. *Ther. Deliv.* **2011**, *2*, 493-521.
(6) Sunshine, J. C.; Akanda, M. I.; Li, D.; Kozielski, K. L.; Green, J. J. *Biomacromolecules* **2011**, *12*, 3592-3600.
(7) Green, J. J. *Ann. Biomed. Eng.* **2012**, *40*, 1408-1418.
(8) Green, J. J.; Langer, R.; Anderson, D. G. *Acc. Chem. Res.* **2008**, *41*, 749-759.
(9) Shmueli, R. B.; Sunshine, J. C.; Xu, Z. H.; Duh, E. J.; Green, J. J. *Nanomed.-Nanotechnol.* **2012**, *8*, 1200-1207.
(10) Sunshine, J.; Green, J. J.; Mahon, K. P.; Yang, F.; Eltoukhy, A. A.; Nguyen, D. N.; Langer, R.; Anderson, D. G. *Adv. Mater.* **2009**, *21*, 4947-+.
(11) Tzeng, S. Y.; Guerrero-Cazares, H.; Martinez, E. E.; Sunshine, J. C.; Quinones-Hinojosa, A.; Green, J. J. *Biomaterials* **2011**, *32*, 5402-10.
(12) Bhise, N. S.; Shmueli, R. B.; Gonzalez, J.; Green, J. J. *Small* **2012**, *8*, 367-73.
(13) Akinc, A.; Lynn, D. M.; Anderson, D. G.; Langer, R. *J. Am. Chem. Soc.* **2003**, *125*, 5316-23.
(14) Akinc, A.; Langer, R. *Biotechnol. Bioeng.* **2002**, *78*, 503-8.
(15) Sunshine, J. C.; Peng, D. Y.; Green, J. J. *Mol. Pharm.* **2012**, *9*, 3375-83.
(16) Sunshine, J. C.; Sunshine, S. B.; Bhutto, I.; Handa, J. T.; Green, J. J. *PloS one* **2012**, *7*, e37543.
(17) Huang, Y. H.; Zugates, G. T.; Peng, W.; Holtz, D.; Dunton, C.; Green, J. J.; Hossain, N.; Chernick, M. R.; Padera, R. F., Jr.; Langer, R.; Anderson, D. G.; Sawicki, J. A. *Cancer Res.* **2009**, *69*, 6184-91.
(18) Eltoukhy, A. A.; Siegwart, D. J.; Alabi, C. A.; Rajan, J. S.; Langer, R.; Anderson, D. G. *Biomaterials* **2012**, *33*, 3594-3603.
(19) Wang, J.; Gao, S. J.; Zhang, P. C.; Wang, S.; Mao, M. Q.; Leong, K. W. *Gene Ther.* **2004**, *11*, 1001-1010.
(20) Zelikin, A. N.; Trukhanova, E. S.; Putnam, D.; Izumrudov, V. A.; Litmanovich, A. A. *J. Am. Chem. Soc.* **2003**, *125*, 13693-13699.
(21) Plank, C.; Tang, M. X.; Wolfe, A. R.; Szoka, F. C., Jr. *Hum. Gene Ther.* **1999**, *10*, 319-32.
(22) Schaffer, D. V.; Fidelman, N. A.; Dan, N.; Lauffenburger, D. A. *Biotechnol. Bioeng.* **2000**, *67*, 598-606.
(23) Leong, K. W.; Mao, H. Q.; Truong-Le, V. L.; Roy, K.; Walsh, S. M.; August, J. T. *J. Control. Release* **1998**, *53*, 183-193.
(24) Tam, P.; Monck, M.; Lee, D.; Ludkovski, O.; Leng, E. C.; Clow, K.; Stark, H.; Scherrer, P.; Graham, R. W.; Cullis, P. R. *Gene Ther.* **2000**, *7*, 1867-1874.
(25) Yu, R. Z.; Geary, R. S.; Leeds, J. M.; Watanabe, T.; Fitchett, J. R.; Matson, J. E.; Mehta, R.; Hardee, G. R.; Templin, M. V.; Huang, K.; Newman, M. S.; Quinn, Y.; Uster, P.; Zhu, G.; Working, P. K.; Horner, M.; Nelson, J.; Levin, A. A. *Pharm. Res.* **1999**, *16*, 1309-1315.

(26) Green, J. J.; Zugates, G. T.; Tedford, N. C.; Huang, Y. H.; Griffith, L. G.; Lauffenburger, D. A.; Sawicki, J. A.; Langer, R.; Anderson, D. G. *Adv. Mater.* **2007**, *19*, 2836-+.
(27) van der Aa, M. A. E. M.; Huth, U. S.; Hafele, S. Y.; Schubert, R.; Oosting, R. S.; Mastrobattista, E.; Hennink, W. E.; Peschka-Suss, R.; Koning, G. A.; Crommelin, D. J. A. *Pharm. Res.* **2007**, *24*, 1590-1598.
(28) Ketola, T. M.; Hanzlikova, M.; Urtti, A.; Lemmetyinen, H.; Yliperttula, M.; Vuorimaa, E. *J. Phys. Chem. B* **2011**, *115*, 1895-1902.
(29) Vuorimaa, E.; Ketola, T. M.; Green, J. J.; Hanzlikova, M.; Lemmetyinen, H.; Langer, R.; Anderson, D. G.; Urtti, A.; Yliperttula, M. *J. Control. Release* **2011**, *154*, 171-176.
(30) Vuorimaa, E.; Urtti, A.; Seppanen, R.; Lemmetyinen, H.; Yliperttula, M. *J. Am. Chem. Soc.* **2008**, *130*, 11695-700.
(31) Nanduri, V.; Sorokulova, I. B.; Samoylov, A. M.; Simonian, A. L.; Petrenko, V. A.; Vodyanoy, V. *Biosens. Bioelectron.* **2007**, *22*, 986-92.
(32) Michel, D. *Biophys. Chem.* **2007**, *129*, 284-288.
(33) Gelamo, E. L.; Tabak, M. *Spectrochim. Acta A* **2000**, *56*, 2255-2271.
(34) Gelamo, E. L.; Silva, C. H. T. P.; Imasato, H.; Tabak, M. *BBA-Protein Struct. M* **2002**, *1594*, 84-99.
(35) Ketola, T. M.; Hanzlikova, M.; Leppanen, L.; Ravina, M.; Bishop, C. J.; Green, J. J.; Urtti, A.; Lemmetyinen, H.; Yliperttula, M.; Vuorimaa-Laukkanen, E. *Journal of Physical Chemistry B* **2013**, *117*, 10405-10413.

4 Chapter 4: Degradable Polymer-Coated Gold Nanoparticles for Co-delivery of DNA and siRNA

4.1 Introduction

There is a need for improved nanobiotechnologies that enable intracellular delivery of difficult to deliver biologics such as nucleic acids. Ideally, a delivery material would be capable of delivering both large molecules such as DNA as well as small molecules such as siRNA, and thus be capable of both positive and negative regulation of genes. It also is necessary that such a delivery material is non-cytotoxic and desirable that it can enable multi-functionality through imaging and/or other therapeutic modalities.

Gold nanoparticles (AuNP) are easy to synthesize [1], monodisperse [1], biocompatible in various applications [2,3], have optical properties [2] useful for colorimetric sensor applications, and can be diversely functionalized with chemical moieties via thiol (R-SH) groups [2]. They can be used as biosensors or imaging agents, and can also be used as a therapeutic for theranostic applications. Their nanoscale size allows for the ability to passively target tumors via the enhanced permeability and retention (EPR) effect, and they can be functionalized with tumor/cancer-specific small molecules or antibodies for active targeting [4-6]. It has been shown that NPs up to 400 nm can leak through neovasculature around tumors due to abnormal endothelial cell fenestrations [7,8].

AuNPs have been imaged *in vitro, ex vivo*, and *in vivo* via various modalities, either natively or with further chemical modification, such as: x-ray computed

---

Chapter 4 was published as "Bishop CJ, Tzeng SY, Green JJ. Degradable polymer-coated gold nanoparticles for co-delivery of DNA and siRNA. *Acta Biomater.* 2015;11:393-403."

tomography, transmission electron and dark-field microscopies, multiphoton, and surface enhanced Raman spectroscopies, two-photon luminescence and photoacoustic tomography [9-11].

AuNPs are also able to be physicochemically tuned for use in photothermal therapy. When light is directed to AuNPs at the surface plasmon resonance (SPR) wavelength, heat is produced. If the nanoparticles (NPs) are engineered appropriately, cellular damage due to heat can be directed towards tumors through NP targeting and by the decreased ability of tumors to self-thermoregulate [12]. SPR wavelengths may be tuned in the near infrared (NIR) region which is useful as NIR is transparent to biological tissue on the order of centimeters [13].

AuNPs are able to deliver a payload through conjugation or ionic complexation to small molecules [14], or various nucleic acids, such as DNA [15], short hairpin RNA or short interfering RNA (siRNA) [16] for promoting or inhibiting protein expression. Layer-by-layer (LbL) approaches coat a surface or a core with multiple layers of charge-alternating polyelectrolytes [15,17-21]. NP LbL approaches are ideal for complexing ionically charged macromolecules into EPR-relevant sizes. LbL approaches can be accomplished using aqueous solvents, are versatile regarding molecular structure as natural and synthetic polyelectrolytes are able to be used, and are easily tuned by varying the number and order of the layers [18,22].

Although viruses may be effective nucleic acid delivery vectors, many have been associated with immune complications and/or insertional mutagenesis and therefore we have focused our efforts using safer, non-viral methods [23]. In this work, we report a proof of concept of simultaneous non-viral knockdown and exogenous gene expression via an

LbL theranostic platform technology with biodegradable polymers as outer layers. This system was validated *in vitro* using human primary glioblastoma multiforme (GBM) cells [24,25]. The hybrid NPs employ two uniquely degrading polymers for release, one based on hydrolysis of ester groups and the other based on environmentally-triggered degradation of disulfide linkages once the particles are in the cytoplasm. The ability to both inhibit and generate proteins of interest simultaneously with these NPs has many applications in cancer therapeutics, such as overcoming drug resistance, promoting apoptosis, and inhibiting migration as well as the rectification of diseases caused by aberrant proteins [26,27].

4.2 Materials and Methods

4.2.1 Materials

Materials: The AuNPs were synthesized using tetrachloroauric acid ($HAuCl_4$) trihydrate (Ted Pella, Inc.), sodium citrate (Na_3-Citrate) tribasic dehydrate (Sigma Aldrich), a reflux condenser (Sigma Aldrich), mineral oil (Sigma Aldrich), a hot plate with magnetic stir bar (Fisher Scientific), and 11-mercaptoundecanoic acid (11-MUA). The polymers were synthesized from commercially available monomers N,N'-bis(acryloyl)cystamine (BSS) (Alfa Aesar), 3-amino-1-propanol (S3) (Alfa Aesar), and 1-(3-Aminopropyl)-4-methylpiperazine (E7) (Alfa Aesar), 1,4-Butanediol diacrylate (B4) (Alfa Aesar), and 4-amino-1-butanol (S4) (Alfa Aesar). Other reagents used included sodium acetate (NaAc), ethanol (EtOH), anhydrous dimethyl sulfoxide (DMSO) (Sigma Aldrich), methanol (MeOH) (Sigma Aldrich), 25 kDa branched polyethyleneimine (Sigma Aldrich), anhydrous tetrahydrofuran (THF) (Sigma Aldrich), anhydrous ethyl ether (Fisher

Scientific), Lipofectamine® 2000 (Invitrogen), OptiMEM I (Invitrogen), YO-PRO®-1 (Y3603; Invitrogen), Picogreen® (P7589; Invitrogen), Ribogreen® (Q10213; Invitrogen), Fluoraldehyde™ OPA assay (26025; Thermo Scientific). Cell culturing reagents included: fetal bovine serum (FBS), DMEM:Ham's F12 (1:1) (Invitrogen), 1x antibiotic-antimycotic (Invitrogen), anti-eGFP siRNA (sense: 5′-CAAGCUGACCCUGAAGUUCTT; anti-sense: 3′-GAACUUCAGGGUCAGCUUGCC), scrambled siRNA as a negative control (sense: 5′-AGUACUGCUUACGAUACGGTT; anti-sense: 3′-CCGUAUCGUAAGCAGUACUTT), plasmid enhanced green fluorescent protein DNA (eGFP-N1; referred to as eGFP) (Clontech), amplified and purified by Aldevron, pDsRed-Max-N1 DNA (dsRed) (Addgene), and CellTiter 96® AQueous One Solution Cell Proliferation Assay (Promega).

4.2.2 Colloidal Gold Nanoparticle Synthesis

Similar to the Frens Method [1], 20 mL of 0.01% solution of $HAuCl_4$ was vigorously boiling in a round bottom flask using mineral oil, a hot plate with magnetic stirring capabilities and a reflux condenser when 1 mL of a 1% solution of Na_3-Citrate was quickly injected therein and boiled for an additional 6 min. As the nucleation and growth of the AuNPs proceeded, the solution turned from a slightly yellow to a deep red solution. After boiling, the citrate-stabilized AuNPs (CAu) were cooled on ice for approximately 10 minutes. 11-MUA was conjugated to the AuNPs (MAu) to help ensure charge stability throughout the layering process. To do so, a 20 mM solution of 11-MUA was made in 95% EtOH and diluted to 1 mM using 70% EtOH which had been diluted

from 95% using 150 mM NaAc. The CAu was centrifuged at 20 krcf for 10 minutes and after the supernatant was removed an equal amount of the 1 mM 11-MUA solution was used to resuspend the CAu. The solution was sonicated at an amplitude of 1 for 2 seconds using a Misonix Ultrasonic Liquid Processor. The conjugation took place over 48 hours at room temperature and sonicated at approximately 4 hours and 40 hours during the conjugation process. The solution was washed in water twice by centrifugation (21 krcf for 10 minutes) and became a deep purple and cloudy with sonication as the 11-MUA crashed out of solution in the water. This solution was washed twice in ethanol again and then twice in 4.5 mg mL^{-1} of Na_3-citrate via centrifugation (21 krcf for 10 minutes). The solution retained its purple hue but was no longer cloudy. The resulting MAu solution in 4.5 mg mL^{-1} of Na_3-citrate was stable. The MAu solution was diluted to 0.31 nM and used in the LbL process.

4.2.3 Citrate-stabilized and 11-mercaptoundecanoic acid-stabilized Gold Nanoparticle Characterization

Transmission Electron Microscopy (TEM; Philips/FEI BioTwin CM120) was used to ascertain the diameter of the AuNPs on carbon-coated copper grids (FCF400-Cu; Electron Microscopy Sciences) which was also used to calculate the extinction coefficient ε according to Huo, et al. according to Equation 1 [28]:

$$\ln \varepsilon = 3.32111 \ln Diameter_{AuNP\ in\ nm} + 10.80505 \quad (1)$$

The concentration was determined by dividing the normalized absorbance (A cm^{-1}) which was measured using UV-Vis spectroscopy (Synergy2, Biotek®, Gen5 software) by ε according to the Beer-Lambert Law. The aggregation differences of naked CAu and

MAu were assessed by placement into increasingly more concentrated sodium acetate solutions which was the buffer used for layering (pH 5.2). The final concentration of sodium acetate after the first layer (PEI) was added to the AuNPs was 63 mM.

4.2.4 Polymer Synthesis and Characterization

The reducible disulfide-containing poly(amido amine) (BSS-S3-E7 or SS37) [29-31] and the hydrolytically degradable poly(beta-amino ester) (B4-S4-E7 or 447) [24] polymers were synthesized as previously reported **(Scheme S1)**.

Briefly, polymer SS37 was synthesized by adding the BSS monomer in a 4:1 v/v mixture of MeOH and water, and subsequently adding the S3 monomer in a 1.05:1 molar ratio under nitrogen. The reaction was kept in the dark, with constant stirring under positive nitrogen pressure via a balloon syringe at 45°C for 14 days **(**Scheme S1**)**. The solution became clear after the first couple of hours. Once the reaction was complete the polymer was purified using reverse-dialysis with a molecular weight cut-off of 2 kDa in 2 L of pH 3 Milli-Q water with constant stirring for 24 hours. Fresh pH 3 water was changed out at 8 hours. After washing in water using centrifugation, the polymer was frozen in liquid nitrogen and lyophilized. The polymer was then made into a 167 mg mL^{-1} solution using anhydrous DMSO. 0.5 M E7 in DMSO was added to dilute the 167 mg mL^{-1} solution to 100 mg mL^{-1} in a 0.5 M solution.

Polymer 447 was synthesized by mixing neat monomers B4 and S4 in a 1.2:1 molar ratio. The reaction was carried out for 24 hours at 90°C in the dark with constant stirring. The diacrylate-terminated base polymer was dissolved in anhydrous THF. E7 in anhydrous THF was added for a final concentration of 100 mg mL^{-1} B4-S4 base polymer

and 0.2 M E7 endcap, and the mixture was left to react for 1 hour while shaking at 1000 RPM (Scheme S1). The endcapped polymer was then precipitated into anhydrous ethyl ether in a 4:1 v/v ratio of ether to THF. The polymer was collected by centrifugation at 4000 RPM for 5 min, the supernatant was decanted, and the polymer was washed once more with ether and collected by centrifugation. Polymer was allowed to dry for 2 days under vacuum, was then dissolved in anhydrous DMSO at a final polymer concentration of 100 mg mL^{-1}, and was subsequently stored at -20 °C with desiccant until use.

GPC (Waters®, Breeze 2 software) was used to assess the M_n, M_w, and PDI using three 37.8 x 300 mm columns in series at a flow rate of 1 mL min^{-1} of GPC solvent (94% THF, 5% DMSO, 1% piperidine containing approximately 10 mg of butylated hydroxytoluene).

4.2.5 Polyelectrolyte Layering Process

The layering process is depicted in **Scheme 1** [18,22] 80 µL of 25 kDa branched PEI was added to 112 µL of the 0.31 nM MAu ($1.9x10^{11}$ particles mL^{-1}) in water, shaken for 30 minutes at 500 RPM at room temperature, and centrifuged twice at 10 krcf for 10 minutes to remove uncomplexed polyelectrolytes (extracted 182 µL). The supernatant after the first and second washing was replaced with 182 µL and 102 µL of 150 mM NaAc, respectively. Each subsequent layer was added to the previous resuspended complexes using 80 µL of the polyelectrolyte in 150 mM NaAc. The order in which the polyelectrolytes were layered with their associated concentrations are as follows: MAu (0.31 nM)-PEI (10 mg mL^{-1})-DNA (0.5 mg mL^{-1})-PEI (10 mg mL^{-1}) or SS37 (5 mg mL^{-1}) or 447 (5 mg mL^{-1})-DNA (0.5 mg mL^{-1}) or anti-eGFP siRNA (4 µM)-447 (1.25, 2.5, or 5

mg mL^{-1}) or PEI (0.25 mg mL^{-1}). The supernatant of the second wash just prior to adding the last layer was replaced with 25 mM NaAc and the last polyelectrolyte layer was also added in 25 mM NaAc.

4.2.6 Diameter and Zeta Potential

The diameter and ZP at each of the layered stages of the DNA/siRNA co-delivery NP formulation with a 447 concentration of 5 mg mL^{-1} were ascertained via NP tracking analysis using a NanoSight NS500 ($n \geq 2$), and a Malvern Zetasizer Nano ZS (Malvern Instruments, detection angle 173°, 633 nm laser; Smoluchowski model) (n=3), respectively. The diameters were calculated after the two washing steps, just prior to adding the subsequent layer in the same diluent (0 to 3.1-fold dilution) as in the usual polyelectrolyte layering process. The unknown diffusivity (D) was calculated from the root mean square distance (<x>) and time (t) in Equation 2 (2-dimensional) below:

$$< x >= \sqrt{4Dt} \quad (2)$$

which can then be used to calculate the unknown hydrodynamic radius using the Stokes-Einstein equation shown in Equation 3 (K_B = Boltzmann constant, T = temperature in Kelvin, μ = viscosity, r = hydrodynamic radius):

$$D = \frac{K_B T}{6\pi\mu r} \quad (3)$$

The ZPs were measured after the second washing at each layer after a 3.6-fold dilution in ultra pure distilled water.

Although the diameter quantified using the NanoSight NS500 instrument is also an indicator of aggregation, we endeavoured to corroborate these findings via TEM. In doing so, 30 μL of the sample of interest was placed onto corona plasma-treated, carbon-

coated copper grids. CAu in water was air dried; the PEI to 447 layers (using the 11-MUA conjugated CAu or MAu) layers were adsorbed for 30-45 minutes, followed by wicking and rinsing in water. Similar to when the diameter and ZP were assessed, the 447 layer was at 5 mg mL^{-1}.

4.2.7 Nucleic Acid Loading and Layering Efficiency

To quantify the amount of nucleic acid loaded in the various formulations, three different nucleic acid-intercalating probes were used. When quantifying the amount of DNA in the absence of siRNA, YO-PRO®-1 was used. YO-PRO®-1 can fluoresce in the presence of either DNA or siRNA, therefore nucleic acid-specific intercalating probes were used when quantifying DNA and siRNA in the presence of the other, namely, Picogreen® and Ribogreen®, respectively.

When quantifying the amount of nucleic acid present using DNA intercalators, it is important to ensure that ionically complexed nucleic acid is all detected as the complexed form is less accessible to the nucleic acid-intercalating probes. To ensure all nucleic acid present was detected in the presence of polymer, branched PEI with a known amount of DNA or siRNA using 10 w/w was used for optimization of the disassembly process ($n \geq 3$) by adjusting the salt and heparin concentrations. When quantifying the amount of DNA in the absence of siRNA, the formulation is brought to 10 μM YO-PRO®-1, 650 mM salt (PBS and NaAc) and 300 μg mL^{-1} of heparin and measured using a fluorescence plate reader (excitation and emission of 485 nm and 528 nm). When quantifying the amount of DNA in the presence of siRNA, the formulation tested is brought to 650 mM salt (PBS and NaAc) and 110 μg mL^{-1} of heparin at the completion of

the layering process and measured using a 1:200 dilution of Picogreen® in a 1x tris and EDTA (TE) buffer using an excitation and emission of 485 and 528 nm (1 μL of sample + 199 μL of 1:200 dilution Picogreen® in 1x TE buffer). When quantifying siRNA in the presence of DNA, the formulation is brought to 8 mM salt (PBS and NaAc), 1040 μg mL^{-1} heparin and was measured using a 1:200 dilution of Ribogreen® in the provided RNA BR buffer using an excitation and emission of 644 and 673 nm (10 μL of sample + 200 μL of 1:200 dilution Ribogreen® in RNA BR buffer). The co-delivery DNA/siRNA LbL formulation's DNA and siRNA content was quantified after adding polymer 447 at 5 mg mL^{-1} (highest w/w formulation). The same DNA and siRNA content was used to calculate the w/w values when 2.5 or 1.25 mg mL^{-1} of polymer 447 was added as the last layer as there is the same amount of nucleic acid present before the 447 polymer is complexed (**Table S1**).

The content of DNA and siRNA quantified in the supernatants during the washing steps was performed with a NanoDrop 2000 Spectrophotometer (Thermo Scientific). The layering efficiency was calculated by multiplying the amount of nucleic acid ionically complexed per vial by 100 and dividing by the total amount of nucleic acid added per vial.

4.2.8 Polymer Weight/DNA Weight Ratio

The w/w values for the layered formulations were calculated by dividing the mass of the unwashed polymer on the outer layer of the various formulations per mass of DNA or siRNA loaded per vial. Although the majority of the polymer in the layered formulations is the unwashed outer layer, we investigated the extent to which an earlier

washed polymer layer could be contributing to the w/w values. The amount of PEI complexed was calculated by subtracting the uncomplexed PEI extracted in the supernatants from the amount of PEI added which was calculated using a Fluoraldehyde™ OPA assay which detects primary amines using an excitation and emission of 340 and 420 nm, respectively.

4.2.9 Cell Culture and Transfection

The human glioblastoma multiforme cell line (GBM319) was derived from brain tumor stem cells (79 year old patient) and cultured as previously described [25] in a humid 37°C and 5% CO_2 atmosphere using DMEM:Ham's F12 (1:1) (Invitrogen) and supplemented with 1x antibiotic-antimycotic (Invitrogen) and 10% FBS. These eGFP negative cells were used to assess expression in layered formulations delivering DNA only (eGFP). To assess the ability to co-deliver DNA and siRNA using layered formulations (termed LD or HD), stably expressing eGFP-positive GBM319 cells were used which were previously transfected with B4-S5-E3/eGFP polyplex and retained eGFP positivity in 1.2% of the cells 3 months post-transfection [32]; these cells were cell sorted multiple times to obtain a more pure eGFP positive population of 81%. Knockdown in the stably expressing eGFP-positive GBM319 cells was assessed using anti-eGFP siRNA and a scrambled siRNA as a control. Expression in the stably expressing eGFP-positive cells was assessed using red fluorescence protein transcribed and translated from dsRed DNA. Lipofectamine® 2000 was used as a positive control for knockdown and expression. All formulations were delivered as 20 μL, except for Lipofectamine® 2000 delivering dsRed DNA.

The GBM319 cells (eGFP-positive and negative) were seeded in 96-well plates at 10,000 cells well^{-1} 1 day prior to transfection. The positive controls and various layered formulations were delivered to the cells and the 96-well plates were gently rocked manually. 2 hours after delivery the media was changed.

4.2.10 Transfection Assessment and Quantification

Fluorescence microscope images (Zeiss) were taken of the various formulations on days 1 through 3 (10x magnification) for expression and day 7 (5x magnification) for knockdown. The exposure times for the eGFP and dsRed channels were 200 and 600 ms, respectively.

A Synergy2 fluorescence plate reader was used to assess knockdown each day until the strongest knockdown reached a maximum, and then the knockdown was assessed using the more sensitive method of flow cytometry. To ensure the knockdown assessment is due solely to RNA interference and not as a result of cytotoxicity, a scrambled control was used. The knockdown was calculated using Equation 4 using an excitation and emission of 485 and 528 nm (F_{si} = fluorescence of the well using anti-eGFP siRNA; F_{sc} = fluorescence of the well using scrambled siRNA; $F_{Background}$ = fluorescence background of media without cells; F_{osi} = initial fluorescence of well just prior to delivery for the anti-eGFP formulations; F_{osc} = initial fluorescence of well just prior to delivery for the scrambled siRNA formulations):

$$Knockdown\ \% = 100\left(1 - \frac{[F_{si} - F_{Background}]}{F_{osi}} \frac{F_{osc}}{[F_{sc} - F_{Background}]}\right) \quad (4)$$

ImageJ analysis was performed on days 1 through 3 to determine the day of maximal expression. A BD Accuri™ C6 flow cytometer equipped with an automatic

HyperCyt sampler was used to assess expression at day 2 and knockdown at day 7. The singlet population was identified using FSC-H vs SSC-H; the FL1-H vs FL3-H channel was used to assess the eGFP and dsRed population percentages. When the stably expressing eGFP GBM319 cells were used to assess co-delivery of DNA and siRNA, an FL1 90% filter was used to ensure the FL1 detector was not saturated. FL1-H vs FL3-H were chosen as this minimizes overlapping fluorescence. Knockdown was calculated by flow cytometry by quantifying the geometric mean for the anti-eGFP siRNA and scrambled groups of the eGFP-positive region using FL1-A, according to Equation 5:

$$Knockdown\ \% = 100 - 100\frac{anti{-}eGFP\ siRNA\ Geometric\ Mean}{scrambled\ siRNA\ Geometric\ Mean} \quad (5)$$

4.2.11 Cytotoxicity

An MTS assay, CellTiter 96®, was used to assess the RMA relative to an untreated group which was normalized to 100% 24 hours post-transfection. The MTS assay is an indicator of cytotoxicity or viability. We wished to evaluate if the nanoparticles became increasingly cytotoxic following the degradation of the outer layer, which was composed of biodegradable polymer 447. This polymer has been shown to have a half-life of 2-5 hrs [33]. We therefore incubated the particles at 37°C in complete media for 18 hrs and then subsequently, these particles were added to GBM319 cells at the same concentration and dosage as the HD5 formulation. Cellular viability was measured using an MTS assay at 24 hours post-transfection. A two-tailed Student's t-test was used to compare the degraded and the non-degraded HD5 formulations.

4.2.12 Cellular Uptake

TEM was also used to assess cellular uptake of the co-delivery LbL formulation. The GBM319 cells, after 2 hours of LbL formulation incubation using the 300 ng DNA and 240 ng of siRNA formulation at respective w/w values of 56 and 69, were fixed, dehydrated, and infiltrated with Epon, and then using an ultramicrotome were sectioned into 70-100 nm slices.

More specifically, the cells were washed with PBS and were fixed using a glutaraldehyde buffer (2.5% v/v; 0.1 M sodium cacodylate buffer (CaCO), 3 mM CaCl, 1% sucrose, pH 7.2-7.4) and rocked overnight at 4°C. The following day, the cells were washed 3x in a new glutaraldehyde buffer (0.1 M CaCO, 3 mM CaCl, 3% sucrose) for 15 minutes each while being vigilant to not allow the cells to dry out. The cells were then left in the dark with a 1% osmium tetroxide solution (0.1 M CaCO, 3 mM CaCl) for at least 1 hour on ice and then the cells were washed twice in fresh deionized water for 5 minutes. Filtered (0.22 μm) 2% uranyl acetate solution in water was used to cover the cells for a maximum of 1 hour in the dark. The cells then underwent a dehydration series using 50, 70, 90 and then freshly opened 100% ethanol. Subsequently, Epon (1:1 solution of propylene oxide: Epon) was added in a swirling fashion and left overnight. The following day Epon with 1.5% DMP-30 (Ted Pella, Inc.) catalyst was added and placed in a vacuum chamber (15 inches of Hg) for two hours twice and then placed on a rocker for another 2 hours. The Epon was again replaced and put into an oven at 37°C and was allowed to cure for 72 hours. The cells were then placed at 60°C for 24 hours. Pliers were then used to break the edges carefully. The dish was snapped off to allow clean breaks and to minimize the creation of aberrant lines in the sample. The samples were then cut

out and sliced using an ultramicrotome and imaged on formvar-coated notched grids (Electron Microscopy Sciences).

4.2.13 Statistics

All errors reported are standard error of the means (SEM). The errors reported in **Figure 2A** ($n \geq 2$) and **1B** ($n = 3$) are independently prepared samples with at least 3 TR, except CAu and MAu are technical replicates (TR) ($n = 3$) as they are from a single batch synthesis. The errors in **Figure S3** are TR ($n \geq 3$). The errors reported in **Table 1** and **Figure S4** are $n \geq 3$ with at least 3 TR. **Figure 3** errors are TR (LD and HD $n = 20$; Lipofectamine® 2000 $n = 4$); a one-way ANOVA was performed using a Bonferroni's Multiple Comparison Test to assess knockdown differences between the day of maximum knockdown and day 7 when flow cytometry was performed (p-value > 0.05 is not significant). Errors reported in **Figure 4** are TR (LD, HD, and untreated are $n \geq 16$; Lipofectamine® 2000 is $n = 4$); a one-way ANOVA was performed using a Bonferroni's Multiple Comparison Test post hoc where *** is a p-value < 0.0001. **Figure S6**, **S7**, and **S9** are TR with $n = 4$, $n \geq 4$, and $n \geq 4$, respectively. A one-way ANOVA was performed on **Figure 7** and **Figure S9** using a Dunnett's Multiple Comparison Test to assess significance between Lipofectamine® 2000 where *** is a p-value < 0.0001.

4.3 Results

4.3.1 Citrate-stabilized and 11-mercaptoundecanoic acid-stabilized Gold Nanoparticle Characterization

Citrate-stabilized AuNP (CAu) batches were synthesized following a modified Frens Method [1] (see methods). CAu NPs were then conjugated with 11-mercaptoundecanoic acid (11-MUA) to obtain MAu NPs that were 17 ± 2 nm in diameter **(Figure 1; far left).** Based on the TEM diameter of the CAu, the extinction coefficient, ε, was calculated to be $6.3x10^8$ M^{-1} cm^{-1}. Using the absorbance from UV-Visible (UV-Vis) spectrometry, the working concentration of MAu was calculated to be 0.31 nM which is equivalent to $1.9x10^{11}$ particles mL^{-1}. The SPR wavelength of the 11-MUA-unconjugated CAu was 520 nm in 4.5 mg mL^{-1} (pH 7.1) of sodium citrate (Na_3-citrate) and was red-shifted to 526 nm after 11-MUA conjugation (**Figure S1**) indicating the 11-MUA was conjugated successfully. The MAu solution aggregated far less than the CAu solution as indicated by the degree to which the SPR wavelengths red-shifted when placed in acidic NaAc buffer (**Figure S2**).

4.3.2 Polymer Characterization Via Gel Permeation Chromatography

1-(3-aminopropyl)-4-methylpiperazine end-modified poly(N,N'-bis(acryloyl)cystamine-co-3-amino-1-propanol) (abbreviated here as SS37) containing disulfide bonds. The 1-(3-aminopropyl)-4-methylpiperazine end-modified poly(1,4-butanediol diacrylate-co-4-amino-1-butanol) (abbreviated here as 447) is a poly(beta-amino ester) (PBAE) containing ester linkages.

Polymer molecular weight was ascertained by gel permeation chromatography (GPC). SS37 had a number average molecular weight (M_n) and weight average

molecular weight (M_w) of 2.5 kDa and 2.7 kDa respectively. 447 had an M_n of 10.2 kDa and an M_w of 39.8 kDa.

4.3.3 Layer-by-layer Notation

Throughout the paper the notation to describe layered NPs is as follows: polyethyleneimine (PEI) is abbreviated as "P"; DNA as "D"; and the synthetic polymers as "SS37" and "447." The specific mutilayered formulation that contains DNA and siRNA, MAu-P-D-SS37-siRNA-447, are referred to as "LD" or "HD," corresponding to low nucleic acid dose (LD) or high nucleic acid dose (HD). We investigated 6 different co-delivery multilayer particle formulations: 2 nucleic acid dosages at 3 different 447 concentrations (1.25, 2.5 or 5 mg mL^{-1}) as the last layer. These formulations are referred to as the low (LD) or high dosage (HD), following by 1.25, 2.5, or 5 mg mL^{-1} to indicate the polymer concentration of the last layer (for example: "LD2.5" or "HD5").

4.3.4 Diameter and Zeta Potential

By dynamic light scattering (DLS; Malvern Zetasizer) the measured intensity-weighted diameters for CAu and MAu were 23 ± 1 and 27 ± 2 nm, respectively. NanoSight calculated the concentration of layered particles for the HD5 formulation (MAu-P-D-SS37-siRNA-447) to be $(2.6 \pm 0.5)x10^9$ particles per mL. The largest increase in size following layering was observed when transitioning from MAu-P to MAu-P-D, when the DNA was added, leading to AuNP clusters consisting of several AuNPs within

each larger particle of approximately 230 nm (**Figure 2A**). Despite using higher concentrations of DNA (0.75 and 1.0 mg/mL) the diameter of the MAu-P-D formulation was not able to be significantly decreased. The diameters of the MAu-P-D formulation using 0.75 and 1.0 mg/mL were 180 ± 10 nm (n=3; p-value=0.20) and 170 ± 10 nm (n=3; p-value=0.18). As each subsequent polyelectrolyte layer was added to the NPs and washed, the zeta potential (ZP) of the NPs reversed in charge (**Figure 2B**).
TEM indicated a progressive increase in size up to the DNA layer. At this layer, TEM showed clustering of AuNPs into larger nanoparticles (**Figure 1**).

4.3.5 Nucleic Acid Loading and Layering Efficiency

Nucleic acid loading and layering efficiency was determined through evaluation with nucleic acid binding dyes. For measurements, heparin and salt concentrations (phosphate buffered saline (PBS) and NaAc) were optimized to displace polymer and allow the intercalating fluorescence dyes to detect the total nucleic acid present in the presence of 25 kDa PEI at 10 weight/weight (w/w; mass ratio of polymer to nucleic acid). YO-PRO®-1, Picogreen, and Ribogreen were able to detect 94.8 ± 0.8%, 101 ± 2%, and 100 ± 2% of the present nucleic acid, respectively (**Figure S3**). The amount of nucleic acid delivered per 96-well plate well in 20 μL volumes for the layered formulations is shown in **Table 1** (w/w discussed in section 2.6). The DNA doses delivered by the layered formulations ranged from 200 to 2400 ng DNA and the siRNA doses ranged from 160 and 240 ng siRNA.

In contrast to the MAu-P-D-P-D-447 formulation, the loading of the MAu-P-D-447-D-447 and MAu-P-D-SS37-D-447 formulations were determined to have lower loading than would be otherwise anticipated based on the loading of the MAu-P-D formulation. We observed that DNA loading was maximum when only non-degradable, highly charged polymers were used in the middle layers of the formulation, rather than more weakly charged and biodegradable polymers. This loading difference may be due to the differences in binding affinity between the varying cationic polymers and DNA [24,34].

When one DNA layer was utilized, the average percent of nucleic acid retained in the layering process, or the layering efficiency, was 24.1 ± 0.4%. When either polymers SS37 or 447 were used as the middle polymer layers with two layers of DNA, the average layering efficiency decreased to 5.8 ± 0.5%. When nondegradable and highly charged PEI was used as the first and middle layer with two layers of DNA, the layering efficiency was similar to the single DNA layer efficiency at 29 ± 1%. The nucleic acid layering efficiencies of DNA and siRNA for the co-delivery formulations were 12 ± 2% and 80 ± 3%, respectively. Further details on the quantification of layering efficiencies (**Supplemental Experimental Section**), nucleic acid content contained in the supernatants washes (**Figure S4**), and nucleic acid adsorbed to plasticware during formulation (**Figure S5)** are discussed in the supplemental information.

4.3.6 Polymer Weight/DNA Weight Ratio

The 447 polymer w/w for LbL formulations are listed in **Table 1** and **Table S1**. The DNA and siRNA co-delivery formulations were assessed at two different dosages and

three different concentrations of the outer polymer layer (1.25, 2.5 and 5 mg mL^{-1} of 447). The siRNA-free, "DNA only" LbL formulations had a polymer to nucleic acid weight ratio (w/w) that ranged from 0 to 92. The 447 w/w for the DNA and siRNA co-delivery formulations ranged from 14 to 83 w/w for DNA and 17 to 104 w/w for siRNA. The degree to which the inner ionically complexed layer of polymer could contribute to w/w was investigated using the PEI layer and was determined to range from 6-9 and 8-12 w/w for DNA and siRNA, respectively, according to the OPA assay.

4.3.7 Transfection and Cytotoxicity

4.3.7.1 siRNA-mediated Knockdown

SiRNA-mediated knockdown over time in human brain cancer cells was obtained by measuring decreased endogenous GFP expression of GFP+ human brain cancer cells following transfection with LbL particles containing GFP siRNA (**Figure 3**). The maximum knockdown during the time course for each co-delivery formulation occurred on days 5 and 6 and was highest with MAu-P-D-SS37-siRNA-447 LD5 and HD5, the formulations with the greatest concentration of polymer 447 as the outside layer of the particles. Relative fluorescence over time was measured by fluorimetry on a plate reader and fluorescence of individual cells was measured by flow cytometry at 7 days. There were no significant differences between the maximum and day 7 which was when flow cytometry was performed on all formulations (p-value > 0.05).

The knockdown varied according to the siRNA dosage and w/w, ranging from near 0% to 44 ± 5% according to the plate reader by measuring average fluorescence (**Figure 3**) and near 0% to 34 ± 3% by flow cytometry (**Figure 4**). Relative metabolic

activity (RMA) or normalized viability (to the untreated group) ranged from 73 ± 4% to 91 ± 6% among the layered NP formulations.

Lipofectamine® 2000, a commercially available leading non-viral transfection reagent, was used as a positive control at the same dosages as the co-delivery LD and HD formulations. According to the plate reader and flow cytometry assessment, the strongest knockdown observed with Lipofectamine® 2000 was with a volume to siRNA mass ratio (μL:μg) of 0.5:1 and 2.5:1 with an siRNA dosage of 240 and 160 ng, respectively. The 240 (0.5:1) and 160 ng (2.5:1) dosages reached their maximum knockdown on days 6 and 7, respectively (**Figure S6**). According to the flow cytometer and the plate reader, the 240 ng dosage reached 20 ± 2% and 25 ± 7% knockdown, respectively, and the 160 ng dosage reached 6 ± 3% and 19 ± 5% knockdown, respectively with the human brain cancer cells (**Figure S6 and S7**). The 160 ng 2.5:1 Lipofectamine® 2000 condition was quite toxic, with an RMA of 44 ± 1%, whereas the 240 ng 0.5:1 was 90 ± 2% (**Figure S7**). **Figure S6** shows all knockdown time courses of Lipofectamine® 2000 positive controls tested at various dosages and ratios to siRNA with RMAs greater than 70% according to the CellTiter assay.

Fluorescence microscope images of the enhanced green fluorescence protein (eGFP) channel showing the strength of knockdown at day 7 from the co-delivery DNA and siRNA LbL formulations with varying dosages and w/w, as well as Lipofectamine® 2000 at 240 ng (0.5:1) and 160 ng (2.5:1) as positive controls are shown in **Figure 5**.

4.3.7.2 DNA-mediated Expression

The exogenous DNA expression of the co-delivery DNA and siRNA LbL formulation reached maximal expression on day 2 and day 2 was chosen to assess

expression efficacy for all formulations in the study [24,35] The expression of each of the co-delivery LbL formulation dosages at various w/w are shown in fluorescence micrograph images (**Figure 6**). The expression ranged from near zero to 10.8 ± 0.5% (**Figure 7**). There was no statistical difference in the expression efficacy as measured by the percentage of positively transfected cells between HD5 and Lipofectamine® 2000 at a 100 ng dosage (2.5 μL:1 μg DNA). The RMA ranged from 73 ± 4 to 91 ± 6%.

The fluorescence images of the expression at day two of other non-siRNA containing LbL formulations, as well as their quantified expression according to flow cytometry are shown in **Figure S8** and **S9**, respectively. The expression for the DNA only layered formulations ranged from near 0 to 37 ± 2%. The MAu-P-D-P formulation was associated with approximately 3% transfection and an RMA of 26 ± 2% which was the most cytotoxic layered formulation investigated. The layered NP formulation that delivered two nucleic acid layers of DNA (no siRNA) that resulted in the highest transfection (28 ± 1%) was MAu-P-D-SS37-D-447. This is the same formulation of polymer layers chosen to co-deliver DNA and siRNA and was associated with a high RMA of 91 ± 2%. Lipofectamine® 2000 at a 100 ng dosage (2.5 μL:1 μg DNA) was associated with a transfection of 14 ± 2% and an RMA of 72 ± 5%. Formulations MAu-P-D-447, MAu-P-D-SS37-D-447, and MAu-P-D-447-D-447 were statistically significantly higher (p-value < 0.0001) than the Lipofectamine® 2000 positive control for exogenous DNA expression by 2.6, 2.0, and 1.6 fold, respectively (**Figure S9**).

4.3.8 Cytotoxicity of the Co-delivery HD5 Formulation 18 Hr Post-degradation

The HD5 formulation which had undergone 18 hours of degradation was statistically similar (p-value=0.34) to the non-degraded formulation in terms of its relative metabolic activity (cytotoxicity).

4.3.9 Cellular Uptake

Cellular uptake of the co-delivered LbL formulation HD5 is shown in **Figure 8** as measured by TEM. Inlaid images **Figure 8A** and **Figure 8B** show particles on the order of ~200 nm. **Figure 8C** shows putative endosomes (far two left arrows) containing multiple aggregates of AuNPs in the endosome.

4.4 Discussion

4.4.1 Citrate-stabilized and 11-mercaptoundecanoic acid-stabilized Gold Nanoparticle Characterization

The tendency for MAu to aggregate less throughout the layering process indicates that MAu was superior for layering purposes in comparison to CAu. The differences in the UV-Vis spectra in **Figure S2** also further validate that the 11-MUA conjugation was successful.

4.4.2 Polymer Characterization Via Gel Permeation Chromatography

SS37 is a disulfide-containing poly(amido amine) that was chosen as a degradable polyelectrolyte for layering because: 1) it is cationic to allow for nucleic acid complexation; 2) it contains tertiary amines to contribute to the proton sponge effect and endosomal escape [36]; 3) it contains disulfide linkages to facilitate triggered degradation following cytoplasmic delivery as the cytosol is a reducing environment. The 447 PBAE was chosen as a degradable polyelectrolyte for layering as: 1) it is also cationic; 2) it contains tertiary amines for aiding in the proton sponge effect and endosomal escape [36]; 3) it degrades hydrolytically due to its ester groups [37].

When we evaluated two layers of PEI coating AuNPs without using biodegradable polymers, we found the system to be less effective and excessively toxic (refer to section 3.5.2) compared to LbL AuNPs with less PEI that utilized biodegradable polymers. When we evaluated two layers of PEI coating AuNPs without using biodegradable polymers, we found the system to be less effective and excessively toxic (refer to section 3.5.2) compared to LbL AuNPs with less PEI that utilized biodegradable polymers. This finding is in agreement with previous literature, which has shown that PBAE polyplexes, such as 447/DNA polyplexes that have polymer 447 on their surface, have improved cellular uptake and are more effective than PEI/DNA polyplexes for gene delivery [38-40]. We believe this same phenomenon makes 447 better than PEI as an outer layer on our particles. Further variation of the degradability of the polymers that make up the multilayers may be useful for controlling expression and knockdown over time.

4.4.3 Diameter and Zeta Potential

The NanoSight NS500 is able to directly measure number-averaged NP diameter by Nanoparticle Tracking Analysis (NTA), rather than intensity-averaged NP diameter like DLS in aqueous media. In our testing, the uncoated CAu and MAu were unable to be accurately measured by NTA as the particle sizing limitation of the NanoSight NS500 with these materials was near 40 nm. However, for particles larger than 40 nm, the NanoSight measurements were similar to DLS measurements when measuring polyplexes or AuNPs layered with polymer. For example, DLS reported the diameters for MAu-P to be 80 ± 10 nm which is near the NanoSight measurement of 113 ± 3 nm (errors are standard deviation; n=6). Based on the TEM images (**Figure 1**) and the DLS particle size data (**Figure 2**), most MAu-P were singlets that had a PEI layer thickness of approximately 30 nm.

We hypothesize that the clustering effect during the layering process of positively charged polymer-coated AuNPs is due to multivalent interactions with DNA, as DNA is a large, anionic biomolecule. As the layering process proceeded, the NPs with outermost layers of SS37, siRNA, and 447 were all relatively similar in diameter to the DNA layer, approximately 200 nm. Assuming that no MAu was lost throughout the layering process, this would suggest that there are 43 ± 9 MAu cores per layered NP (initial number of MAu nanoparticles divided by the final number of LbL particles based on NTA). Because of the 3D aggregation of the MAu, it is difficult to directly count individual MAu in the final LbL nanoparticles by TEM (**Figure 1**, far right). Assuming the highest possible density of packing by the 17 nm MAu in a packed regular lattice to be 0.74, the maximum theoretical number of MAu that could fit into the volume of a 200 nm diameter spherical NP would be approximately 1200. Because we estimate that there are

approximately 43 MAu, rather than 1200, in an LbL NP this finding suggests approximately 4% of the occupied volume is MAu.

The reversal of the ZP demonstrates successful ionic complexation of each subsequent layer as the LbL coatings were built. TEM agreed well with the NanoSight measurements in that the largest increase in diameter occurred at the DNA layer and that the layered particles reached approximately 200 nm in size.

The inclusion of PEG-conjugated 447 as the last layer could perhaps further optimize the system and minimize clearance by the reticulo-endothelial system [41]. Furthermore, hyaluronic acid could be another polyelectrolyte candidate to help control biodistribution [42].

4.4.4 Nucleic Acid Loading and Layering Efficiency

PEI was demonstrated to be more efficient at binding nucleic acid than the degradable and less positively charged polymer 447. On a mass basis, the siRNA had higher loading efficiency into the LbL NPs than the DNA did (**Figure S4**). The packing densities for the HD5 formulation by volume for DNA and siRNA were approximately $3x10^{-4}$ and $5x10^{-2}$ molecules per nm^3, respectively (the mass per particle was calculated using the particle concentration determined by NTA). **Figures S4** and **S5** demonstrate that the two washing steps during the layering process are sufficient to ensure removal of free polyelectrolyte from solution prior to the addition of subsequent polyelectrolyte layers to the particles. Previous work by our group has shown that it is possible to lyophilize PBAE/DNA polyplexes in the presence of a cryoprotectant, such as sucrose,

resulting in the ability to store the gene delivery formulations long-term (>2 years) without compromising transfection efficacy [43].

Nucleic acid in solution during layering steps that does not electrostatically coat the NP is recovered in the supernatant following centrifugation or is removed from the solution due to adsorption to the surface of the plasticware used during fabrication. These inefficiencies were calculated during the fabrication of the LbL NPs. The accumulation of nucleic acid content contained in the two supernatants during washing steps is shown in Figure S4. Approximately 80% of all nucleic acid was accounted for in the LbL NPs and in the supernatants. The remainder of nucleic acid was observed adsorbed to the plasticware that was in contact with the nucleic acid solution during layering steps (Figure S5**)**. A pipette tip and vial without the LbL solution are shown in Figures S5A-B. The LbL solution in the vial without and with YO-PRO®-1 are shown in Figures S5C-D, respectively. Figure S5E-F shows the vial and pipette tip that came in contact with the LbL solution with YO-PRO®-1 to quantify nucleic acid.

Knowing the amount of nucleic acid in the second supernatant washings allows the calculation of the amount of free DNA or siRNA in the layered formulations when the subsequent polyelectrolyte layer is added. The amount of free DNA and siRNA after the second washing was determined to be negligible, less than the error of measurement of the dosages listed in Table 1. This finding supports the two washings during the layering process are sufficient to ensure a negligible amount of free polyelectrolyte in solution prior to the addition of the subsequent layer.

4.4.5 Transfection and Cytotoxicity

4.4.5.1 siRNA-mediated Knockdown

The w/w values in large part determined the time course of the knockdown; as the w/w increased for either 160 ng (LD) or 240 ng (HD) dosages, the knockdown increased in all cases. A decreased siRNA dosage did not necessarily result in decreased knockdown, depending on the w/w. The knockdown of the LD5 and HD5 formulations were statistically significantly higher than Lipofectamine® 2000 at 160 ng 2.5:1 by 1.4 and 1.8 fold, respectively, whereas formulations HD2.5, LD5, and HD5 were statistically significantly higher than Lipofectamine® 2000 at 240 ng 0.5:1 (**Figure 4**) by 5.8, 4.7, and 2.3 fold. The trends observed in the qualitative images are in agreement with the fluorescence plate reader and the flow cytometer's assessment of knockdown as well.

4.4.5.2 DNA-mediated Expression

The expression of the co-delivery HD and LD formulations increased with increasing dosage and w/w. Generally, the RMA increased as the expression efficacy decreased. The most efficacious NP formulation for expression of DNA was MAu-P-D-447. The biodegradable polymer 447 was demonstrated to be superior to the conventionally used nondegradable polymer, PEI, as an outer layer. It was necessary to have an outer layer of 447 polymer as the last layer in light of MAu-P-D-P's results as well as the observation that MAu-P-D (0 w/w) was associated with very low transfection

(0.12 ± 0.07%). MAu-P-D's results suggest that the inner layer of PEI was insufficient alone at promoting transcription and translation and was not contributing substantially to toxicity.

4.4.6 Cytotoxicity of the Co-delivery HD5 Formulation 18 Hr Post-degradation

The relative metabolic activities of the degraded and freshly prepared, non-degraded HD5 formulations were similar. Neither of these conditions showed significant cytotoxicity in GBM319 cells.

4.4.7 Cellular Uptake

One of the advantages of using gold as the core of the NPs is that it can be tracked by imaging. The hybrid LbL particles were able to enter the cells, be tracked by TEM, release siRNA into the cytoplasm to achieve knockdown, and release DNA that reaches the nucleus for exogenous expression. In contrast to viruses where a multiplicity of infection of even 1 can result in transduction, non-viral methods are less efficient and therefore require a much higher effective multiplicity of infection to get sufficient number of plasmids within the cell for sufficient expression, as just a few particles are observed to be within the cell in **Figure 8**. However, further studies would need to be conducted to correlate the number of particles uptaken with the resulting expression or knockdown.

4.5 Conclusions

We have successfully demonstrated that we can layer siRNA and DNA for co-delivery on AuNPs using polymers which degrade through different mechanisms. We found that the zeta potential reverses upon the addition of each oppositely charged layer of polyelectrolytes and the diameter reaches approximately 200 nm in size. PEI was found to be the most efficient polymer for loading nucleic acid, and polymer 447, the most effective outer layer polymer for gene delivery. The gene knockdown achieved with the HD5 and LD5 formulations was superior to optimized Lipofectamine® 2000 at comparable dosages in human brain cancer cells. These formulations also enabled exogenous DNA expression and intracellular tracking of the AuNPs by TEM. These LbL formulations are an enabling theranostic technology that can deliver combinations of genetic therapies along with an agent for potential imaging and photothermal therapy.

4.6 Figures

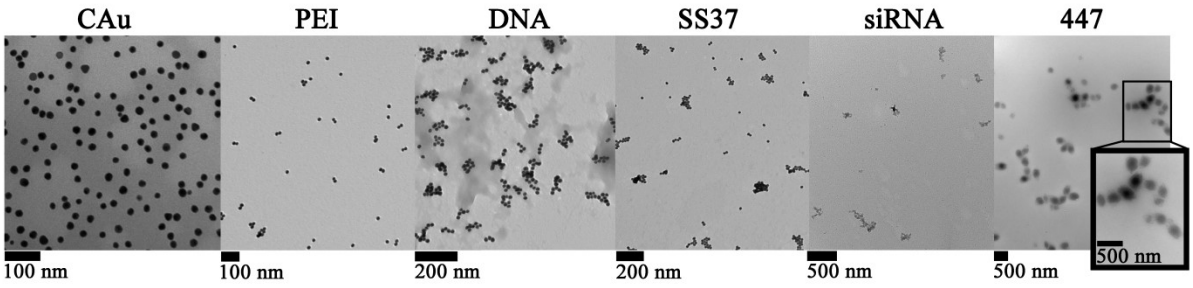

Figure 1. TEM images of each of the layered stages showing nanoparticle size. The addition of the DNA layer results in initial clustering of multiple gold nanoparticle cores together to form a single particle.

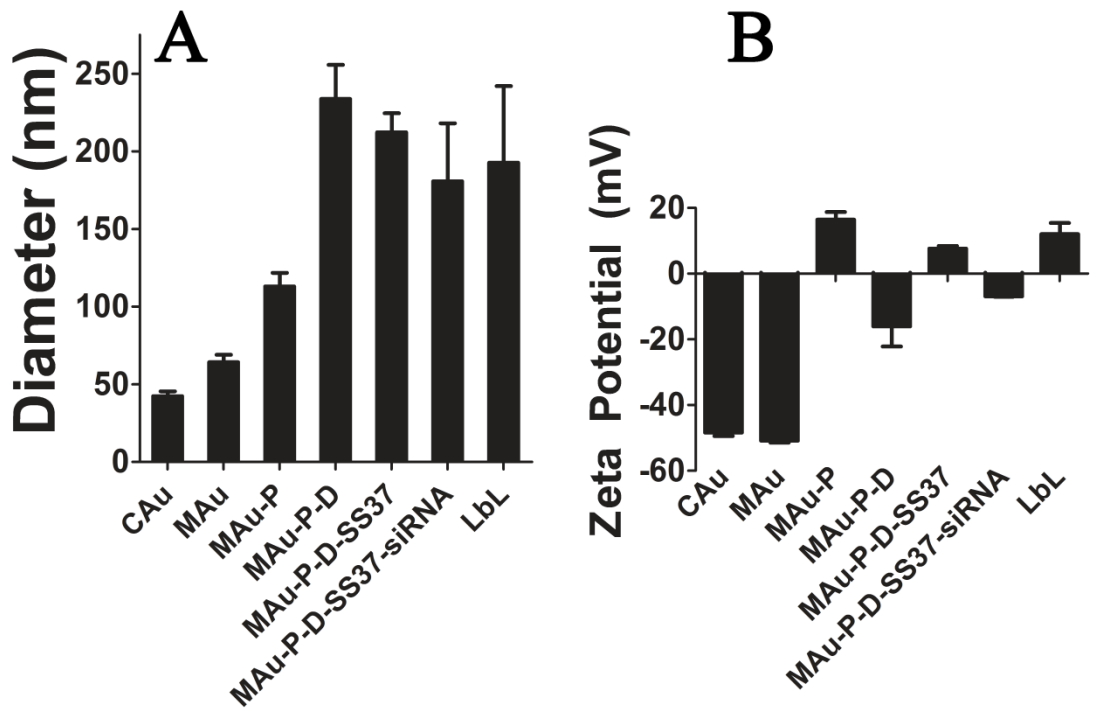

Figure 2. Diameter (A) and zeta potential (B) at each of the layering stages.

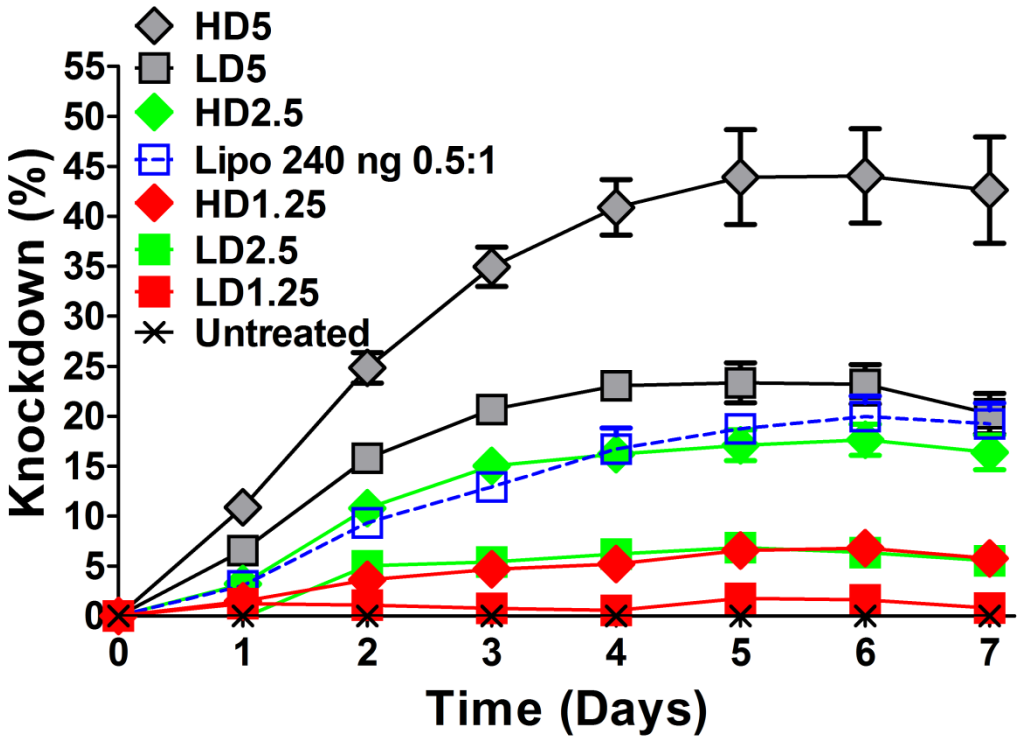

Figure 3. SiRNA-mediated knockdown over time of GFP in human brain cancer cells resulting from delivery of MAu/DNA/siRNA LbL particles. Nanoparticle dosages and amount of 447 polymer in the outer layer were varied. Optimized particles had higher knockdown than the optimized formulation of the leading commercially available reagent Lipofectamine® 2000.

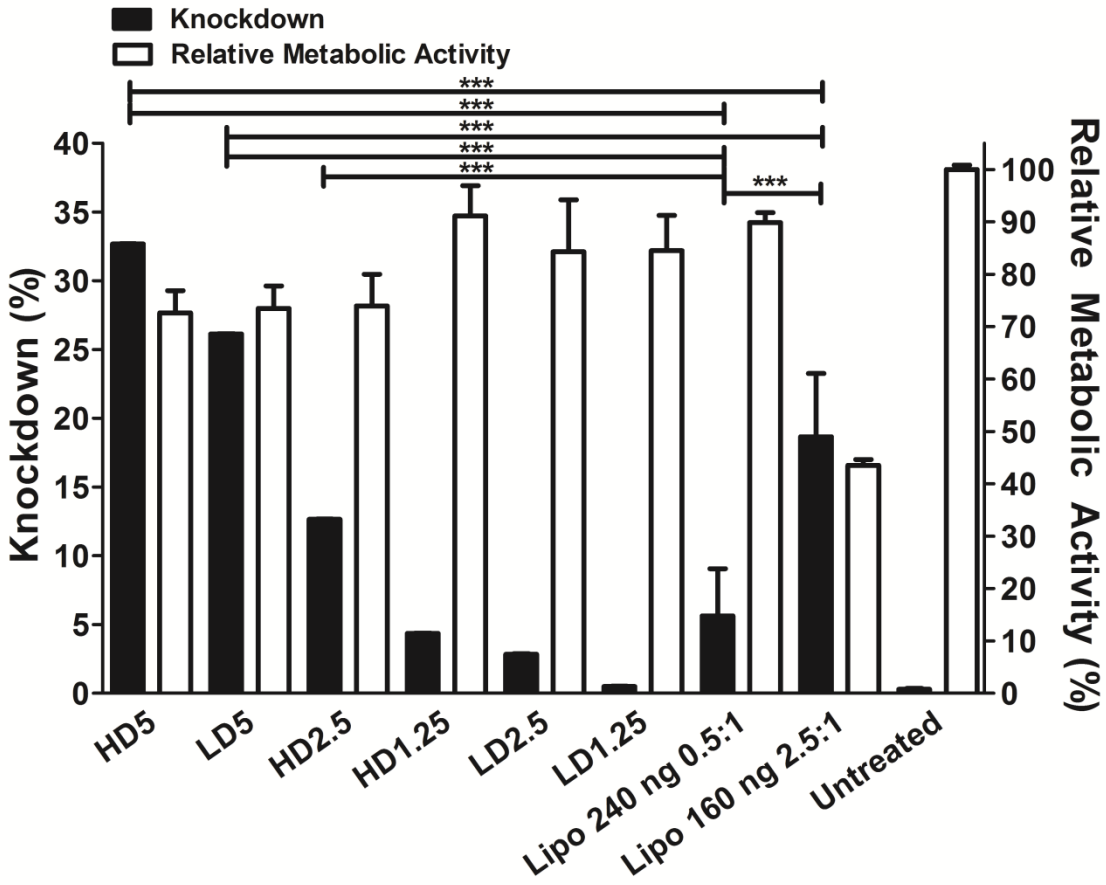

Figure 4. SiRNA-mediated knockdown of MAu/DNA/siRNA LbL particles on day 7 and relative metabolic activity at 24 hours post transfection of LbL NPs.

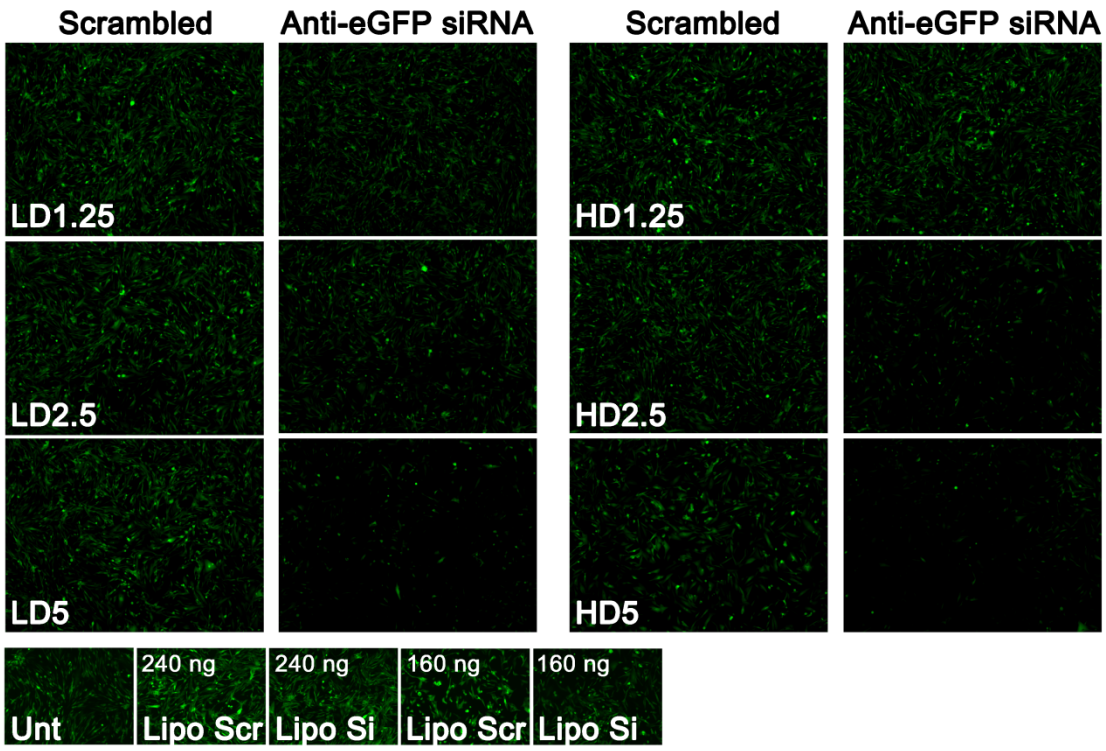

Figure 5. Fluorescence microscope images of the eGFP channel showing GFP knockdown following transfection with various MAu/DNA/siRNA LbL nanoparticles; the Lipofectamine® 2000 conditions shown are 240 ng 0.5:1 and 160 ng 2.5:1 (200 ms eGFP exposure time; magnification of 5x; "scr" refers to scrambled siRNA and "si" refers to active anti-eGFP siRNA).

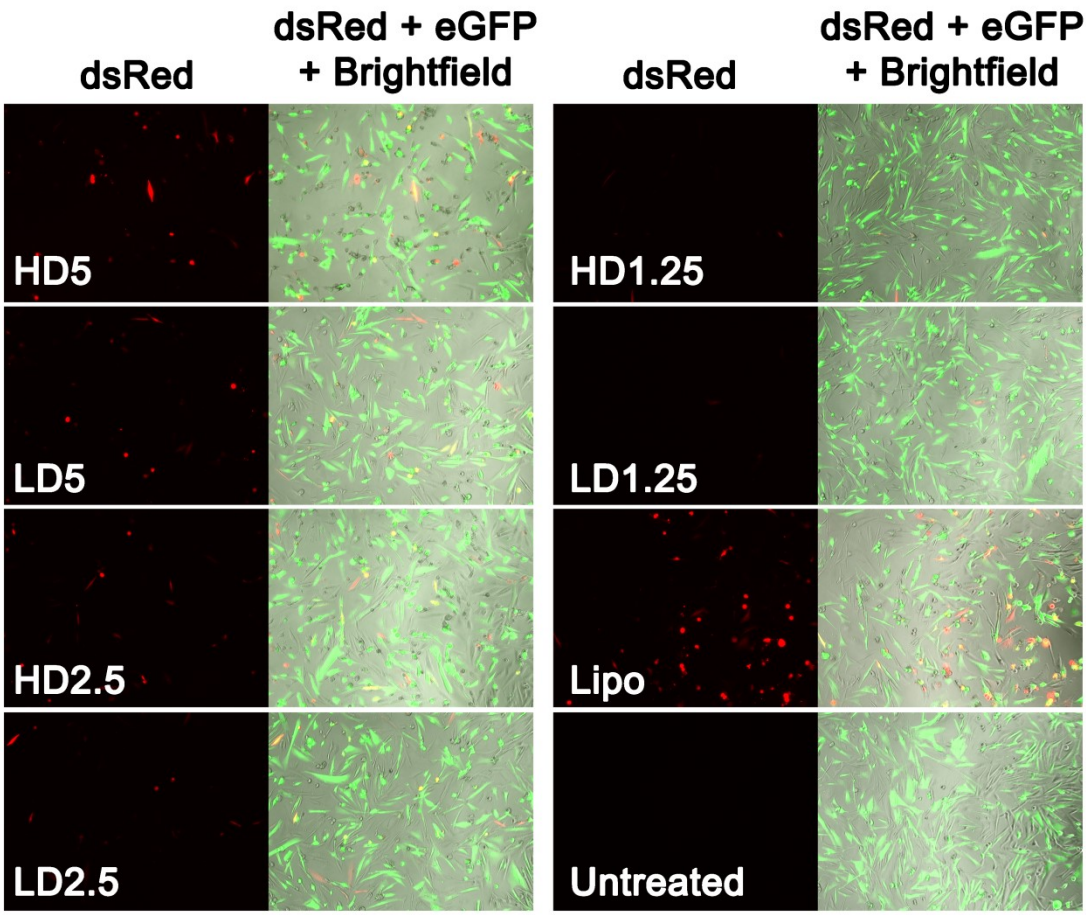

Figure 6. Fluorescence microscope images showing exogenous dsRed expression following transfection of MAu/DNA/siRNA LbL nanoparticles. Lipofectamine® 2000 was added at a 100 ng dosage 2.5 µL:1 µg dsRed DNA; (200 ms eGFP and 600 ms dsRed exposure time; magnification of 10x).

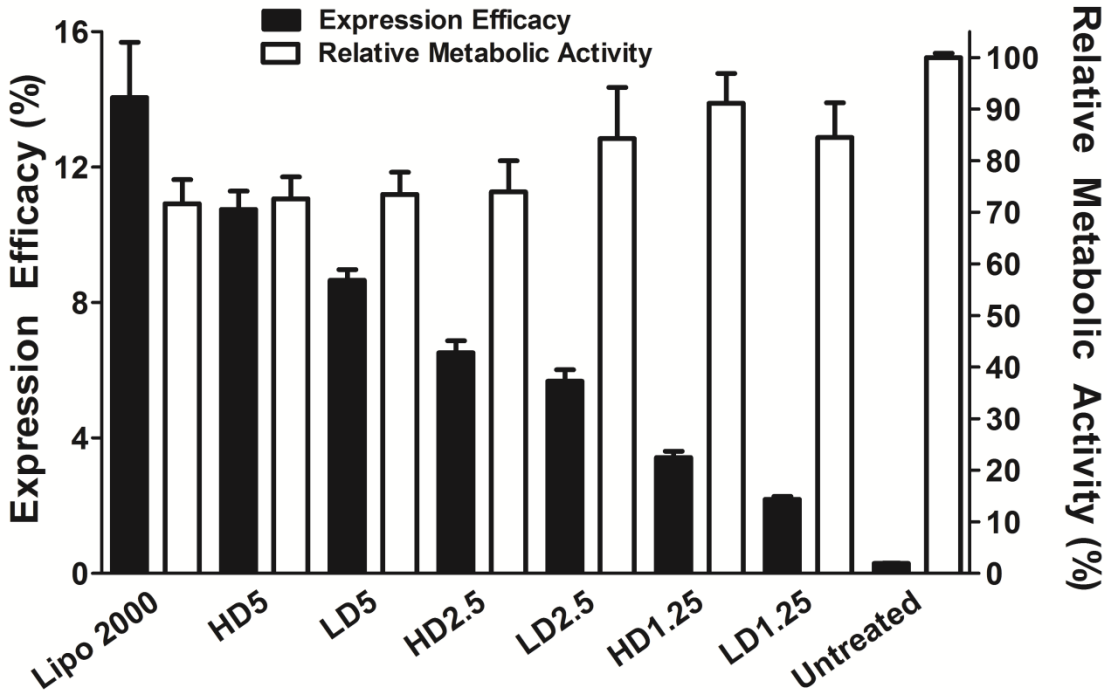

Figure 7. DNA transfection efficacy and relative metabolic activity of MAu/DNA/siRNA LbL nanoparticles. Lipofectamine® 2000 was added at a 100 ng (2.5:1) dose and is not statistically different from nanoparticle formulation HD5. Lipofectamine® 2000's expression was statistically significantly greater than all other formulations (p-value < 0.0001).

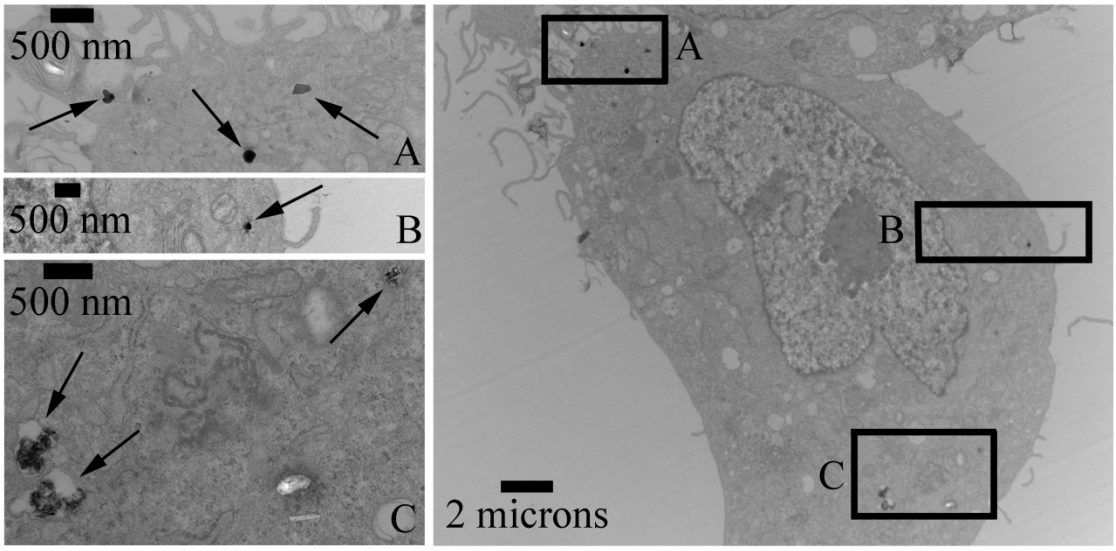

Figure 8. TEM of MAu/DNA/siRNA LbL nanoparticles of formulation HD5 in GBM319 cells. **A** and **B**: show particles that are ~200 nanometers. **C**: Two left arrows indicate putative endosomes with multiple gold nanoparticle aggregates.

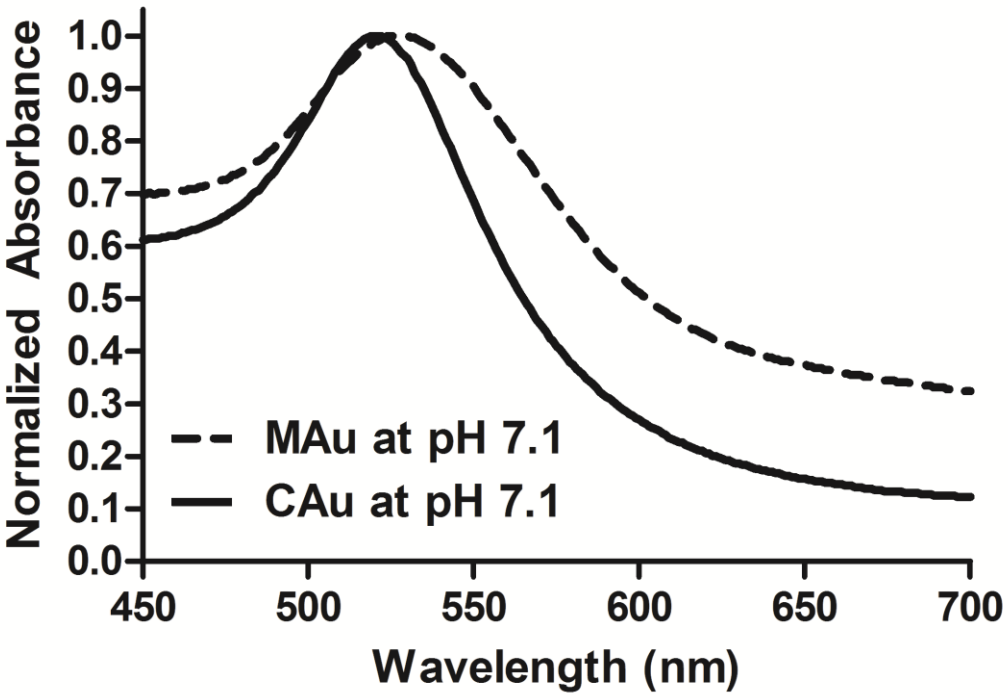

Figure S1. Absorbance spectra of citrate-stabilized CAu and 11-MUA-conjugated MAu at pH 7.1, similar to the storage conditions. MAu resists aggregation whereas CAu aggregates as indicated by the increase in the SPR wavelength.

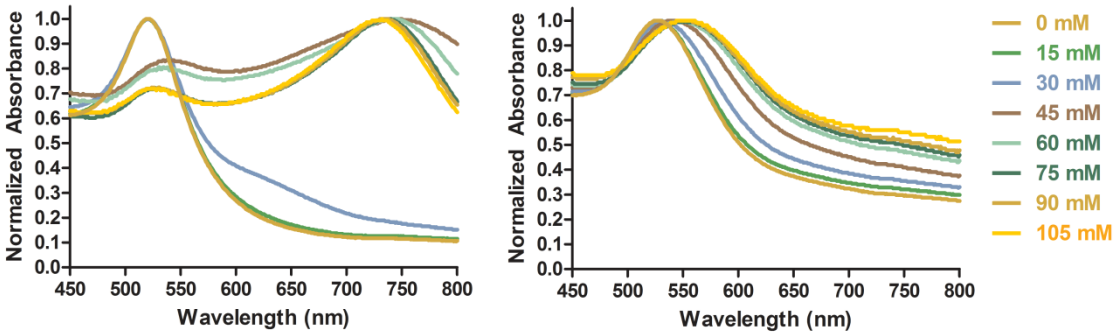

Figure S2. UV-Vis spectra of CAu (left) and MAu (right) solutions in various concentrations of NaAc ranging from 0 to ~100 mM. The NaAc concentration after the first layer (PEI) is ionically complexed to AuNPs is approximately 60 mM.

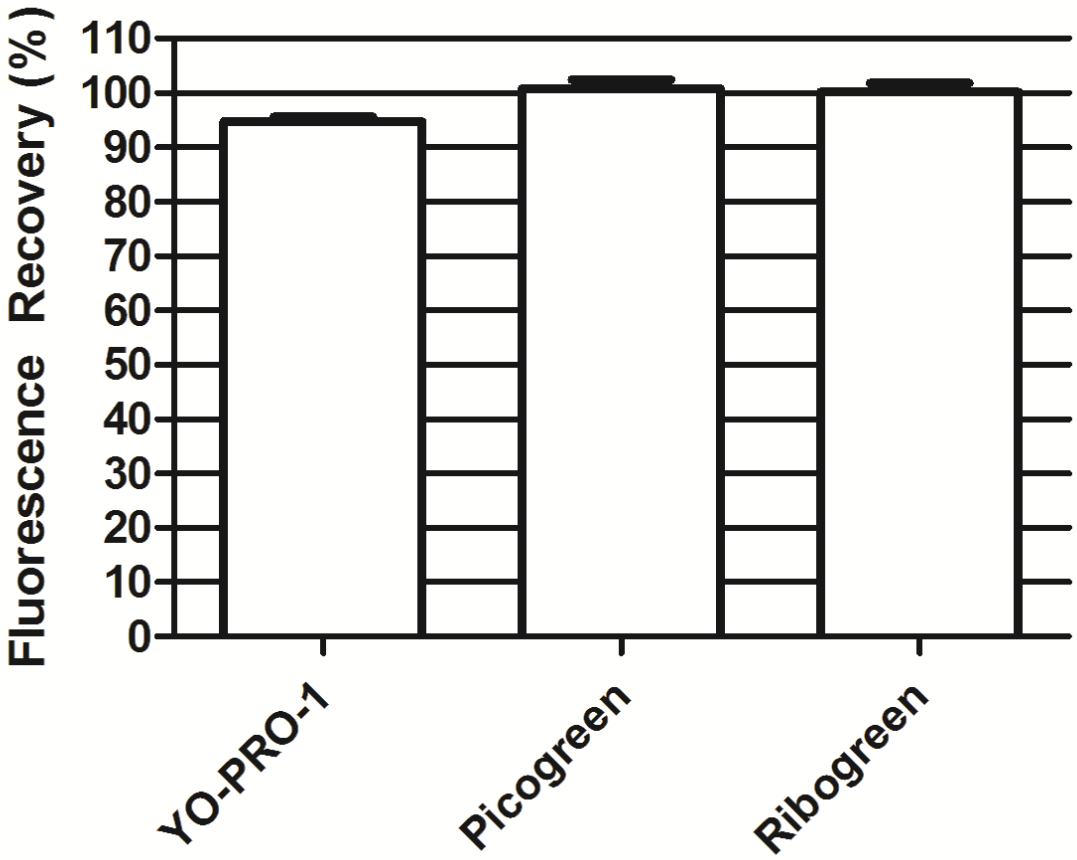

Figure S3. Fluorescence recovery percentages using YO-PRO®-1, Picogreen, and Ribogreen to quantify nucleic acid.

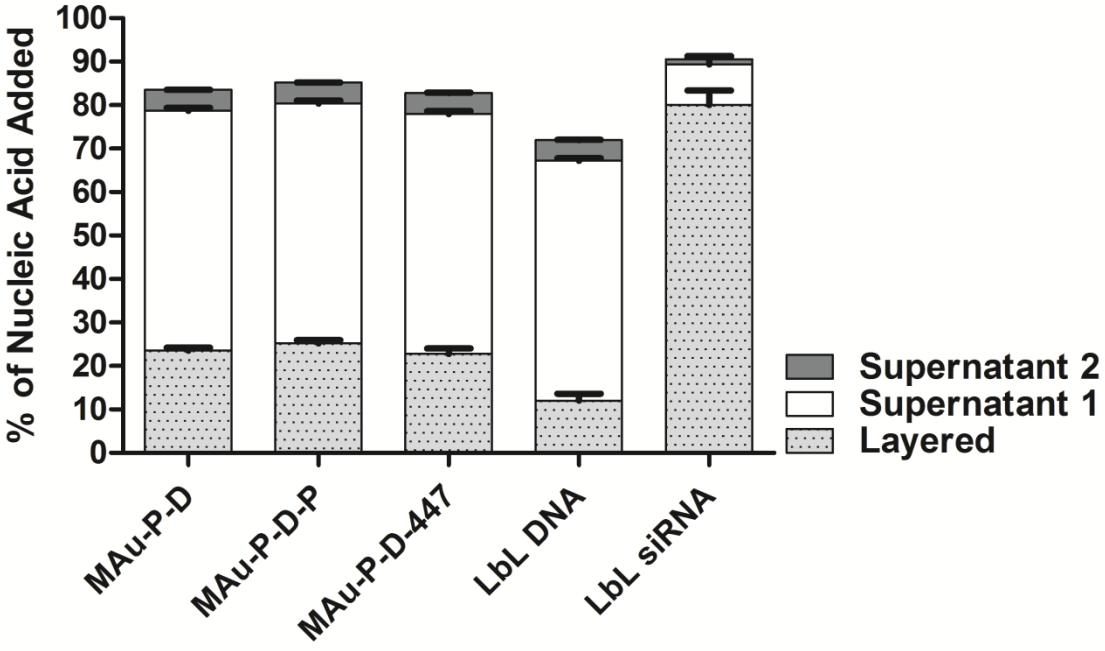

Figure S4. Compartmentalization percentages of nucleic acid. DNA and siRNA content of what was ionically complexed during the layering process and in the two supernatants during the washing steps.

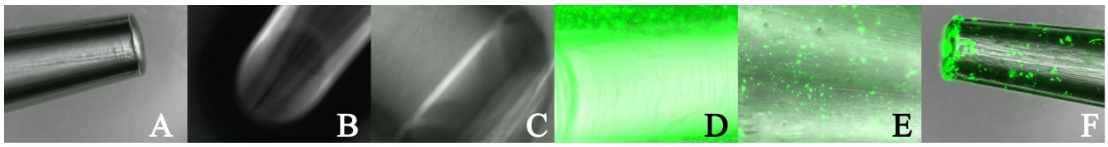

Figure S5. Nucleic acid lost to plasticware surface contact. **A**-**B**: Pipette tip and vial without contact with the co-delivery LbL formulation and without YO-PRO®-1, respectively. **C**: Vial with LbL formulation without YO-PRO®-1. **D**: Vial with LbL formulation and YO-PRO®-1. **E-F**: Vial and pipette tip with all of the LbL formulation removed with YO-PRO®-1, showing DNA and or siRNA not retained in the layering process.

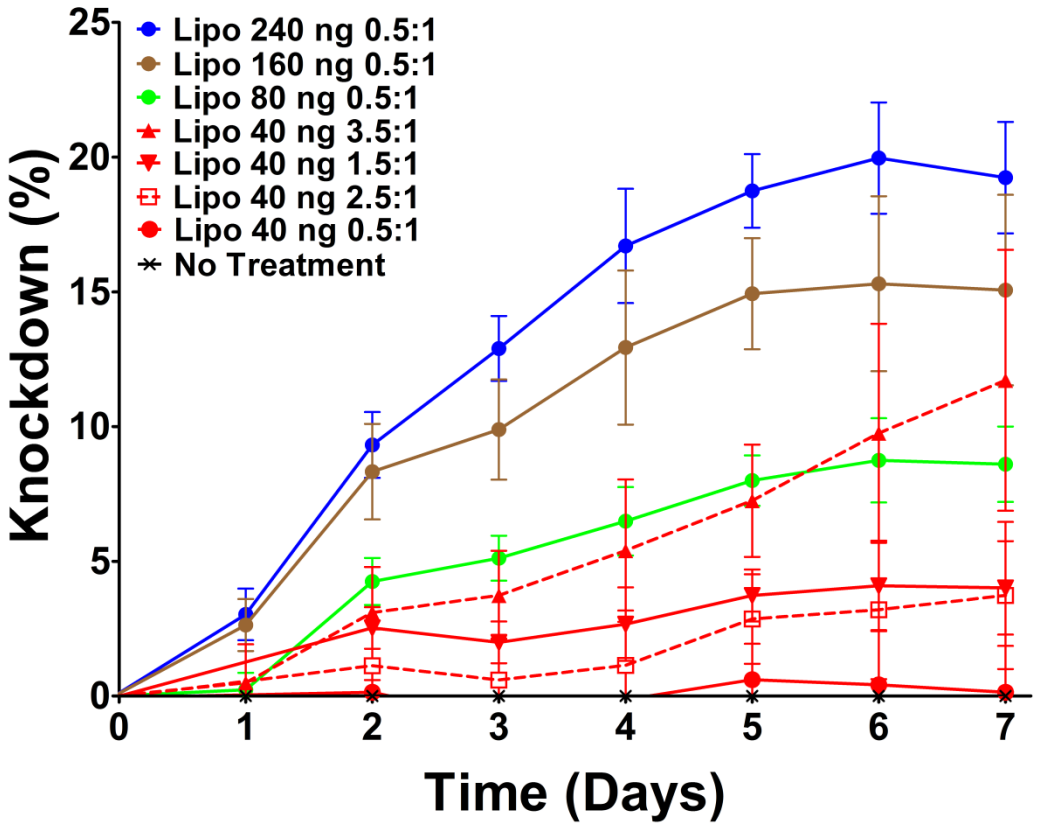

Figure S6. Optimization of siRNA delivery to human brain cancer cells using Lipofectamine® 2000 over time with varying ratios. Efficacy measured by fluorescence on a plate reader for conditions where the relative metabolic activity was greater than 70%, normalized to the untreated group.

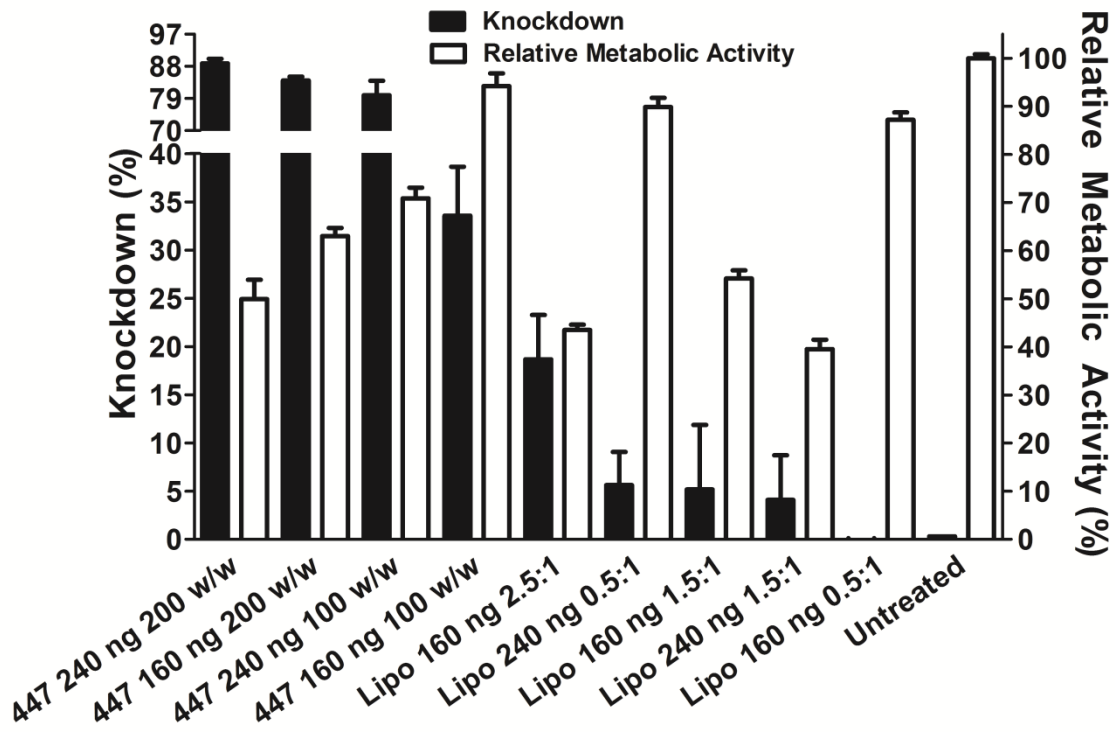

Figure S7. Optimization of siRNA delivery to human brain cancer cells using Lipofectamine® 2000 and polymer 447 on day 7. Knockdown on day 7 and relative metabolic activity at 24 hours post transfection using Lipofectamine® 2000 (Lipo X:Y; where X = Lipo μL; Y = μg DNA) and 447.

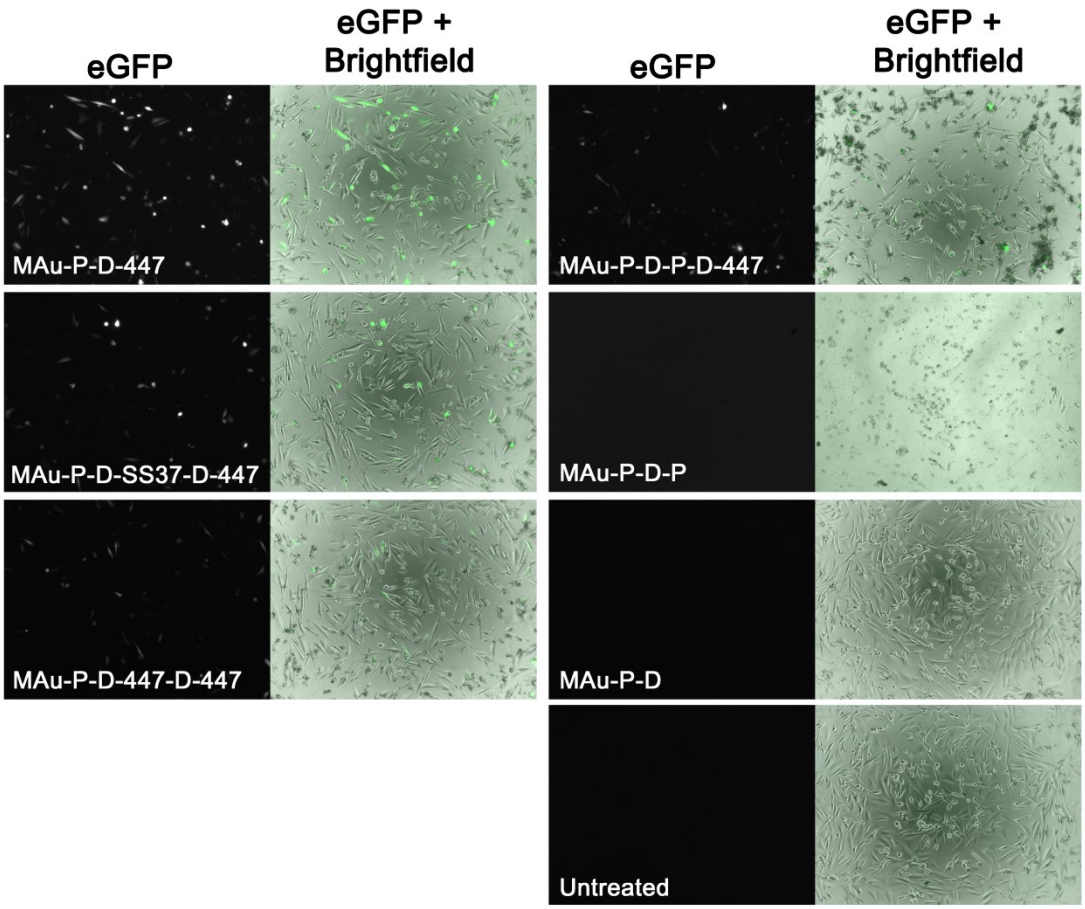

Figure S8. Fluorescence images of the various LbL formulations showing eGFP expression and their associated brightfield images overlaid to their right.

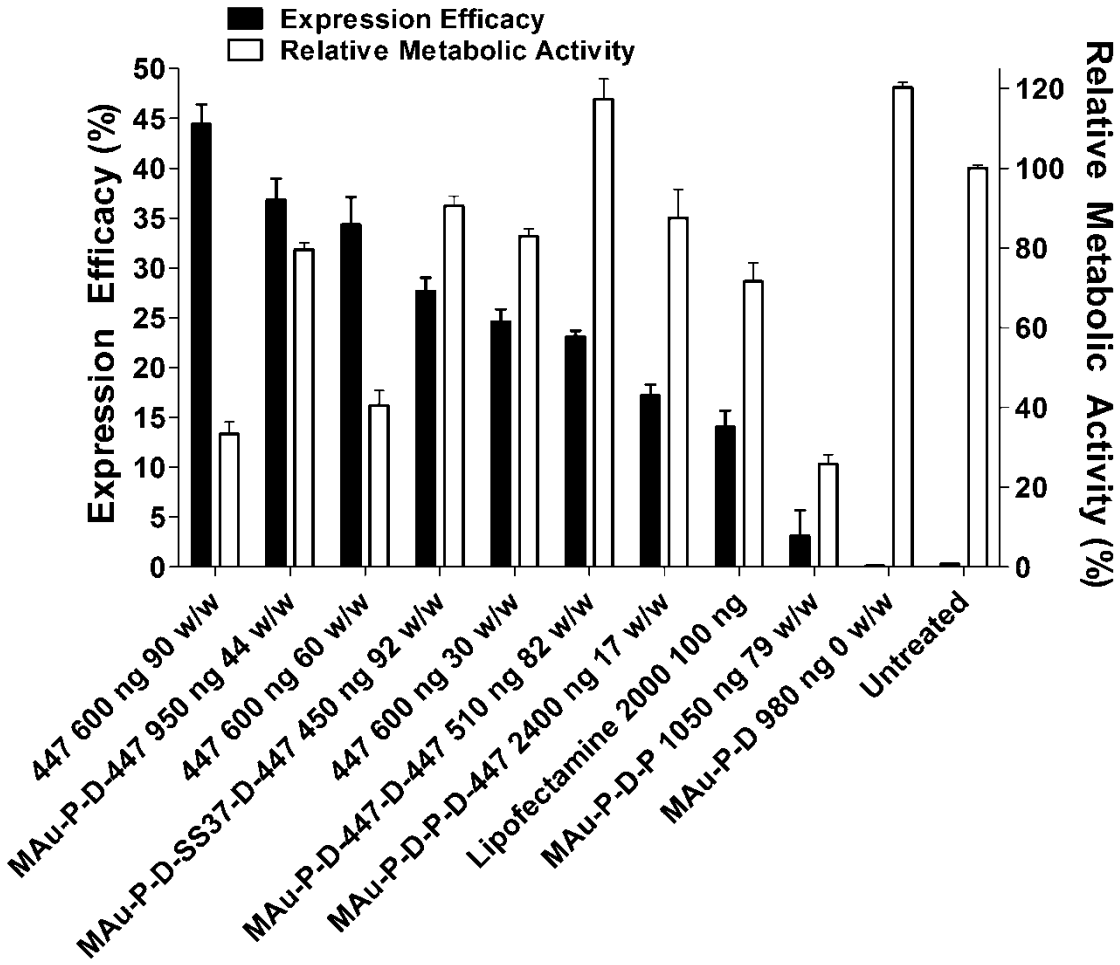

Figure S9. DNA transfection efficacy of dsRed expression and relative metabolic activity of various formulations. Lipofectamine® 2000 was delivered using 2.5 μL:1 μg DNA.

4.7 Schemes

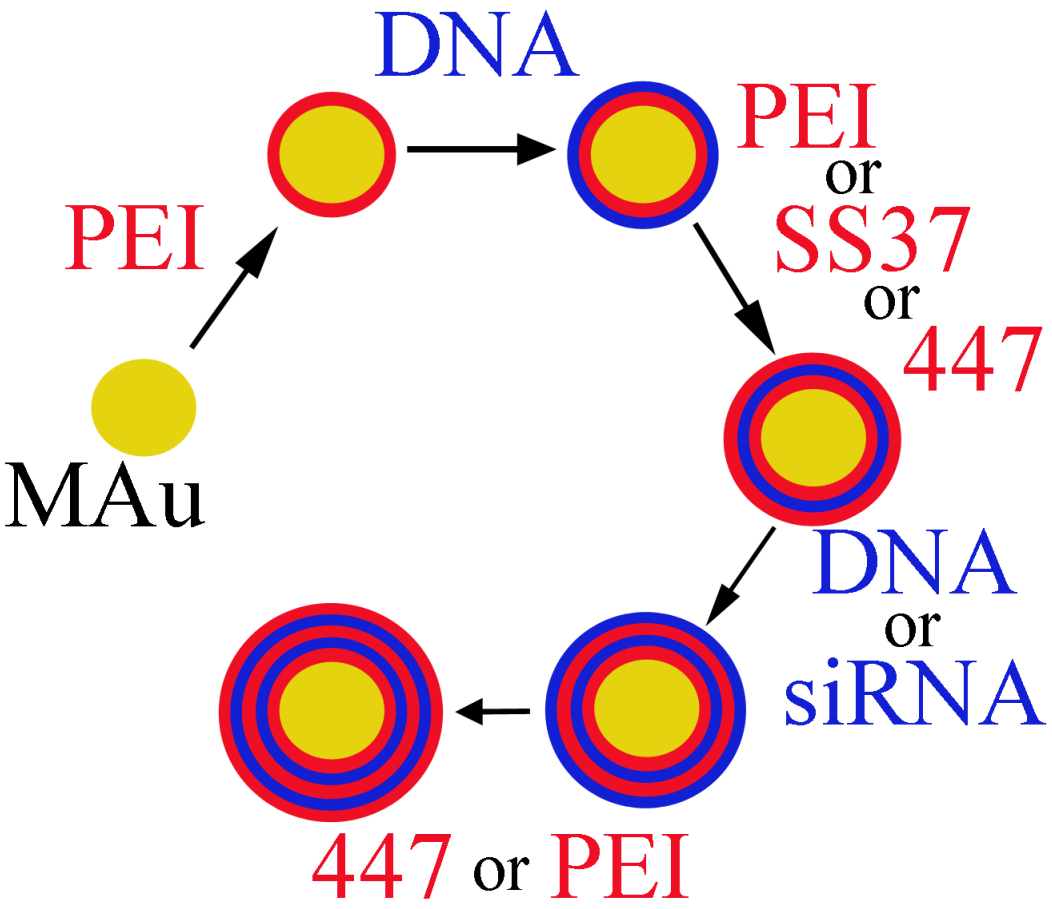

Scheme 1. LbL process starting with MAu.

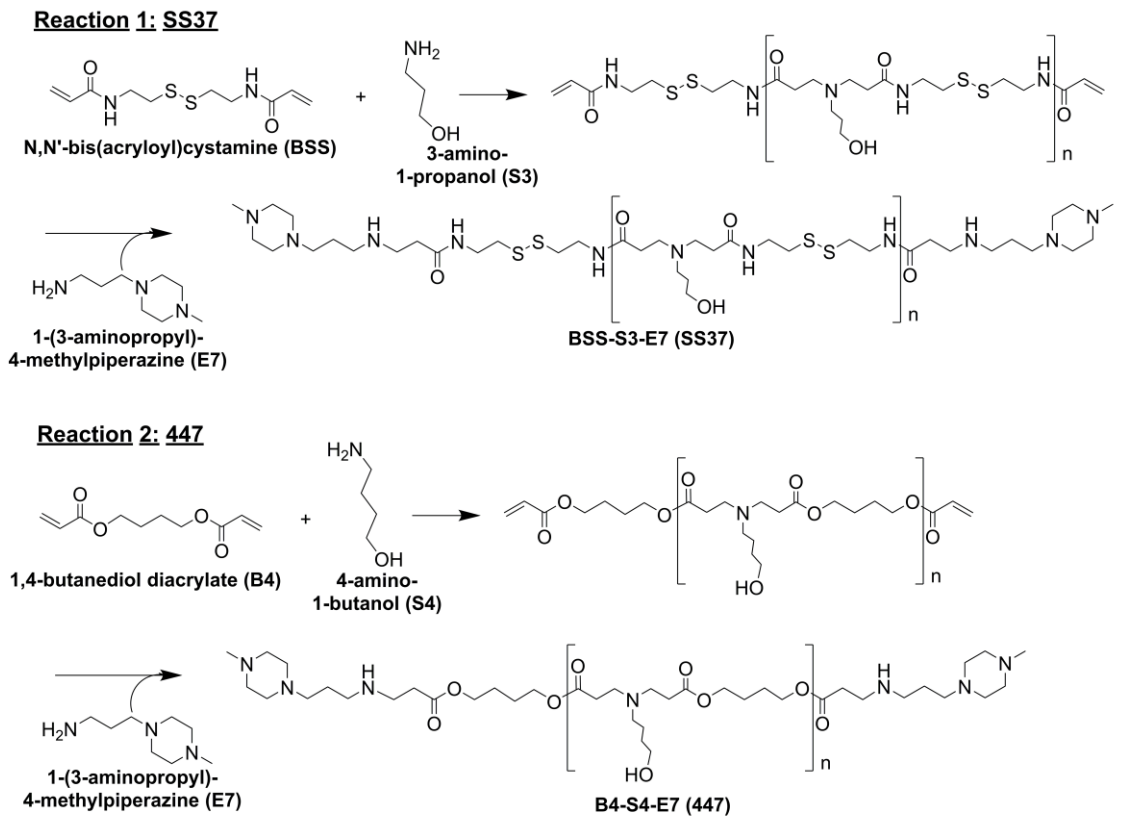

Scheme S1. Reaction scheme for SS37 (Reaction 1) and 447 (Reaction 2).

4.8 Tables

Table 1. Nucleic acid dosages and mass ratio of the 447 polymer to DNA (w/w) values of the various layered formulations. The w/w values are calculated from the most outer layer of polymer as described in section 2.6.

Formulation	DNA [ng]	Mass Ratio [w/w]
MAu-P-D	980 ± 30	0
MAu-P-D-P	1050 ± 30	79
MAu-P-D-447	950 ± 50	44
MAu-P-D-P-D-447	2400 ± 100	17
MAu-P-D-447-D-447	510 ± 20	82
MAu-P-D-SS37-D-447	450 ± 40	92
LD and HD	See section 2.6 and Table S1	See section 2.6 and Table S1

Table S1. Nucleic acid dosages and weight/weight (w/w) values of the various layered formulations of polymers 447 for DNA and siRNA.

Formulation	DNA [ng]	447/DNA [w/w]	siRNA [ng]	447/siRNA [w/w]
LD1.25	**200 ± 20**	**21**	**160 ± 9**	**26**
HD1.25	**300 ± 40**	**14**	**240 ± 10**	**17**
LD2.5	**200 ± 20**	**42**	**160 ± 9**	**52**
HD2.5	**300 ± 40**	**28**	**240 ± 10**	**35**
LD5	**200 ± 20**	**83**	**160 ± 9**	**104**
HD5	**300 ± 40**	**56**	**240 ± 10**	**69**

4.9 References

(1) Frens, G. *Nature-Phys. Sci.* **1973**, *241*, 20-22.
(2) Pissuwan, D.; Niidome, T.; Cortie, M. B. *J. Control. Release* **2011**, *149*, 65-71.
(3) Qian, W.; Curry, T.; Che, Y.; Kopelman, R. *Colloidal Nanocrystals for Biomedical Applications Viii* **2013**, *8595*.
(4) Hainfeld, J. F.; O'Connor, M. J.; Dilmanian, F. A.; Slatkin, D. N.; Adams, D. J.; Smilowitz, H. M. *Br. J. Radiol.* **2011**, *84*, 526-533.
(5) Park, C.; Youn, H.; Kim, H.; Noh, T.; Kook, Y. H.; Oh, E. T.; Park, H. J.; Kim, C. *J. Mater. Chem.* **2009**, *19*, 2310-2315.
(6) Peng, C.; Qin, J. B.; Zhou, B. Q.; Chen, Q.; Shen, M. W.; Zhu, M. F.; Lu, X. W.; Shi, X. Y. *Polym. Chem.* **2013**, *4*, 4412-4424.
(7) Chawla, J. S.; Amiji, M. M. *AAPS PharmSci* **2003**, *5*.
(8) Bae, Y. H.; Park, K. *J. Control. Release* **2011**, *153*, 198-205.
(9) Wang, T. Y.; Halaney, D.; Ho, D.; Feldman, M. D.; Milner, T. E. *Biomed. Opt. Express* **2013**, *4*, 584-595.
(10) Yuan, H.; Register, J. K.; Wang, H. N.; Fales, A. M.; Liu, Y.; Tuan, V. D. *Anal. Bioanal. Chem.* **2013**, *405*, 6165-6180.
(11) Zhang, Q.; Iwakuma, N.; Sharma, P.; Moudgil, B. M.; Wu, C.; McNeill, J.; Jiang, H.; Grobmyer, S. R. *Nanotechnology* **2009**, *20*, 395102.
(12) Huang, X. H.; Jain, P. K.; El-Sayed, I. H.; El-Sayed, M. A. *Laser Med. Sci.* **2008**, *23*, 217-228.
(13) Loo, C.; Lowery, A.; Halas, N.; West, J.; Drezek, R. *Nano Lett.* **2005**, *5*, 709-11.
(14) Jang, H.; Ryoo, S. R.; Kostarelos, K.; Han, S. W.; Min, D. H. *Biomaterials* **2013**, *34*, 3503-3510.
(15) Elbakry, A.; Wurster, E. C.; Zaky, A.; Liebl, R.; Schindler, E.; Bauer-Kreisel, P.; Blunk, T.; Rachel, R.; Goepferich, A.; Breunig, M. *Small* **2012**, *8*, 3847-3856.
(16) Lee, J. S.; Green, J. J.; Love, K. T.; Sunshine, J.; Langer, R.; Anderson, D. G. *Nano Lett.* **2009**, *9*, 2402-2406.
(17) Blacklock, J.; Mao, G. Z.; Oupicky, D.; Mohwald, H. *Langmuir* **2010**, *26*, 8597-8605.
(18) Elbakry, A.; Zaky, A.; Liebkl, R.; Rachel, R.; Goepferich, A.; Breunig, M. *Nano Lett.* **2009**, *9*, 2059-2064.
(19) Flessner, R. M.; Jewell, C. M.; Anderson, D. G.; Lynn, D. M. *Langmuir* **2011**, *27*, 7868-7876.
(20) Flessner, R. M.; Yu, Y.; Lynn, D. M. *Chem. Commun.* **2011**, *47*, 550-552.
(21) Saurer, E. M.; Flessner, R. M.; Sullivan, S. P.; Prausnitz, M. R.; Lynn, D. M. *Biomacromolecules* **2010**, *11*, 3136-3143.
(22) Lee, S. K.; Han, M. S.; Asokan, S.; Tung, C. H. *Small* **2011**, *7*, 364-370.
(23) Sunshine, J. C.; Bishop, C. J.; Green, J. J. *Ther. Deliv.* **2011**, *2*, 493-521.
(24) Bishop, C. J.; Ketola, T. M.; Tzeng, S. Y.; Sunshine, J. C.; Urtti, A.; Lemmetyinen, H.; Vuorimaa-Laukkanen, E.; Yliperttula, M.; Green, J. J. *J. Am. Chem. Soc.* **2013**, *135*, 6951-6957.
(25) Tzeng, S. Y.; Guerrero-Cazares, H.; Martinez, E. E.; Sunshine, J. C.; Quinones-Hinojosa, A.; Green, J. J. *Biomaterials* **2011**, *32*, 5402-10.

(26) Zhao, Y. H.; Zhang, Y.; Yang, Z.; Li, A.; Dong, J. L. *Biochem. Biophys. Res. Commun.* **2008**, *370*, 509-513.
(27) Kang, H. C.; Bae, Y. H. *Biomaterials* **2011**, *32*, 4914-4924.
(28) Liu, X. O.; Atwater, M.; Wang, J. H.; Huo, Q. *Colloid Surface B* **2007**, *58*, 3-7.
(29) Lin, C.; Blaauboer, C. J.; Timoneda, M. M.; Lok, M. C.; van Steenbergen, M.; Hennink, W. E.; Zhong, Z. Y.; Feijen, J.; Engbersen, J. F. J. *J. Control. Release* **2008**, *126*, 166-174.
(30) Lin, C.; Zhong, Z. Y.; Lok, M. C.; Jiang, X. L.; Hennink, W. E.; Feijen, J.; Engbersen, J. F. J. *J. Control. Release* **2006**, *116*, 130-137.
(31) Lin, C.; Zhong, Z. Y.; Lok, M. C.; Jiang, X. L.; Hennink, W. E.; Feijen, J.; Engbersen, J. F. J. *Bioconjug. Chem.* **2007**, *18*, 138-145.
(32) Tzeng, S. Y.; Green, J. J. *Adv. Healthcare Mater.* **2013**, *2*, 468-480.
(33) Sunshine, J. C.; Peng, D. Y.; Green, J. J. *Mol Pharm* **2012**, *9*, 3375-83.
(34) Ketola, T. M.; Hanzlikova, M.; Leppanen, L.; Ravina, M.; Bishop, C. J.; Green, J. J.; Urtti, A.; Lemmetyinen, H.; Yliperttula, M.; Vuorimaa-Laukkanen, E. *Journal of Physical Chemistry B* **2013**, *117*, 10405-10413.
(35) Eltoukhy, A. A.; Siegwart, D. J.; Alabi, C. A.; Rajan, J. S.; Langer, R.; Anderson, D. G. *Biomaterials* **2012**, *33*, 3594-603.
(36) Boussif, O.; Lezoualc'h, F.; Zanta, M. A.; Mergny, M. D.; Scherman, D.; Demeneix, B.; Behr, J. P. *Proc. Natl. Acad. Sci. U. S. A.* **1995**, *92*, 7297-301.
(37) Sunshine, J. C.; Peng, D. Y.; Green, J. J. *Mol. Pharm.* **2012**, *9*, 3375-3383.
(38) Tzeng, S. Y.; Higgins, L. J.; Pomper, M. G.; Green, J. J. *J Biomed Mater Res A* **2013**, *101*, 1837-45.
(39) Kim, J.; Sunshine, J. C.; Green, J. J. *Bioconjug Chem* **2014**, *25*, 43-51.
(40) Bhise, N. S.; Wahlin, K. J.; Zack, D. J.; Green, J. J. *Int. J. Nanomedicine* **2013**, *8*, 4641-4658.
(41) Shmueli, R. B.; Anderson, D. G.; Green, J. J. *Expert Opin. Drug Deliv.*, *7*, 535-50.
(42) Poon, Z.; Lee, J. B.; Morton, S. W.; Hammond, P. T. *Nano Lett.* **2011**, *11*, 2096-2103.
(43) Guerrero-Cazares, H.; Tzeng, S. Y.; Young, N. P.; Abutaleb, A. O.; Quinones-Hinojosa, A.; Green, J. J. *Acs Nano* **2014**, *8*, 5141-5153.

5 Chapter 5: Inorganic/Polymeric Layer-by-Layer Approach for Gene Delivery: Controlling Protein Expression

5.1 Introduction

Gene therapy is capable of curing or treating many genetic disorders and cancer [1]. Polymeric gene delivery techniques have advantages over viral methods in that they are chemically customizable, are able to be manufactured on a large scale, are associated with far less insertional mutagenesis, and are less immunogenic. However, the balance between safety and efficacy remains elusive, as there are yet any U.S. FDA approved viral or non-viral gene therapies available.

Delivering DNA in conjunction with biocompatible gold nanoparticles (AuNP)s enables a therapeutic function (gene/thermotherapy) as well as a diagnostic (imaging). AuNPs are effective clinical X-ray contrast agents with extended imaging times and sharper contrast than traditional iodine-based agents [2]. AuNPs are also able to be imaged via photoacoustics [3]. Additionally, photothermal therapy, in which AuNPs are excited by incident electromagnetic radiation (at its surface plasmon resonance wavelength typically in the near-infrared region as it is transparent to tissue on the order of centimeters), has been shown to effectively thermally ablate tumors in mammalian *in vivo* models [4]. AuNPs are also attractive due to their monodispersity [5], their ability to be highly charged

for layer-by-layer (LbL) complexation processes, their ability to be easily chemically modified via thiol groups [6], and their optical properties.

LbL assembly involves the sequential addition of oppositely charged polyelectrolytes onto a given substrate. DNA loading can be modified by the number and the order of the DNA layers [7]. If DNA layers were able to be transcribed and translated at different time points, it would improve temporal control over the cellular microenvironment. Stem cell differentiation is one type of potential application that could benefit from such control over expression time profiles, as exposure to growth factors at different time points can heavily influence differentiation pathways [8,9]. As a proof of principle, this work demonstrates the ability to control the expression time profiles of two proteins using a single theranostic-enabling AuNP LbL platform.

5.2 Materials and Methods

5.2.1 Gold Nanoparticle Synthesis and Characterization

The AuNPs used in this study were synthesized via a modified Frens method [5] and previously reported [10]. Briefly, a 0.01% tetrachloroauric acid trihydrate, $HAuCl_4$ (Fisher Scientific), in ultra pure distilled water was vigorously boiling when a 1% sodium citrate tribasic dihydrate (Sigma Aldrich) solution (in water) was injected to reduce the gold ions.

5.2.2 Gold Nanoparticle 11-MUA Stabilization

To maintain monodispersity and create a stably charged anionic coating on the AuNPs, 11-mercaptoundecanoic acid (MUA) was conjugated to the AuNPs via a thiol

bond as previously reported and was previously shown to be superior for ionic complexation LbL processes compared to citrate-stabilized AuNPs [10]. The 11-MUA at 1 mM in ethanol was added to the citrate stabilized AuNPs and allowed to thiolate for 48 hours. The solution was then washed twice in ethanol and re-solvated in a 0.45% solution of sodium citrate. The resulting conjugated AuNPs were then diluted to 0.31 nM in preparation for the layering process.

5.2.3 Polymer Synthesis and Characterization

To synthesize the hydrolytically degradable cationic poly(β-amino ester) (PBAE) polyelectrolyte layer, diacrylate (1,4-Butanediol diacrylate) and amine small molecules (4-amino-1-butanol) were reacted neat in a 1.2:1 molar ratio [11]and were allowed to react for 24 hours (>100 RPMs) before being end-capped for 1 hour at 1000 RPM via 1-(3-aminopropyl)-4-methylpiperazine in anhydrous tetrahydrofuran (THF), resulting in poly(1,4-butanediol diacrylate-co-4-amino-1-butanol). The cationic PBAE polymer is referred to as B4-S4-E7 or 447 (**Figure S1**). Polymer 447 was then ether-purified to remove any unreacted monomers and then solvated to 100 mg/mL in anhydrous dimethyl sulfoxide (DMSO) and was stored at -20°C until use. We have previously reported NMR spectra on 447 [1].

The molecular weight was quantified using gel permeation chromatography (Waters®, Breeze 2 software). The solvent constituted 94% THF, 5% DMSO, 1% piperidine and a trace amount of butylated hydroxytoluene at a flow rate of 1 mL min^{-1}.

5.2.4 Multilayer Particle Formation

The LbL process is shown in **Scheme 1**. 80 μL of 25 kDa branched polyethyleneimine (PEI) was added to 112 μL of 0.31 nM ($1.9x10^{11}$ particles mL^{-1}) aqueous AuNPs which had been MUA-conjugated. The AuNP-PEI solution was shaken at room temperature for 30 minutes at 500 RPM, and then washed twice at 4°C via centrifugation for 10 minutes at 10 krcf. The supernatant was replaced with 150 mM sodium acetate (NaAc) up to 192 μL for the first wash, and then up to 112 μL for the second wash. Subsequent layers were deposited by adding 80 μL of polyelectrolyte suspended in 150 mM NaAc, followed by the same washing procedure. PEI was added at 10 mg mL^{-1} (Layers 1, 3, 5), dsRed-Max-N1 (dsRed; Addgene) plasmid DNA (pDNA) at 0.5 mg mL^{-1} (Layer 2), poly(acrylic acid) (PAA; M_w ~1800 Da; Sigma Aldrich) at 0.5 mg mL^{-1} (Layer 4), enhanced Green Fluorescent Protein (eGFP-N1, referred to as eGFP; Clontech) pDNA at 0.5 mg mL^{-1} (Layer 6), and PBAE 447 at 2.5 mg mL^{-1} (Layer 7). To reduce cell toxicity 25 mM NaAc was used instead of 150 mM NaAc for the final wash of the eGFP pDNA layer. In addition, PBAE 447 was solvated in 25 mM NaAc and was not washed as we have previously found excess 447 is necessary for transfection [10].

The rationale behind having 3 polymer layers between the dsRed and eGFP pDNA layers was to space the layers such that the outer eGFP layer would be transcribed and translated first, followed by the expression of the more inner dsRed layer at a later point in time.

5.2.5 Particle Diameter and Zeta Potential

Nanoparticle tracking analysis (NTA) was performed with a NanoSight NS500 at each of the 7 layering stages (n=2). Particles were diluted up to a total of 500 uL in 150

mM NaAc and mixed thoroughly immediately prior to loading into the NanoSight. Transmission electron microscopy (TEM) was accomplished on the complete LbL formulation to confirm the diameter ascertained via NTA (n=3). ImageJ (NIH) was also used to quantify diameters of the TEM images based on the area of the particles.

Dynamic light scattering (DLS) analysis was performed with a Zetasizer (Malvern) at each of the 7 layers after the washing steps (except for the last layer) to measure the zeta potential (n=2 per layer). Particles were diluted up to a total of 700 uL in UltraPure™ Distilled Water (Invitrogen).

5.2.6 Nucleic Acid Loading

Based on our previously reported decomplexation process [10], the nucleic acid content was quantified via a calibration curve; A fluorescence dye at 10 μM (YO-PRO®-1) at a high salt (650 mM) and heparin (300 μg/mL) concentration was used to quantify the decomplexed nucleic acid content using a fluorescence plate reader (Synergy2; 485/528 nm excitation/emission). Previously reported data shows that the salt and heparin concentration used was sufficient to measure the nucleic acid content present in the layered formulation [2]. The nucleic acid content was assessed after the dsRed layer and after both the dsRed and eGFP layers were complexed. The eGFP content was quantified via simple arithmetic by subtracting the total nucleic acid content from the dsRed content. The uncomplexed nucleic acid content was also assessed in the supernatants of the washing steps just after the dsRed and eGFP layers as well. The efficiency of layering was calculated by multiplying 100 by the fraction of nucleic acid retained in the LbL formulation to the total nucleic acid content used for layering.

5.2.7 Cell Culture and Transfection

Human glioblastoma cells (GB319) cultured in T-75 flasks were cultured at 37°C and 5% $C0_2$ atmosphere using DMEM:F12 (1:1), 1x antibiotic-antimycotic and 10% fetal bovine serum (FBS). The cells were seeded at 10,000 cells/well in 96-well tissue culture treated polystyrene plates. Transfection was accomplished by diluting the 192 µL of the final LbL formulation up to 256 uL using 25 mM NaAc. From the diluted 256 µL, 20 µL was delivered per well and allowed to incubate with the seeded cells in the 96-well plates for 2 hours at 37°C before the media was replaced with complete media. The full layered nanoparticles were incubated using 10 and 50% serum by volume for the 2 hour time period to assess any differences, as the 50% serum concentration more closely resembles *in vivo* conditions.

As a positive control, Lipofectamine® 2000 (Lipo2k) was also incubated with the cells in like manner. Lipo2k was mixed with dsRed and eGFP pDNA using ratios of 0.5:1, 1.5:1, 2.5:1, and 3.5:1 (Lipo2k µL: pDNA µg) at the same dsRed:eGFP pDNA ratio and dosages as the LbL formulation. Total dosages of dsRed:eGFP pDNA of 100 and 200 ng were also assessed at the same Lipo2k:pDNA (µL:µg; n=4) ratios.

5.2.8 Expression and Relative Metabolic Activity

Fluorescence microscopy images were obtained with a Carl Zeiss fluorescence microscope on days 2, 5, 9, 14, and 21 post-transfection (5x magnification). The eGFP and dsRed channel exposure times were 300 and 600 ms, respectively.

Flow cytometry was performed with a BD Accuri™ C6 flow cytometer on days 2, 5, 9, 14, and 21 post-transfection as well; a HyperCyt sampler was used to automate data collection. Cells were detached via incubation at 37°C with trypsin-

ethylenediaminetetraacetic acid (0.05%) for five minutes, followed by immediate quenching with 2% FBS in phosphate buffered saline (PBS). FSC-H vs. SSC-H was used to isolate the singlet population; expression of eGFP and dsRed were analyzed using FL1-H vs. FL3-H (FloJo).

An MTS-based Promega assay CellTiter 96® was used to determine the relative metabolic activity of transfected cells as compared to untreated controls at 24 hours for 10 and 50% serum conditions which is an indicator of viability.

5.2.9 Statistics

Figure 2: left (n=2): A one-way ANOVA with a Bonferroni post-hoc analysis was performed; right: n=2. **Figure 3**: 10% serum: n=12; 50% serum: n=4. **Figure S2**, **S4**, and **S5** were n≥4, ≥4, =4, respectively. When comparing the positive control (**Figure 3** vs **Figure S5**) to the LbL formulation at 2 days post-transfection, a two-tailed Student's t-test was used. All error bars in figures are standard errors of the mean (SEM). Other error bars reported which are standard deviations are otherwise indicated (StDev).

5.3 Results

5.3.1 Gold Nanoparticle Characterization and 11-MUA Stabilization

TEM analysis confirmed that the stabilized AuNPs were monodisperse as well as uniform in size at 17 ± 2(StDev) nm [10]. SPR results showed a red-shift of the wavelength from 520 nm for solely citrate stabilized AuNPs to 526 nm for 11-MUA conjugated nanoparticles [10].

5.3.2 Polymer Characterization

The number-average (M_n) and weight-average (M_w) molecular weights of PBAE 447 were 11.9 kDa and 35.5 kDa, respectively, with a polydispersity index of 2.98.

5.3.3 Particle Diameter and Zeta Potential

The TEM of the complete LbL formulations with all 7 layers is shown in **Figure 1**. The arithmetic and geometric means of cores per aggregate were 4.3 and 2.7, respectively. According to the area of the particles assessed by ImageJ, the dry core diameters were 104 ± 0.8 nm (StDev) in diameter and the larger dry aggregate diameters were 210 ± 10 nm (StDev) between the 3 images. The diameter according to TEM corroborated the hydrodynamic diameter findings according to NTA, which was approximately 300 nm for all 7 layers (**Figure 2**; left).

According to NTA, the hydrodynamic radius increased with each layer out to layer 6. There was no statistical difference in diameter between layers 5-7. The largest increase in diameter occurred at the first DNA layer similarly to what was observed previously [10]. The zeta potential reversed at each of the 7 stages (**Figure 2**; right).

5.3.4 Nucleic Acid Loading

The inner (dsRed) and outer (eGFP) pDNA layers contained 208 ± 9 and 120 ± 10 ng/well, respectively, with a total of 328 ± 9 ng of pDNA. The layering efficiency of the inner and outer layers were 6.6 ± 0.6 and 4 ± 1%. The nucleic acid content in the

supernatant of the first and second washings accounted for 79 ± 2% and 4 ± 1% of the dsRed pDNA used for layering, respectively; for eGFP, 77 ± 3% and 4 ± 2%, respectively. The mass ratio of polymer 447 to pDNA was 48.

5.3.5 Expression and Relative Metabolic Activity

In regards to the 10% serum condition (**Figure 3**; left), the transfection levels of the outer (eGFP) pDNA layer was 22 ± 2% (**Figure 3**; top) and remained similar out to day 9 and then decreased to approximately 7% thereafter. In contrast, the inner (dsRed) pDNA layer (**Figure 3**; top) had low expression initially and steadily increased to a maximum at 16 ± 6% on day 9. The expression thereafter was similar to the outer eGFP levels near 7%. **Figure S3** shows the dot plots of the dsRed and eGFP fluorescence channels (FloJo) for the 10% serum condition on days 2, 5, 9, 14, and 21. Qualitatively, it can be seen that the eGFP and dsRed expression maxima are on days 2 and 9, respectively. The fluorescence microscope images showing the 10% serum condition in **Figure 4** also qualitatively corroborate these findings.

In regards to the 50% serum condition (**Figure 3**; right) the outer (eGFP) layer was higher at 12 ± 1% initially and steadily decreased to near 0% on day 14 (**Figure 3**; top). The inner (dsRed) layer was similar to the 10% serum condition, except there was a peak on day 5 rather than 14 and the transfection efficacy was lower, with a maximum at 6.5 ± 0.8% (**Figure 3**; top).

Figure 3 (bottom) shows the normalized transfection levels for the 10% serum condition (bottom left) and the 50% serum condition (bottom right) which accentuates the time differences in the maximum expression levels; the outer layers for the 10 and 50%

serum conditions were highest on day 2 whereas the inner layers for the 10 and 50% serum conditions peaked on days 9 and 5, respectively.

The relative metabolic activities (untreated = 100%) of the 7 layers incubated in 10% and 50% serum at 24 hours post-transfection were 93 ± 4% and 88 ± 2%, respectively, as shown in **Figure S4**.

Generally speaking, as the dosage increased for the Lipo2k formulations both the transfection efficacies of eGFP and dsRed increased and the relative metabolic activities decreased (**Figure S5**). At comparable dosages to the full 7 layers (eGFP: 120 ± 10 ng; dsRed: 208 ± 9 ng; see *Nucleic acid loading* section), the 3.5:1, 2.5:1, 1.5:1, and 0.5:1 (Lipo2k μL: μg pDNA) had relative metabolic activities of 30 ± 2%, 53 ± 1%, 79 ± 1%, and 96 ± 1%, respectively. The transfection levels for the same Lipo2k:pDNA ratios for eGFP and dsRed were 21 ± 5%, 22 ± 4%, 27 ± 4%, 22 ± 1% and 28 ± 2%, 25 ± 2%, 32 ± 3%, 13 ± 1%, respectively. The highest transfection level achieved with the positive control at the same dosage as the LbL formulation was thus with the 1.5:1 formulation which was similar statistically to the full 7 layers in 10% serum for both eGFP (p-value = 0.53) and dsRed (p-value = 0.14) (**Figure S5**).

While holding the eGFP and dsRed mass ratio for the Lipo2k similar to the full 7 layers (0.34:0.66 ng), the highest transfection level was found to be using a pDNA dosage of 200 ng and a Lipo2k μL: μg pDNA ratio of 2.5:1. The eGFP and dsRed transfection levels were 28 ± 1% and 32 ± 3% which were statistically similar to the full 7 layers in 10% serum as well for both eGFP (p-value = 0.38) and dsRed (p-value = 0.13). However, the optimized Lipo2k formulation (200 ng; 2.5:1) also had a much lower relative metabolic activity of 65 ± 1% (**Figure S5**).

5.4 Discussion

As expected the hydrodynamic radius of the LbL formulation was slightly larger than the dry diameter and the reversal of the zeta potential at each successive layer after multiple washings indicated successful ionic complexation of each subsequent layer.

The layering efficiencies of the LbL formulation of interest were comparable to our previously reported layering efficiencies (2 layers of nucleic acid with polymers SS37 or 447 as a middle layer) [10]. Future endeavors to minimize formulation costs by re-using the nucleic acid supernatants would be potentially worthwhile. The supernatants' concentration would decrease with each layering process; the supernatants could be potentially lyophilized and re-constituted at the original concentration. Post-lyophilization, the NaAc could be removed with multiple washings. However, possible uncomplexed polyelectrolytes may be present in the supernatant and would need to be fully characterized. For quality control and reproducibility purposes, re-using the supernatant was not investigated for the purposes of this study [10].

Because the backbones of the plasmids are similar, any differences in the expression time profiles could possibly be contributed to the inner plasmid being secluded from transcription and translation for a longer time period within the non-degradable inner polymer layers of PEI and PAA. Despite there being approximately 75% more dsRed pDNA than eGFP, the dsRed was secluded sufficiently that there was still a separation of the expression in time.

Interestingly, the maximum expression efficacy for the 10% serum condition for the outer and inner layers were on days 2 and 9, respectively, whereas the 50% serum resulted in the inner layer to be maximally expressed on day 5; little toxicity was

observed in either case. In the 50% serum condition, it is possible that the decomplexation process may be enhanced by the presence of more serum proteins. We have found that not all uptake mechanisms (i.e., clathrin, caveolae, and macropinocytosis) are equally effective for the eventual transcription and translation of exogenous plasmids [12]. It is possible that the LbL nanoparticles in the presence of more serum proteins may be uptaken by the cell through a different mechanism, which could in part explain the disparity between the expression profiles between the 10 and 50% serum conditions. Further studies would be required to elucidate the mechanism.

At the same pDNA dosages, the LbL formulation was comparable in both the dsRed and eGFP expression in comparison to the optimized Lipo2k formulation (1.5:1; Lipo2k μL: pDNA μg) on day 2.

5.5 Conclusions

Using an LbL approach, we were able to successfully develop a theranostic-enabling platform technology which is capable of loading two different types of plasmids separated by a polymer barrier: PEI-PAA-PEI. The most inner layer is transcribed and translated at a later point in time than the most outer plasmid layer. Such control over the timing of expression is of great interest to the scientific community for controlling the cellular microenvironment.

5.6 Figures

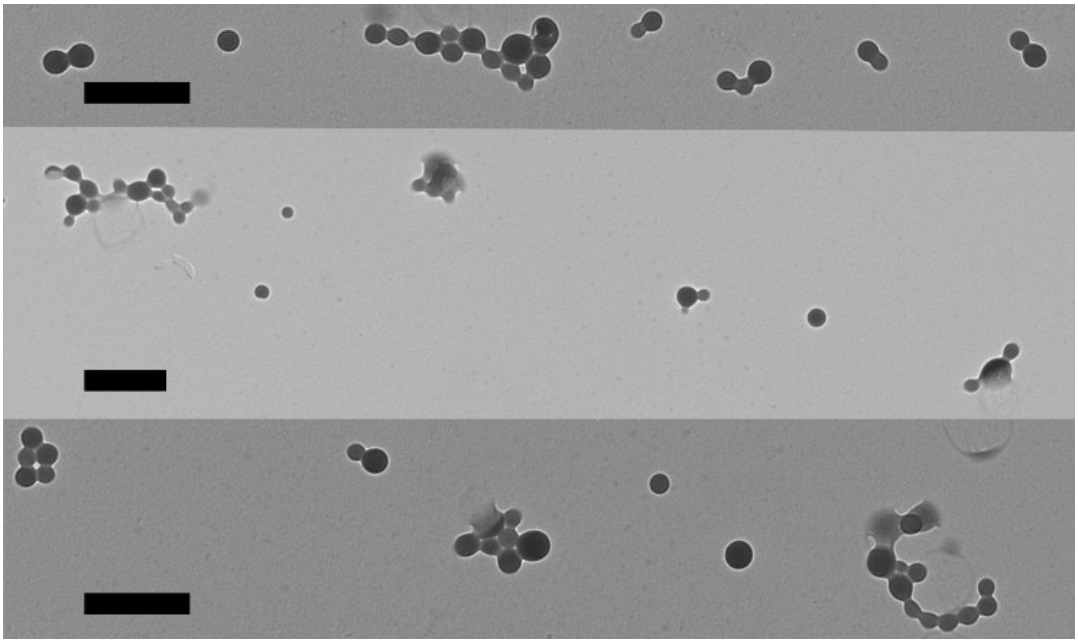

Figure 1. TEM of complete LbL formulation. Scale bars are 500 nm.

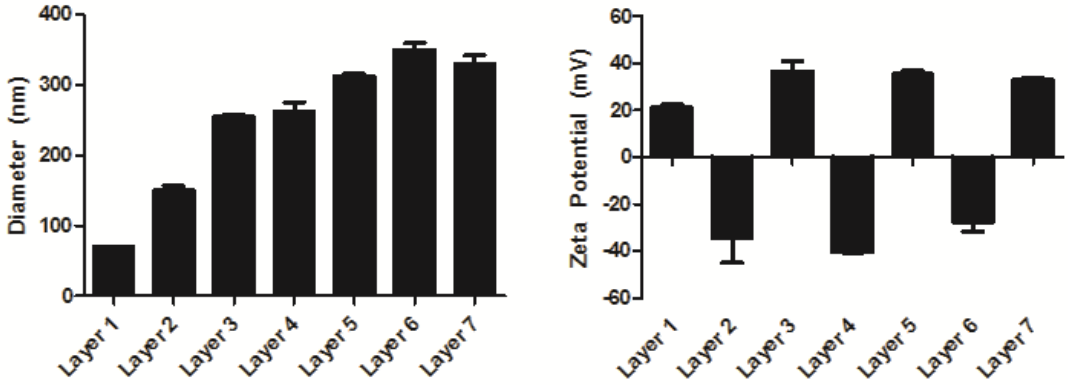

Figure 2. Hydrodynamic diameter (left) and zeta potential (right) of each of the 7 layers, respectively.

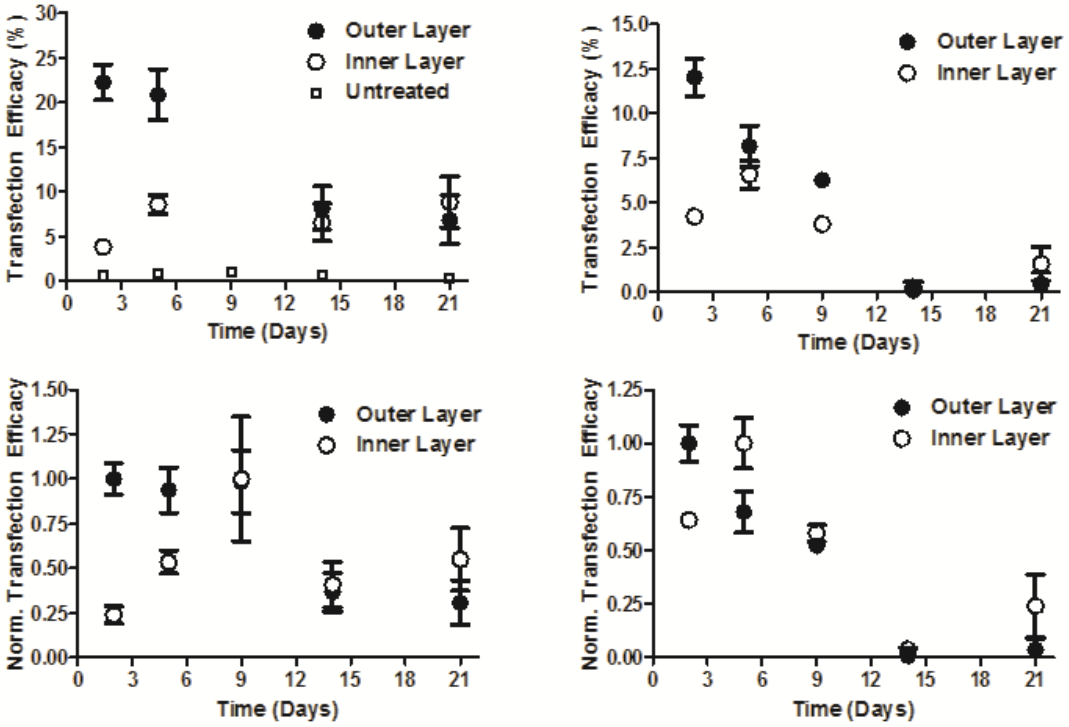

Figure 3. Transfection efficacies (top) and normalized transfection efficacies (bottom) in time for the outer (eGFP) and inner (dsRed) pDNA layers using 10% (left) and 50% (right) serum conditions.

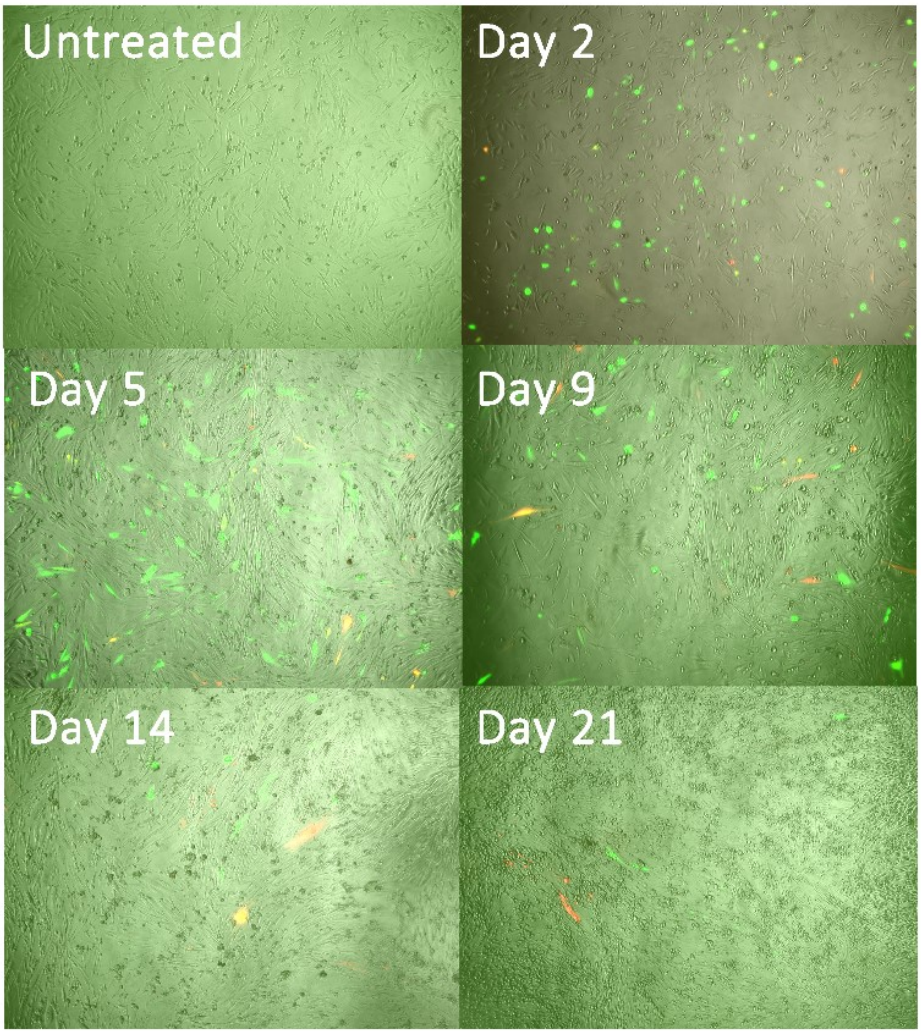

Figure 4. Fluorescence microscopy images of the GB319 cells in 10% serum transfected with the full 7 layers on days 2, 5, 9, 14, and 21 post-transfection.

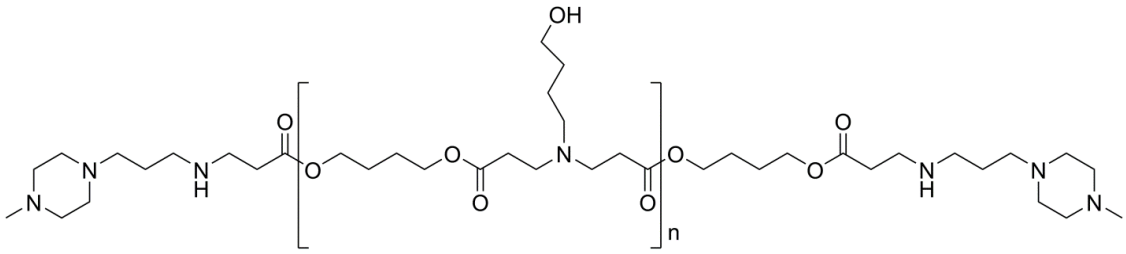

Figure S1. Polymer structure of B4-S4-E7 (447).

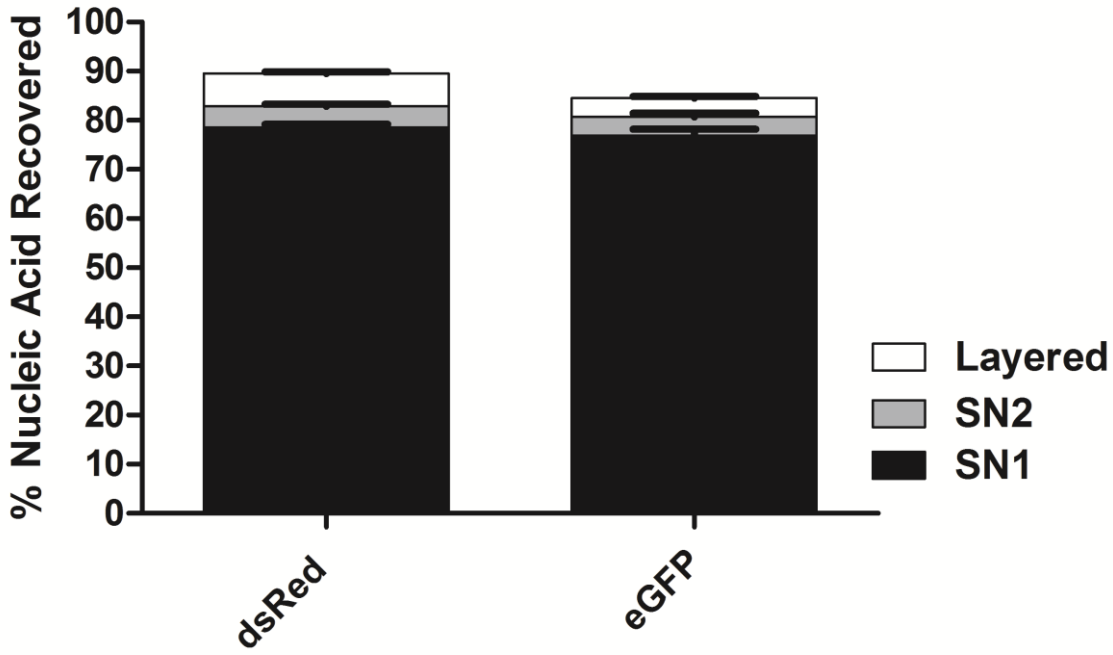

Figure S2. Layered nucleic acid content of the inner (dsRed) and outer (eGFP) pDNA layers; nucleic acid content in the supernatant of the first and second washings (SN1 and SN2) after the nucleic acid layer incubation.

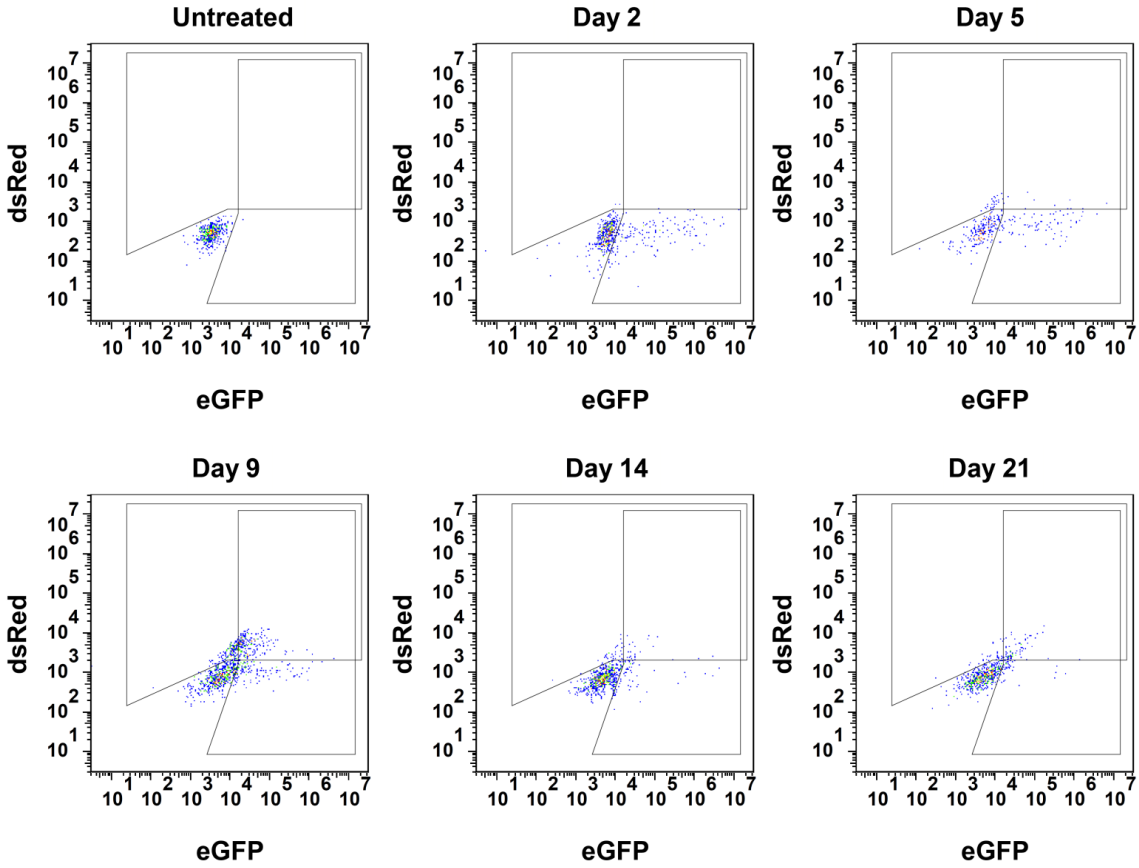

Figure S3. The flow cytometry dot plots of the eGFP and dsRed channels in time of the 10% serum condition which qualitatively shows the expression maxima of the outer (eGFP) and inner (dsRed) pDNA layers to be on days 2 and 9, respectively.

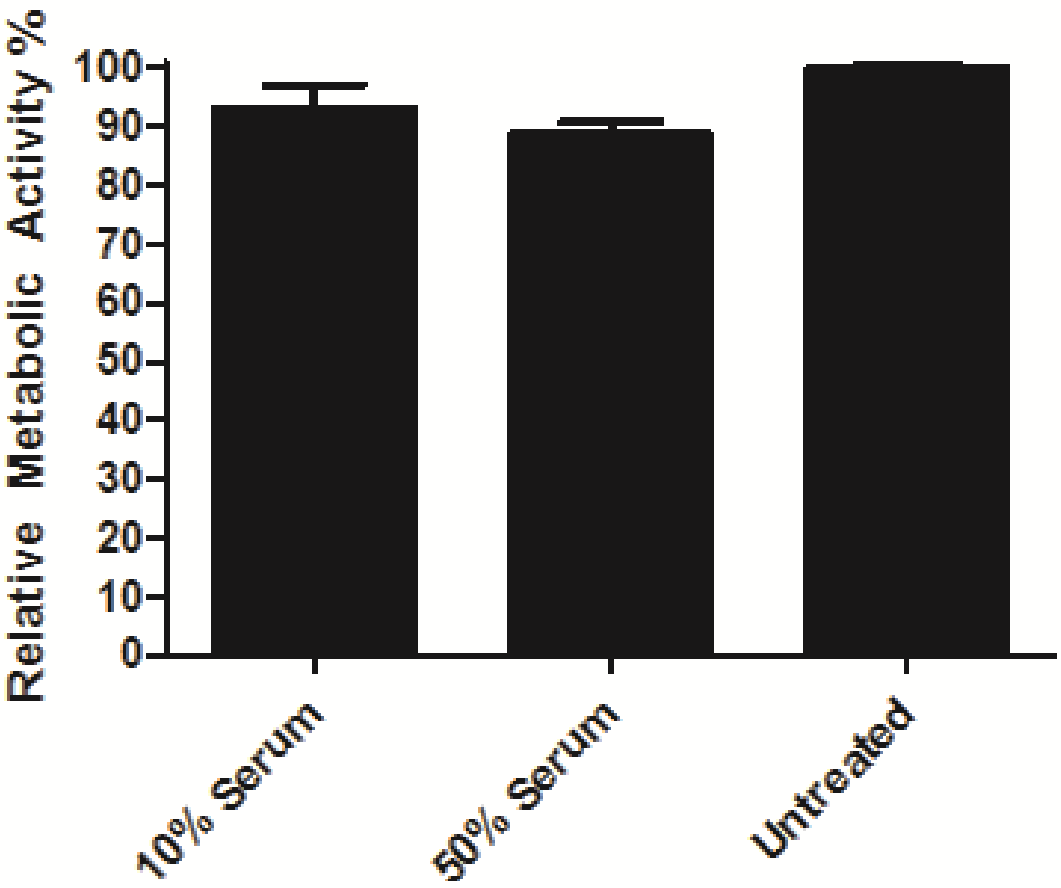

Figure S4. The relative metabolic activities of GB319 cells incubated with the full 7 layers in either 10% or 50% serum.

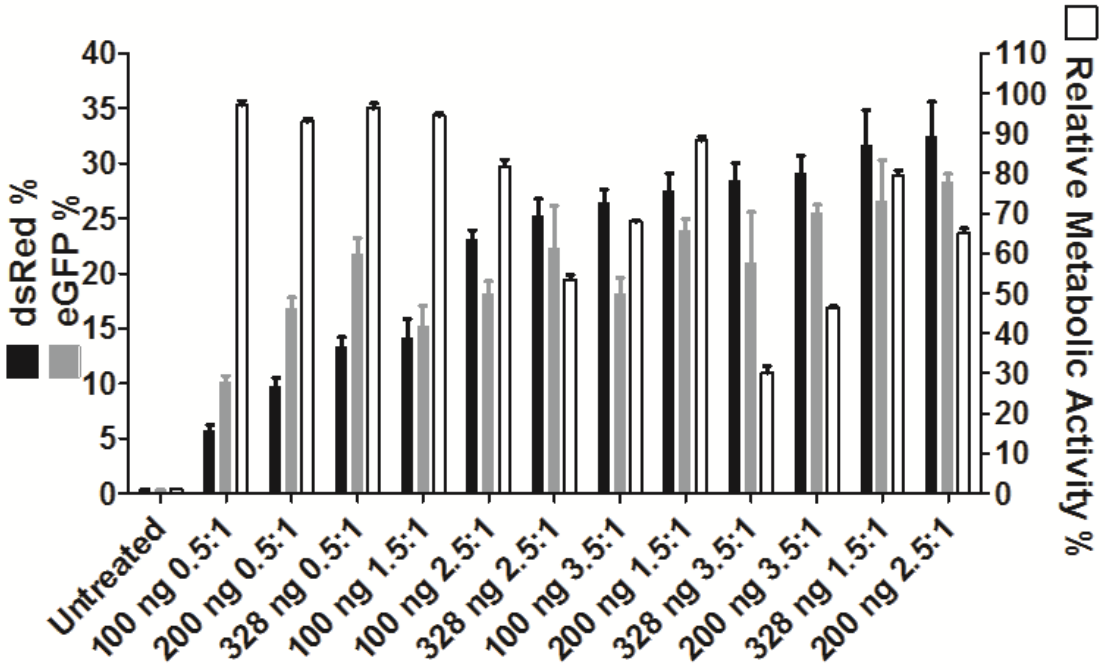

Figure S5. dsRed and eGFP expression efficacies of Lipo2k dosages at 100, 200, or 328 ng (same dsRed:eGFP pDNA ratio) at varying Lipo2k µL:pDNA µg ratios.

5.7 Schemes

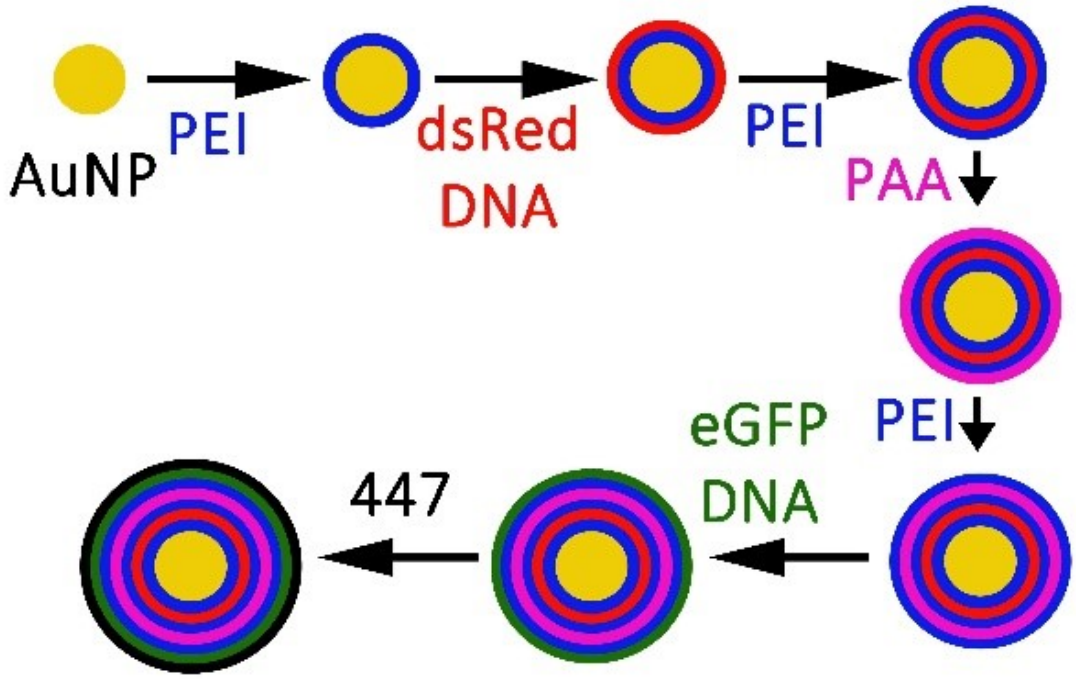

Scheme 1. LbL process of 7 layering steps beginning with the MUA-conjugated AuNPs.

5.8 References

(1) Bishop, C. J.; Kim, J.; Green, J. J. *Ann. Biomed. Eng.* **2014**, *42*, 1557-1572.
(2) Hainfeld, J. F.; Slatkin, D. N.; Focella, T. M.; Smilowitz, H. M. *Br. J. Radiol.* **2006**, *79*, 248-253.
(3) Zhang, Q.; Iwakuma, N.; Sharma, P.; Moudgil, B. M.; Wu, C.; McNeill, J.; Jiang, H.; Grobmyer, S. R. *Nanotechnology* **2009**, *20*.
(4) El-Sayed, I. H.; Huang, X. H.; El-Sayed, M. A. *Cancer Lett.* **2006**, *239*, 129-135.
(5) Frens, G. *Nature-Phys. Sci.* **1973**, *241*, 20-22.
(6) Zhang, Z. W.; Jia, J.; Lai, Y. Q.; Ma, Y. Y.; Weng, J.; Sun, L. P. *Bioorg. Med. Chem.* **2010**, *18*, 5528-5534.
(7) Blacklock, J.; Mao, G. Z.; Oupicky, D.; Mohwald, H. *Langmuir* **2010**, *26*, 8597-8605.
(8) Indrawattana, N.; Chen, G. P.; Tadokoro, M.; Shann, L. H.; Ohgushi, H.; Tateishi, T.; Tanaka, J.; Bunyaratvej, A. *Biochem. Biophys. Res. Commun.* **2004**, *320*, 914-919.
(9) Worster, A. A.; Brower-Toland, B. D.; Fortier, L. A.; Bent, S. J.; Williams, J.; Nixon, A. J. *J. Orthop. Res.* **2001**, *19*, 738-749.
(10) Bishop, C. J.; Tzeng, S. Y.; Green, J. J. *Acta Biomater.* **2014**, *11*, 393-403.
(11) Bishop, C. J.; Ketola, T. M.; Tzeng, S. Y.; Sunshine, J. C.; Urtti, A.; Lemmetyinen, H.; Vuorimaa-Laukkanen, E.; Yliperttula, M.; Green, J. J. *J. Am. Chem. Soc.* **2013**, *135*, 6951-6957.
(12) Kim, J.; Sunshine, J. C.; Green, J. J. *Bioconjug. Chem.* **2014**, *25*, 43-51.

6 Chapter 6: Cellular and Nuclear Uptake Rate Evaluation of Exogenous DNA via Flow Cytometry

6.1 Introduction

Gene therapy has the potential to treat and cure inheritable diseases such as cystic fibrosis [1], Duchenne muscular dystrophy [4,10], and hemophilia [15]. In general, viruses are highly efficient in delivering nucleic acid with a multiplicity of infection as low as one, but are immunogenic and can cause insertional mutagenesis. Non-viral methods, although generally less efficient at delivering nucleic acids, are easier to scale-up from a manufacturing standpoint, are easily chemically modified for optimization of function and toxicity, and have a low host immune response, comparatively.

Although high-throughput methods have enabled the screening of vast numbers of monomer combinations and polymer types for non-viral gene delivery, understanding the polymeric structure-function relationships would enable a more rational engineering approach for designing new delivery vectors. Quantifying plasmid cellular and nuclear uptake rate differences elucidates salient functional differences between polymer structures and reveals bottlenecks associated with specific vectors. PCR is a well-established method to quantify the number of plasmids within the cell or nucleus [7,8], however, lysing cells and nuclei, isolating and purifying DNA, and then subsequently running PCR on the samples is a time-consuming process compared to flow cytometry analyses.

This work lays forth the foundation as a proof of principle to quantify the number of plasmids within the cell and associated or internalized within isolated nuclei based on flow cytometry. Through the use of mathematical fitting to a system of differential equations, this method also allows the quantitative determination of cellular and nuclear uptake rate constants. We synthesized an already well-established vector, poly(β-amino ester) B4-S4-E7 or 447 [3,5] to transfect human primary glioblastoma multiforme (GBM319) cells and subsequently used a set of first order mass-action differential equations to quantify the rate constants associated with cellular entry, nuclear envelope association, and nuclear internalization. This more efficient flow cytometry method to quantify rate constants can be used to methodically elucidate how polymer structure determines intracellular gene delivery function.

6.2 Materials and Methods

6.2.1 Polymer Synthesis

Polymer B4-S4-E7 (447) was synthesized via a Michael addition reaction (**Scheme S1**) by adding 4-amino-1-butanol (S4) neat to 1,4-butanediol diacrylate (B4) in a 1.2:1 B4:S4 monomeric ratio, immediately vortexed, and placed in a 90ºC oven for 24 hours in the dark using a stir bar greater than 100 RPM, resulting in a B4-S4 acrylate-terminated base polymer [3]. The B4-S4 polymer was then solvated to 166.7 mg/mL using anhydrous tetrahydrofuran (THF) and subsequently endcapped using a 0.5 M solution of 1-(3-aminopropyl)-4-methylpiperazine, or E7, solvated in anhydrous THF for 1 hour at a final concentration of 100 mg/mL (**Scheme S1**). We have previously reported NMR data for polymer 447 [3,12]. The polymer was then precipitated using anhydrous

ethyl ether using two centrifugation washing steps at 4000 RPM for approximately 4 minutes. After decanting the ether the second time, the polymer was placed in a vacuum chamber for at least 24 hours in the dark. The polymer was then stored neat at -20ºC until the fractionation process.

6.2.2 Polymer Fractionation

Gel permeation chromatography (GPC) (Waters Corp.) was used to obtain a similar number- and weight-average molecular weight (M_n and M_w, respectively) of polymer 447 used previously which had high transfection efficacy in GBM319 cells [3]. The GPC setup included an autosampler, a refractive index detector, a Styragel column (WAT025861), and an autofractionator (Waters Corporation). The GPC diluent flowed at 1 mL/min and constituted 94% THF, 5% dimethyl sulfoxide (DMSO), 1% piperidine and a few 100 mg of butylated hydroxytoluene to inhibit free radical formation. The 39.7-41.7 minute time fraction was collected and again precipitated and vacuum dried as previously described. The polymer was then solvated in anhydrous DMSO to 100 mg/mL and frozen in 20 µL aliquots at -20ºC until use. Each aliquot used for further study underwent one freeze-thaw cycle only. Post-fractionation, the M_n and M_w was quantitated via GPC against polystyrene standards.

6.2.3 Cy3-plasmid DNA conjugation

A Mirus Label IT® Tracker™ Cy™3 Kit was used to conjugate Cy3 to enhanced Green Fluorescent Protein (eGFP-N1; 4733 base pairs (bp)) plasmids. In brief, 75 µg plasmid DNA (pDNA; 1 µg/µL), 60 µL of Mirus Buffer A and 415 µL of ultrapure

distilled water (DNase and RNase free) was added to 50 µL of the Cy3 dye reagent and incubated for at least 3 hours; at each hour the vials were briefly centrifuged to ensure all reagents were homogeneously reacting. Subsequently, 60 µL of 3 M sodium acetate (NaAc) and 1880 µL of ice cold 190 proof ethanol (EtOH) was added and the solution was kept at -20 ºC for at least 30 additional minutes. After which, the sample was centrifuged at 4 ºC for 15 minutes at 13 krcf, the supernatant was discarded and the pellet was then resuspended in 2 mL of 70% EtOH at room temperature. The sample was again centrifuged and the supernatant was discarded and the pellet was resuspended in 300 µg (1 mg/mL) of Cy3-unconjugated eGFP pDNA (1 µg:4 µg conjugated:unconjugated). Prior to adding the unconjugated pDNA the cap was left open and covered with aluminum to protect from light to allow the EtOH to evaporate for approximately 10 minutes. The sample was then characterized via a NanoDrop 2000 Spectrophotometer (Thermo Scientific). The absorbance of the DNA was corrected for Cy3-spectral overlap using the following equation (obtained from Mirus):

$$A_{base} = A_{260\,nm} - 0.08A_{550\,nm}$$

The nucleotide:dye ratio (N:D) was calculated using the following equation (obtained from Mirus):

$$N{:}D = \frac{A_{base}}{(\varepsilon_{\text{base}} = 6{,}600\ \text{M}^{-1}\text{cm}^{-1})} \frac{\left(\varepsilon_{\text{dye}} = 250{,}000\ \text{M}^{-1}\text{cm}^{-1}\right)}{A_{260\,nm}}$$

The eGFP-N1 plasmid contained a 77 bp Simian virus-40 (SV40) DNA-targeted sequence (DTS): 5'-AACCAGCTGT GGAATGTGTG TCAGTTAGGG TGTGGAAAGT CCCCAGGCTC CCCAGCAGGC AGAAGTATGC AAAGCAT-3'. The sequence binds to a transcription factor which then undergoes a morphological

change, revealing its nuclear localization signal (NLS) [17]. The DNA and its indirectly associated NLS can then be transported into the nucleus.

6.2.4 Cy3 pH-sensitivity

Various uptake pathways such as macropinocytosis, and caveolae- and clathrin-mediated endocytosis lead to the lysosomal degradation pathway, referred to as the proton sponge effect [6]. The cargo must have the ability to buffer the endosome to escape without degradation [6]. Because the pH of the Cy3-conjugated pDNA during the delivery process may range anywhere from approximately 5 to 7.4, the pH-sensitivity of Cy3 was assessed using a fluorescence plate reader (excitation and emission of 550 and 570 nm, respectively; Synergy2, Gen5) by using equal molar concentrations of the Cy3-eGFP pDNA in 150 mM sodium acetate (pH 5.2) and 150 mM phosphate buffered saline (PBS; pH 7.4) in triplicate. A Student's t-test was used to assess significance ($\alpha = 0.05$).

6.2.5 Cell Culturing

The GBM319 cells used for transfection were derived from human primary brain cancer and were cultured in a 5% CO_2 atmosphere at 37ºC, using DMEM:Ham's F12 (1:1) (Invitrogen) and was supplemented with 10% fetal bovine serum and 1x antibiotic-antimycotic (Invitrogen).

6.2.6 Polyplex Formation and Cell Incubation

Polymer 447 at a working concentration of 100 mg/mL in anhydrous DMSO was

diluted to 1.35 mg/mL which was used for preparing the 30 weight/weight (w/w; mass of polymer to mass of DNA) in 25 mM NaAc and mixed in a 1:1 v/v ratio with 45 μg/mL of plasmid DNA which was diluted from 1 mg/mL (originally in water) using 25 mM NaAc. Uptake studies utilized Cy3-conjugated pDNA, whereas qPCR and expression studies used Cy3-unconjugated pDNA, as the presence of Cy3 within such close proximity to the pDNA would inhibit primer annealing or the transcription and translation processes. Polyplex diameter and concentration were assessed in PBS via nanoparticle tracking analysis in triplicate via a NanoSight NS500 (Malvern Instruments, Ltd.). 24-well plates (2.0 μm^2) were seeded with 93,750 GBM319 cells (625 μL) 24 hours prior to transfection. 125 μL (2813 ng of pDNA) was delivered to each well. Separate 24-well plates for each time point were used to ensure that the cells containing Cy3-pDNA at later time points did not have more exposure to light, ensuring photobleaching was not a confounding factor.

6.2.7 Nuclei Isolation

Nuclei isolation was accomplished using an isolation kit (Nuc101; Sigma Aldrich). At each time point of interest after transfection the cells were placed on ice and 1 mL of an ice cold solution of heparin sodium salt from porcine intestinal mucosa (Sigma-Aldrich H3393) at 50 μg/mL in PBS (refer to the *Washing Extracellular and Extranuclear pDNA* section below) was quickly used to wash the cells twice with gentle trituration. Subsequently, 150 μL of ice cold lysis buffer (Nuc101; Sigma Aldrich) was placed on the cells and the cells were immediately scraped thoroughly and transferred to a 15 mL conical tube on ice. The cells were then homogenized using a round-bottom

glass tube while on ice and were by volume approximately 1/3 froth at completion and sat on ice for an additional 5 minutes. The samples were then transferred to 0.5 mL microcentrifuge tubes and centrifuged at 4ºC for 5 minutes at 500 rcf. The supernatant was carefully aspirated as to not agitate the pellet. 30 µL of ice cold lysis buffer was used to resuspend the pellet, followed by vortexing for 1-2 seconds. 120 µL of ice cold lysis buffer was then added to the samples and vortexed for a fraction of a second. The samples were placed on ice for another 5 minutes. The centrifugation and resuspension were completed twice and the samples were filtered into a new 0.5 mL microcentrifuge tube with a 40 µm nylon filter. The time points were divided into two tubes. 350 µL of ice cold 50 µg/mL heparin was added to half of the divided tubes and vortexed briefly. Samples were then centrifuged for 6 minutes at 600 rcf at 4ºC, the tubes were carefully aspirated, and the pellets were resuspended in 30% glycerol (3:7 v:v glycerol: ultrapure distilled water), and frozen at -80 ºC until further use for either flow cytometry analysis or genomic DNA (gDNA)/pDNA isolation and purification.

The nuclei isolation efficiency was calculated via a hemacytometer by dividing the number of cells used for the nuclei isolation process by the number of 2-(4-amidinophenyl)-1H-indole-6-carboxamidine (DAPI)-stained nuclei isolated and multiplying by 100 (n=3).

6.2.8 Nuclei Purity from Cytoplasm

To confirm nuclei purity, stably expressing eGFP(+) GBM319 cells [5] underwent the same culturing, transfection, and nuclear isolation process and were assessed via flow cytometry (n=2). The singlet nuclei population was identified using

FSC-H and SSC-H. The percent of eGFP(+) cells and nuclei were quantified by multiplying the ratio of the number of eGFP(+) cells to singlets by 100. Furthermore, DAPI stained nuclei with a combined brightfield image for qualitative purposes were taken to show the purity of the nuclei.

6.2.9 Washing Extracellular and Extranuclear Plasmid DNA

To ensure the heparin washing was sufficient to remove uninternalized plasmid pDNA from the cells (n=3) and nuclei (n≥2), the 24-well plates were placed at 4 ºC to inhibit ATP-dependent uptake mechanisms. Any fluorescence above the untreated groups associated with the cells or nuclei was thus attributed to unwashed plasmids on the phospholipid bilayer membrane of the cells or nuclei.

To assess how well cells were washed, polymer 447-pDNA polyplexes were incubated with the cells for 1 hour using 30 w/w (and 60 w/w which would likely be more difficult to wash). After the incubation period, the cells were either not washed or quickly washed with gentle trituration using heparin twice (1 mL; 50 μg/mL of heparin in PBS) and subsequently washed with 1 mL of PBS. Heparin is a highly anionic macromolecule used to destabilize the uninternalized polyplexes which frees the pDNA, causing the pDNA to be easily removed. The washed cells were immediately trypsinized after the PBS wash, quenched using 2% fetal bovine serum (FBS) in PBS, and then used for flow cytometry.

The nuclei were also challenged similarly at 4 ºC for 1 hour. Similar to the nuclei isolation process, one heparin wash was used (350 μL at 50 μg/mL) which was followed by centrifugation (600 rcf for 6 minutes). Furthermore, to more closely assimilate the

intracellular condition, rather than polyplexes, naked pDNA was used to challenge the nuclei as the plasmid in contact with the nuclei would likely have little or even no polymer ionically complexed at that stage due to degradation and dissociation from charged intracellular molecules (Varga and et al., used an unpackaging rate of $1x10^{9}$ min^{-1} in their model) [18–20]. The amount of plasmids per nuclei ($1x10^{5}$ plasmids/nuclei) used to assess the thoroughness of the heparin washing procedure was chosen to be exceedingly higher than previously reported values for plasmids found in the nucleus using non-viral methods [7,8].

For cellular and nuclear uptake studies all samples were washed at either the time point of interest up to two hours (0 (aspirated nearly simultaneously), 1, and 2 hours) or at two hours for all time points thereafter (4, 7, 18, and 24 hours). Cells were washed before nuclei isolation at the time point of interest. Unwashed and washed nuclei were then used for flow cytometry to assess the amount of plasmids either tightly associated (extranuclear (P_{ne}) + intranuclear (P_{ni})) or internal to the nuclei (P_{ni}), respectively. The word "tightly" is used as pDNA which is loosely associated with nuclei would likely not retain association with the nuclei throughout the nuclei isolation process.

6.2.10 Cellular and Nuclear Uptake

Cellular and nuclear uptake were assessed in triplicate at 0, 1, 2, 4, 7, 18, and 24 hours. To prepare the cells (n=3) for flow cytometry, the cells were washed as previously discussed (refer to the section entitled *Washing Extracellular and Extranuclear pDNA*). After the PBS washing step, 150 µL of warm 0.05% Trypsin-ethylenediaminetetraaceteic acid (EDTA) was added. After incubating at 37ºC for approximately 5 minutes, 850 µL

of 2% Trypsin in PBS was added to each well to quench the reaction. Each well was transferred to a 1.5 mL microcentrifuge tube and placed on ice before analysis. To prepare the nuclei (n=3) for flow cytometry, nuclei were taken from the -80 ºC freezer, thawed and diluted to approximately 150 µL using 2% FBS in PBS. Flow cytometry using a BD Accuri™ C6 Cytometer at a flow rate of 66 µL/min (note FL2-A = function of flow rate) was then used to identify the singlet populations and to assess the presence and intensity of Cy3. All gating and analysis was accomplished using FloJo. The singlet populations of nuclei and cells were identified using FSC-H and SSC-H; the amount of Cy3 per cell or nucleus was quantified using the geometric mean of FL2-A of the singlet population and normalized to an untreated group.

Of note, we would like to emphasize that what is being directly measured by the flow cytometer are fluorescences of the cell (plasmids within the cytoplasm ($P_{cyto} + P_{ne} + P_{ni}$), the unwashed nuclei ($P_{ne}+P_{ni}$), and washed nuclei ($P_{ni}$)). By simple arithmetic, the fluorescences associated with each compartment could be quantified.

6.2.11 Plasmid and Genomic DNA Isolation and Purification

The cells at their respective time points after transfection with unconjugated pDNA were prepared in triplicate for gDNA/pDNA isolation and purification by washing with heparin as previously described, trypsinizing, quenching with 2% FBS, and then doing a centrifugation washing step in a 1.5 mL tube to remove the trypsin. After the supernatant was trypsinized the samples were resuspended in 30 µL of PBS. The samples (7 time points in triplicate and the untreated group) were then incubated in a lysis buffer which constituted 0.5% sodium dodecyl sulfate (SDS), 100 µg/ml proteinase K, and 20 µg/ml DNase-free RNase [8]. The samples were placed in an oven at 50ºC while shaking

at 200 rpm for 4 hours. Tris-EDTA-saturated phenol was used to do a 1x volume extraction where an appropriate amount of phenol was added and the emulsion was vortexed briefly. To separate the layers, the samples were placed in a quickspin apparatus. The aqueous top layer was placed in a new vial and a 1x volume extraction with 25:24:1 phenol/chloroform/isoamyl alcohol was completed twice. The same procedure from the previous extraction was followed and the aqueous top layer was collected. The samples were set on ice and washed with ice-cold water-saturated ether twice. Water-saturated ether was prepared by mixing ultrapure distilled, RNase-/DNase-free water and ether in a 1:1 volume ratio. After the water-saturated ether was added, the samples were briefly vortexed and spun to separate the layers. The top ether layer was aspirated and the aqueous bottom layer was set on ice. To evaporate the remaining ether in the solution, the vials were left open for ~5 minutes. DNA was precipitated using 3x volumes of ice cold 95% EtOH at a final concentration of 0.3 M NaAc. The samples were incubated for at least 30 minutes at -20 ºC, and then centrifuged at 21 krcf at 4 ºC for 15 minutes. The supernatants were then removed and the pellets were resuspended in 3x volumes of 70% EtOH at room temperature. The same centrifugation steps were followed, and the supernatant was aspirated. The samples were allowed to dry by leaving the caps open for ~15 minutes. Ultrapure distilled, RNase-/DNase-free water was used to resuspend the samples to 30 µL before storing at -80 ºC. After storage, the concentrations of the isolated and purified gDNA and pDNA at each of the respective time points were assessed via UV-vis spectroscopy. The 260 nm/280 nm absorbance ratios were also assessed (n=24) as an indicator for nucleic acid purity. Aromatic amino acids absorb at the 280 nm wavelength which can used as an indicator of protein contamination.

6.2.12 Cy3 Fluorescence to Plasmid Number Conversion for Cells

The normalized geometric mean (NGM) of the samples were calculated using flow cytometry by dividing FL2-A (Cy3) by the untreated FL2-A. Because there may be slight variations in the intensity of the flow cytometry from day to day, the samples were normalized to their own untreated at each time point. When there is no Cy3 present in the samples the NGM is 1. Since we are interested in the increase in the fluorescence in time above the untreated group, $NGM_{Sample} - (NGM_{Unt} = 1)$ versus time was plotted thus Cy3's fluorescence began at 0 at the 0 hour time point. $NGM_{Sample} - NGM_{Unt}$ is the equivalence of the relative-fold fluorescence of Cy3 above the untreated. Within the manuscript NGM will refer to $NGM_{Sample} - NGM_{Unt} = \frac{Fluor_{Above\ Unt}}{Cell}$. Other values needed in converting Cy3 fluorescence to plasmid number included the bulk fluorescence (550/570 nm excitation/emission) via a fluorescence plate reader ($Fluor_{PR}$) associated with a known number of cells, quantified via a hemacytometer ($\#\ cells_{Hemacytometer}$). The plasmid number ($\#\ Plasmids$) contained within all of the cells was calculated using a pre-determined calibration curve ($n = 4;\ \#\ Plasmids = (m = slope)Fluor_{PR} + (b = y\ intercept)$). The following equation was used to calculate how much fluorescence (above the untreated group) is associated per plasmid according to flow cytometry:

$$\frac{Fluor_{Above\ Unt\ (Cells)}}{Plasmid} = \frac{\left(\frac{Fluor_{Above\ Unt}}{Cell}\right)}{\left(\frac{(\#\ Plasmids = mFluor_{PR} +\ b)}{\#\ cells_{Hemacytometer}}\right)}$$

In order to be above the bulk fluorescence background 3 wells of a 24-well plate were combined in order to have sufficient Cy3 signal (n=3; 9 wells total). The

$\frac{Fluor_{Above\ Unt\ (Cells)}}{Plasmid}$ value was measured (n=3) multiple times at multiple time points to ensure it was constant.

6.2.13 Cy3 Fluorescence to Plasmid Number Conversion for Nuclei

It was more challenging to calculate the $\frac{Fluor_{Above\ Unt\ (Nuclei)}}{Plasmid}$ in the same way as the cells with the fluorescence plate reader for two reasons: 1) there are far fewer plasmids per nucleus than plasmids per cell and thus the Cy3 fluorescence signal was not able to break out of the background fluorescence even when 12 wells of isolated nuclei were combined (with volume held constant at 100 µL similar to calibration curve); 2) we lose fluorescence signal due to the nuclei isolation process itself as the nuclei isolation efficiency is approximately 25%. Re-optimizing the isolation protocol to accommodate larger volumes may alter variables, such as the washing process, and may confound results further.

As an alternative, we were able to scale the $\frac{Fluor_{Above\ Unt\ (Cells)}}{Plasmid}$ value to be applicable for nuclei by multiplying by the relative fluorescence of untreated cells and nuclei which was confirmed with qPCR (Student's t-test) as follows:

$$\frac{Fluor_{Above\ Unt\ (Nuclei)}}{Plasmid} = \left(\frac{Fluor_{Above\ Unt\ (Cells)}}{Plasmid}\right)\left(\frac{Unt\ Cells}{Unt\ Nuclei}\right)$$

For each time point for either the cells or nuclei the fluorescence by flow cytometry was converted to the number of plasmids by the following equation:

$$Plasmid_{PR} = \frac{\left(\frac{Fluor_{Above\ Unt}}{Cell\ or\ Nucleus}\right)}{\left(\frac{Fluor_{Above\ Unt\ (Cells\ or\ Nuclei)}}{Plasmid}\right)}$$

6.2.14 Intracellular Plasmid DNA Degradation Kinetics

Cy3 is not an intercalating dye and its fluorescence intensity does not change if the plasmids structural integrity is compromised because Cy3 is conjugated to the pDNA via a reactive alkyl group to heteroatoms within the plasmid. Because quantifying fluorescence of Cy3-pDNA does not necessarily correspond to intact plasmids, qPCR was used in order to correct for pDNA degradation in time.

After the isolated and purified gDNA/pDNA samples from the GBM319 cells (n=3) were quantified via NanoDrop of, each sample was diluted to 1 μg/mL in ultrapure distilled water (DNase and RNase free). Each qPCR well contained 6 ng of the purified gDNA/pDNA, 14 μL of SYBR® Green PCR Master Mix (2x concentration; Life Technologies), and 2 μL of the reverse and forward primers for eGFP and human β-cytoskeleton actin (β-actin), totaling 20 μL. β-actin is a housekeeping gene and was used to compare the relative amounts of eGFP present. The eGFP and β-actin primer amplicons were 95 and 250 nucleotides in length, respectively. The eGFP and β-actin sequences were as follows: forward eGFP primer: AGGGCATCGACTTCAAGG (55.6% GC; Tm: 54.7ºC); reverse eGFP primer: CTACGTCTATATCATGGCCG (50% GC: %Tm: 52.1ºC); forward β-actin primer: CATGTACGTTGCTATCCAGGC (52.4% GC; Tm: 60.8ºC); reverse β-actin primer: CTCCTTAATGTCACGCACGA (50.0% GC; Tm: 60.2ºC). The thermal cycling conditions for qPCR were set at 95ºC for the first 10 minutes to fully denature the template and activate the enzymes. Immediately thereafter, a temperature cycle was repeated between 95ºC and 60ºC for 15 seconds and 1 minute, respectively, 40 times.

PCR was performed on a dilution series for each gene of interest in order to calculate the efficiency of replication (ER) and was calculated using the cycle threshold value (CT) as follows:

$$ER = -1 + (fold\ dilution\ between\ samples)^{1/|average\ \Delta CT\ between\ dilutions|}$$

We ensured the ERs for the eGFP and the β-actin amplicon amplifications were between 0.95-1.05 which allowed $2^{-\Delta\Delta CT}$ to be a valid quantification of the relative amounts of genes present [13]. It is important to note the log(DNA content: concentration or mass) versus CT plot is sigmoidal. The ER should be calculated for the linear range in this plot and the unknown samples' CT values should also be within this same linear CT range. ΔΔCT was calculated as follows:

$$\Delta\Delta CT = \left(CT_{eGFP\ sample} - CT_{\beta-actin\ sample}\right) - \left(CT_{eGFP\ Untreated} - CT_{\beta-actin\ Untreated}\right)$$

Because β-actin is a single copy gene, there are two copies per cell. By multiplying $2^{-\Delta\Delta CT}$ by 2, the total number of plasmids per cell can be obtained [8]. Thus:

$$Plasmid_{qPCR} = 2(2^{-\Delta\Delta CT})$$

Once qPCR was completed, melt curves of the qPCR products were examined for quality control; furthermore, the qPCR products were assessed for off-target amplification and primer dimers using gel electrophoresis (4% agarose; 1µg/mL ethidium bromide) and a DNA ladder.

The structural integrity of the plasmids was taken into account ($Plasmid_{Corr}$) by multiplying $Plasmid_{PR}$ by the ratio of intact plasmids (of the 447 polymer in the GBM319 cells) at each time point, using the following equation:

$$Plasmid_{Corr} = Plasmid_{PR}\left(\frac{Plasmid_{qPCR\ 447}}{Plasmid_{PR\ 447}}\right)$$

The polymer chosen for this poof of principle paper has a $Plasmid_{Corr}$ value equal to the $Plasmids_{qPCR\ 447}$ value. If additional polymer structures were compared to assess structure-function relationships at gene delivery, the $\left(\frac{Plasmids_{qPCR\ 447}}{Plasmids_{PR\ 447}}\right)$ ratios at each time point could be used without repeating qPCR. The corrected plasmid values for the cytoplasm, the extranuclear space, and the intranuclear space are represented as follows: $P_{Corr\ cyto}$, $P_{Corr\ ne}$, and $P_{Corr\ ni}$, respectively. Each plasmid compartment (P_{cyto}, P_{ne} and P_{ni}) was assumed to have the same degradation kinetics for simplicity. For the investigation of other polymers, the polymer-pDNA binding strength would also likely need to be relatively similar for the degradation kinetics to be comparable [3,14].

The intracellular plasmid degradation time constants were calculated from using exponential decay fittings from 2 to 24 hours. The reason we chose to not include 0-2 hours was because there are plasmids being imported from the media 0-2 hours which would confound the intracellular degradation computation. We investigated fittings with both mono- and bi-exponential terms, which was accomplished using the MatLab function nlinfit.

6.2.15 Expression Efficacy and Relative Metabolic Activity

Fluorescence microscopy (10x magnification, 200 ms eGFP exposure time) and flow cytometry (66 μL/min) were performed to assess expression 48-hours post transfection (n=3). The relative metabolic activity (viability) was assessed using a CellTiter 96® AQueous One assay at an absorbance of 490 nm using a UV-Vis spectrophotometer (Synergy2, Gen5) (n=3).

6.2.16 Modeling via First Order Mass-action Kinetics

The set of first order mass-action differential equations used in this work was simplified to the extent possible such that the experimental data could be sufficiently recapitulated using the minimum number of fitted variables and without taking information from a variety of sources which can confound the interpretation [2]. The model included 4 compartments from 0 to 2 hours: the media, cytoplasm, nuclear envelope (ne; tightly-associated extranuclear space), and nucleus (ni; intranuclear space) (**Scheme 1**) and 3 compartments after 2 hours because the plasmid number in the media drops to zero at the completion of the polyplex-cell incubation time period.

The number of plasmids in the media, cytoplasm, associated with the nuclear envelope, and internal to the nucleus are represented by P_{media}, P_{cyto}, P_{ne}, and P_{ni}, respectively. The rate contributing term transferring plasmids from the media into the cytoplasm, $k_{cell}P_{media}$, in the set of differential equations included a Heaviside or unit step function ($\mathfrak{A}$) which was able to bring the non-zero term to zero at 2 hours by multiplying $k_{cell}P_{media}$ by $\mathfrak{A}[-(t-2)]$; where t = time (hours). The Heaviside step function greatly simplified the differential equations because without the unit step function, two sets of differential equations would have been required. Using the plasmid number at 2 hours

from the 4 compartmental model for the 3 compartmental model's initial conditions would have rendered the same results had the Heaviside step function not been used.

The rate constants for plasmids transferring from the media to the cytoplasm, the cytoplasm to the nuclear envelope, and the nuclear envelope to the nucleus are represented as k_{cell}, k_{ne}, and k_{ni}, respectively (**Scheme 1**). k_{bd} is a backflow rate term from the nuclear envelope and the nucleus back to the cytoplasm. The backflow could be due to active plasmid transport from the nucleus or from nuclear envelope breakdown.

In some cases rate constants are normalized to volume; in this model because P_{ne} represents plasmids on a surface area and P_{media}, P_{cyto} and P_{ni} represent plasmids within a volume, it is not reasonable to normalize the compartments plasmid variables or their respective rate constants to a volume or a surface area.

Any plasmids that were tightly associated with the extranuclear space or within the intranuclear space would be effectively in the cytoplasm at the time of nuclei isolation if the cell were undergoing mitosis. For simplification, we used the same k_{deg} term for all intracellular compartments. The differential equation set used was as follows:

$$\frac{dP_{cyto}}{dt} = k_{cell}\, P_{media}\, \mathfrak{A}[-(t-2)] + k_{bd}(P_{ne} + P_{ni}) - \big(k_{ne} + k_{deg}\big)P_{cyto}$$

$$\frac{dP_{ne}}{dt} = k_{ne}\, P_{cyto} - \big(k_{ni} + k_{bd} + k_{deg}\big)P_{ne}$$

$$\frac{dP_{ni}}{dt} = k_{ni}\, P_{ne} - \big(k_{bd} + k_{deg}\big)P_{ni}$$

The MatLab code automatically fitted the experimental data through for loops. Random rate constants from 0.0000 to 1.0000 hours^{-1} were assigned to k_{ne}, k_{ni}, and k_{bd}. At every value varied for k_{cell}, MatLab's ODE23s solver was used to assess the model plasmid

values (P_{cyto}, P_{ne}, P_{ni}) and the sum of the residuals squared (SRS) was calculated using the experimental data as follows:

$$SRS = \sum_{t=0\ hour}^{24\ hours} \left(\left| P_{Corr\ cyto} - P_{cyto} \right|^2 + |P_{Corr\ ne} - P_{ne}|^2 + |P_{Corr\ ni} - P_{ni}|^2 \right)$$

After varying k_{cell}, the minimum SRS was determined and used as a constant value. After which the other 3 remaining rate constants were independently scanned in like manner one at a time to find the rate constant values associated with their SRS minima. Once all 4 rate constants were optimized once, these same rate constant values were used for the whole process again rather than using random variables. This continued until the rate constants were optimized and did not change with further iterations. The entire process where random variables were used and optimized until there were no changes in the rate constants was repeated 25 times.

6.2.17 Statistics

All errors reported are standard errors of the mean and are independently prepared samples. Sample numbers are reported in their respective method sections. A Student's t-test was performed for **Figure S1** (n=3) and **Figure S2** (n=2). Two independent one-way ANOVAs were performed for cells (n=3) and nuclei (n≥2) for **Figure 2**.

6.3 Results

6.3.1 Polymer Synthesis and Fractionation

Polymer 447's M_n and M_w were 9.5 kDa and 12.3 kDa, respectively. A polydispersity index (PDI) close to unity of 1.30 was obtained.

6.3.2 Cy3-plasmid DNA Conjugation

The number of nucleotides per dye immediately post-conjugation and before dilution into unconjugated pDNA was approximately 35 nucleotides/dye.

6.3.3 Cy3 pH-sensitivity

The Cy3 fluorescence at pH 7.4 (150 mM PBS) and 5.2 (150 mM NaAc) were not different (p-value = 0.63) as shown in **Figure S1**.

6.3.4 Polyplex Formation

The diameter of the polyplexes was 98 ± 7 nm. The polyplex concentration was $(4.3 \pm 0.7)x10^{10}$ particles/well. Based on the dosage delivered there were $6.0x10^{11}$ plasmids per well assuming 600 Da/base pair. This would suggest there were 14 ± 2 plasmids on average per polyplex. At the time of seeding there were approximately 93,750 cells, which suggests there were on average $6.4x10^6$ plasmids available per cell and $(4.6 \pm 0.7)x10^5$ polyplexes available per cell.

6.3.5 Nuclei Isolation and Purity from Cytoplasm

The isolated nuclei were close to 20 μm in diameter. The efficiency of the nuclei isolation process was 25 ± 5%. **Figure 1** shows isolated nuclei stained with DAPI. The background fluorescence of the gated nuclei (eGFP negative) from the eGFP-stably expressing cells (79%+) according to flow cytometry was 0.4%+ as shown in **Figure S2** (p-value = 0.02), which is more than a 99% drop in eGFP.

6.3.6 Washing Extracellular and Extranuclear Plasmid DNA

The heparin wash regimen was sufficient in removing the pDNA from both cells and nuclei which would not have been uptaken at 4 ºC as endocytosis is an ATP-dependent process for both cells (30 and 60 w/w) and nuclei (100k plasmids/nucleus) (**Figure 2**).

6.3.7 Cellular and Nuclear Uptake

As expected, the nuclei on flow cytometry was associated with a lower FSC-H than the cells which can be qualitatively seen in the ungated FSC-H vs SSC-H dot plot (**Figure S3**; top) and in the FSC-H histogram of gated singlet cells and nuclei (**Figure S3**; bottom). The 0 hour time point for the cells and nuclei were as expected in that the fluorescence values were near the untreated groups'. As an example, a dot plot of FL1-A and FL2-A for the untreated, and 0 and 2 hour time points for cells are shown in **Figure S4**. This can also be observed for cells and nuclei by the 0 hour time points' closeness in proximity to the origin in **Figure 3**.

The percent positive time profiles for Cy3-pDNA in cells (top left) and nuclei (bottom left) are shown in **Figure 3**. The Cy3(+) percent for cells increased from zero to

a relatively constant value of ~75% at 2 hours (top left), with the 18 and 24 hour time points being ~80%; the Cy3(+) percent value for nuclei (bottom left) reached a maximum at 2 hours. The NGM fluorescence increased from 0 to a maximum at 2 hours for both cells (top right) and nuclei (bottom right) (**Figure 3**).

It was determined that the maximum uptake occurred at the time the particles were washed from the cells and nuclei by also observing that the maximum was at 4 hours when the cells were allowed to incubate with polyplexes for 4 hours rather than 2 hours.

6.3.8 Plasmid and Genomic DNA Isolation and Purification

The concentrations of the gDNA and pDNA isolated and purified from the cells for qPCR was 16 ± 2 μg/mL. The 260 nm/280 nm absorbance ratio was 2.03 ± 0.08.

6.3.9 Cy3 Fluorescence to Plasmid Number Conversion for Cells and Nuclei

The background fluorescence for cells without Cy3 was equivalent to the background for the known plasmid standard below $1x10^8$ plasmids per well which was approximately 1000. A calibration curve (**Figure S5**) was used to convert the bulk fluorescence on the plate reader to a plasmid number.

The $\frac{Fluor_{Above\ Unt\ (Cells)}}{Plasmid}$ and $\frac{Fluor_{Above\ Unt\ (Nuclei)}}{Plasmid}$ values were $(1.8 \pm 0.2)x10^{-4}$ per plasmid and $(3.5 \pm 0.4)x10^{-3}$ per plasmid, respectively. Because the deviation between multiple time points was small, it demonstrates a linear relationship which helps validate that the different compartments' fluorescences can be calculated through simple arithmetic.

Confirming the scaling of the $\frac{Fluor_{Above\ Unt\ (Nuclei)}}{Plasmid}$ value, a Student's t-test at the 2 hour time point between the $Plasmid_{qPCR}$ and $P_{Corr\ ni}$ values showed no statistical difference (p-value = 0.25).

6.3.10 Intracellular Plasmid DNA Degradation Kinetics

The replication efficiencies of the eGFP and β-actin primers were 0.97, and 0.95, respectively. The eGFP and β-actin qPCR products were the same lengths as the amplicon lengths; 95 and 250 bp, respectively, according to gel electrophoresis (**Figure S6**). No primer dimers or off-target amplification was observed on the gel as well which corroborated the melt curve findings.

Figure S7 shows the plasmid numbers in time of cells ($P_{cyto} + P_{ne} + P_{ni}$) based on $Plasmid_{PR}$ and $Plasmid_{qPCR}$ which separated further in time as intracellular nucleases continued degrading the exogenous pDNA. The similarity of the $Plasmid_{PR}$ and $Plasmid_{qPCR}$ values for the initial time points further validate the conversion from fluorescence to plasmid number. The $Plasmid_{PR}$ and $Plasmid_{Corr}$ values for both cells and nuclei are shown in **Figuare S8** on the top and bottom, respectively.

The $Plasmid_{qPCR}$ values in time from 2 to 24 hours are shown in **Figure S9** with mono-(dotted line) and bi-exponential degradation (solid line) fittings. The bi-exponential degradation fits the experimental data more stringently, suggesting there are likely two terms involved in the degradation process. For simplicity, we initially used the mono-exponential k_{deg} value of 0.350 $hours^{-1}$ in the model and the plasmid values reached zero at a much earlier time point after the 2 hour peak than the experimental data suggested which prompted us to explore the bi-exponential degradation approach for k_{deg}. The bi-

exponential degradation analysis is based on a mechanism of faster degradation in one state (such as when the DNA is free from polymer) and slower degradation of the DNA when it is in a second state (such as bound to polymer). The k_{deg} incorporating the two exponential degradation terms in the set of differential equations was calculated using ***Supplemental derivation 1***, where A, B, k_{deg1}, and k_{deg2} were obtained from the bi-exponential fitting (**Figure S9**; Plasmids ($P_{cyto} + P_{ne} + P_{ni}$) = $Ae^{-k_{deg1}t} + Be^{-k_{deg2}t}$) and is as follows:

$$k_{deg} = \frac{\left(k_{deg1}Ae^{-k_{deg1}t} + k_{deg2}Be^{-k_{deg2}t}\right)}{\left(Ae^{-k_{deg1}t} + Be^{-k_{deg2}t}\right)}$$

The initial number of plasmids available per cell for uptake in the media was $6.36x10^6$, which was based on the dosage delivered per well (2813 ng). The number of plasmids available to be uptaken per cell in time is shown in **Figure S10** which was calculated by subtracting the amount of plasmids uptaken in time from the initial dosage. At 2 hours, all plasmids in the media were washed away, which is why **Figure S10** drops to zero immediately after 2 hours.

6.3.11 Expression Efficacy and Relative Metabolic Activity

The expression efficacy of 447 30 w/w (2813 ng; 2 hour polyplex incubation) 48 hours post transfection was 70.6 ± 0.6% (**Figure S11**; bottom). The relative metabolic activity was 101 ± 3%, normalized to the untreated group (100%).

6.3.12 Modeling via First Order Mass-action Kinetics

19 iterations of optimization were required to obtain the converged rate constant values for the bi-exponential degradation model (**Figure S12**). k_{cell}, k_{ne}, k_{ni}, and k_{bd} were

$6.8x10^{-4}$, 0.72, 1.1, and 1.8 $hour^{-1}$, respectively. The minima of the sum of the residuals squared (SRS) between the experimental data and the bi-exponential model are shown in **Figure S13** for the last iteration of the optimization. The experimental data in conjunction with the bi-exponential and mono-exponential degradation models are shown in **Figure 4** and **Figure S14** (k_{cell}, k_{ne}, k_{ni}, and k_{bd} were $7.1x10^{-4}$, 0.85, 1.3, and 2.1 $hour^{-1}$, respectively), respectively.

6.3.13 Polymer Rate Comparison

Polymers 44, 446, and 447 (**Scheme 2** in chapter 3.6.2) were assessed in like manner, according to the methods outlined above. The experimental data and the first-order mass action kinetic models overlaid can be found in **Figure 5** for polymers 44 (**Figure 5A**), 446 (**Figure 5B**), and 447 (**Figure 5C**). The auto-fitted rate constants can be found in **Table 1**, as well as the M_n, M_w, and PDIs**.**

6.4 Discussion

The fractionation process allowed for the targeted molecular weight to be obtained which had shown to previously work well in GBM319 cells [3]. The obtained PDI of 1.30 was similar to previously reported PDIs of fractionated polymer [3]. Because Cy3 is not pH-sensitive in the range of interest (pH 5.2-7.4), no intracellular fluorescence intensity corrections based on the intracellular location of the plasmids were needed for the uptake experiments. The gated nuclei from stably-expressing eGFP(+) cells were nearly free from a detectable amount of eGFP by flow cytometry, indicating there was very little false-positive Cy3-pDNA signal in the cytoplasm on the nuclei. The washing experiments successfully demonstrated the feasibility of removing extracellular and

extranuclear plasmids from the surface of the cells and nuclei, which would have otherwise contributed false-positively to the fluorescence.

The percentage of cells with a detectable amount of eGFP according to flow cytometry increased from zero and even increased slightly after 2 hours which may have been because the cells preparing to enter mitosis would have an increased endocytosis rate, enabling the expansion of their phospholipid bilayer membranes [16]. This could result in a greater proportion of cells with a detectable amount of Cy3-pDNA after the polyplex incubation time period. Asynchronous cell populations with respect to cell cycle stages were used for uptake studies because there have been reports suggesting that the cell cycle stage synchronization process itself affects multiple cellular processes, confounding the interpretation of the results [9]. Furthermore, an asynchronous cell population would more closely resemble an *in vivo* environment.

There was a decrease in FL2-A's fluorescence intensity after the incubation time period which corroborates the heparin washing experiments; we have found that when not all of the unuptaken Cy3-pDNA is washed sufficiently from the wells that the NGM FL2-A values at later time points can be 2-3 fold higher. The decrease in the fluorescence was likely due to dilution from cell division (doubling time of GBM319 cells is approximately 1 day) and also, to some degree, exocytosis or the endosome recycling pathway.

The mono-exponential degradation value for k_{deg} of 0.350 $hour^{-1}$ was similar to Varga, et al.'s reported value of $5x10^{-3}$ min^{-1} or 0.3 $hour^{-1}$ [21]. Usage of the bi-exponential degradation allowed for a better fit for the first order mass-action kinetic model which suggested that there may be two different plasmid states as has been

reported previously in literature: 1) an unbound or free plasmid state where the plasmids are more susceptible to nuclease activity and 2) the plasmid-polymer bound state, where the plasmids are better protected from nuclease activity [14]. The polymer degradation or unpacking of the plasmid cargo would lead to more degradation in time accounting for the greater differences between the $Plasmid_{PR}$ and $Plasmid_{qPCR}$ values in time [14].

When utilizing this approach, the degradation rate constants should be re-evaluated for each cell type of interest using qPCR as the plasmid degradation rate constants can vary by cell type. If the binding affinity between the polymer types of interest vary substantially it may also be beneficial to assess the degradation rate even within the same cell type [3]. Furthermore, if the Cy3 density conjugated to pDNA varies, re-calibrating the plasmid conversion would also be necessary.

The cellular and nuclear uptake rates observed were similar to other rates previously reported in literature [2,11,21,22] which further validates the flow cytometry approach used. The bi-exponential degradation model provided superior fits compared to the mono-exponential degradation model as the latter caused the plasmid values to drop to zero prematurely compared to the experimental data. The maximum plasmid number for each compartment (P_{cyto}, P_{ne}, and P_{ni}) as indicated by the model shifted slightly in time with P_{cyto} at 2 hours and P_{ni} nearer to 2.5 hours.

Despite there being $6.4x10^6$ plasmids ($4.6x10^5$ polyplexes) available per cell, around ~25% of the cells did not uptake plasmids sufficiently to be Cy3(+) and ~30% of cells did not transcribe and translate enough protein to be considered eGFP(+) according to flow cytometry. Only 0.1% of the pDNA delivered in the media was uptaken by the cells. The high number of unuptaken plasmids for non-viral gene delivery delineates the

need for more efficient delivery systems at the cellular level. Of the 0.1% of the plasmids containing the DTS, 12% of what was in the cell successfully entered the nucleus. The rate limiting barrier for polymer 447 was at the cellular level. Incorporating a cell penetrating/targeting ligand may improve the cellular uptake efficiency and perhaps require far fewer plasmids for successful transfection.

The rate constants demonstrate that the plasmid amount present in one compartment at any given time is dependent upon the concentration in the compartment(s) driving the mass transfer. Therefore, for comparison of different polymers, the overall rate transfer should be compared and not just the rate constants. The rate constants also indicate the bottlenecks in intracellular delivery for each polymer. The content of DNA in the nucleus was directly proportional to the amount of eGFP expressed in all 3 polymer cases.

6.5 Conclusions

In these experiments, we were able to develop a new flow cytometry based method to quantify intracellular steps in gene delivery. We were able to demonstrate the needed methodlolgy including: washing cells and nuclei sufficiently to remove uninternalized false-positive Cy3-pDNA; Isolating nuclei with a minimal amount of cytoplasm to assess the amount of labeled Cy3-pDNA in the cytoplasm, on the nuclear envelope, and internal to the nucleus; first order mass-action modeling using MatLab to auto-fit the relevant rate constants using a minimal number of compartments and with no information extrapolated from literature. A bi-exponential degradation model was also able to recapitulate the experimental data with good agreement. This methodology can

be easily combinatorially combined with other intracellular fluorescent measurments to better elucidate intracellular gene delivery. It can also be scaled with high-throughput plate-based flow cytometry to assay arrays of biomaterials and/or cell lines for intracellular delivery in a quantitative manner.

6.6 Figures

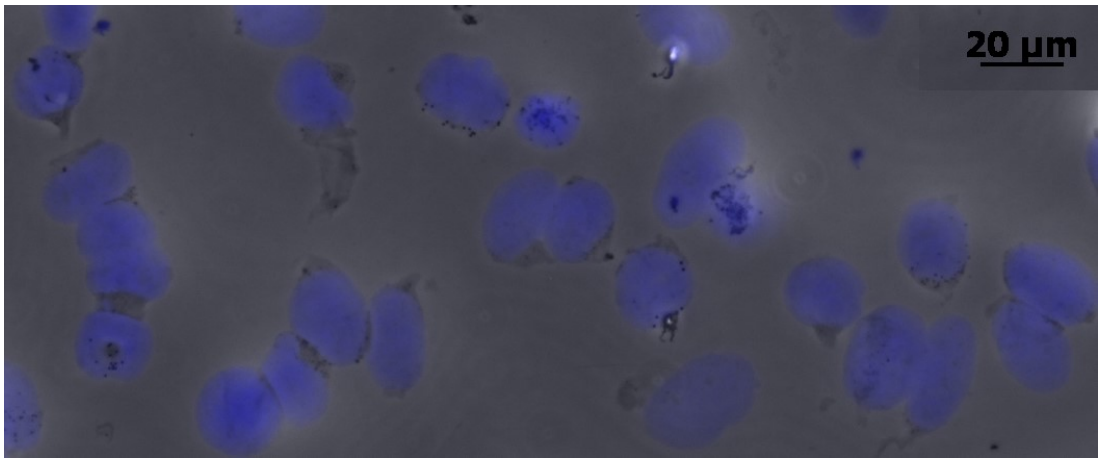

Figure 1. Isolated nuclei stained with DAPI.

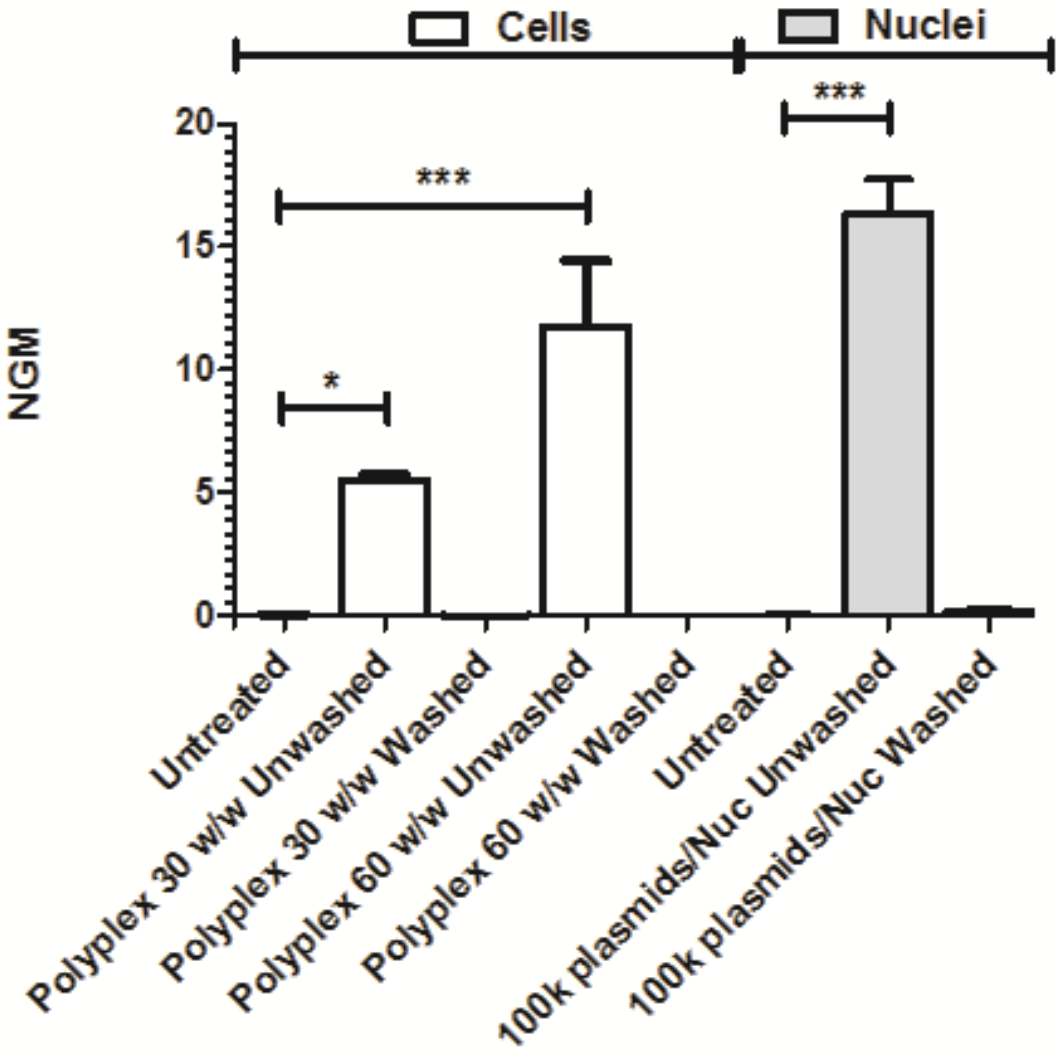

Figure 2. Cells and nuclei washing challenge (polyplex incubation for 1 hour at 4ºC) using 50 μg/mL heparin in PBS to eliminate associated DNA or DNA that was not uptaken. The washed cells and nuclei returned to their untreated fluorescence values, indicating successful washing.

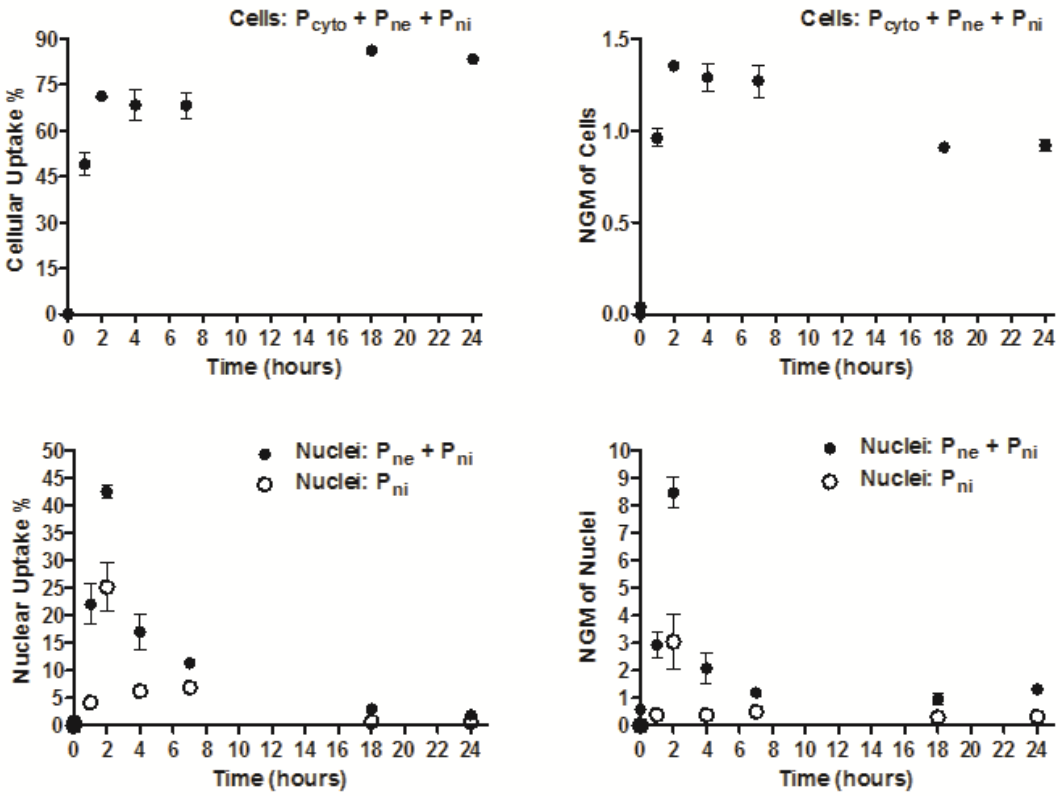

Figure 3. Percentages (left) and NGM (right) of Cy3 for both cells (top) and nuclei (bottom). Pcyto, Pne, and Pni are plasmids which are in the cytoplasm, and plasmids which are extranuclear and intranuclear, respectively.

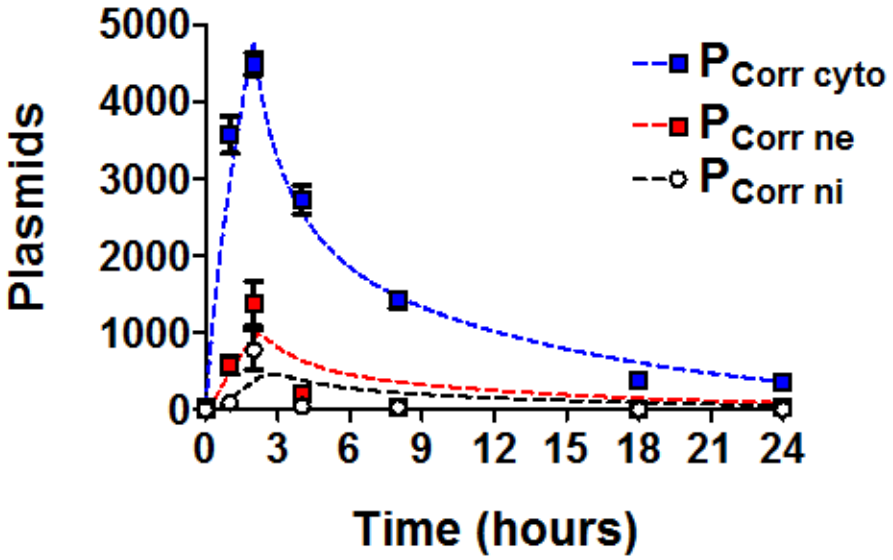

Figure 4. First order mass-action model (dotted lines; bi-exponential degradation) for the $P_{Corr\ cyto}$, $P_{Corr\ ne}$, and $P_{Corr\ ni}$ experimental data points.

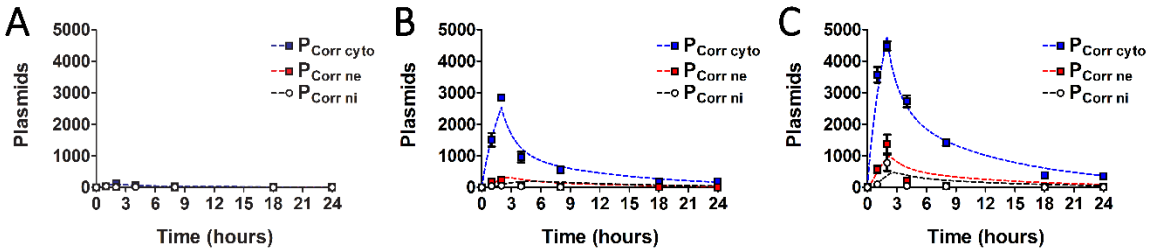

Figure 5. The experimental and first order mass action kinetic models overlaid for polymers 44 (**A**), 446 (**B**), and 447 (**C**).

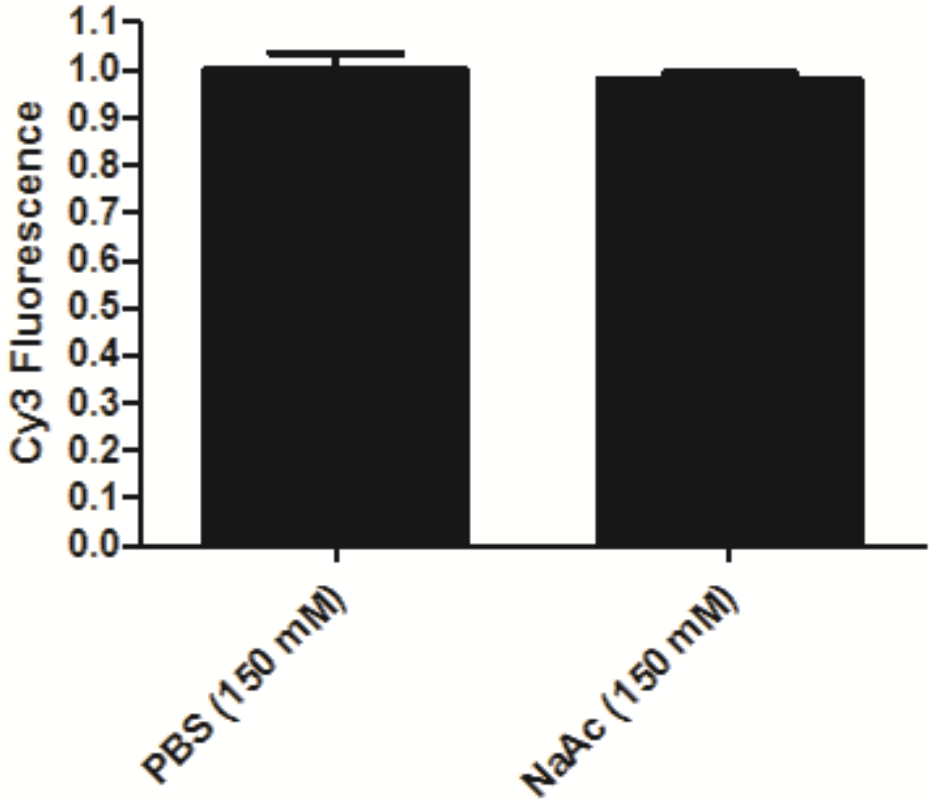

Figure S1. Normalized fluorescence of Cy3, showing no statistical difference at pH 7.4 (150 mM PBS) and 5.2 (150 mM NaAc).

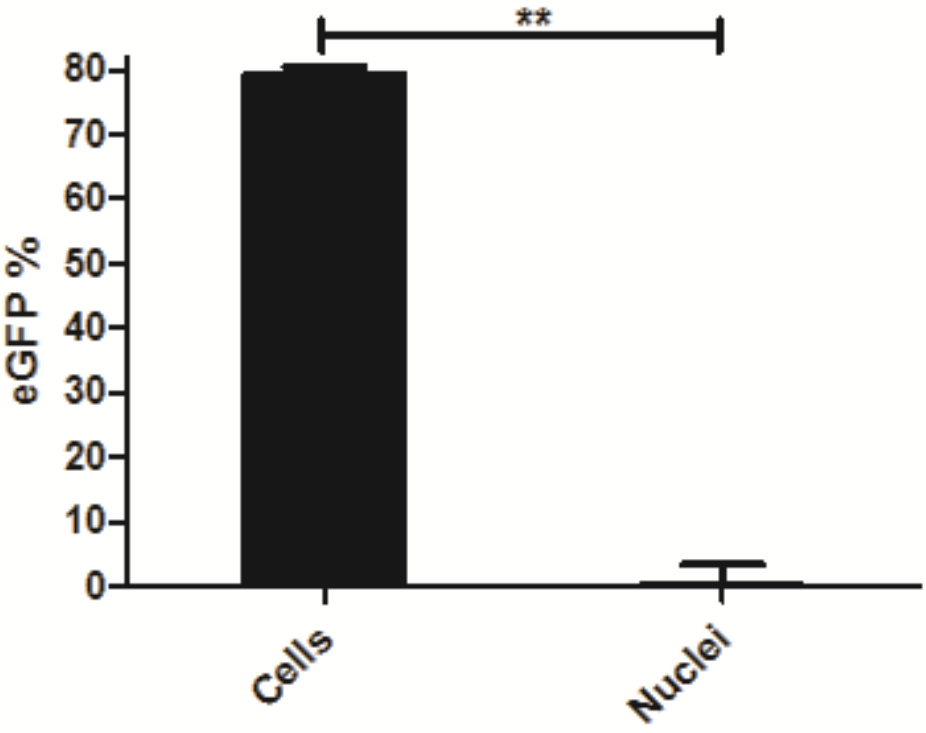

Figure S2. Purity of nuclei. Flow cytometry was used to assess the eGFP presence of eGFP-stably expressing cells and their isolated nuclei to ascertain the purity of the nuclei; the eGFP protein in adhered cytoplasm would have caused nuclei to fluoresce.

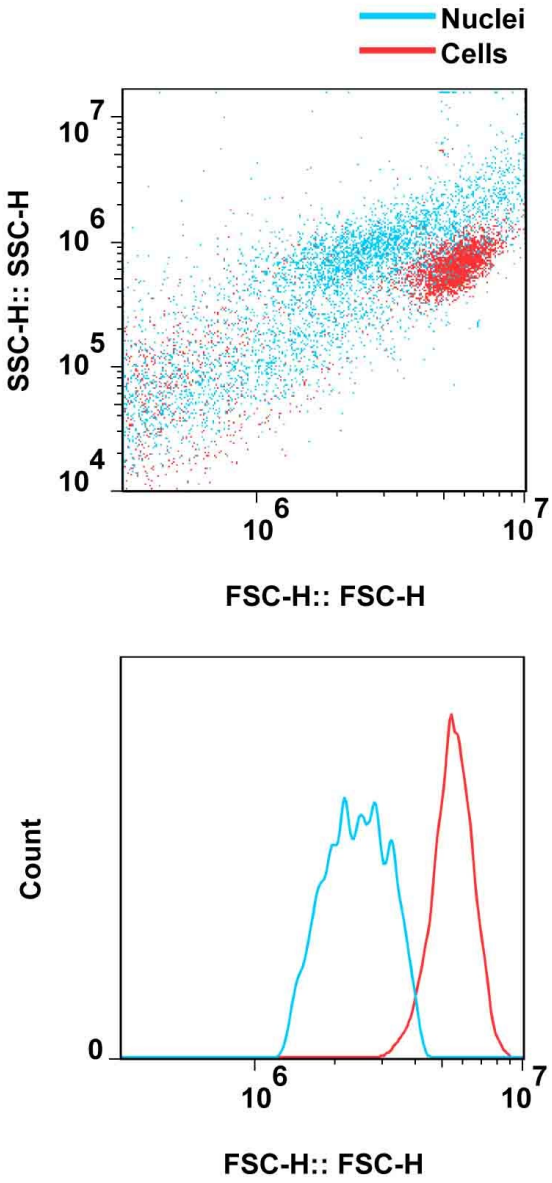

Figure S3. Top: Ungated cells and nuclei (FSC-H vs SSC-H). The nuclei had a lower FSC-H value as expected due to their smaller size. Bottom: FSC-H Histogram for gated cells and nuclei.

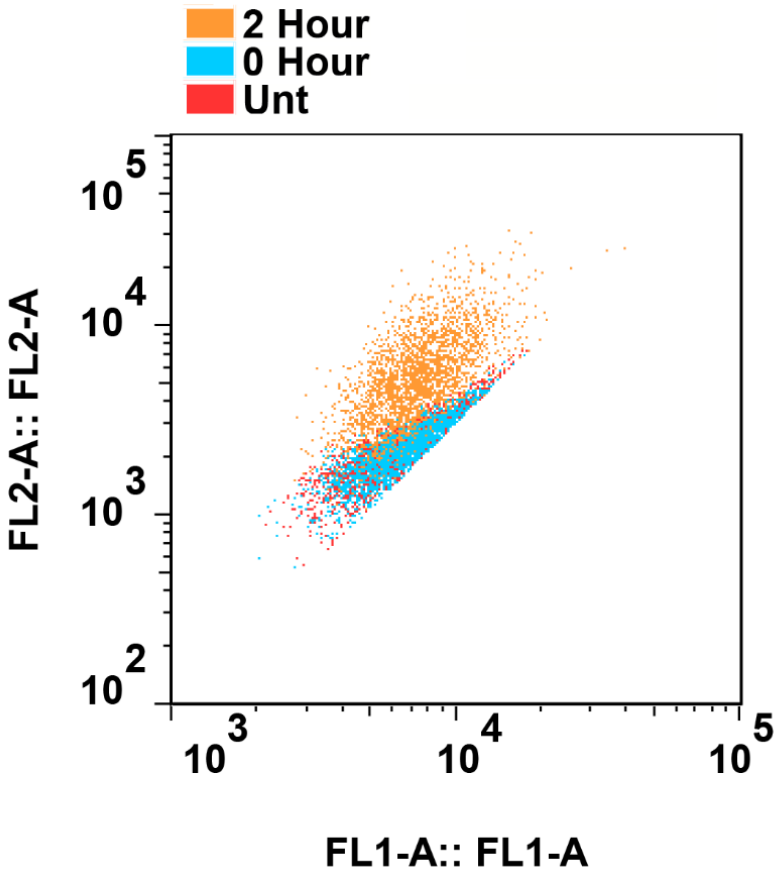

Figure S4. Cell flow cytometry data for the untreated, and the 0 and 2 hour time points. There is a great deal of population overlap for the untreated and the 0 hour time point, as would be expected.

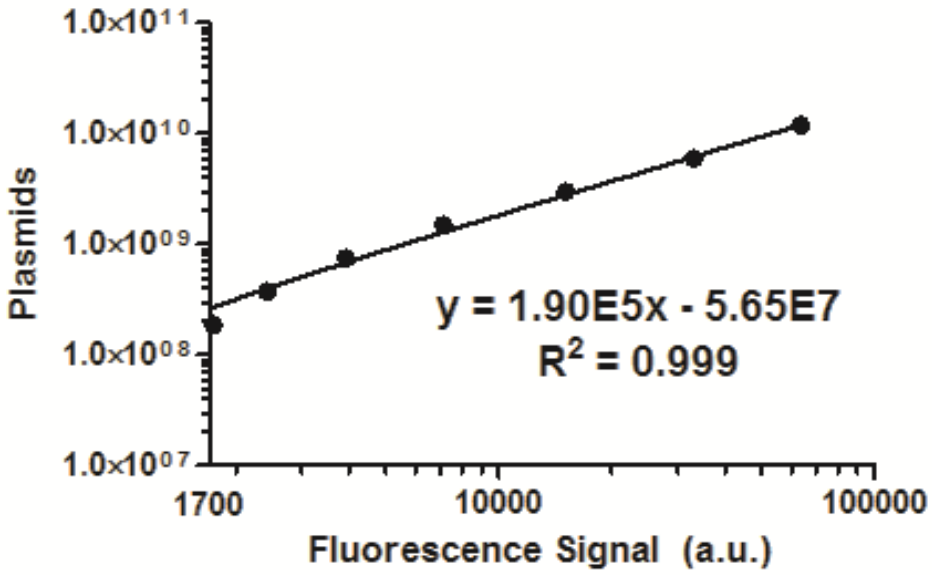

Figure S5. Calibration curve for converting bulk fluorescence on a plate reader to a plasmid number.

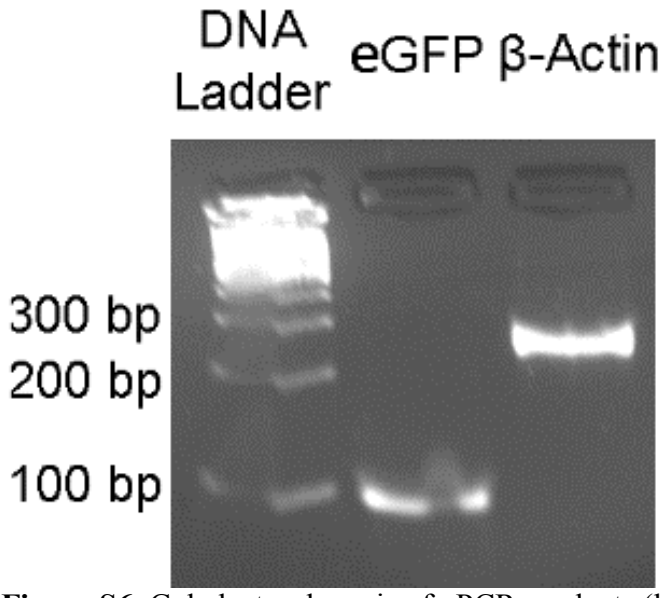

Figure S6. Gel electrophoresis of qPCR products (left, middle and rights lanes: DNA ladder, and qPCR products of eGFP and β-actin, respectively).

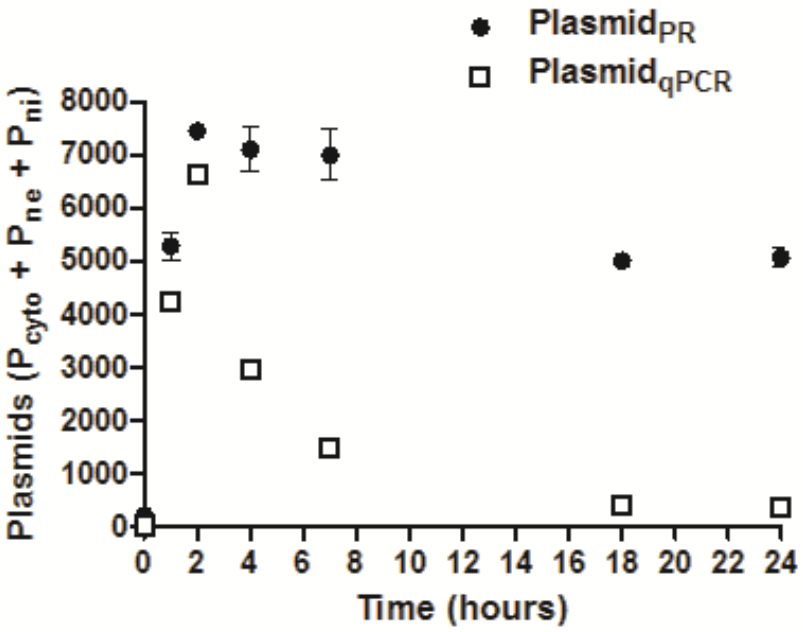

Figure S7. Plasmids in time calculated using the plate reader (Plasmid$_{PR}$) method compared to qPCR (Plasmid$_{qPCR}$).

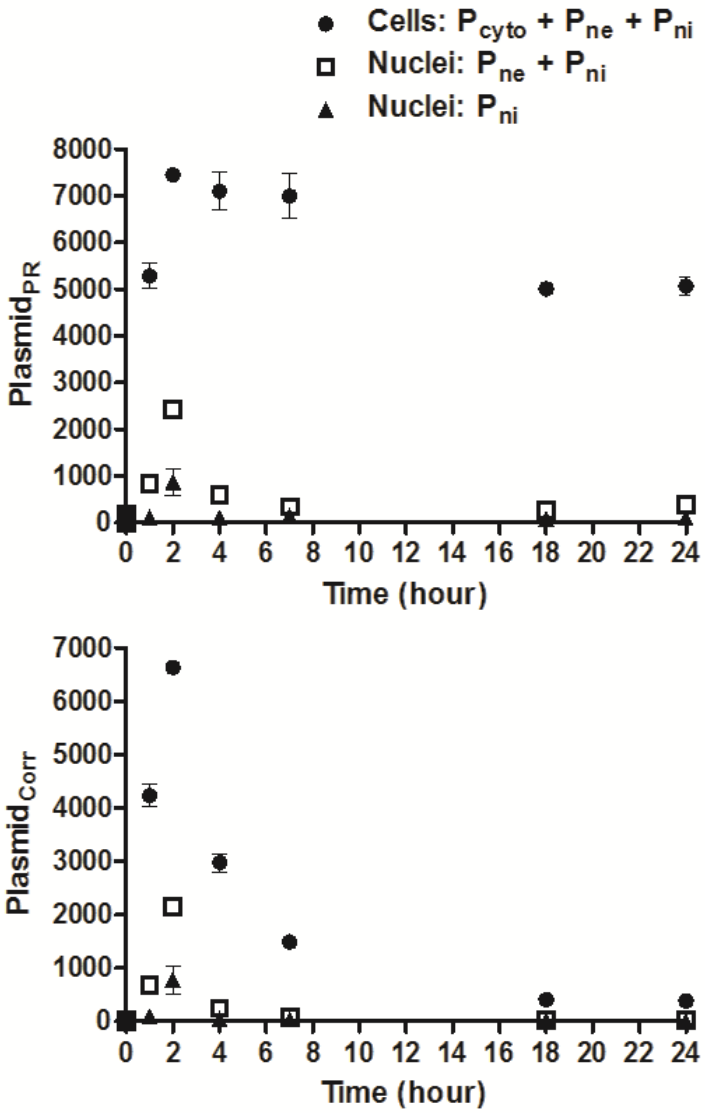

Figure S8. $Plasmid_{PR}$ (top) and $Plasmid_{Corr}$ (bottom) in time for cells and nuclei.

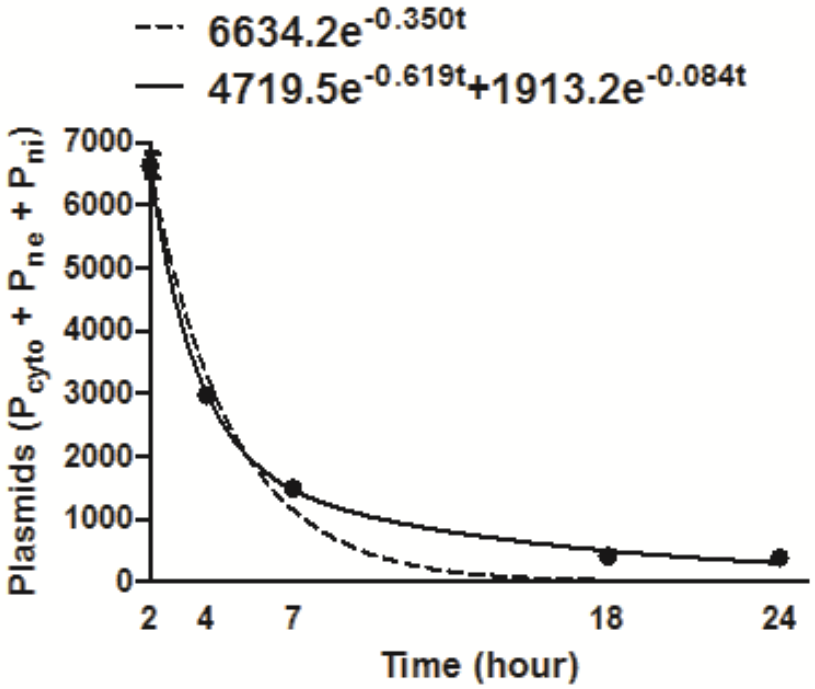

Figure S9. Plasmid$_{qPCR}$ values from 2 to 24 hours for fitting the degradation constant, k_{deg}, showing mono- (dotted line) and bi-exponential degradation fittings.

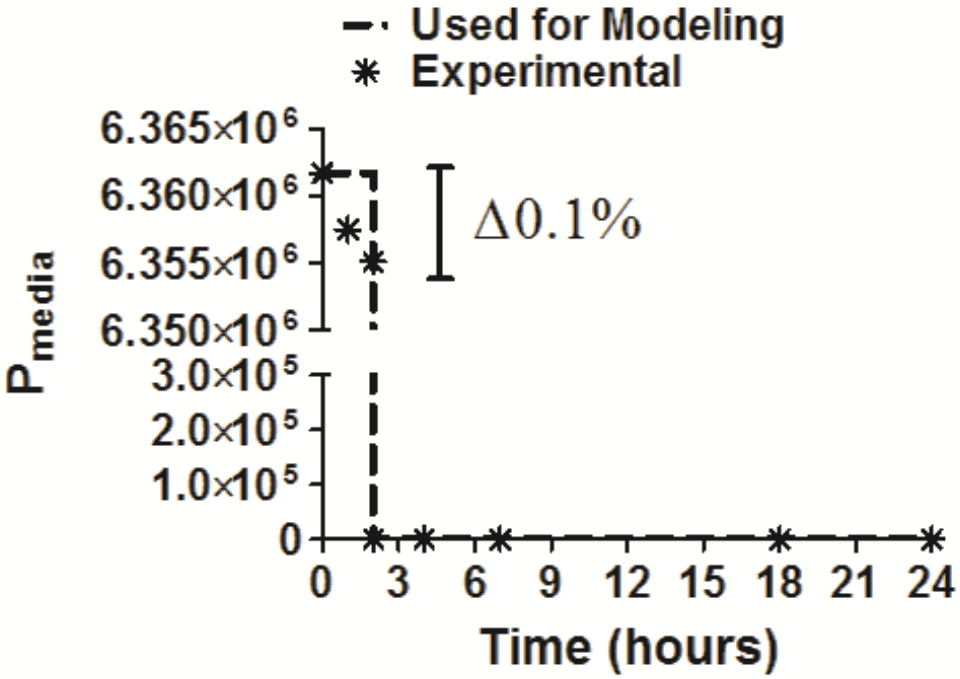

Figure S10. Available number of plasmids in the media per cell in time. The dotted line shows what was used for modeling purposes.

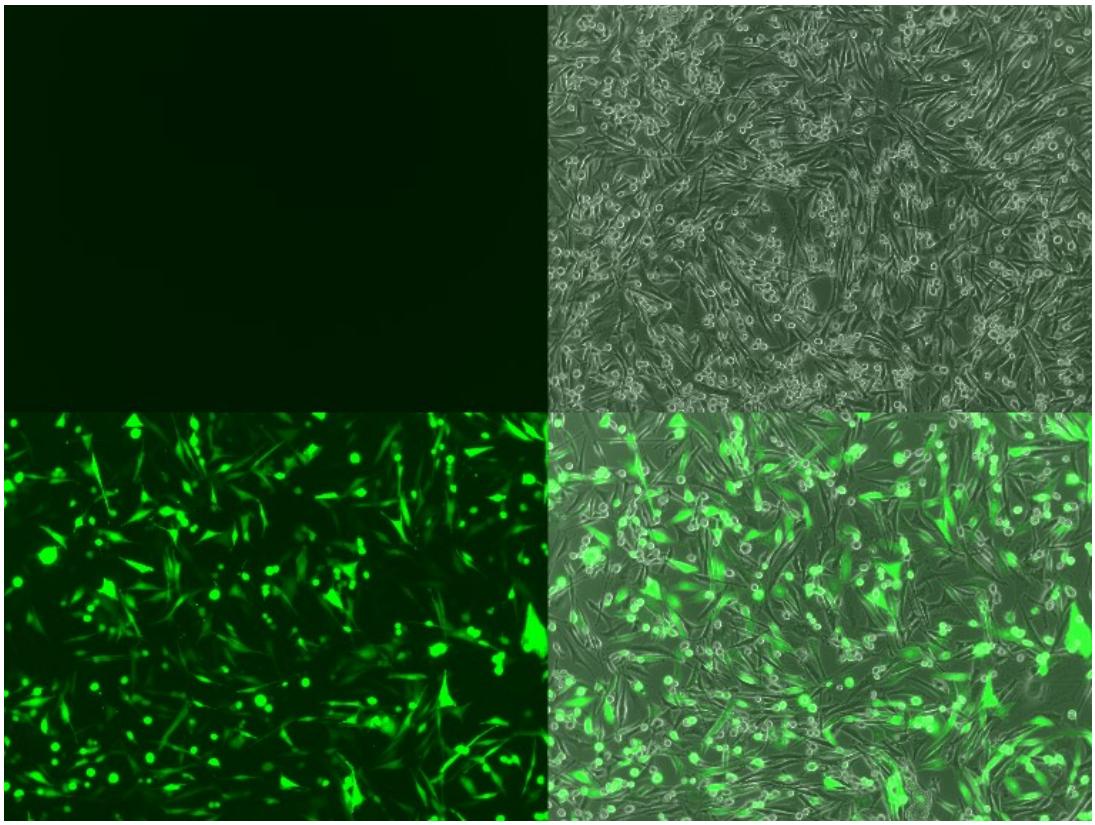

Figure S11. Fluorescence microscopy images of the eGFP channel (left) and the eGFP and brightfield channels combined (right) for untreated (top) and for 447 30 w/w (bottom) at 48 hours post transfection.

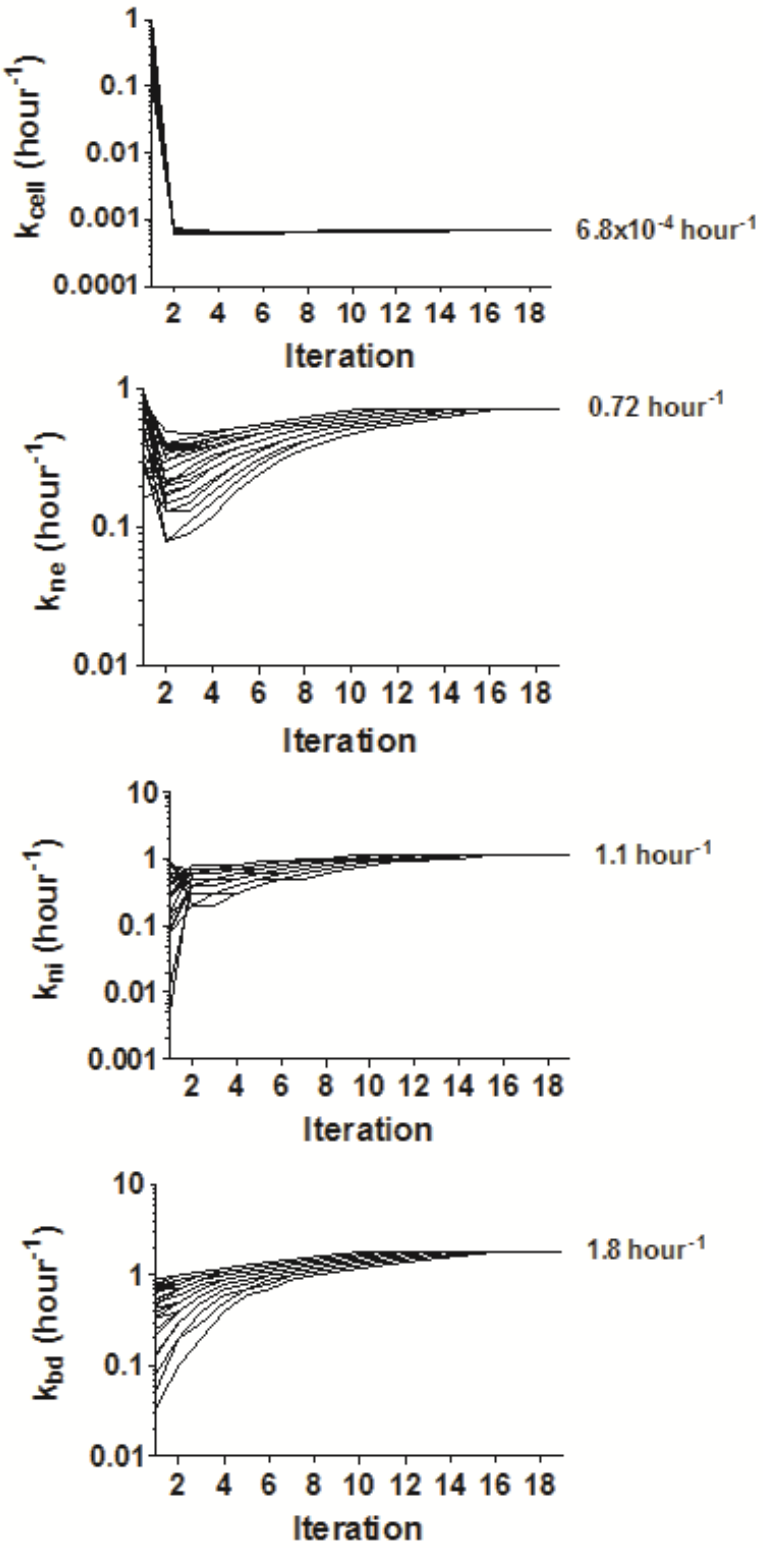

Figure S12. Convergences of k_{cell}, k_{ne}, k_{ni}, and k_{bd} through optimization iterations.

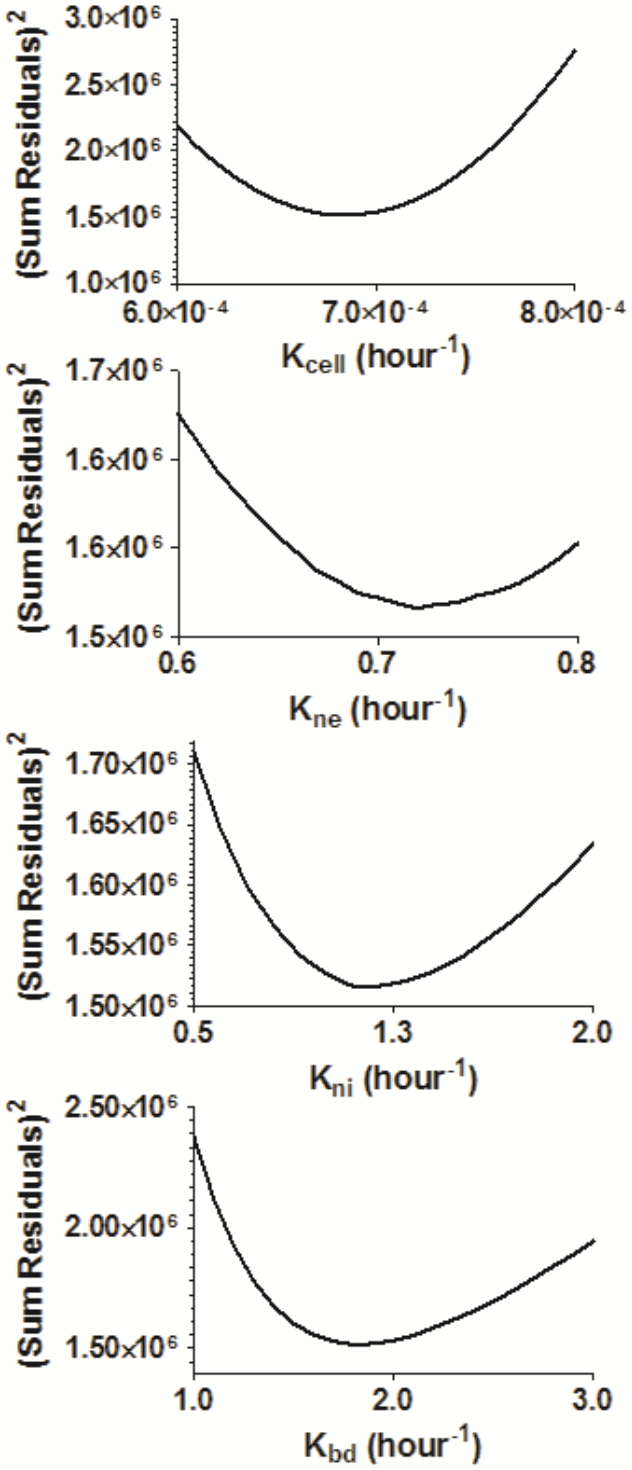

Figure S13. Error minimizations for the 19th or last iteration of optimization for k_{cell}, k_{ne}, k_{ni}, and k_{bd}.

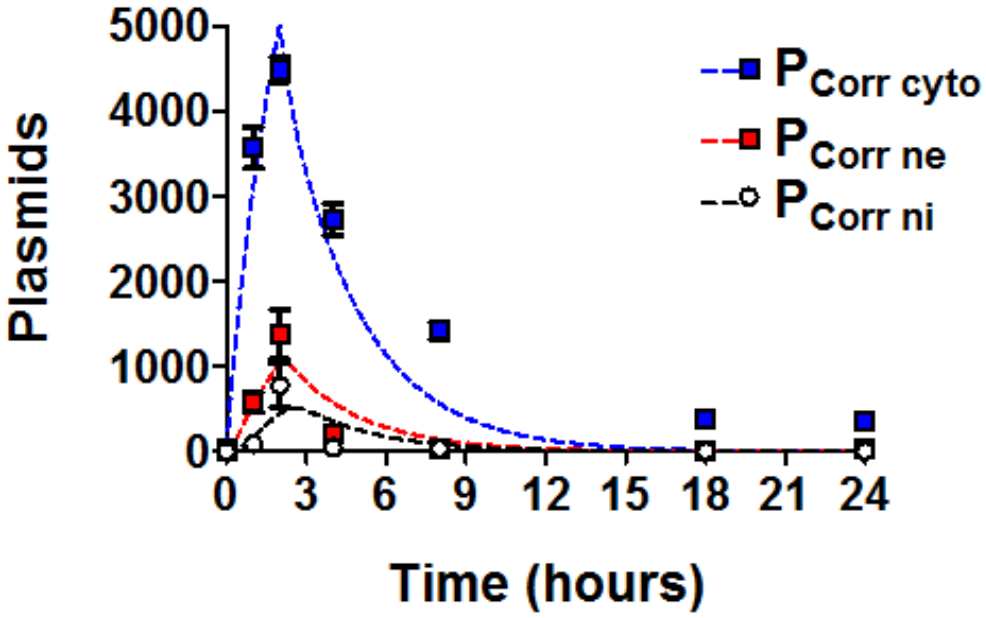

Figure S14. First order mass-action model (dotted lines; mono-exponential degradation) for the $P_{Corr\ cyto}$, $P_{Corr\ ne}$, and $P_{Corr\ ni}$ experimental data points.

6.7 Schemes

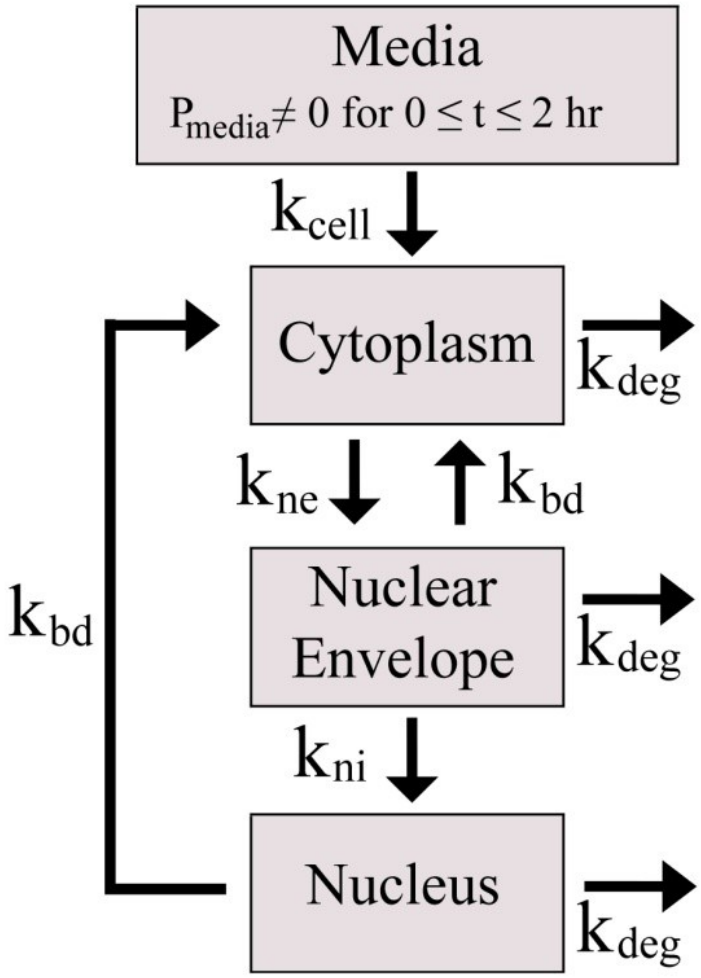

Scheme 1. Compartmental model depicting the direction of plasmid transfer.

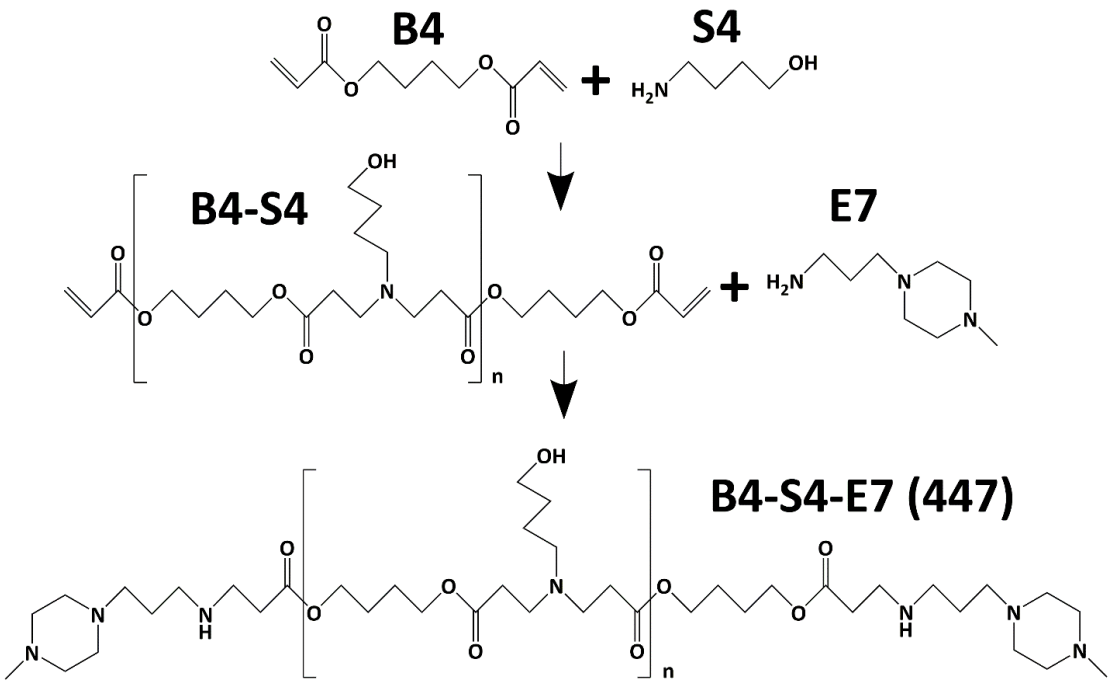

Scheme S1. Reaction scheme of polymer B4-S4-E7 (447). 1,4-butanediol diacrylate (B4) was mixed neat with 4-amino-1-butanol (S4) and endcapped with 1-(3-aminopropyl)-4-methylpiperazine (E7).

6.8 Tables

Table 1. GPC data (M_n, M_w, PDI) and rate constants for polymers 44, 446, and 447.

Polymers	M_n (Da)	M_w (Da)	PDI	k_{cell} (hr^{-1})	k_{ne} (hr^{-1})	k_{ni} (hr^{-1})	k_{bd} (hr^{-1})
44	**9590**	**12300**	**1.30**	**1.5E-5**	**1.4**	**11**	**5.8**
446	**8650**	**11700**	**1.35**	**3.2E-4**	**0.16**	**0.48**	**0.29**
447	**10600**	**11900**	**1.12**	**6.8E-4**	**0.72**	**1.1**	**1.8**

6.9 Supplemental Derivation

Derivation 1. Derivation of degradation term in the differential equations.

$$P = Ae^{k_{deg1}t} + Be^{k_{deg2}t}$$

$$\ln P = \ln(Ae^{k_{deg1}t} + Be^{k_{deg2}t})$$

$$d(\ln P) = d\left(\ln\left(Ae^{k_{deg1}t} + Be^{k_{deg2}t}\right)\right)$$

$$\frac{dP}{dt}d(\ln P) = \frac{dP}{dt}d\left(\ln\left(Ae^{k_{deg1}t} + Be^{k_{deg2}t}\right)\right)$$

$$\frac{dP}{dt}\frac{d(\ln P)}{dP} = \frac{d\left(\ln\left(Ae^{k_{deg1}t} + Be^{k_{deg2}t}\right)\right)}{dt}$$

$$\frac{dP}{dt}\frac{1}{P} = \frac{d\left(\ln\left(Ae^{k_{deg1}t} + Be^{k_{deg2}t}\right)\right)}{dt}$$

$$\frac{dP}{dt} = \frac{d\left(\ln\left(Ae^{k_{deg1}t} + Be^{k_{deg2}t}\right)\right)}{dt}P$$

$$\frac{dP}{dt} = \frac{d(\ln u)}{dt}P; u = Ae^{k_{deg1}t} + Be^{k_{deg2}t}$$

$$\frac{du}{dt} = Ak_{deg1}e^{k_{deg1}t} + Bk_{deg2}e^{k_{deg2}t}$$

$$\frac{du}{Ak_{deg1}e^{k_{deg1}t} + Bk_{deg2}e^{k_{deg2}t}} = dt$$

$$\frac{dP}{dt} = \frac{d(\ln u)}{\frac{du}{Ak_{deg1}e^{k_{deg1}t} + Bk_{deg2}e^{k_{deg2}t}}} P$$

$$\frac{dP}{dt} = \frac{d(\ln u)\left(Ak_{deg1}e^{k_{deg1}t} + Bk_{deg2}e^{k_{deg2}t}\right)}{du} P$$

$$\frac{dP}{dt} = \frac{\left(Ak_{deg1}e^{k_{deg1}t} + Bk_{deg2}e^{k_{deg2}t}\right)}{u} P$$

$$\frac{dP}{dt} = \frac{\left(Ak_{deg1}e^{k_{deg1}t} + Bk_{deg2}e^{k_{deg2}t}\right)}{Ae^{k_{deg1}t} + Be^{k_{deg2}t}} P$$

6.10 References

1. Alton EW, Middleton PG, Caplen NJ, Smith SN, et al. Non-invasive liposome-mediated gene delivery can correct the ion transport defect in cystic fibrosis mutant mice. Nat. Genet. 1993;5:135–42.

2. Banks G a, Roselli RJ, Chen R, Giorgio TD. A model for the analysis of nonviral gene therapy. Gene Ther. [Internet]. 2003;10(20):1766–75. Available from: http://www.ncbi.nlm.nih.gov/pubmed/12939643

3. Bishop CJ, Ketola T-M, Tzeng SY, Sunshine JC, et al. The effect and role of carbon atoms in poly(β-amino ester)s for DNA binding and gene delivery. J. Am. Chem. Soc. [Internet]. 2013;135(18):6951–7. Available from: http://www.ncbi.nlm.nih.gov/pubmed/23570657

4. Bishop CJ, Kim J, Green JJ. Biomolecule delivery to engineer the cellular microenvironment for regenerative medicine. Ann. Biomed. Eng. 2014;42(7):1557–72.

5. Bishop CJ, Tzeng SY, Green JJ. Degradable polymer-coated gold nanoparticles for co-delivery of DNA and siRNA. Acta Biomater. [Internet]. 2015;11:393–403. Available from: http://www.ncbi.nlm.nih.gov/pubmed/25246314

6. Boussif O, Lezoualc'h F, Zanta MA, Mergny MD, et al. A versatile vector for gene and oligonucleotide transfer into cells in culture and in vivo: polyethylenimine. Proc. Natl. Acad. Sci. U. S. A. 1995;92(August):7297–301.

7. Carapuça E, Azzoni AR, Prazeres DMF, Monteiro GA, et al. Time-course determination of plasmid content in eukaryotic and prokaryotic cells using Real-Time PCR. Mol. Biotechnol. 2007;37:120–6.

8. Cohen RN, van der Aa MAEM, Macaraeg N, Lee AP, et al. Quantification of plasmid DNA copies in the nucleus after lipoplex and polyplex transfection. J. Control. Release. 2009;135:166–74.

9. Cooper S. Cellular and Molecular Life Sciences Rethinking synchronization of mammalian cells for cell cycle analysis. 2003;60:1–8.

10. Filareto A, Parker S, Darabi R, Borges L, et al. An ex vivo gene therapy approach to treat muscular dystrophy using inducible pluripotent stem cells. Nat. Commun. [Internet]. 2013;4:1549. Available from: http://www.pubmedcentral.nih.gov/articlerender.fcgi?artid=3595133&tool=pmcentrez&rendertype=abstract

11. James MB, Giorgio TD. Nuclear-associated plasmid, but not cell-associated plasmid, is correlated with transgene expression in cultured mammalian cells. Mol. Ther. [Internet]. 2000;1(4):339–46. Available from: http://www.ncbi.nlm.nih.gov/pubmed/10933952

12. Kim J, Sunshine JC, Green JJ. Differential polymer structure tunes mechanism of cellular uptake and transfection routes of poly(β-amino ester) polyplexes in human breast cancer cells. Bioconjug. Chem. 2014;25:43–51.

13. Livak KJ, Schmittgen TD. Analysis of relative gene expression data using real-time quantitative PCR and the 2(-Delta Delta C(T)) Method. Methods [Internet]. 2001;25(4):402–8. Available from: http://www.ncbi.nlm.nih.gov/pubmed/11846609

14. Mullen PM, Lollo CP, Phan Q, Amini A, et al. Strength of conjugate binding to plasmid DNA a ¡ ects degradation rate and expression level in vivo. 2000;1523.

15. Nathwani AC, Tuddenham E, Rangarajan S, Rosales C, et al. Adenovirus-Associated Virus Vector–Mediated Gene Transfer in Hemophilia B. N. Engl. J. Med. 2011;365(25):2357–65.

16. Raucher D, Sheetz MP. Membrane Expansion Increases Endocytosis Rate during Mitosis. 1999;144(3):497–506.

17. Sacramento CB, Moraes JZ, Denapolis PMA, Han SW. Gene expression promoted by the SV40 DNA targeting sequence and the hypoxia-responsive element under normoxia and hypoxia. Brazilian J. Med. Biol. Res. 2010;43:722–7.

18. Schaffer D V, Fidelman N a, Dan N, Lauffenburger D a. Vector unpacking as a potential barrier for receptor-mediated polyplex gene delivery. Biotechnol. Bioeng. [Internet]. 2000;67(5):598–606. Available from: http://www.ncbi.nlm.nih.gov/pubmed/10649234

19. Sunshine JC, Peng DY, Green JJ. Uptake and transfection with polymeric nanoparticles are dependent on polymer end-group structure, but largely independent of nanoparticle physical and chemical properties. Mol. Pharm. 2012;9:3375–83.

20. Varga CM, Hong K, Lauffenburger D a. Quantitative analysis of synthetic gene delivery vector design properties. Mol. Ther. [Internet]. 2001;4(5):438–46. Available from: http://www.ncbi.nlm.nih.gov/pubmed/11708880

21. Varga CM, Tedford NC, Thomas M, Klibanov a M, et al. Quantitative comparison of polyethylenimine formulations and adenoviral vectors in terms of intracellular

gene delivery processes. Gene Ther. [Internet]. 2005;12(13):1023–32. Available from: http://www.ncbi.nlm.nih.gov/pubmed/15815703

22. Zhou J, Yockman JW, Kim SW, Kern SE. Intracellular kinetics of non-viral gene delivery using polyethylenimine carriers. Pharm. Res. 2007;24:1079–87.

7 Chapter 7: Poly(β-amino ester) Monomer and Polymer Structure Function Relationships Elucidated Via Principal Component Analysis

7.1 Introduction

Viral methods for gene therapy have been actively investigated for many years in more than 2,000 world-wide clinical trials, but due in part to reported toxicological and immunological concerns, have not been approved for use in the United States.[1] Polymeric vectors are an alternative for gene delivery worth investigating as they can be physico-chemically modified to enhance function and minimize toxicity. They also benefit by being easier and less expensive to manufacture than viruses and, unlike viruses, do not have a restriction to their nucleic acid cargo capacity. While high-throughput screening methods have recently been adapted to allow for evaluation of biomaterial libraries, it is difficult to use this data to isolate key structural drivers of biological activity or to predict characteristics of untested structures.[2,3] Understanding fundamental structure-function relationships for gene delivery polymers would allow for improved rational engineering and enhanced chemical delivery systems.

Principal Component Analysis (PCA) is a powerful tool for reducing complex data sets that contain many variables with unknown correlations. The data set is reduced into orthogonal, linearly uncorrelated variables, termed principal components (PC). PCs are

useful in helping to determine underlying relationships between variables.[4,5] While to our knowledge these methods have not been previously used to elucidate how polymer structure can affect biological function including gene delivery efficacy, we hypothesized that we would find trends based on our recent work on evaluating how polymer structure can tune DNA binding and gene delivery.[6] We chose hydrolytically degradable poly(β-amino ester)s (PBAE) to study as a PBAE polymer library can be readily synthesized by semi-high throughput methods and we have previously shown utility of these polymers for both *in vitro* and *in vivo* gene therapy applications.[7,8] We report the use of PCA to aid our understanding of the physico-chemical properties of polymers that drive transfection, uptake, and viability in human cells.

7.2 Methods, Results, and Discussion (Communication Format)

7.2.1 Polymer Library

A PBAE library consisting of 75 polymers with varying backbone (B), sidechain (S), or endcap (E) were synthesized as previously reported (**Scheme 1**).[9] In brief, the base polymer was synthesized by mixing B and S monomers (**Scheme 1**) neat in 1.05:1, 1.1:1, or 1.2:1 B:S monomeric ratios and the reaction was allowed to stir for 24 hours at 90˚C in the dark; after which the B-S base polymer solvated in anhydrousn dimethyl sulfoxide (DMSO) to 167 mg/mL. 480 μL of the 167 mg/mL base polymer was then endcapped in DMSO for 1 hr (no shaking) using approximately a 10:1 E (0.5 M solution in DMSO;

320 μL) to B-S ratio (Scheme 1).[9] The 100 mg/mL endcapped polymer was then stored at -20˚C until use.[9]

The B to S monomeric ratio (B:S) dictates the molecular weight of the polymer, with molecular weight increasing as the ratio approaches unity. The numbers associated with the B and the S monomer names are the number of carbons between the backbone's acrylate groups and the sidechain's amine and hydroxyl groups, respectively (**Scheme 1**). "B+S" refers to the sum of these numbers for an individual polymer, or the number of carbons in its repeating unit. As the carbons in the backbone and sidechain increase, the overall hydrophobicity of the polymer increases. The numbers associated with the "E" term are randomly assigned and are not indicative of endcap structure.

The polymers were characterized using gel permeation chromatography (GPC). In brief, the polymers were solvated in 94% tetrahydrofuran (THF), 5% DMSO, 1% piperidine with a few 100 mg of butylated hydroxytoluene.[9] The solvated polymer was then filtered using a 0.2 μm polytetrafluoroethylene filter and compared against polystyrene standards using GPC (Waters, Milford, MA) to obtain the number- and weight-average molecular weights (Mn and Mw), the polydispersity indices (PDI) and the degree of polymerization (DP).[9]

7.2.2 Physicochemical Properties

Other physical parameters were calculated with the aid of ChemDraw, the Joback fragmentation method, and the Crippen's fragmentation method. These include boiling point (BP); melting point (MP); critical volume (CV), which is the volume of 1 mole at the critical temperature and pressure; Gibb's free energy (GFE), which is the

thermodynamic potential to perform work; LogP, the partition-coefficient between two immiscible phases at equilibrium which is proportional to hydrophobicity; molar refractivity (MR), which is a measurement of the total polarizability of 1 mole; the heat of formation (HtF), which is the change in enthalpy of 1 mole from the formation the elemental constituents; and the topological polar surface area (tPSA), which is the total area of all polar atoms (predominantly oxygen and oitrogen) including their affixed hydrogen atoms. Properties associated with the polymer repeating unit are differentiated from those of the full polymer, by the presence of an asterisk in their name (i.e., LogP* vs. LogP). *In vitro* studies were performed on primary human glioblastoma cells using this described cationic PBAE library as previously reported (**Supplementary Methods**).[9]

7.2.3 Transfection and Viability

In vitro studies were performed on primary human glioblastoma multiforme cells using the library set and previously reported [9]. In brief, the primary human glioblastoma cells were seeded in 96-well tissue cultured plates at 15,000 cells/well (100 μL) and incubated overnight at 37˚C and 5% CO_2 for 24 hours.[9] eGFP-N1 plasmid DNA was diluted to 0.06 mg/mL in sodium acetate (NaAc) and mixed in a 1:1 vol:vol ratio with each of the polymers at 3.6 mg/mL in NaAc (diluted from 100 mg/mL); thus the polymer to DNA mass ratio (w/w) was 60.[9] The solution was thoroughly triturated and allowed to ionically complex for 10 minutes at room temperature to self-assemble into nanoparticles.[9] The total incubation time for the polyplexes with the cells (final dose of 5 μg/mL) was 2 hours.[9] To assess uptake Cy™3 (Mirus Bio LLC; MIR 7020)-conjugated

plasmid DNA was used and directly assessed via the flow cytometer after the 2 hour incubation time period.[9] A viability assay (Cell Titer 96®AQueous One) was used at 24 hours to assess cell viability. Transfection efficacy was assessed at 48 hours using flow cytometry.[9]

7.2.4 Principal Component Analysis

PCA was carried out using the standard "princomp" function in MatLab to calculate the coefficients, scores, and variances. All included variables were first scaled from 0 to 1 for normalization and included the following 27 parameters: B, B:S, B+S, BP, BP*, CV, CV*, DP, GFE, GFE*, HtF, HtF*, LogP, LogP*, Mn, MP, MP*, MR, MR*, Mw, MW*, PDI, S, tPSA, transfection efficacy, cell uptake, and cell viability. 24 of the 27 are physico-chemical variables determined by the structure of the polymers; the remaining 3 are cell-based functional variables determined experimentally. As a control, a random variable, the "E" number assigned to each endcap but not meaningful when normalized from 0 to 1, was incorporated into the set of parameters.

7.2.5 Variance Explained

The variance of a particular PC divided by the sum of all of the PC variances multiplied by 100 is the percentage that a particular PC recapitulates the data set. Since there are 27 variables, there is a potential maximum of 27 PCs. The first and second PCs were responsible for 58.2% and 24.3% of the variance in the data set, respectively (**Figure 1**, top). Cumulatively, the first 5 PCs capture 96.6% of the variance in the data

set. Although there are 27 variables, it is striking that 5 PCs can cover almost all the variance in the data and just the first two PCs cover 83% of this variance, significantly decreasing the complexity of this multivariate data.

7.2.6 Variable Contribution to Principal Components

We can rank the variables by the degree to which they contribute positively or negatively to each PC using their associated coefficients. The top four variables contributing to each of the first five PCs are listed above the variances of each PC (**Figure 1**; top) and are indicated in parentheses as "(-)" if it is a negative contribution. **Table S1** contains a full list of the 27 variables ranked for the first five PCs.

7.2.7 Correlative Relationships Between Variables

The loading plot, generated using the first and second coefficients associated with each variable (**Figure 1**; bottom), reveals the correlative relationships between the variables. Variables within the same quadrant of the loading plot indicate that they are positively correlated. B, transfection, uptake, Mn, Mw, PDI, MR, CV and LogP are all positively correlated in quadrant IV. The color in the figure is utilized to enhance contrast between lines. Hydrophobicity (LogP) positively correlating with transfection efficacy has been previously observed[3] as well, corroborating the findings. As expected, increased cellular uptake correlated strongly to higher transfection efficacy.

Variables in opposite quadrants indicate that they are inversely correlated. As such, viability is negatively correlated with the variables in quadrant IV. For example, polymers that transfect strongly generally correlate to also slightly lowering cell viability.

As an example of how PCA reduces the complexity of multiple variables and assembles correlated variables together, the B:S ratio as well as the molecular weights, Mn and Mw, and DP all lie along the PC2 axis, but with B:S in an opposing direction as it is inversely correlated to other parameters. Variables in adjacent quadrants are positively correlated with respect to one PC but not the other. **Figure S1** shows the other variables (PDI, Mn, Mw, MR, CV), which were also positively correlated to transfection and uptake which are difficult to differentiate visibly. As expected, the random variable of the normalized "E" number, when included as a variable for analysis (totaling 28 variables), was found to be at the origin of the loading plot (0.0041, -0.0238). Coefficients of approximately zero were expected for E because the normalized "E" number is not related to polymer structure and therefore should not make a meaningful contribution to the PCs.

7.2.8 Assessing which and to what Degree Physicochemical Properties Drive Transfection, Uptake, and Viability

Based on the loading plot, variables can be ranked according to the degree to which they correlate to a reference variable using Acos(Θ); where A is the magnitude of the vectors of the variables being compared to the reference and Θ is the angle between the variables and the reference. Variables corresponding to a positive Acos(Θ) value are positively correlated with the reference variable of interest; whereas negative Acos(Θ) values are negatively correlated. Thus, the most positive and the most negative variables drive the reference variable. The Acos(Θ) values near neutral contribute relatively little to the reference variable. **Table 1** shows the reference variables of interest, namely, transfection, uptake and viability, and the remaining 26 variables ranked accordingly. As expected, when the random variable E was included in the data set, totaling 28 variables,

the Acos(Θ) values for transfection, uptake, and viability were 0.02, 0.01, and -0.01, respectively, which were the most neutral values observed. This validates that PCA successfully identified the normalized "E" number a random variable and not a chemical parameter for analysis.

The top 4 positively correlated physico-chemical variables driving the biological parameters, transfection, uptake and viability were: B, uptake, LogP*, and B+S; LogP*, B+S, GFE*, and MW*; HtF*, B:S, HtF, and GFE, respectively. Whereas the top 4 negatively correlated variables driving transfection, uptake and viability were: B:S, HtF*, HtF, and GFE; HtF*, B:S, HtF, and GFE; LogP*, MR*, CV*, and MP*, respectively.

Because uptake and transfection are highly positively correlated, it would be expected that many of the variables would rank similarly, which is what was observed. In contrast, because viability is negatively correlated with transfection and uptake, it would be expected that the ranking for the variables would be reversed, which was also observed. For example, LogP* and B+S were highly positively correlated with transfection and uptake but were negatively correlated with viability. This data quantitatively demonstrates how the same factor can both positively and negatively drive biological functional outcomes.

7.2.9 Scores Plot

Because there are 27 variables being analyzed there are 27 scores associated with each of the 75 polymer samples within the PBAE library. The scores plot (**Figure S2**) depicts all of the 1st and 2nd scores of the 75 polymers in the PBAE library associated with the 1st and 2nd PCs. The Mn and Mw are listed in kDa to the right of the polymer

names (i.e., 447, 8.8, 28.3), respectively. According to the ranking in **Table S1**, B+S contributes positively to PC1 and Mn and Mw contribute negatively to PC2 which is observed in the scores plot; as PC1 increases, B+S increases and as PC2 increases, the molecular weight generally decreases.

The PC1 and PC2 scores for the 75 polymers in **Figure S2** were plotted against transfection efficacy in the 3rd dimension in **Figure 2A**. A supplemental auto-rotating video created using MatLab of **Figure 2A** can also be found online. The color in **Figure 2** corresponds to the level of transfection with red being the highest and yellow the lowest. **Figure 2A** demonstrates that the 75 polymers self-cluster into three groups along 3 regions of PC1. These are named as B, C, and D in **Figure 2A** and these three groups are plotted in 2-dimensions vs. PC2 in **Figures 2B**, **2C**, and **2D**, respectively. Surprisingly, the self-clustered regions B, C, and D correspond to polymers that have B+S values equal to precisely 7, 8, and 9, respectively. Intriguingly, the number of carbons within a polymer's repeat unit was found to group the polymer's behavior more than any other parameter. Furthermore, this B+S grouping dictated the role of PC2 on transfection efficacy among the polymers within the group. For example, polymers in group B (B+S=7) had generally very low transfection efficacy, with transfection efficacy increasing to ~half the maximum for more negative PC2 values (indicating a higher molecular weight, higher degree of polymerization, and a smaller B:S ratio closer to unity). For polymers in group C (B+S=8), transfection is higher, reaching the maximum. Like with the B+S=7 group, lower values of PC2 (and higher MW) increased transfection efficacy. In both of these groups, a lower value of PC2 could increase transfection efficacy by larger than an order of magnitude. In contrast, group D (B+S=9) transfection

was uniformly high near the maximum and PC2 did not influence transfection efficacy. Thus these two principal components, PC1 (hydrophobicity, B+S) and PC2 (molecular weight), were found to cluster and elucidate the polymer structures and their biological efficacy in new ways. In general, as B+S increased from 7 to 9, a greater portion of polymers had higher transfection levels. The optimal transfections were associated with PC2 values of -1, -1, and 0 for groups B, C, and D, respectively.

Previous research in our lab[6] has demonstrated that transfection levels can be biphasic with respect to binding constants and also that binding constants increase with increasing molecular weight. Our results in the current PCA study are consistent with these past results as the highest transfection efficacy among all polymers occurs at intermediate values of PC2 (between -1 and 0).

7.3 Conclusions

We have been able to successfully demonstrate that PCA is a useful tool for helping elucidate how physico-chemical properties of polymers drive transfection, uptake, and viability in human primary glioblastoma cells. By determining the principal components, one can design next generation materials by tuning the chemical parameters that matter most (such as hydrophobicity and molecular weight) in the particular ranges determined to lead to the desired biological functional outcomes (such as high transfection). This type of analysis could potentially be used across a wider type of polymeric vectors[10] (i.e., poly(l-lysine), polyethyleneimine, chitosan, dendrimers, and β-cyclodextrin-containing vectors) and various types of cargo (i.e., siRNA/miRNA, shRNA, mRNA). Such a large

scale analysis would undoubtedly further elucidate additional structure-function relationships allowing improved polymer and delivery system design.

7.4 Figures

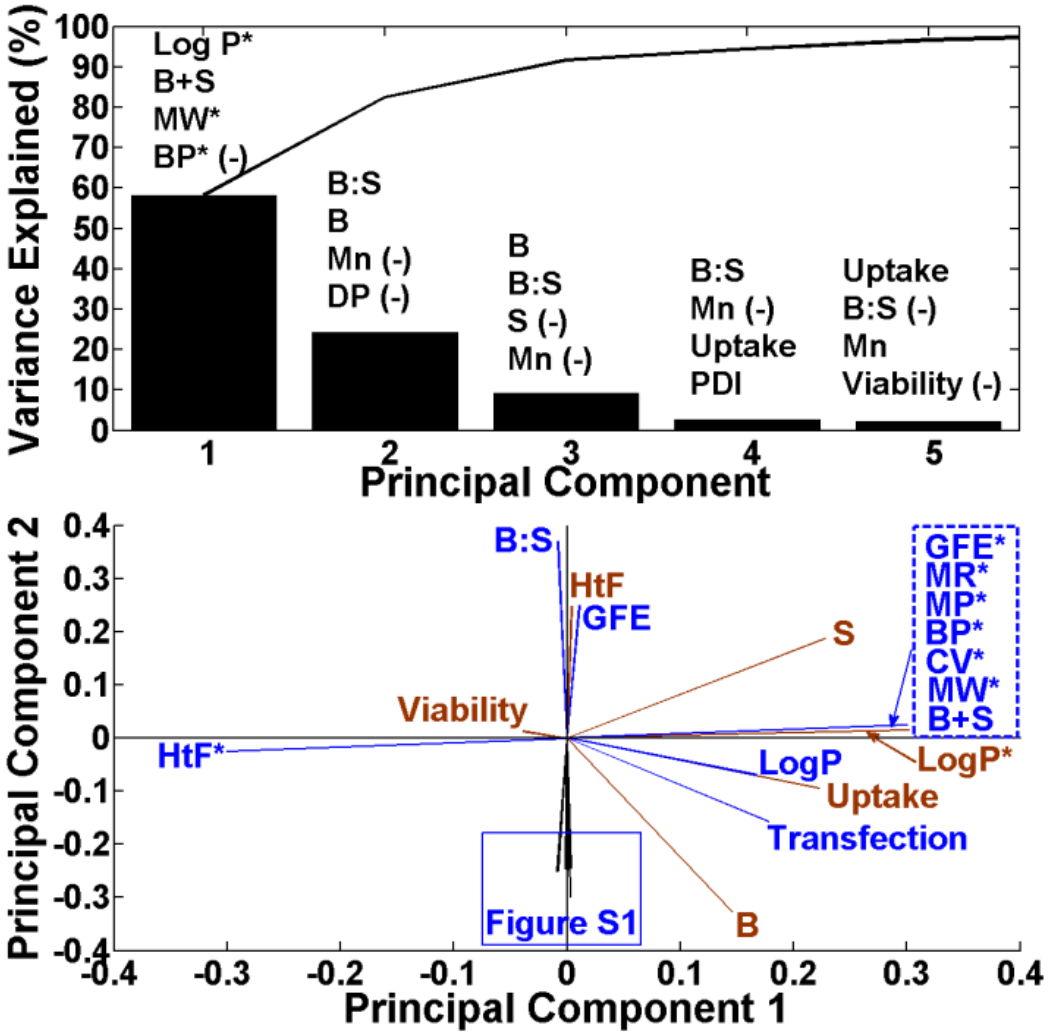

Figure 1. Top: the variances are explained for the first 5 PCs. The top 4 variables of the 27 are ranked by the degree to which they contribute to the PCs according to their associated coefficients and listed above the variances. The "(-)" indicates a negative contribution; Bottom: The loading plot of all of the variables showing relative correlations.

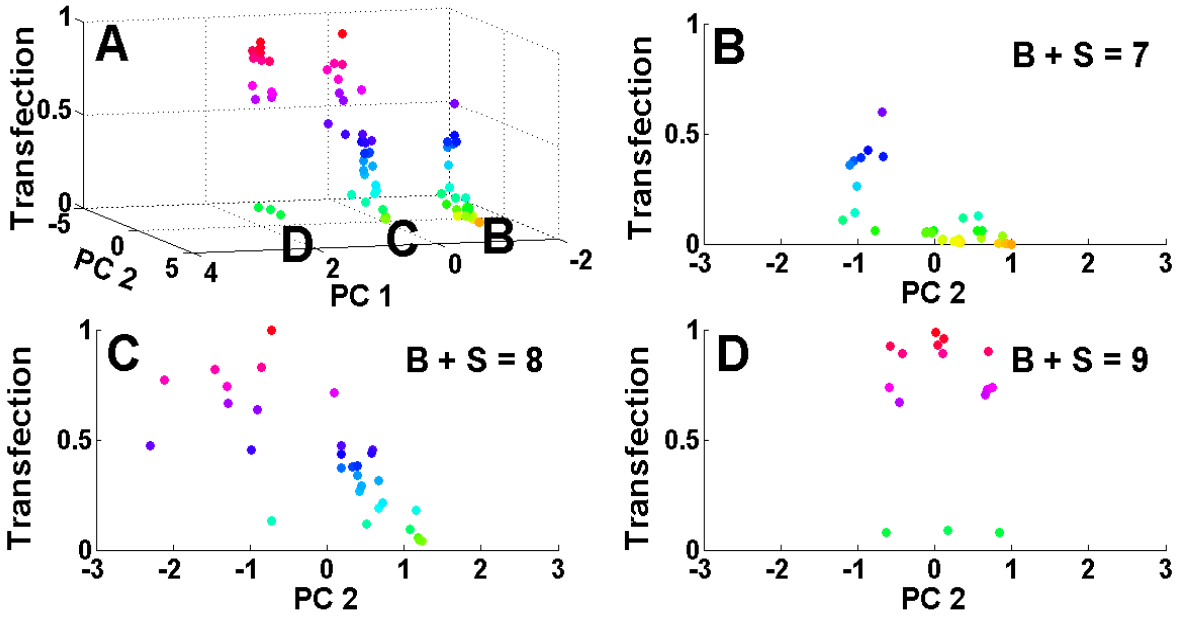

Figure 2: **A**: The scores plot versus transfection efficacy with red being the highest level of transfection; **B**: region B of 3A with a B+S (sum of carbons in backbone and sidechain) value of 7; **C**: region C of 3A with a B+S value of 8; **D**: region D of 3A with a B+S value of 9.

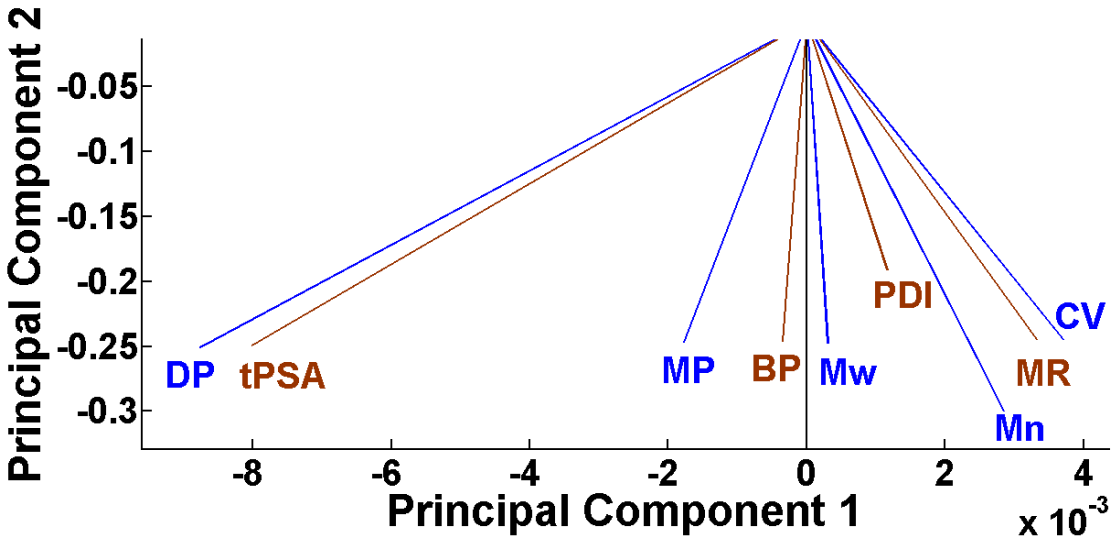

Figure S1. The loading plot of the variables in the boxed region of **Figure 1** showing other variables (Mw, PDI, Mn, MR, CV) which are positively correlated to transfection and uptake (quadrant IV) which are difficult to visibly differentiate.

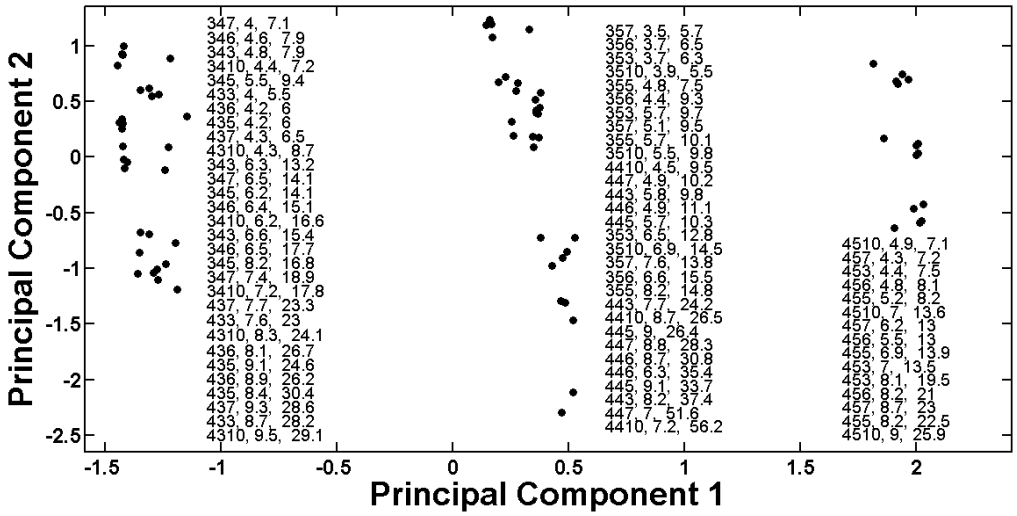

Figure S2. The scores plot of all polymers used for PCA. The numbers listed are the polymer type xyz (Bx-Sy-Ez), Mn (kDa), and Mw (kDa), respectively. The 3 lists are positioned near their respective groups and the list order is the same as the data points with respect to principal component 2.

7.5 Schemes

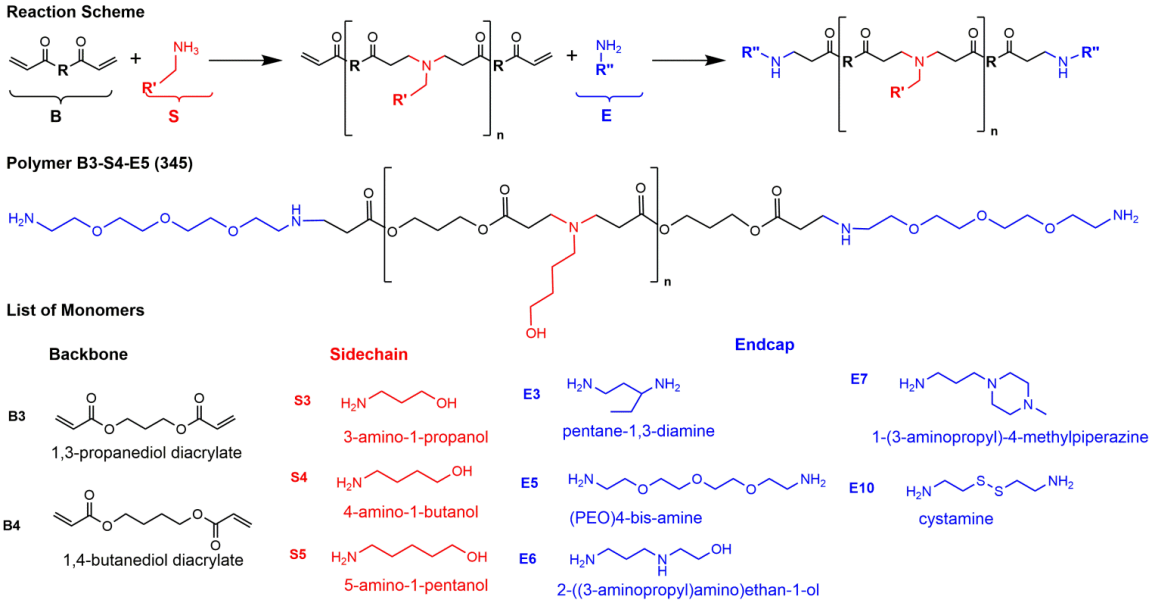

Scheme 1. Top: the general reaction scheme of PBAEs with a representative polymer, B3-S4-E5; bottom: lists of backbone (B), sidechain (S), and endcap (E) monomers used in the PBAE library.

7.6 Tables

Table 1. Ranking of variables for transfection, uptake and viability. The value of Acos(Θ) indicates the strength of the correlation.

	Transfection		Uptake		Viability	
	Variable	A(cosθ)	Variable	A(cosθ)	Variable	A(cosθ)
1	B	0.33	LogP*	0.27	HtF*	0.28
2	Uptake	0.23	B+S	0.27	B:S	0.13
3	LogP*	0.22	GFE*	0.27	HtF	0.08
4	B+S	0.21	MW*	0.27	GFE	0.07
5	GFE*	0.21	BP*	0.27	PDI	-0.06
6	MW*	0.21	MP*	0.27	DP	-0.07
7	BP*	0.21	CV*	0.27	tPSA	-0.07
8	MP*	0.21	MR*	0.27	MP	-0.08
9	CV*	0.21	B	0.26	BP	-0.08
10	MR*	0.21	Transfection	0.23	Mw	-0.08
11	Mn	0.20	LogP	0.18	MR	-0.08
12	LogP	0.17	S	0.14	CV	-0.08
13	CV	0.16	Mn	0.12	Mn	-0.10
14	MR	0.16	CV	0.10	S	-0.15
15	Mw	0.16	MR	0.10	LogP	-0.18
16	BP	0.16	Mw	0.10	Transfection	-0.22
17	MP	0.16	BP	0.10	Uptake	-0.24
18	DP	0.16	MP	0.10	B	-0.25
19	tPSA	0.16	tPSA	0.09	B+S	-0.28
20	PDI	0.13	DP	0.09	GFE*	-0.28
21	S	0.05	PDI	0.08	MW*	-0.28
22	Viability	-0.04	Viability	-0.04	BP*	-0.28
23	GFE	-0.16	GFE	-0.09	MP*	-0.28
24	HtF	-0.16	HtF	-0.09	CV*	-0.28
25	HtF*	-0.21	B:S	-0.15	MR*	-0.28
26	B:S	-0.25	HtF*	-0.27	LogP*	-0.28

Table S1. The ranking of all variables according to the degree to which they contribute to each of the first 5 PCs. The notation '(-)' indicates the contribution is negative.

	Principal Component 1	Principal Component 2	Principal Component 3	Principal Component 4	Principal Component 5
1	LogP*	B:S	B	B:S	Uptake
2	B+S	B	B:S	Mn (-)	B:S (-)
3	MW*	Mn (-)	S (-)	Uptake	Mn
4	BP* (-)	DP (-)	Mn (-)	PDI	Viability (-)
5	MP* (-)	GFE	Uptake	B (-)	PDI (-)
6	CV*	tPSA (-)	MR (-)	Transfection (-)	Transfection (-)
7	GFE*	HtF	MP (-)	LogP	HtF
8	MR*	Mw (-)	BP (-)	MR	CV (-)
9	HtF* (-)	MP (-)	CV (-)	CV (-)	GFE
10	S	BP (-)	Mw (-)	BP (-)	MR (-)
11	Uptake	CV (-)	HtF	MP (-)	tPSA (-)
12	Transfection	MR	tPSA (-)	Mw	BP (-)
13	LogP	PDI (-)	GFE	HtF (-)	MP (-)
14	B	S	DP (-)	tPSA	Mw (-)
15	Viability	Transfection (-)	LogP (-)	GFE (-)	DP (-)
16	GFE	Uptake (-)	Transfection	DP	LogP* (-)
17	DP (-)	LogP (-)	PDI (-)	S	HtF*
18	tPSA (-)	MW*	Viability (-)	Viability	MR* (-)
19	B:S (-)	BP*	GFE* (-)	HtF*	MW* (-)
20	HtF	MP*	MP* (-)	MR* (-)	BP* (-)
21	CV	CV*	B+S (-)	B+S (-)	MP* (-)
22	MR	MR* (-)	MW* (-)	MW* (-)	CV* (-)
23	Mn	B+S	BP* (-)	BP*	B+S (-)
24	MP	GFE*	CV* (-)	CV*	GFE* (-)
25	PDI	HtF* (-)	MR* (-)	MP*	LogP (-)
26	BP	LogP*	HtF*	GFE* (-)	B (-)
27	Mw	Viability	LogP* (-)	LogP* (-)	S (-)

7.7 References

(1) Gene Therapy Clinical Trials Worldwide. http://www.abedia.com/wiley (accessed Jan 2015).
(2) Anderson, D. G.; Lynn, D. M.; Langer, R. *Angewandte Chemie-International Edition* **2003**, *42*, 3153-3158.
(3) Sunshine, J. C.; Akanda, M. I.; Li, D.; Kozielski, K. L.; Green, J. J. *Biomacromolecules* **2011**, *12*, 3592-3600.
(4) Martinerie, J.; Adam, C.; Le Van Quyen, M.; Baulac, M.; Clemenceau, S.; Renault, B.; Varela, F. J. *Nat. Med.* **1998**, *4*, 1173-1176.
(5) Bishop, C. J.; Mason, N. O.; Kfoury, A. G.; Lux, R.; Stoker, S.; Horton, K.; Clayson, S. E.; Rasmusson, B.; Reid, B. B. *J. Heart Lung Transplant.* **2010**, *29*, 27-31.
(6) Bishop, C. J.; Ketola, T. M.; Tzeng, S. Y.; Sunshine, J. C.; Urtti, A.; Lemmetyinen, H.; Vuorimaa-Laukkanen, E.; Yliperttula, M.; Green, J. J. *J. Am. Chem. Soc.* **2013**, *135*, 6951-6957.
(7) Bishop, C. J.; Tzeng, S. Y.; Green, J. J. *Acta Biomater.* **2014**, *DOI: 10.1016/j.actbio.2014.09.020*.
(8) Kamat, C. D.; Shmueli, R. B.; Connis, N.; Rudin, C. M.; Green, J. J.; Hann, C. L. *Mol. Cancer Ther.* **2013**, *12*, 405-415.
(9) Tzeng, S. Y.; Green, J. J. *Adv. Healthcare Mater.* **2013**, *2*, 468-480.
(10) Yin, H.; Kanasty, R. L.; Eltoukhy, A. A.; Vegas, A. J.; Dorkin, J. R.; Anderson, D. G. *Nature Reviews Genetics* **2014**, *15*, 541-555.

8 Chapter 8: Future Perspective

8.1 Biomolecule Delivery to Engineer the Cellular Microenvironment

In this work, I have discussed the work of many world leaders involved in delivering biomolecules for regenerative medicine applications. The different types of delivery include extracellular delivery of soluble biomolecules, either as a bolus or through controlled release systems; delivery of insoluble factors, often through biomaterial-based scaffolds; and intracellular nucleic acid delivery to program a target cell on a genetic level. Examples of applications were presented in diverse areas of regenerative medicine such as tissue engineering of bone[1,2], cartilage, muscle, blood vessels[3-5], the heart, and the eye, neuroengineering[6], and wound healing (**Figure 5**; **Table 1**).

Many of the future directions in this field are associated with delivery that is engineered to be more biomimetic. This includes more precise spatial and temporal control of delivery as well as sequential delivery of multiple factors in the manner that best mimics natural healing mechanisms. Future directions include greater investigation and characterization on the microscale and nanoscale of the microenvironment in developing and healing tissues as well as creating synthetic bioengineered microenvironments that successfully reproduce their complexity of signals, both

---

Chapter 8 is in part published as "Bishop CJ, Kim J, Green, JJ. Biomolecule delivery to engineer the cellular microenvironment for regenerative medicine. *Ann. Biomed. Eng.* 2014;42(7):1557-72" and "Sunshine JC, Bishop CJ, Green, JJ. Advances in polymeric and inorganic vectors for nonviral nucleic acid delivery. *Ther. Deliv.* 2011;2(4):493-521".

insoluble and soluble, to cells developing in that microenvironment. Regulatory hurdles for cellular, tissue, and gene therapies are in many ways more complicated than for small molecules due to the added safety concerns associated with cellular materials. For example, characterization and purity of cells is critical, but as cell populations can often contain heterogeneity, ensuring purity and homogeneity of cells and their combination with biomaterials and signaling biomolecules in a precisely controlled way is a future direction of the field. Cell fate *in vivo* and ensuring that any delivered cells do not differentiate, proliferate, migrate, or behave in an unintended manner is key as well for both safety and efficacy. These concerns make the pathway from discovery of a new regenerative medicine therapy on the bench to translation in the clinic more tortuous.

In the past few years research efforts developing highly specific genome editing tools such as zinc nuclease fingers could possibly open the doors for safer, more efficacious methods to control gene expression to promote regeneration.[7-10] Zinc nuclease fingers alleviate some complications more traditional types of gene vectors face such as insertional mutagenesis, immune reactions, and high long-term expression. Methods to pattern topologies[11,12] for spatially controlled protein expression and presentation of biomolecules, as well as gene switches[13,14] which are able to turn on and off in the presence or absence of a molecule will be invaluable for engineering spatiotemporally controlled materials for regenerative applications. Regenerative medicine has enormous potential to treat many areas of medicine and as new basic discoveries are made and new bioengineered technologies invented, therapeutic modalities move closer to helping patients.

8.2 Polymeric and Inorganic Vectors for Nucleic Acid Delivery

While non-viral nucleic acid delivery remains less effective and efficient than viral delivery, recent advances offer the promise that soon there will be significant clinical effect from these approaches. Cyclodextrin-based polymers have found early clinical successes and additional biocompatible polymers are likely soon to follow suit. Incorporation of inorganic materials into such particles can also enable multimodality and theranostic applications. Several new directions are evolving which offer interesting approaches to achieve the goal of targeted, efficient, non-viral nucleic acid delivery.

Mesenchymal Stem Cells (MSC) and Neural stem/progenitor cells (NSPCs) are capable of migration toward pathological sites such as tumors and associated metastases. MSCs can be used to carry cargo while evading the immune system, as they are hypoimmunogenic and can then engraft into the stroma after arrival [15,16] For these reasons, MSCs are a very promising avenue for non-viral targeted gene delivery. Recently it was shown that virally-transduced NSPCs coud be implanted intracranially as an anti-cancer therapy. The NSPCs were transduced to stably express cytosine deaminase (CD), which converts 5-fluorocytosine (5-FC) to active 5-fluorouracil (5-FU). Following systemic 5-FC treatment 3-days later, there was a significant (71%) reduction in tumor burden [17]. Another group has modified human neural stem cells (NSCs) to secrete anti-HER2 immunoglobulin molecules as a tool to target and attack metastatic breast cancer in the brain. They were able to show that anti-Her2-secreting NSCs exhibit preferential tropism to tumor cells and can deliver antibodies to human breast cancer xenografts in

mice [18]. Potential complications for non-viral delivery approaches using stem cells could include timing of gene expression, differentiation of NSPCs/MSCs, and the possibility that these cells become tumorigenic. It is critical that all potential safety concerns with this approach are thoroughly investigated in non-human primates before clinical trials commence.

Translocation of pDNA to the nucleus and nuclear import remain critical barriers for gene delivery. This is because in many ways, non-viral gene delivery researched has focused on transporting plasmid DNA safetly and effectively into the cell, but has not focused on its subcellular location. Moreover, many biomaterials are designed to release naked DNA to the cytoplasm even though nuclear import is known to be inefficient. Enhancing nuclear import by other modalities in addition to NLS sequences and simple diffusion would be of great interest. Dynein mediates retrograde transport along microtubules towards the nucleus and kinesin mediates transport in opposite direction [19]. It is known that viruses such as HIV are able to exploit the cytoskeleton for directed movement towards the nucleus [20]. With further characterization of microtubule associated transport, perhaps synthetic approaches could similarly use endogenous cell machinery to enhancing nuclear uptake.

Finally, addition of targeting moieties is a widely used and important technique in the field. In addition to targeting ligands to cell surface receptors, a complementary approach is targeting specific enzymes at a specific microenvironment such as matrix metalloproteinases (MMPs). MMPs are upregulated during tumor growth (i.e., MMP-3, 7, and 13) and play a role in cell growth, death, malignant conversion, and tumor-associated angiogenesis [21]. siRNA has been used to downregulate MMP-9 and was

shown to aid the inhibition of invasion and migration of prostate cancer cells, leading to apoptosis both *in vitro* and *in vivo* [22]. In one approach, quantum dots have been conjugated to folic acid which is sterically shielded from the environment by MMP-7 cleavable PEG (exhaustively cleaved at 5 nM)[23]. This work combines the passive targeting of the EPR effect with MMP-sensitive release of cargo to take a two-fold approach for the targeted delivery of the nanoparticles. The cancer stage and type are important in determining which MMP should be used to cleave cargo or be a target itself [21]. Compared to conventional cancer chemotherapies, gene therapy can enable a much wider therapeutic window due to increased specificity. Nanoparticles can be passively targeted by the EPR effect, targeted to a microenvironement through enzyme activity, targeted to a cell receptor through a ligand interaction, and targeted to a cell-type through biomaterial optimization [24]. Once DNA delivered, it can then be transcriptionally targeted to the cell type of interest and the gene product itself could also be specific to the cell type of interest. Thus many layers of targeting can be enabled in a non-viral gene delivery system and particles that use multiple methods of targeting will likely become more widespread in the future. The directions sketched above and other innovations in biology, bioengineering, materials science, and nanotechnology will continue to guide the field of non-viral gene delivery.

8.3 Future Directions

8.3.1 Cellular and Nuclear Uptake Rate Evaluation of Exogenous DNA via Flow Cytometry

The method developed in this thesis for assessing uptake rates is a more high throughput method than purely qPCR methods that have been used. This new method developed can be used to compare multiple cell lines and multiple biomaterial structures to elucidate how biomaterial structure affects gene delivery function. One can compare healthy versus cancerous cell lines to elucidate cell specific differences in gene delivery. For a future direction, it would be interesting to compare cells from different tissues as well as primary normal and cancerous cells from the same tissue to investigate how these differences change DNA cellular uptake and nuclear uptake rates.

8.3.2 Poly(β-amino ester) Monomer and Polymer Structure Function Relationships Elucidated Via Principal Component Analysis

Now that a PCA approach for how biomaterial structure affects gene delivery function has been demonstrated, it would be intriguing to further grow the library of materials used as well as increase the variable parameters considered. For example, incorporating polymer-DNA binding constant data for the principal component analysis would be interesting. Since for PCA analysis, data sets are normalized and high-throughput data acquisition preferable, rather than utilizing the time-correlated single photon counting method, a semi-quantitative binding assay, such as YO-PRO®-1 total fluorescence may be a preferable alternative.

Also, developing a principal component method which is able to assess data library sets with missing data for certain variables would be great because one could include far more data, including partial data sets found in the literature. Currently, the method requires all data for all variables to be present. With further data, it is believed that this

approach could make predictions on how polymer structure affects gene delivery function.

8.4 Tables

Table 1. Literature summary.

Application	Biomaterial / Vector	Biomolecule	Cell Type	Animal Model	References
Biomolecule Delivery of Soluble Signals					
Bone	PLGA microspheres in poly(propylene fumarate) scaffold surrounded by gelatin hydrogel	BMP-2 and VEGF		ectopic / orthotopic implantation into rat	[36]
Bone	SMO-PCLA-PEG-PCLA-SMO hydrogel	hBMP-2	hMSCs	subcutaneous injection into mouse	[17]
Cartilage	collagen sponge	bFGF	chondrocytes	nude mouse	[15]
Cartilage	oligo(poly(ethylene glycol) fumarate) hydrogel with gelatin microparticles	TGF-β1	rabbit marrow mesenchymal stem cells		[32]
neovascularization	alginate hydrogel with PLG microspheres	PDGF and VEGF		ischemic limb i.m. injection into apoE$^{-/-}$ mouse	[33]
wound healing	photocrosslinkable chitosan hydrogel	FGF-2		mutant diabetic mouse	[16]
Insoluble Biomolecule Delivery Affecting Cell-Cell and Cell-ECM Interactions					
Bone	PLGA porous scaffold	GRGDS peptide sequence	human bone marrow cells		[46]
Bone	PEG hydrogel	nanospacing of RGD peptide	rat MSCs		[47]
Neural	self-assembling nanofiber from peptide amphiphile	IKVAV epitope of laminin	murine neural progenitor cells		[49]
Liver		HA, poly-L-lysine	primary rat hepatocytes and murine 3T3-J2 fibroblasts		[42]
stem cell self-renewal	polyacrylamide hydrogel	GKKQRFRHRNRKG peptide (vitronectin-derived, GAG-binding)	hESCs and iPSCs		[48]
Viral Vectors for *Ex Vivo* Cell Engineering					
Bone	Adenovirus	hBMP-2	rat marrow stromal cells	Orthotopic implantation into rat	[59]
Cardiac	Adenovirus	hVEGF	hESC-derived CD133^{+} endothelial progenitors	rat myocardial infarct model	[58]
Cardiac	Adenovirus	hVEGF	human skeletal myoblasts	porcine heart model of chronic infarction	[57]
Neural	herpes simplex virus type-1	rat HGF	rat marrow stromal cells	intracerebral transplantation into rat's ischemic brain	[61]
Viral Vectors for *In Vivo* Regeneration					
Bone	adenovirus coated on allograft	BMP-2	C3H10T1/2 cells for *in vitro*	femoral allograft surgery on female mouse	[62]
Eye	recombinant adenovirus 2/2	RPE-specific 65-kDa protein		subretinal injections into young adult patients	[65]
Non-viral Vectors for *Ex Vivo* Cell Engineering					
Bone	nucleofection with plasmid	recombinant hBMP-6	primary porcine adipose tissue-derived stem cells	injection into lumbar paravertebral muscle in mouse	[66]
Cardiac	PEI nanoparticle	hypoxia-regulated VEGF	rabbit skeletal myoblasts	female rabbit with acute myocardial infarction model	[67]
Non-viral Vectors for *In Vivo* Regeneration					
Bone	liposomal vector	BMP-2		transplantation into peri-implant bone defects on pig calvariae	[69]
wound healing	peptide-DNA condensates in fibrin gel	HIF-1α		intradermal implantation into mouse	[71]
wound healing	poly(β-amino ester) nanoparticle	human sonic hedgehog		intradermal delivery into mouse	[73]

8.5 References

(1) Jiang, T.; Nukavarapu, S. P.; Deng, M.; Jabbarzadeh, E.; Kofron, M. D.; Doty, S. B.; Abdel-Fattah, W. I.; Laurencin, C. T. *Acta Biomater.* **2010**, *6*, 3457-3470.
(2) Kofron, M. D.; Li, X. D.; Laurencin, C. T. *Curr. Opin. Biotechnol.* **2004**, *15*, 399-405.
(3) Jabbarzadeh, E.; Starnes, T.; Khan, Y. M.; Jiang, T.; Wirtel, A. J.; Deng, M.; Lv, Q.; Nair, L. S.; Doty, S. B.; Laurencin, C. T. *Proc. Natl. Acad. Sci. U. S. A.* **2008**, *105*, 11099-11104.
(4) Ferreira, L. S.; Gerecht, S.; Fuller, J.; Shieh, H. F.; Vunjak-Novakovic, G.; Langer, R. *Biomaterials* **2007**, *28*, 2706-2717.
(5) Yang, F.; Cho, S. W.; Son, S. M.; Bogatyrev, S. R.; Singh, D.; Green, J. J.; Mei, Y.; Park, S.; Bhang, S. H.; Kim, B. S.; Langer, R.; Anderson, D. G. *Proc. Natl. Acad. Sci. U. S. A.* **2010**, *107*, 3317-3322.
(6) Santos, T.; Ferreira, R.; Maia, J.; Agasse, F.; Xapelli, S.; Cortes, L.; Braganca, J.; Malva, J. O.; Ferreira, L.; Bernardino, L. *Acs Nano* **2012**, *6*, 10463-10474.
(7) Bedell, V. M.; Wang, Y.; Campbell, J. M.; Poshusta, T. L.; Starker, C. G.; Krug, R. G.; Tan, W. F.; Penheiter, S. G.; Ma, A. C.; Leung, A. Y. H.; Fahrenkrug, S. C.; Carlson, D. F.; Voytas, D. F.; Clark, K. J.; Essner, J. J.; Ekker, S. C. *Nature* **2012**, *491*, 114-U133.
(8) Li, H. J.; Haurigot, V.; Doyon, Y.; Li, T. J.; Wong, S. N. Y.; Bhagwat, A. S.; Malani, N.; Anguela, X. M.; Sharma, R.; Ivanciu, L.; Murphy, S. L.; Finn, J. D.; Khazi, F. R.; Zhou, S. Z.; Paschon, D. E.; Rebar, E. J.; Bushman, F. D.; Gregory, P. D.; Holmes, M. C.; High, K. A. *Nature* **2011**, *475*, 217-U128.
(9) Miller, J. C.; Tan, S. Y.; Qiao, G. J.; Barlow, K. A.; Wang, J. B.; Xia, D. F.; Meng, X. D.; Paschon, D. E.; Leung, E.; Hinkley, S. J.; Dulay, G. P.; Hua, K. L.; Ankoudinova, I.; Cost, G. J.; Urnov, F. D.; Zhang, H. S.; Holmes, M. C.; Zhang, L.; Gregory, P. D.; Rebar, E. J. *Nat. Biotechnol.* **2011**, *29*, 143-U149.
(10) Reyon, D.; Tsai, S. Q.; Khayter, C.; Foden, J. A.; Sander, J. D.; Joung, J. K. *Nat. Biotechnol.* **2012**, *30*, 460-+.
(11) Baraniak, P. R.; Nelson, D. M.; Leeson, C. E.; Katakam, A. K.; Friz, J. L.; Cress, D. E.; Hong, Y.; Guan, J. J.; Wagner, W. R. *Biomaterials* **2011**, *32*, 3062-3071.
(12) De Laporte, L.; Huang, A.; Ducommun, M. M.; Zelivyanska, M. L.; Aviles, M. O.; Adler, A. F.; Shea, L. D. *Acta Biomater.* **2010**, *6*, 2889-2897.
(13) Deans, T. L.; Cantor, C. R.; Collins, J. J. *Cell* **2007**, *130*, 363-372.
(14) Rusk, N. *Nat. Methods* **2007**, *4*, 684-685.
(15) Corsten, M. F.; Shah, K. *Lancet Oncol* **2008**, *9*, 376-84.
(16) Tang, C.; Russell, P. J.; Martiniello-Wilks, R.; Rasko, J. E.; Khatri, A. *Stem Cells*.
(17) Aboody, K. S.; Najbauer, J.; Schmidt, N. O.; Yang, W.; Wu, J. K.; Zhuge, Y.; Przylecki, W.; Carroll, R.; Black, P. M.; Perides, G. *Neuro Oncol* **2006**, *8*, 119-26.
(18) Frank, R. T.; Edmiston, M.; Kendall, S. E.; Najbauer, J.; Cheung, C. W.; Kassa, T.; Metz, M. Z.; Kim, S. U.; Glackin, C. A.; Wu, A. M.; Yazaki, P. J.; Aboody, K. S. *PLoS One* **2009**, *4*, -.
(19) Hirokawa, N. *Science* **1998**, *279*, 519-526.
(20) Arhel, N.; Genovesio, A.; Kim, K. A.; Miko, S.; Perret, E.; Olivo-Marin, J. C.; Shorte, S.; Charneau, P. *Nat Methods* **2006**, *3*, 817-24.
(21) Coussens, L. M.; Fingleton, B.; Matrisian, L. M. *Science* **2002**, *295*, 2387-2392.

(22) Nalla, A. K.; Gorantla, B.; Gondi, C. S.; Lakka, S. S.; Rao, J. S. *Cancer Gene Ther.* **2010**, *17*, 599-613.
(23) Sewell, S. L.; Giorgio, T. D. *Materials Science & Engineering C-Biomimetic and Supramolecular Systems* **2009**, *29*, 1428-1432.
(24) Sunshine, J.; Green, J. J.; Mahon, K. P.; Yang, F.; Eltoukhy, A. A.; Nguyen, D. N.; Langer, R.; Anderson, D. G. *Advanced Materials* **2009**, *21*, 4947-+.

Vita

Corey J. Bishop

Biomedical Engineering Ph.D. Candidate (Expected Graduation: May 2015)
The Johns Hopkins University School of Medicine
400 N. Broadway / Smith Building Rm 5001E
Baltimore, MD 21231
coreybishop@jhmi.edu

Education

7/2010-5/2015	Ph.D., Biomedical Engineering (GPA: 4.0) The Johns Hopkins University School of Medicine Thesis: "An Investigation of Gene Delivery Barriers for Poly(β-amino ester)s and Hybrid Gold-Polymeric Nanoparticles"
5/2009 – 6/2010	Biomedical Engineering Graduate Student (GPA: 3.93) University of Utah, Salt Lake City, UT
8/2005-5/2009	B.S., Biomedical Engineering (GPA: 3.91) University of Utah, Salt Lake City, UT

Honors and Awards

2014	Honorable Mention STAR Award from the Society for Biomaterials
2011-2014	National Science Foundation Graduation Research Fellowship
2011-2012	National Science Foundation Nordic Research Opportunity Fellowship
2011	National Science Foundation International Travel Grant Award
2010-2011	Dean Scholarship, JHU
2010	Invitation to Inventor Recognition by Intermountain Healthcare
2008	Undergraduate Research Award, University of Utah
2008	University of Utah Undergraduate Research Opportunity Grant
2007-2009	Engineering Scholarships, University of Utah
2007-2008	Departmental Bioengineering Scholarship, University of Utah
2007	Tau Beta Pi, Engineering Honors Society
2000	Eagle Scout
1990-2000	Three gold cups in Piano Federations (Black and White Club)

Manuscripts (h-index: 6; Citations: 112)

CJ Bishop, NO Mason, AG Kfoury, et al: A novel non-invasive method to assess aortic valve opening in HeartMate II patients using a modified Karhunen-Loève Transformation. *J Heart Lung Transplant.* 2010, 29:27–31.

NO Mason, **CJ Bishop**, AG Kfoury et al. Noninvasive predictor of HeartMate XVE pump failure by neural network and waveform analysis. *J. Amer. Society for Artificial Internal Organs*. 2010, 56(1):1-5.

AE Raymond, AG Kfoury, **CJ Bishop**, et al. Obesity of left ventricular assist device driveline exit site infection. *J. Amer. Society for Artificial Internal Organs.* 2010, 56(1):57-60.

SA Molokhia, H Sant, J Simonis, **CJ Bishop**, et al: The Capsule Drug Device: Novel Approach for Drug Delivery to the Eye. *Vision Res*. 2010 Mar 31. 50(7):680-5.

JC Sunshine, **CJ Bishop**, JJ Green. Advances in Polymeric and Inorganic Vectors for Non-viral Nucleic Acid Delivery. *Therapeutic Delivery.* 2011, 2(4), 493-521.

CJ Bishop, T Ketola, SY Tzeng, et al. The effect and role of carbon atoms in poly(β-amino ester)s for DNA binding and gene delivery. *J. Am. Chem. Soc.*, 2013, 135(18), 6951-7.

T Ketola, M Hanzlikova, L Leppanen, R Manuela, **CJ Bishop**, et al. Independent vs cooperative binding in polyethyleneimine-DNA and poly(L-lysine)-DNA polyplexes. *J. Phys. Chem. Part B*., 2013, 117(36), 10405-13.

CJ Bishop, J Kim, JJ Green. Biomolecule delivery to engineer the cellular microenvironment for regenerative medicine. *Ann. Biomed. Eng.* 2013, 42(7), 1557-72.

T Wang, DM Gilkes, N Takano, L Xiang, W Luo, **CJ Bishop**, et al. Hypoxia-Inducible factors and RAB22A mediate formation of microvesicles that stimulate breast cancer invasion and metastasis. *Proceed. of the National Academy of Sciences*, 2014, 111(31), 3234-42.

CJ Bishop, J Kim, KL Kozielski, et al. Highlights from the latest articles in nanomedicine. *Nanomedicine*, 2014, 9(7), 945-7.

CJ Bishop, SY Tzeng, JJ Green. Nano-Gold/Degradable Polymer Hybrid Nanoparticles for Co-Delivery of DNA and siRNA. *Acta Biomaterialia,* 2014. 2014, 42(7), 1557-72.

CJ Bishop, B Abubaker-Sharif, TR Guiriba, JJ Green. Gene delivery polymer structure-function relationships elucidated via principal component analysis. ***Biomaterials.*** **In submission.** 2015.

BP Hung, DL Hutton, KL Kozielski, **CJ Bishop**, et al. Platelet-derived growth factor BB enhances osteogenesis of adipose-derived but not bone marrow-derived mesenchymal stromal/stem cells. *Journal of Stem Cells*. Submitted 11.2014. In revision.

CJ Bishop, RL Majewski, TR Guiriba, NS Bhise, JJ Green. Quantifying biomaterial-mediated cellular and nuclear uptake rates of exogenous DNA via flow cytometry. In preparation for submission 2015.

CJ Bishop, AL Liu, DS Lee, et al. Inorganic/polymeric layer-by-layer nanoparticles for gene delivery: controlling protein expression. In preparation for submission 2015.

Abstracts/Poster/Oral Presentations

CJ Bishop, CN Madsen, KM Nelson, et al: Causes for Hospital readmission in Destination Therapy LVAD patients. J Heart Lung Transplant 26(2S):334, 2007. (Oral presentation, San Francisco, 2007)

DM Nelson, ML Eidson, MR Bonnell, **CJ Bishop**, et al: Causes of late mortality in DT LVAD patients. ASAIO J 53(2):36A, 2007. (Poster presentation, Chicago, 2007)

KM Nelson DM Nelson, **CJ Bishop**, et al: Single center experience with the Levitronix Centrimag VAD for temporary support. ASAIO J 53(2):39A, 2007. (Oral Presentation, Chicago, 2007)

CJ Bishop, LN Janicki, DM Nelson, CN Madsen, et al: Outcome in Destination Therapy LVAD patients predicted by the Seattle Heart Failure Model. J Heart Lung Transplant 27(2S): 272, 2008. (Poster presentation, Boston, 2008)

CJ Bishop, NO Mason, RA Khodaverdian, et al.: Reconstructive surgery for LVAD infections. ASAIO J 54(2):32A, 2008. (Poster presentation, San Francisco, 2008)

SA Moore, CN Madsen, **CJ Bishop**, et al.: Destination left ventricular assist device therapy for advanced age patients with heart failure: is there an age limit. J Am Coll Cardiol 2008;51:A68.

AL Raymond, AG Kfoury, **CJ Bishop,** et al: Obesity and Left Ventricular Assist Device driveline exit site infection. ASAIO J 55(2): 127. (Slide Presentation, Dallas, 2009)

CJ Bishop, AG Kfoury, NO Mason, et al: A novel non-invasive method to assess aortic valve opening in HeartMate II patients. ASAIO J 55(2): 159. (Slide Presentation, Dallas, 2009)

NO Mason, AG Kfoury, **CJ Bishop**, et al: Signal characteristics predictors of HeartMate XVE pump failure. ASAIO J 55(2): 161. (Slide presentation, Dallas, 2009)

CJ Bishop, BK Ambati: Pressure findings of a novel intraocular lens-co-implantable drug delivery device for the treatment of age-related macular degeneration. Univ of Utah Undergrad. Research abstracts 9:10-11. (Poster presentation, Park City, UT)

CJ Bishop, HJ Sant, SA Molokhia, et al. Designing and manufacturing a refillable multi-drug capsule ring platform. J ARVO. May 2009; 514:5331/A259. (Poster presentation, Ft. Lauderdale, FL)

RM Burr, SA Molokhia, CJ Bishop, et al. J ARVO. *In vitro* diffusion and permeability of a novel intraocular drug delivery implant. J ARVO. May 2009; 514:5299/A227. (Poster presentation, Ft. Lauderdale, FL)

SA Molokhia, RM Burr, CJ Bishop, et al. *In vivo* pharmacokinetics of a new intraocular drug delivery device. J ARVO. May 2009; 514:5328/A256. (Poster presentation, Ft. Lauderdale, FL)

KM Lin, CJ Bishop, HJ Sant, et al. Refilling mechanism to stabilize a free-floating intraocular capsule drug ring (CDR). AIChE Nov 2010. 15D16:568.

CJ Bishop, JC Sunshine, JJ Green. Nano-gold/degradable polymer hybrid nanoparticles for co-delivery of DNA and siRNA. Nucleic Acid Delivery; BMES Oct. 2011, PS58A. Presented in Hartford, Connecticut.

CJ Bishop, SY Tzeng, JC Sunshine, JJ Green. Nano-gold/degradable polymer hybrid nanoparticles for co-delivery of DNA and siRNA. 23rd Annual Wilmer Research Meeting, April 2012, M5. Poster presentation.

TM Ketola, CJ Bishop, JJ Green, M Hanzlíková, H Lemmetyinen, A Urtti, M Yliperttula, E Vuorimaa. The influence of pH and polymer structure on the cationic polymer-DNA complexes revealed by time-resolved fluorescence studies. XXIV IUPAC Symposium on Photochemistry, 15-20 July 2012, Coimbra, Portugal. Poster presentation.

CJ Bishop, SY Tzeng, JJ Green. A Layer-by-Layer Approach to Co-deliver DNA and siRNA Via AuNPs: A Potential Platform for Modifying Release Kinetics; BMES Oct. 2012; PS269A. Presented in Atlanta, Georgia.

CJ Bishop, SY Tzeng, JJ Green. A Layer-by-layer Gene Therapy Approach for Promoting Exogenous and Inhibiting Endogenous Protein Expression. *Society for Biomaterials.* April 2014 Denver Colorado; Oral Presentation; Honorable Mention STAR Award

CJ Bishop, SY Tzeng, JJ Green. Structure-Functional Relationships Between Poly(β-amino ester)s for DNA Binding and Gene Delivery. American Society for Gene and Cell Therapy. May 2014, 351, Poster presentation in Washington D.C.

Patents

Physiological Characteristic Determination for Medical Device User: 20100087742

Nanocomposites of Gold and Polymers: WO 2,013,056,113

Professional Experience

7/2010-5/2015	Ph.D. Graduate Research Student The Johns Hopkins University School of Medicine
7/2011-7/2014	National Science Foundation Graduate Research Fellow The Johns Hopkins University School of Medicine

12/2011-3/2012	National Science Foundation Nordic Research Fellow University of Helsinki/Tampere University of Technology
5/2009-6/2010	Graduate Research Assistant, University of Utah

Ambati/Wasatch Microfluidics Lab, Moran Eye Center/Merrill Engineering Building, Salt Lake City, UT

7/2007-6/2009	Bioengineering Research Associate

Utah Artificial Heart Program, LDS Hospital and Intermountain Medical Center

5/2008-12/2008	Biomedical Engineer for the Undergraduate Research Opportunity Program, University of Utah
5/2006-7/2007	Bioengineering Research Assistant Utah Artificial Heart Program, LDS Hospital

Utah Artificial Heart Program

On-call engineer for cardiac surgeons, physicians, nurses, and patients for implanting and explanting ventricular assist devices and total artificial hearts, as well as for troubleshooting equipment malfunctions (on-site and off-site). I would control the ventricular assist devices and artificial hearts during implant and explant procedures to maintain proper pressures in the devices as well as the patients. I assembled the inflow and outflow conduits, and primed the ventricular assist devices and total artificial hearts under a sterile field for the cardiac surgeon. I reported mechanical and physiological adverse events to the Interagency Registry for Mechanically Assisted Circulatory Support. I maintained databases for our patients' survival statistics to ensure we were meeting quality of care standards. I also trained new bioengineers coming into the program. Whenever I was not helping in a surgery or with a patient I would be doing research (see Research Publications).

IND Application Preparation for Intraocular Drug Delivery Device):

Eye Research - Graduate Research Assistant, University of Utah

From 5/2009-6/2010 I helped manufacture a polycarbonate-based polyether urethane refillable drug delivery reservoir that sits in the periphery of an intraocular lens and is implanted at the time of phacoemulsification. The drug reservoir was a PVA matrix encapsulating Avastin. We found that in rabbits the Avastin was able to successfully reach the retina. I helped prepare portions of the IND application that was in preparation to be submitted to the FDA; in particular, I was writing the manufacturing methods and the GLP protocols for developing the drug delivery devices.

Teaching Experience

2013 spring: Teaching Assistant for Tissue Engineering (undergraduate/graduate level)

2013 summer intersession: Course instructor for Nanoparticles for drug delivery applications in medicine

Students Mentored

6 Undergraduates (Rebecca Majewski, Josh Murdock, Kavan Reddy, David Lee, Allen Liu, Toni-Rose Guiriba); High school student (Evan Smith): Intel ISEF Finalist (Bruno Kessler Foundation Fellowship to participate in an interdisciplinresearch program in Italy)

Journal Reviewer
Soft Matter, ACS Nano, Acta Biomaterialia, Nanomedicine, Journal of Gene Medicine

Professional Societies
Tissue Engineering and Regenerative Medicine International Society, 2014

American Society for Gene and Cell Therapy, 2014

Society for Biomaterials, 2014-2015

Biomedical Engineering Society, 2011 - 2013

Association for Research in Vision and Ophthalmology, 2009 - 2010

American Society for Artificial Internal Organs, 2007 – 2010

International Society for Heart and Lung Transplantation, 2007 – 2010

Technical Skills
Software: MatLab (principal component analysis, Fouriér transform analysis, graphical user interface, differential equation modeling), SolidWorks, COMSOL (finite element analysis, drug diffusion).

Instrumentation: flow cytometry (Accuri C6/HyperCyt, FACScan, FACSCalibur), dynamic light scattering/Zetasizer (Malvern), nanoparticle tracking analysis (NanoSight/Malvern), UV-vis absorbance spectroscopy (Synergy2) and NanoDrop, multiphoton/confocal microscopy (Zeiss LSM 710NLO-Meta), transmission electron microscopy (Philips CM120, Hitachi 7600), scanning electron microscopy (Leo-Zeiss Field Emission), nuclear magnetic resonance, quantitative/relative polymerase chain reaction, enzyme-linked immunosorbent assay, time-correlated single photon counting, fluorescence microscopy (Zeiss), gel permeation chromatography (characterization/ preparative; Waters), rheometry, differential scanning calorimetry, lyophilization with sucrose stabilization.

Other: microfluidic chips, drug release studies (nucleic acid and small molecules), nanoparticle/microparticle drug encapsulation formation and drug synthesis, aqueous and organic soluble gold nanoparticle nucleation, quantum dot synthesis, gel electrophoresis, non-viral gene delivery of DNA and siRNA, cell synchronization, cell cycle assessment, nuclei isolation, acrylate gel synthesis.

Languages: English and Korean

References: Available upon request
U.S. Citizen